ROLE OF TRANSCRIPTION FACTOR EB (TFEB) IN CARDIAC HEALTH AND DISEASE

by

Purvi C. Trivedi

Submitted in partial fulfilment of the requirements

for the degree of Doctor of Philosophy

at

Dalhousie University

Halifax, Nova Scotia

December 2020

Table of Contents

List of Tables

.

List of figures

Abstract

Cardiomyopathy is prevalent, and the leading cause of mortality among obese and diabetic patients. Abnormalities in cardiac energy metabolism trigger myocyte dysfunction that precedes the onset of cardiomyopathy. Lack of insulin function triggers metabolic remodeling, rendering cardiomyocytes susceptible to detrimental effects of hyperglycemia and fatty acid (FA) overutilization. Glucolipotoxicity precipitates ER stress, mitochondrial dysfunction, impairment in Ca^{2+}-handling and protein degradation, leading to myocyte injury and death. Using *in-vivo* and *ex-vivo* models, data from my doctoral thesis demonstrated that glucolipotoxicity impairs the protein degradation pathway of lysosomal autophagy, causing cardiomyocyte injury. Gene expression of lysosomal proteins governing lysosomal metabolism and proteolytic (autophagy) function are under the direct control of transcription factor EB (TFEB), belonging to the microphthalmia/TFE family. My data show that glucolipotoxicity following nutrient-overload causes cardiomyocyte injury by inhibiting TFEB and suppressing lysosomal function. I next ascertained if types of FA and duration of FA exposure regulate TFEB action and dictate cardiomyocyte viability. Saturated FA, palmitate, but not polyunsaturated FAs, decreased TFEB content in a concentration- and time-dependent manner in cardiomyocytes. Hearts from high-fat high-sucrose diet-fed mice showed a temporal decline in nuclear TFEB content with a marked elevation of distinct lipid species suggesting that myocyte lipid loading and loss of TFEB are concomitant molecular events. To identity signaling and metabolic pathways modulated by the loss of TFEB action in cardiomyocytes, transcriptome analysis in murine cardiomyocytes with targeted deletion of TFEB ($TFEB^{-/-}$) was conducted. The RNA-sequencing analysis revealed enrichment of differentially expressed genes (DEGs) representing pathways of nutrient metabolism, cell death/apoptosis and cardiac function. Transcriptome analysis also showed upregulation of genes involved in lipid biosynthesis and storage, whereas genes associated with lipid catabolism were downregulated in myocyte with TFEB deletion. $TFEB^{-/-}$ cardiomyoblasts exhibited higher lipid droplet accumulation and increased caspase-3 activation, whereas constitutive activation of TFEB abrogated the phenotype. Notably, electrically stimulated $TFEB^{-/-}$ cardiomyocytes displayed an increase in Ca^{2+} transient amplitude. Together, our data demonstrated that TFEB plausibly regulates non-canonical energy metabolism pathways other than the canonical pathway of autophagy in cardiomyocytes. Loss of TFEB function in cardiomyocytes remodels energy metabolism and renders cardiomyocyte susceptible to nutrient-overload-induced injury. Probing intramyocellular mechanisms regulating TFEB and identifying pathways targeted by TFEB offers promising therapeutic options for treating patients with metabolic heart failure.

List of Abbreviations and Symbols

AA	arachidonic acid
ACC	acetyl CoA carboxylase
ACSL	long-chain fatty acyl-CoA synthase
AGE	advanced glycation end product
AMCM	adult mouse cardiomyocytes
AMPK	5’ AMP-activated protein kinase
ARCM	adult rat cardiomyocyte
Atg	autophagy-related
ATGL	adipose triglyceride lipase
ATP	adenosine triphosphate
AU	arbitrary units
bHLH	basic helix loop helix
BMI	body mass index
CD36	membrane of fatty acid translocase
CLEAR	Coordinated Lysosomal Expression and Regulation
Clu	clusterin
CMA	chaperone mediated autophagy
CPT	carnitine palmitoyl transferase
CQ	chloroquine
CREB	cyclic AMP response element binding protein
CRP	C-reactive protein
CTGF	connective tissue growth factor
Cts	cathepsin protease
CVD	cardiovascular disease
DAG	diacylglycerol

DEG	differentially expressed gene
DOX	doxorubicin
EC	excitation-contraction
ECM	extracellular matrix
EPA	eicosapentaenoic acid
ER	endoplasmic reticulum
ERK1/2	extracellular receptor kinase 1/2
ETC	electron transport chain
FA	fatty acids
FABP	fatty acid binding protein
FAO	fatty acid oxidation
FATP	fatty acid transport protein
FXR	farnesoid X receptor
G6P	glucose-6-phosphate
GABARAP	GABAA receptor-associated protein
Gba	beta glycosidases
GFP	green fluorescent protein
GLP-1	glucagon-like peptide-1
GLUT	glucose transporter
GP	glucose/palmitate
gpd1	glycerol-3-phosphate dehydrogenase 1
GS	glycogen synthase
GSK	glycogen synthase kinase
HbA1c	glycated hemoglobin
HBP	hexosamine biosynthetic pathway
HDAC	histone deacetylase

Hexb	beta-hexosaminidase
HFHS	high fat high sucrose
HFpEF	HF with preserved ejection fraction
HFrEF	HF with reduced ejection fraction
HK-1	hexokinase-1
Hsc70	heat shock cognate protein 70
HSL	hormone sensitive lipase
Hsp90	heat shock protein 90
InsR	insulin receptor
IRS	insulin receptor substrate
JNK	c-jun amino-terminal kinase
LA	linoleic acid
LAMP	lysosome associated membrane protein
LC3B	microtubule associated protein light chain 3 subtype B
LCFA	long-chain fatty acids
LDH	lactate dehydrogenase
LPL	lipoprotein lipase
LPS	lipopolysaccharide
LSD	lysosomal storage disease
LTCC	L-type Ca^{2+} channels
LV	Left ventricle
LVH	left ventricular hypertrophy
LYNUS	lysosome nutrient sensing machinery
MCOLN1	mucolipin1
MEFs	mouse embryonic fibroblast
MG	monoacylglycerol

MiTF	micropthalmia-associated transcription factor
Mlycd	malonyl-CoA decarboxylase
mRNA	messenger RNA
MTCO1	mitochondrially encoded cytochrome C oxidase I
mTORC1	mammalian target of rapamycin complex 1
MUFA	monounsaturated fatty acid
NCX	Na^{+}/Ca^{2+} exchanger
NOGP	nonoxidative glucose pathways
NRCM	neonatal rat cardiomyocytes
P	palmitate
PDH	pyruvate dehydrogenase
PDHK	pyruvate dehydrogenase kinase
PDHP	PDH phosphatase
PDK	pyruvate dehydrogenase kinase
PE	phosphatidylethanolamine
PFK	phosphofructokinase
PGC1α	peroxisome proliferator-activated receptor gamma co-activator α
pgm5	phosphoglucomutase 5
PI3K	phosphoinositol-3-kinase
PINK1	PTEN-induced putative kinase 1
PIP2	phosphatidylinositol (4,5)-diphosphate
PIP3	phosphatidylinositol (3,4,5)-trisphosphate
PLN	phospholamban
pmp22	peripheral myelin protein 22
PP2B	protein phosphatase 2 B
PPARα	peroxisome proliferator-activated receptor α

PTP	protein tyrosine phosphatase
PUFA	polyunsaturated fatty acids
RFU	relative fluorescence units
RIP1	receptor interacting protein 1
ROS	reactive oxygen species
RYR	ryanodine receptor
SERCA	SR Ca^{2+} ATPase pump 2a
SGLT-2	sodium-glucose cotransporter-2
Sgpl1	sphingosine-1-phosphate lyase 1
Sqstm1	sequestosome 1
SR	sarcoplasmic reticulum
STZ	streptozotocin
T1DM	type-1 diabetes mellitus
T2DM	type-2 diabetes mellitus
TAG	triacylglycerol
TCA	tricarboxylic acid cycle
TFE3	transcription factor E3
TFEB	transcription factor EB
TFEC	transcription factor EC
TGFβ1	transforming growth factor β 1
Tnfrsf1a	TNF receptor superfamily member 1A
TPC	two-pore channel
TRPML	transient receptor potential cation channel
Ub	ubiquitin
ULK1/2	unc-51 like kinase 1/2
UPP	ubiquitin proteasome pathway

UPR	unfolded protein response
vATPase	vacuolar ATPase
VPS	vacuolar protein sorting
WIPI	WD-repeat protein interacting with phosphoinositides

ACKNOWLEDGEMENTS

I take this opportunity to thank and regard the enormous support, encouragement, and knowledge garnered from different minds during this intensive training program. First, I would like to extend my deep sense of gratitude and respect to my research supervisor Dr. Thomas Pulinilkunnil. It has been a great privilege and honor to be mentored by Thomas, especially for his meticulous thinking, constructive criticisms, perseverance and unflagging devotion towards research. As his first graduate student, he taught me the skills to pose significant research questions, achieve systematic solutions, and understand the research philosophy. His painstaking efforts and untiring enthusiasm invested in me yielded two full-length first-authored manuscripts, one review article, two book chapters and five co-authored articles from my graduate program. I thank him for all the guidance, support, encouragement and friendship. I am also thankful to Dr. Petra Kienesberger and Dr. Keith Brunt for their patience, support, and counsel to move forward in my training program.

I am also grateful to my supervisory committee members Dr. T. Alexander Quinn, Dr. Neale Ridgway and Dr. Aarnoud Van Der Spoel, for their valuable suggestions and encouragement during the graduate training program. I would also like to take this opportunity to thank Dr. T. Alexander Quinn for providing his assistance and guidance with contractility and calcium transient data analysis.

I sincerely acknowledge the friendship, support and encouragement of my colleagues from Pulinilkunnil and Kienesberger labs. Their intellect and brilliant presence provided a professionally stimulating atmosphere in the lab. I would also like to thank trainees and staff from Brunt and Reiman lab for their technical assistance and gracious collegiality during my program. I also take pride in thanking DMNB, Department of Biochemistry and Molecular Biology, Faculty of Medicine, Dalhousie University, for providing an excellent graduate training program. I thank the faculty, technical and administrative staff for the help, support and encouragement during this program.

I would like to express my gratefulness to the Nova Scotia Health Research Foundation and Dalhousie Medicine New Brunswick for their graduate studentship support during my graduate program.

My special thanks to all my friends and well-wishers within and outside the faculty for their cheerful companionship and support.

Finally, no words of esteem can suffice to express my love and appreciation for my family. Without their moral, selfless support and sacrifice, accomplishing my goal to acquire a Doctoral degree would have been impossible.

Chapter 1: Introduction

This chapter contains materials (sections 1.5 and 1.6) originally published in:

Trivedi, P.C.; Bartlett, J.J.; Pulinilkunnil, T. Lysosomal Biology and Function: Modern View of Cellular Debris Bin. Cells. 2020, 9(5):1131 [1].

1.1 Obesity, diabetes and cardiovascular disease

1.1.1 Prevalence of obesity and diabetes mellitus

Obesity is a pathophysiological state that is globally prevalent among all age groups, sexes and cultures. Clinically, obesity is established when body mass index (BMI) is higher than 30. Obesity is further sub-divided into class-1 (BMI of 30-34.9), class-2 (BMI of 35-39.9) and class-3 (BMI ≥40) obesity [2]. Obesity occurs due to positive energy imbalance, wherein nutrient and energy supply outweigh physiological demand and usage. Between the years 1985 and 2011, the prevalence of obesity has increased in Canada, from 6.1 to 18.3% [2]. In 2018, 9.9 million adults were classified as overweight, bringing the total population with increased health risks due to excess weight to 63.1% [3]. Obesity rates have roughly doubled across all age groups over the past three decades. Disturbingly, 20% of the Canadian youth is overweight or obese, and the number continues to rise, notably in Maritime provinces [4].

Obesity is a major risk factor for type 2 diabetes mellitus (T2DM), which accounts for 90 to 95% of total diabetes cases. Type 1 diabetes mellitus (T1DM) accounts for 5 to 10% of cases, an early-onset diabetes characterized by pancreatic β-cell destruction, resulting in decreased insulin production and secretion, leading to the deficiency of insulin content and function [5]. T1DM is an insulin-dependent autoimmune disease that appears to have a genetic basis [6] and will not be discussed here. Trends in the prevalence and incidence of T2DM closely mirror the upward trend in obesity [7]. In 2013, 422 million adults lived with diabetes worldwide compared to 108 million in 1980 [8]. T2DM is a global epidemic, and its prevalence is increasing every year, and by 2035

is expected to affect over 592 million people [9] globally. 7.3% of Canadians over the age of 12 and older were diagnosed with diabetes in 2017 [9]. Between 2016 and 2017, the proportion of males who reported being diagnosed with diabetes increased from 7.6% in 2016 to 8.4%. The proportion of females with diabetes remained consistent in the last two years [9]. Chronic diabetes is characterized by hyperglycemia, hyperlipidemia and insulin resistance [8,10]. Numerous etiological factors contribute to the onset of T2DM and insulin resistance. These include pancreatic β-cell dysfunction [11], increased inflammatory serum content of interleukin-6 (IL-6) and C-reactive protein (CRP) [12,13], insulin signaling suppression through inflammation [14] and upregulation of cell death pathways in pancreatic β-cells [15,16]. Comorbidities of obesity and diabetes include cancers (pancreatic, colon and rectal cancers), microvascular diseases (retinopathy, nephropathy and neuropathy) and macrovascular diseases (hypertension, hyperlipidemia, heart failure, coronary artery disease, strokes, perivascular and cerebrovascular diseases), including muscle-specific heart disease [17-19].

1.1.2 Obesity- and diabetes mellitus-related heart disease

Etiology/prevalence/epidemiology: Patients with diabetes have twice the risk of developing heart failure (HF) than patients without diabetes. HF is the primary cause of mortality in individuals with diabetes [20]. Over the last two decades, with increasing morbidity of both obesity and diabetes, the prevalence of HF among diabetic patients has significantly increased worldwide [21]. The prevalence of HF in diabetic patients is astoundingly high, ranging from 19% to 26% [22]. Underdiagnoses of diabetic complications increase patient's susceptibility to HF by two- to three-fold compared to those with non-diabetic complications. Additionally, each 1% increase in glycated hemoglobin (HbA_{1c}) is linked to a 15% increase in HF risk [23,24]. Data from a twenty-year follow-up of Framingham Heart Study suggests that diabetes independently increases the risk of developing HF up to two-fold in men and five-fold in women compared to their age-matched controls, also highlighting sexual dimorphism in diabetes-induced heart disease [25]. A higher incidence of HF in diabetic patients is associated with increased left ventricular (LV) wall

thickness [25]. From Strong Heart Study and the Multi-Ethnic Study of Atherosclerosis, differences in LV mass and wall thickness and increased diastolic and systolic dysfunctions in diabetic patients are evident compared to non-diabetic patients [26]. Moreover, the prevalence of HF in patients with T2DM has risen from 12% to 22% with increasing age, suggesting diabetes is an independent risk factor for HF [27].

1.1.3 Current therapeutic strategies

Advanced understanding of the disease pathogenesis has provided us with improved disease treatment and management options for obese and diabetic patients with cardiovascular complications. These management options include improving lifestyle, improving glycemic control and using lipid-lowering agents and therapies to target molecular events such as fibrosis, hypertrophy, oxidative stress, and inflammation.

Lifestyle modification: Regular physical training and healthy eating are key habits for managing obesity and diabetes. Exercise improves glycemic control, insulin sensitivity and cardiac metabolic flexibility in the heart, augmenting cardiac function in diabetic patients [28-30]. Zucker diabetic fatty (ZDF) rat, a preclinical model, simulating clinical T2DM when subjected to aerobic exercise training, exhibits improved glycemic control and lipid profile with a concomitant reduction in anti-inflammatory cytokines [31]. Likewise, healthy eating, caloric restriction and intermittent fasting benefit diabetic patients [32]. Prolonged caloric restriction in T2DM patients reduces BMI and improved glycemic control associated with lower myocardial triacylglycerol (TAG) content and improved diastolic dysfunction [33]. However, both intermittent fasting and caloric restriction approaches are considered safe with frequent personal glucose monitoring practices in diabetic patients only when carried out under the supervision of the patient's healthcare provider.

Anti-diabetic therapies: Glucose overload is a driver of cardiovascular complications in diabetic patients. Epidemiological analysis demonstrates that each 1% reduction in $HbA1_C$ is associated with a 21% reduction in diabetes-related cardiovascular outcomes [34]. Therefore, a therapeutic strategy to improve hyperglycemia and hyperinsulinemia is expected to reduce cardiac

dysfunction in diabetic patients. Although the treatment of hypertension that co-exists with HF is cardioprotective, the beneficial effect of glycemic control in HF is still not clearly defined [35]. Different glucose-lowering therapies such as dipeptidyl peptidase-4 inhibitors (Sitagliptin, Linagliptin), thiazolidinediones (Glitazones) and sulfonylureas (Glibenclamide and Glimepiride) are not beneficial in diabetic patients with HF [36,37], whereas studies utilizing Metformin to treat HF have shown conflicting results. These results suggest that targeting hyperglycemia is insufficient to reduce major macrovascular complications, including accelerated cardiovascular diseases resulting in atherosclerosis and myocardial infarction. However, recent clinical studies such as the LEADER (Liraglutide Effect and Action in Diabetes: Evaluation of Cardiovascular Outcome Results) trial and SUSTAIN-6 trial with glucagon-like peptide-1 (GLP-1 such as Liraglutide and Semaglutide) receptor agonist improve cardiovascular outcomes in diabetic patients [38,39]. Notably, the new class of anti-diabetic drug sodium-glucose cotransporter 2 (SGLT-2) inhibitor such as Empagliflozin has shown the most promising outcome of reducing cardiovascular complications and hospitalization in HF patients with diabetes [40]. However, more studies are warranted to investigate the underlying mechanisms by which GLP-1 receptor agonists and SGLT-2 inhibitors improve cardiovascular complications in diabetic patients.

Dyslipidemia is yet another frequently observed comorbidity in patients with obesity, diabetes and insulin resistance. A higher level of low-density lipoprotein cholesterol is a significant risk factor for atherosclerotic cardiovascular disease (CVD). Also, statin treatments prevent CVD and mortality by controlling hyperlipidemia, likely benefiting T2DM patients [41,42]. Together, these findings suggest that cardiovascular complications in diabetic patients can be managed by lifestyle modification, controlling glycemia and treatment focusing on dyslipidemia, hypertension and HF. Most importantly, since no drug has been approved for HF in diabetic patients, additional pre-clinical studies are warranted to develop therapies and mitigate lipotoxicity in diabetic patients with HF.

1.2 Structural and functional abnormalities in left ventricular heart disease

In the obese and diabetic heart, anatomical and functional changes in the myocardium cause clinicopathological consequences culminating in HF. Pathological alterations in myocardial metabolism, structure and Ca^{2+} signaling are early defects that precede clinically defined HF. The progression of cardiovascular complications to HF during obesity and diabetes is described in three distinct stages with different clinical outcomes and pathophysiological features. In the early stage of disease progression, metabolic disturbances such as insulin resistance and hyperglycemia are not accompanied by substantial changes in myocardial structure and function [43,44]. The diabetic heart is characterized by diastolic dysfunction with preserved ejection fraction [45,46]. Clinically impaired myocardial relaxation is detected by echocardiography and MRI with no systolic dysfunction, indicating optimal ejection fraction. In the advanced stage of disease progression, increased myocardial fibrosis due to increased cell death and oxidative stress initiates a significant decline in diastolic function followed by systolic dysfunction [47]. In the late stage, persistent metabolic inflexibility, neurohumoral activation, and myocardial fibrosis exacerbate diastolic and systolic dysfunction, leading to HF [43,48].

1.2.1 Left ventricular hypertrophy (LVH)

LVH is characterized by an increase in LV mass and is a hallmark of morphological changes observed in the obese and diabetic heart. Initially, LVH overlaps with conserved LV function but chronically results in ventricular dysfunction. The disproportionate enlargement of the LV relative to cardiac work renders the myocardium sensitive to ischaemic and arrhythmic disturbances. Echocardiograms of diabetic patient's hearts show an increase in LV posterior and septal wall thickness [49]. Individuals with obesity are presented with greater LV mass and LV wall thickness than individuals with normal weight [49,50]. Additionally, central obesity is a risk factor for LVH and causes concentric LVH independent of hypertension [51]. Emerging evidence suggests the involvement of cytokines (IL-6 and leptin) and adipokine (resistin) in the development of LVH [52]. Importantly, insulin resistance and hyperinsulinemia are strongly correlated with

increased LV mass, corroborating the association of cardiac hypertrophy to obesity [53]. Despite the clinical knowledge that regressing LVH is cardioprotective during obesity and diabetes, the mechanisms and therapeutic targeting of LVH development and/or progression at the level of the cardiac myocyte are unclear due to the complexity of intracellular pathways regulating cardiac hypertrophy.

1.2.2 Myocardial fibrosis

Myocardial fibrosis develops due to increased collagen deposition secondary to the disarray of ECM (extracellular matrix) protein structure and turnover. Collagen type-I and -III are primarily accumulated in epicardial and perivascular regions of the heart, whereas type-IV is accumulated in the endocardial layer [54]. Histopathological scans of the diabetic heart reveal interstitial fibrosis, capillary basal laminae thickening, narrowing of the lumen due to increased proliferation of endothelial cells and increased thickness of the arteriolar wall [55,56]. In a diabetic heart, an increase in the expression of profibrotic factors such as transforming growth factor β 1 (TGFβ1) and connective tissue growth factor (CTGF) triggers excessive ECM protein accumulation [57]. This effect is secondary to the decrease in the activity of the ECM-degrading enzyme, metalloproteinase-2 and increase in activity of tissue inhibitor of MMP-2 (TIMP2) [58].

Hyperglycemia induces the non-enzymatic reaction between amine residues of proteins, lipids or sugars to form advanced glycosylation end-products (AGEs). This chemical modification of proteins is an important mechanism that could contribute to myocardial fibrosis. Once formed, AGEs cross-link with collagen molecules, which increase their resistance to proteolysis and decrease their turnover [59]. AGEs bind to its putative receptor for advanced glycation end products (RAGE) on the cardiac cell membranes, promoting pro-inflammatory signaling and increasing the expression of oxidative stress mediators, a process which is accelerated in diabetic patients [60]. Biomarkers of collagen synthesis such as inflammatory cytokines, CTGF, metalloproteinases and galectin-3 are used clinically to ascertain the severity of myocardial fibrosis [57,58,61-63].

1.2.3 Diastolic dysfunction

HF resulting from impaired myocardial relaxation and compliance is termed as diastolic HF [64,65]. Diastolic dysfunction in diabetic patients is characterized by a reduction in early diastolic filling and an increase in atrial filling and enlargement, leading to elevated LV end-diastolic pressure and systolic dysfunction [66,67]. The echocardiographic indices for diastolic dysfunction include E/E' and E/A ratios (where E and A are the mitral peak velocity of early and late ventricular filling, respectively and E' is the early diastolic mitral annular velocity), which are impaired in type-2 diabetic patients [66,67]. Indeed, the use of flow and tissue Doppler techniques suggest a prevalence of diastolic dysfunction as high as 40-75% in T1DM and T2DM patients [68]. Diastolic dysfunction is also observed in animal models, including *ob/ob*, *db/db* and ZDF rats, which exhibit obesity, insulin resistance and mild to severe hyperglycemia [69-73].

TAG deposition, impaired insulin signalling, lipotoxicity, increased cytokine activity and increased formation of AGEs are purportedly the causative drivers of diastolic dysfunction [71,74]. Furthermore, diastolic dysfunction is accelerated by impaired mitochondrial energy production by altered substrate supply, and utilization and mitochondrial uncoupling are likely reducing cardiac efficiency [75,76]. Additional drivers and/or triggers include alteration in Ca^{2+} handling, sympathetic overdrive, endothelial dysfunction and LV concentric remodelling, all of which contribute to diastolic dysfunction [77-79].

1.2.4 Systolic dysfunction

With the progression of diabetic cardiomyopathy, diastolic dysfunction and reduced cardiac compliance are accompanied by systolic dysfunction. Systolic dysfunction is characterized by reduced ejection fraction, prolonged pre-ejection performance, an enlarged LV chamber and shortened ejection period [80]. Importantly, when considering sex-specific estimates, the prevalence of LV systolic dysfunction among men with T2DM is 9% compared to 2% in women [81]. Animal studies have demonstrated an association of diabetes with LV systolic dysfunction, wherein diabetic animals display reduced heart rate, systolic blood pressure and fractional

shortening compared to control animals [82-84]. Additionally, LV systolic dysfunction may cause a degree of myocyte loss due to increased myocyte injury, resulting in decreased contractility and ejection fraction. Furthermore, abnormal contractile and regulatory protein expression and activity lead to impaired Ca^{2+} sensitivity, contributing to systolic cardiac dysfunction [85].

1.2.5 HFpEF and HFrEF

HF is clinically defined as a structural or functional abnormality that impairs the ability of the LV to eject blood (Systolic Heart Failure) or to fill with blood (Diastolic Heart Failure). Congestive heart failure is a complex clinical syndrome characterized by abnormalities of LV function and neurohormonal regulation, which are accompanied by effort intolerance, fluid retention, and reduced longevity. However, the above descriptions of HF do not account for HF cases where systolic dysfunction is absent but still exhibit clinical symptoms of HF. Recently, HF has been classified into HF with reduced ejection fraction (HFrEF; LVEF ≤ 40%) [86], HF with preserved ejection fraction (HFpEF; LVEF ≥ 50%) [86,87] and HF with a mid-range ejection fraction (HFmEF; LVEF = 41%-49%) [86,88]. Up to 50% of patients presenting in the emergency room with HF have preserved systolic function (HFpEF). Despite the high prevalence of HFpEF, the mechanisms underlying this type of HF are poorly understood, and currently, there is no effective therapy for HFpEF. Aging, frailty, sex and comorbidities such as atrial fibrillation, hypertension, diabetes, obesity, pulmonary hypertension, and renal dysfunction are often associated with HFpEF. Yet, the relationship and contribution of these clinical manifestations with HFpEF remain ill-defined. Preliminary studies suggest that metabolic maladaptation is the initial trigger for HFpEF pathology. Obesity and diabetes have different outcomes in HFpEF versus HFrEF. Diabetic patients with HFpEF display increased myocardial stiffness, whereas patients with HFrEF exhibit fibrosis [89]. Almost half of HF patients with T2DM exhibit HFpEF, more common in older, hypertensive female patients. These patients are often presented with mild symptoms and are difficult to diagnose, but symptoms appear when patients are subjected to strenuous physical

activity [90]. The severity and duration of hyperglycemia are critical determinants of the development of LV dysfunction. Patients with milder T2DM symptoms usually show HFpEF, whereas HFrEF is observed in patients with severe T2DM complications [91]. Clinically, both HFpEF and HFrEF are characterized by different systemic biomarker profiles. In patients with HFpEF, high plasma levels of inflammatory biomarkers such as interleukin-1 receptor-like 1 (IL1RL1) and CRP are observed [92,93]. Whereas HFrEF patients presented with higher levels of high-sensitivity troponin T (hsTNT, a marker for myocardial injury) or N-terminal pro-B-type natriuretic peptide (NT-proBNP, a marker for myocardial wall stress) [92,93]. The standard diagnostic criteria for HFpEF and HFrEF in diabetic versus non-diabetic patients include LV diastolic volumes and higher LV filling pressure (higher mitral E/A ratio) [92]. Regarding cardiac remodeling, eccentric hypertrophy predominates in HFrEF, and concentric hypertrophy is frequently observed in HFpEF patients [94]. Although the pathogenesis of obesity- and diabetes-related cardiovascular complications are multifactorial, abnormal cardiac metabolism, systemic dyslipidemia, myocardial lipid accumulation and impaired Ca^{2+} signaling are the key defining pathological features during HF. The heterogeneity in HFpEF pathophysiology, insufficient diagnosis and limited evidence-based therapies compound extremely poor outcomes of this disease. The success of interventions for HFrEF have resulted from an advanced molecular understanding of its metabolic, hemodynamic and neurohormonal pathophysiology. Advances in understanding HFpEF can be achieved by deciphering mechanisms perturbing myocyte energy metabolism.

1.3 Cardiac energy metabolism in the obese and diabetic heart

One of the early biochemical transformations in the obese and diabetic heart includes impairment in cardiac energy remodeling, which has primarily been uncovered and extensively studied in preclinical models [95] and verified clinically [79,96]. Cardiac metabolic remodeling is followed by the precipitation of pathological events such as LV wall stiffness, deposition of collagen and impairment in Ca^{2+} homeostasis [97]. However, metabolic changes are underestimated in the clinical scenario due to the rapidity of metabolic transformation, underdiagnoses and delayed

detection in obese and diabetic humans exhibiting cardiomyopathy [98]. Therefore, it stands to reason that reversal of altered cardiac substrate utilization or reversing the detrimental effects of abnormal cardiac energy metabolism during obesity and diabetes will prevent cardiovascular complications. A thorough understanding of the mechanisms by which abnormalities in myocardial energy metabolism trigger disruptions in myocyte signaling and function is vital to achieving this goal.

1.3.1 Glucose and fatty acid utilization

The heart is an energy-intensive organ, requiring a continuous and uninterrupted supply of 3.5–5 KG of ATP/day to maintain adequate pumping action [98,99]. To support higher ATP consumption, the heart relies on multiple substrates such as fatty acids (FA), carbohydrates, amino acids and ketones, with FA and glucose being the principal fuels [99]. In the healthy heart, oxidation of long-chain fatty acids (LCFA) accounts for approximately 65–80% of ATP production, and hence they are the preferred energy substrate for the heart [98,99]. Whereas glucose and lactate oxidation accounts for ATP production, representing 15–25% and 5–10%, respectively [98,99]. Although FA is the most preferred substrate, the heart has a limited capacity to synthesize this substrate and relies on continuous exogenous supply. FAs can be imported to the heart from two systemic sources: 1) FAs released from the adipose tissue and bound to albumin, which is then taken up by the heart and 2) hydrolysis of TAG-rich lipoproteins to FAs **(Figure 1.1 A)** [100]. Exogenous FAs importation is necessary to maintain optimal β-oxidative function, which is accomplished by the concerted action of lipoprotein lipase (LPL) and myocyte FA transporters [101]. FAs entry into the cardiomyocyte is insulin sensitive and occurs via passive diffusion or via protein-mediated transporters such as CD36 (a member of FA translocase), FA transport protein (FATP) **(Figure 1.1 A)** [102-104]. Once inside the cardiomyocyte, Long-chain fatty acyl-CoA synthase (ACSL1) converts FAs into fatty acyl-CoA esters in an ATP-dependent manner **(Figure 1.1 B)** [105,106]. The acyl group from fatty acyl-CoA is transferred from CoA to carnitine to form acylcarnitine by carnitine palmitoyl-transferase-1 (CPT-1),

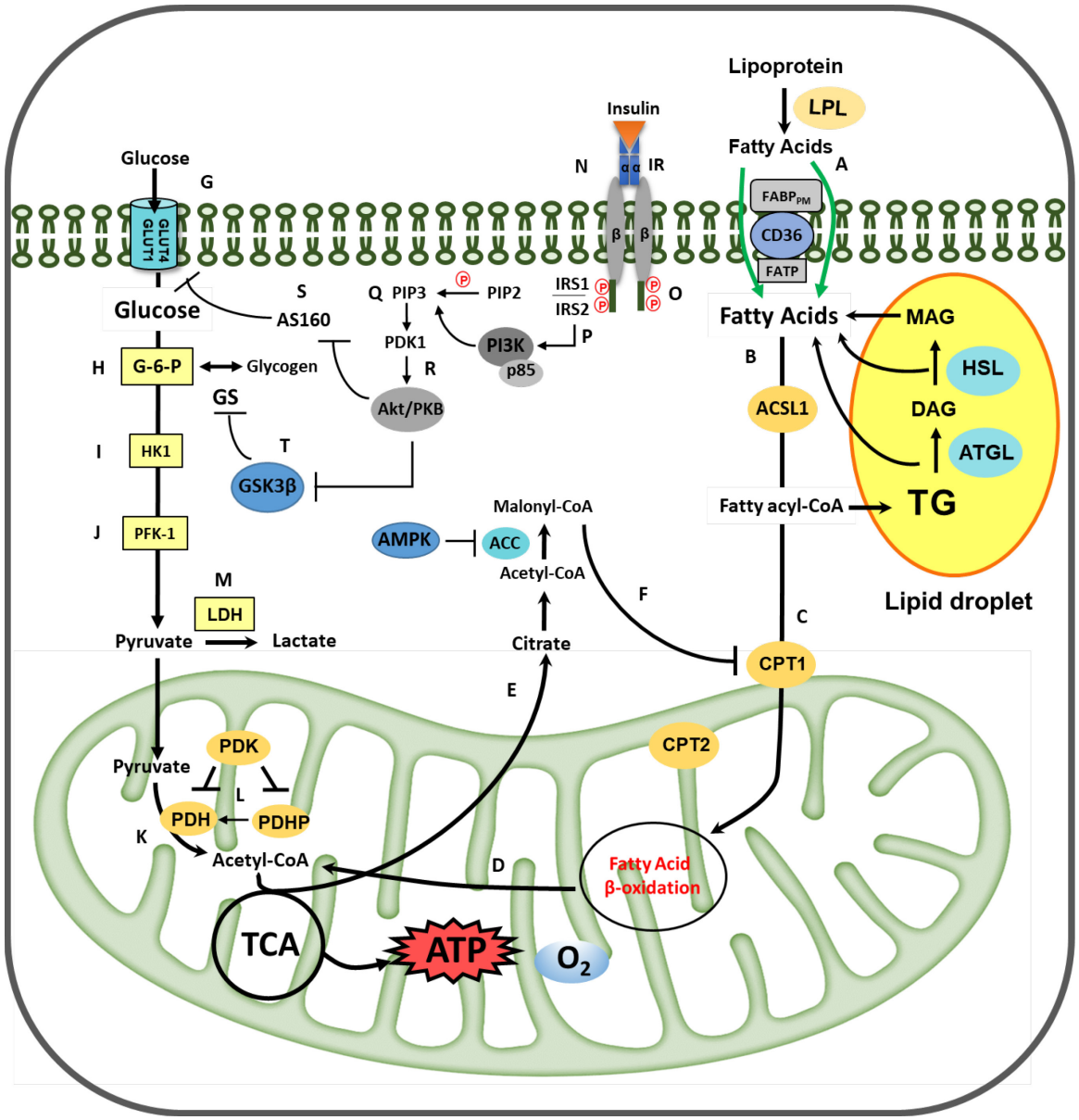

Figure 1.1 Role of insulin in regulating cardiac energy metabolism in a healthy heart. The heart relies on ATP derived from FAO to meet the contractile demands. LPL-derived FA enters the myocardium via the concerted action of CD36 and FABP/FATP **(A-D)**. Within the mitochondria, citrate generated during the TCA cycle translocates into the cytosol to form acetyl-CoA, which is further converted to malonyl-CoA by the action of ACC **(E)**. Insulin increases malonyl-CoA levels, which inhibits CPT-1 and the ensuing mitochondrial β-oxidation of FAs **(F).** Insulin inhibits FAO and directs the incorporation of FAs into TAG **(G).** Insulin limits the reliance of the heart on FAO oxidation by augmenting glucose utilization **(H).** Insulin's binding to its transmembrane receptor initiates an intracellular autophosphorylation cascade that activates IRS-1 and promotes PI3K-phosphorylation of PIP2 to increase intracellular PIP3 concentrations **(O-R).** Increased PIP3 concentrations facilitate the recruitment of PDK1 and Akt to the cardiomyocyte membrane, whereby PDK1 phosphorylates Akt **(S).** Subsequently, Akt inhibits AS160 and relieves inhibition

on GLUT translocation **(T).** GLUT4 facilitates the transport of glucose through the cardiomyocyte sarcolemma **(H).** Insulin-induced GLUT4 translocation facilitates cellular glucose uptake and utilization. Intracellularly, glucose is converted to G-6-P that is either shunted into glycogen storage via glycogen synthase or processed further via the glycolytic pathway **(I-K).** The glycolytic end-product pyruvate is transported into the mitochondrial matrix and converted by PDH to form acetyl-CoA, which is processed via the TCA cycle to generate ATP **(L).** PDH is regulated by either PDHK-dependent inhibitory phosphorylation or PDHP-induced activating dephosphorylation of PDH **(M).**

an enzyme residing in the outer mitochondrial membrane. Subsequently, CPT-2, an enzyme of the inner mitochondrial membrane, catalyzes the transfer of the acyl group from carnitine to CoA in the mitochondrial matrix **(Figure 1.1 C)** [107,108]. Within the mitochondrial matrix, fatty acyl-CoA molecules are sequentially broken down by β-oxidation to liberate acetyl-CoA **(Figure 1.1 D)**, which is then metabolized through the tricarboxylic acid cycle (TCA) to generate ATP. The rate of β-oxidation is regulated by the intracellular levels of malonyl-CoA, synthesized from the cytosolic citrate, an intermediate of the TCA cycle. Citrate is an important precursor for cytosolic acetyl-CoA, required to drive FA synthesis **(Figure 1.1 E)**. Citrate activates acetyl-CoA carboxylase (ACC) enzyme to generate malonyl CoA from acetyl CoA and signals a feedback response to decrease FA uptake into the mitochondria [107,108]. Malonyl CoA is a robust inhibitor of CPT-1 and FA β-oxidation **(Figure 1.1 F)** [109]. Adenosine monophosphate-activated protein kinase (AMPK), the "cellular fuel gauge", inhibits ACC activity and relieves ACC inhibition of CPT-1, thereby augmenting flux of ACSL1 into β-oxidation [110]. FAs derived from TAG hydrolysis are also important cardiac energy substrates for forming complex lipids and the construction of membranes [111]. TAG hydrolysis represents a tightly regulated process involving the concerted action of ATGL (adipose triglyceride lipase generates DAG), HSL (hormone-sensitive lipase generates mono[112]acylglycerol (MG)), and MGL (monoacylglycerol lipase generates FA) **(Figure 1.1 G)** [113,114].

In addition to FA, the heart metabolizes approximately 25% of glucose and 15% of lactate for ATP generation, and the rest of the ATP (~5%) is derived from amino acids and ketones [99]. In an insulin-dependent process, glucose from the circulation is transported into the cardiomyocyte via glucose transporters (GLUTs), GLUT1 and GLUT4 isoforms, which are predominantly expressed in cardiac tissue **(Figure 1.1 H)** [97]. Heart muscle expresses the highest levels of the "insulin sensitive" GLUT4 isoform. GLUT1 isoform is an insulin-independent GLUT present in high abundance in erythrocytes and at lesser amounts within the heart, allowing the heart to uptake glucose in the absence of insulin [112]. GLUT mediated glucose uptake involves serine/threonine

kinase, AMPK, which promotes GLUT1 and GLUT4 translocation to sarcolemma [115]. Once in the cytosolic compartment of the sarcolemma, glucose is phosphorylated by hexokinase to glucose-6-phosphate (G-6-P) **(Figure 1.1 I)**. Hexokinase-I is the abundant isoform in the fetal heart, and hexokinase-II is the dominant isoform in the adult heart **(Figure 1.1 J)** [116-118]. Insulin-dependent glycolysis results from PI3K (Phosphatidylinositol 3-Kinase)/PDK (phosphoinositide-dependent kinase-1)-mediated activating phosphorylation of phosphofructokinase-2 (PFK-2), generating fructose-2-6-bisphosphate (F-2,6-BP) [119], a potent activator of glycolysis [120]. F-2,6-BP activates PFK-1 [119], a control node in glycolysis **(Figure 1.1 K)** [120]. During nutrient abundance, pyruvate generated by glycolysis is transformed via three sets of reactions: 1) conversion to oxaloacetate or malate via a carboxylation reaction, 2) conversion to lactate, and/or 3) decarboxylation to acetyl-CoA through the multienzyme complex pyruvate dehydrogenase (PDH) **(Figure 1.1 L)**. PDH is regulated by either pyruvate dehydrogenase kinase (PDHK)-mediated inhibitory phosphorylation on the E1 subunit of PDH or by PDH phosphatase (PDHP)-induced dephosphorylation of PDH leading to its activation **(Figure 1.1 M)**. Acetyl-CoA derived from pyruvate enters the TCA cycle for ATP generation with the concomitant production of H_2O and CO_2. In oxygen-rich conditions, pyruvate is converted to acetyl-CoA, whereas during the hypoxic state, pyruvate is converted to lactate by the enzyme lactate dehydrogenase (LDH) **(Figure 1.1 N)**. Pyruvate and lactate derived from glucose are transported into the mitochondria via monocarboxylate carrier [121-123].

1.3.2 Metabolic inflexibility and insulin resistance in the obese and diabetic heart

Although FA is the most preferred energy substrate, the heart exhibits extreme dependence on glucose consumption amounting to 25-50 g in a 24 h period in humans [97]. In the heart, insulin plays a critical role in regulating cellular metabolism, particularly glucose transport, glycolysis, glucose oxidation, glycogen synthesis and protein synthesis. Circulating insulin binds to the insulin receptor (InsR) in the heart, which acts as a 'gate-keeper' of insulin-glucose communication between extra- and intra-cellular environments. The InR is a hetero-tetrameric structure consisting

of two extracellular α-subunits and two transmembrane β-subunits **(Figure 1.1 O)** [119]. Two β-subunits have tyrosine-kinase catalytic activity and facilitate an autophosphorylation cascade upon insulin binding on α-subunits **(Figure 1.1 P*)*** [119]. InsR activation following autophosphorylation leads to InsR-mediated phosphorylation of two indispensable molecular targets: insulin-receptor substrate-1 & -2 (IRS-1/2) and Shc [119]. IRS-1 phosphorylation by several tyrosine residues induces IRS-1 activation by recruiting SH2-domain containing proteins including Grb2, Nck, and lipid kinase PI3K to IRS-1 **(Figure 1.1 Q)** [124]. Recruitment of PI3K to the plasma membrane stimulates its catalytic phosphorylation of phosphatidylinositol (4,5)-diphosphate (PIP2) to phosphatidylinositol (3,4,5)-trisphosphate (PIP3) **(Figure 1.1 R)** [124]. Increases in the PIP3 level at the plasma membrane mediates the recruitment of Akt along with PDK1 [124]. Subsequently, PDK1 phosphorylates and activates Akt isoforms to relay insulin's signal to downstream targets, facilitating glucose metabolism **(Figure 1.1 S)**. Activated Akt phosphorylates and inhibits Rab-GTPase-activating protein, TBC1D4 (Akt substrate of 160 kDa, AS160), releasing its inhibitory control over GLUT4 translocation and increasing glucose uptake in the myocardium **(Figure 1.1 T)** [115,125,126]. Insulin regulated glycogen synthesis is dependent on glycogen synthase (GS) enzyme, which is inactivated by glycogen synthase kinase α/β (GSK3α/β) through its phosphorylation at Ser641, Ser645, Ser549 and Ser653 **(Figure 1.1 U)** [127]. Insulin activates Akt, which phosphorylates and inactivates GSK3α/β [128], renders GS active, resulting in increased glycogen synthesis. In addition to insulin's control over cardiac glycogen stores, insulin promotes cardiac glycolysis. Reduced cardiac glycolysis due to impaired insulin signalling in the mouse heart resulted in hypertrophy, fibrosis and reduced cardiomyocyte function [129]. Furthermore, insulin augments glucose oxidation by inactivating PDK1 and activating PDHP, renders PDH active for facilitating pyruvate conversion to acetyl-CoA.

In addition to insulin's effect on glucose metabolism, insulin is an anti-lipolytic hormone, inhibiting FA metabolism by reducing FA entry into the cardiomyocytes. Insulin facilitates the "selectivity and usage" of substrates within the heart by inhibiting LPL activation and promoting

glucose utilization [130]. Notably, cardiac-specific knock-out of LPL switches the cardiac substrate selection preference to glucose [131], signifying the competing traits of different substrates. In the cardiac muscle, insulin inhibits CPT-1 and subsequent FAO rates by increasing malonyl-CoA [106]. In the absence of insulin action, FAs regulate cardiac function by transcriptional regulation of peroxisome proliferator-activated receptor α (PPARα), a nuclear receptor in the heart, which increases FA uptake, mitochondrial transport and β-oxidation [132]. Overexpression of PPARα in mouse model increases FA uptake, FA oxidation and reduced glucose utilization, producing a cardiac phenotype similar to a diabetic or an insulin-resistant heart [133]. The flux of acetyl-CoA into mitochondria derived from either glucose or FA acts as the nodal point for substrate metabolism, proposed by Randle [99]. During states of nutritional abundance, glucose utilization dominates, wherein pyruvate-derived acetyl-CoA is favoured for oxidation by relieving the inhibition of PDH by PDHK. However, negative feedback from high matrix acetyl-CoA concentrations stimulates PDK and reduces PDH activity. PDHK is also activated in response to low insulin levels observed during starvation and during elevation in systemic and intramyocellular FA levels. Activation of PDHK inactivates PDH and inhibits glucose oxidation [134], signifying the impact of insulin on substrate competition within the heart and the resultant remodeling of cardiac metabolism following the loss of insulin or its action.

Since insulin is the central regulator of the systemic and intracellular flux of glucose and FAs, disruptions in insulin signaling result in abnormal substrate utilization, compromising cardiac ability to partition nutrients for metabolism. Insulin helps cardiomyocyte maintain “metabolic flexibility”, which is the heart's ability to switch back and forth between glucose and FA to generate energy based on the demand and availability for contractile function [135]. However, during obesity and diabetes, lack of insulin or insulin action triggers “metabolic inflexibility,” which is the inability of cardiomyocytes to use glucose, leading to an exclusive dependence on FAs for energetic needs. Preclinical and clinical data have confirmed that metabolic health deteriorates as mitochondria lose their capacity to switch freely between alternative forms of carbon energy [136].

A chronic manifestation of this metabolic inflexibility is observed in the obese and diabetic heart independent of vascular complications, including an imbalance in Ca^{2+} homeostasis, defects in contractility and an increase in fibrosis. Metabolic inflexibility in the obese and diabetic heart results in the underutilization of glucose and accumulation of FA metabolites, leading to glucotoxicity and lipotoxicity, together with being referred to as "glucolipotoxicity." Metabolic remodeling following "glucolipotoxicity" is manifested at the biochemical, structural, and functional level in the cardiomyocyte hypothesized to be causative for inducing metabolic cardiomyopathy during obesity diabetes.

1.3.2.1 Glucolipotoxic stress

During obesity and diabetes, lack of insulin or insulin function impairs GLUT4 translocation, leading to inadequate cardiac glucose transport and glucose oxidation, resulting in hyperglycemia **(Figure 1.2 A)**. GLUT4 protein expression is reduced in the obese and diabetic heart, resulting in impaired glucose uptake and utilization, causing hyperglycemia [137,138]. Germline deletion of GLUT4 (GLUT4-null) causes cardiac hypertrophy in 2 to 4 months old mice. Furthermore, GLUT4-null mouse hearts demonstrate increases in glucose uptake, resulting from enhanced insulin-independent GLUT1 expression [139,140]. Hyperglycemia precipitates "glucotoxicity" in the diabetic heart by generating reactive oxygen species (ROS). Excess ROS also activates poly (ADP ribose) polymerase (PARP), which subsequently diverts glucose from the glycolytic pathway into nonoxidative glucose pathways (NOGPs). These NOGPs include advanced glycation end product (AGE) formation, hexosamine biosynthetic pathway (HBP), polyol pathway and protein kinase C (PKC) activation, causing glucotoxic signalling cascade in the obese and diabetic heart **(Figure 1.2 B)** [97,141-143].

To maintain function in the diabetic heart, adaptive molecular events facilitate uninterrupted FA supply and oxidation. Enhanced lipolysis in adipose tissue and higher very-low-density lipoprotein secretion from the liver dramatically increases systemic FA and lipoprotein TAG. This increase in systemic FA and TAG enhances the uptake of FA by cardiomyocytes

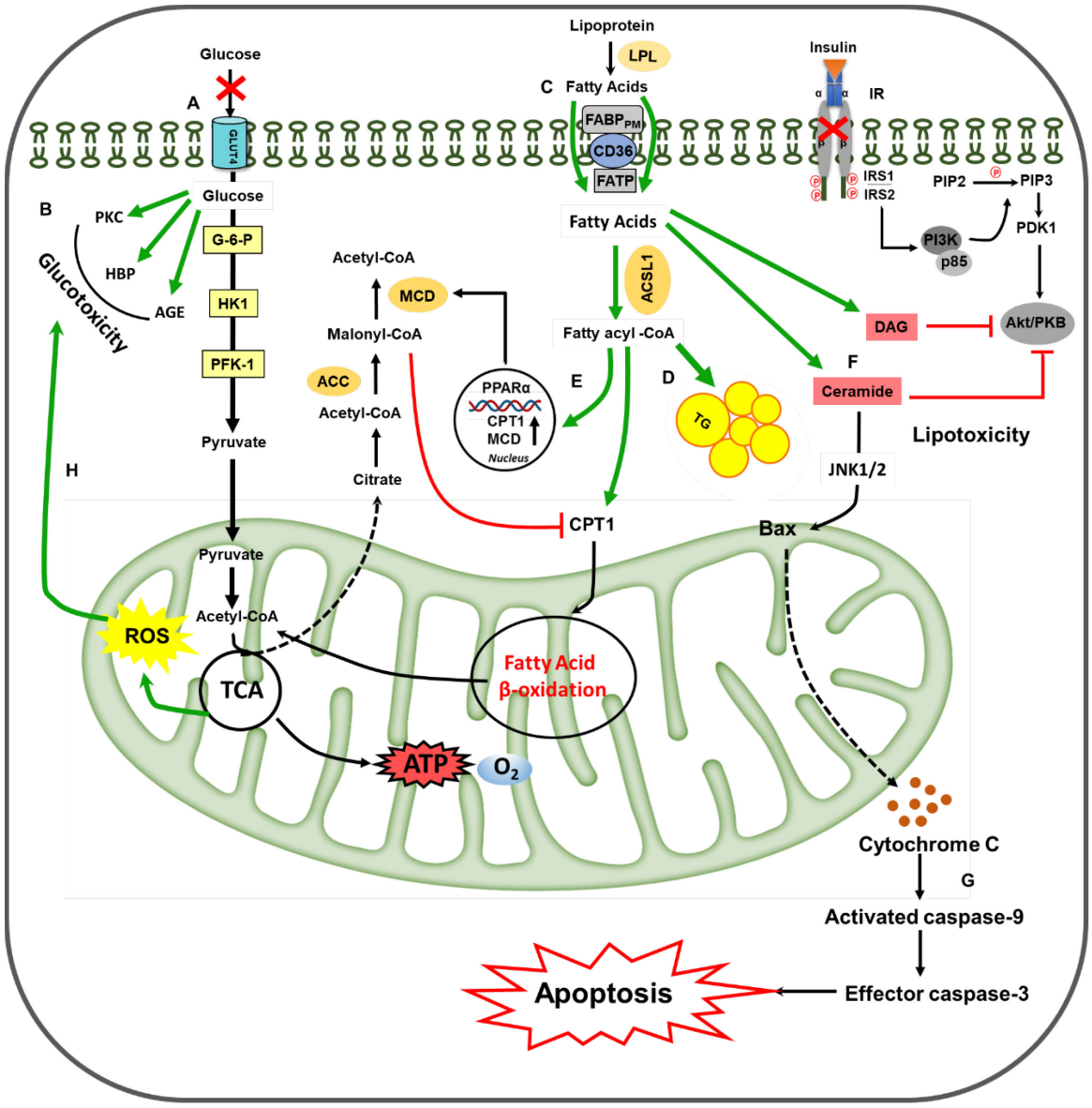

Figure 1.2 Altered cardiac energy metabolism and utilization in the obese and diabetic heart. During cardiac insulin resistance, impaired insulin signaling disrupts glucose utilization redirecting glucose intermediates into the HBP, AGEs and PKC, concomitantly increasing ROS production **(A-B, H).** Decreased reliance on glucose is compensated by enhanced cardiac dependence on FAO via the Randle cycle. Intracellular FA is processed by ACSL1, generating intermediate fatty acyl-CoA that is further processed for mitochondrial β-oxidation pathway via CPT1 to generate ATP through the TCA cycle. A part of the fatty acyl-CoA is stored as TAG **(D),** and the rest forms lipotoxic intermediates such as DAGs and ceramides **(F).** Following diabetes or diet-induced obesity, increased FA load within the cardiomyocyte activates PPARα, which exacerbates maladaptive use of FA by increasing expression of CPT1 **(E).** FA also augment the expression of malonyl CoA decarboxylase (MCD), depleting malonyl-CoA and releasing its inhibition on FAO. Additionally, Akt functions as the facilitator of glucose metabolism and myocyte survival is inhibited by the lipotoxic DAGs and ceramides **(F)**. Thus, when cardiac insulin signaling is

dysfunctional, glucose oxidation is attenuated and FAO is augmented, leading to metabolic inflexibility within the cardiomyocyte and the ensuing accumulation of lipotoxic intermediates ceramide and DAG. Ceramide activates JNK1/2, which interacts with Bax on the mitochondrial membrane and initiates apoptosis signaling **(G).** Solid black arrow: indicates the reaction is proceeding forward in a single-step; Solid green arrow: indicates the response is pathologically increased; Solid red line: indicates the reaction is inhibited. Solid red X: indicates the reaction is impaired.

(Figure 1.2 C), increasing the activity of TAG synthesizing enzymes and TAG accumulation, which is associated with lipotoxicity **(Figure 1.2 D)** [144]. Elevated intracellular FAs activate PPARα **(Figure 1.2 E)**, which increases the transcription of genes involved in FA oxidation (FAO) and concomitantly compromising glucose utilization during diabetes [145]. Indeed, cardiomyocyte-specific PPARα overexpressing mice display mitochondrial ultrastructural abnormalities, lipotoxicity and cardiac steatosis, causing systolic dysfunction and cardiomyopathy [133,146]. Accumulation of FA also enlarges the pool of intracellular FA metabolites, such as fatty-acyl-CoA, ceramides, DAGs **(Figure 1.2 F)**, long-chain acyl CoAs and/or acylcarnitines that are collectively referred to as "lipotoxic" intermediates [147]. Furthermore, uncontrolled FAO disrupts the mitochondrial inner membrane, releases cytochrome c, leading to overproduction of ROS and mitochondrial dysfunction [148].

The amount of FA and the type of FA influence cardiac metabolism during health and disease [149]. *In-vivo*, saturated (palmitate and stearate) and unsaturated (oleate and elaidate) FAs are preferred substrates for oxidation to generate ATP due to their carbon chain length [149]. Prior studies on neonatal rat cardiomyocytes have reported that saturated FA but not unsaturated FA are lipotoxic to cells [149]. Excess supply of saturated FA, palmitate activates pro-inflammatory signaling and provides substrates for synthesizing lipotoxic species such as DAG and ceramides. Additionally, palmitate directly or indirectly interferes with insulin signaling via various mechanisms, including increased serine/threonine phosphorylation and decreased tyrosine phosphorylation of IRS-1, impaired Akt phosphorylation and GLUT4 translocation to the sarcolemma [97,150]. Saturated FAs also induce endoplasmic reticulum (ER) stress in pancreatic β-cells, cardiomyocytes, hepatocytes and macrophages [151-153]. On the other hand, monounsaturated FA (MUFA) oleate is protective against saturated FA-induced lipotoxicity. MUFA intake, which is highly enriched in olive oil, is associated with reduced cardiovascular complications and improved insulin sensitivity [154-156]. This protective effect of oleate against lipotoxicity is likely due to channeling palmitate into the intracellular pool of TAG, suggesting that

different FA exhibit different effects on cellular signaling and function. Palmitate-induced apoptosis in cardiomyocytes and pancreatic β-cells is ameliorated when palmitate is co-supplemented with oleate [149,157]. Additionally, polyunsaturated FAs (PUFAs), specifically, essential long-chain omega-3 PUFAs such as eicosapentaenoic acid (EPA) and docosahexaenoic acid (DHA), are anti-inflammatory and improve insulin sensitivity in animal studies [158,159]. However, studies on omega-3 PUFAs in humans suggest no beneficial effects on cardiovascular outcomes or glucose homeostasis [158,160]. Taken together, these studies indicate that lipid-derived and glucose-derived toxic intermediates precipitate cardiac maladaptation by triggering organelle stress such as mitochondrial dysfunction, ER stress, myocardial Ca^{2+} mishandling and myocardial oxidative stress.

1.4 Glucotoxic and lipotoxic complications in the cardiomyocyte

1.4.1 Impaired Ca^{2+} handling

Cytosolic Ca^{2+} levels are essential in regulating cellular metabolism, muscle contraction and cell signaling. Typically, during excitation-contraction (EC) coupling, the systolic and diastolic function of the heart is coordinated by intracellular Ca^{2+} homeostasis, which involves numerous ion channels, transporters and Ca^{2+} handling proteins [161,162]. The heart's contractile function is regulated by EC coupling, leading to rapid changes in intracellular Ca^{2+} levels. During systole, action potential depolarizes the sarcolemma and enables Ca^{2+} entry into the cytosol through voltage-gated L-type Ca^{2+} channels (LTCC) **(Figure 1.3 A)**. This results in a ~ 10-fold increase in cytosolic Ca^{2+} concentration from the sarcoplasmic reticulum (SR) via ryanodine receptor (RyR2) channels **(Figure 1.3 B)** [163]. Consequently, Ca^{2+}-sensitive myofilament proteins are activated wherein Ca^{2+} binds to troponin C to activate myofilament proteins, resulting in cardiomyocyte contraction. Following cardiomyocyte contraction, myocyte relaxation occurs by exporting 30% of Ca^{2+} out of the sarcolemma primarily by Na^{+}-Ca^{2+} exchanger (NCX) channels **(Figure 1.3 C)**, while 70% of Ca^{2+} is pumped back into the SR via the SR Ca^{2+} ATPase pump 2a (SERCA2a) **(Figure 1.3 D)** [164]. The activity of SERCA2a is negatively regulated by phospholamban (PLN) [165],

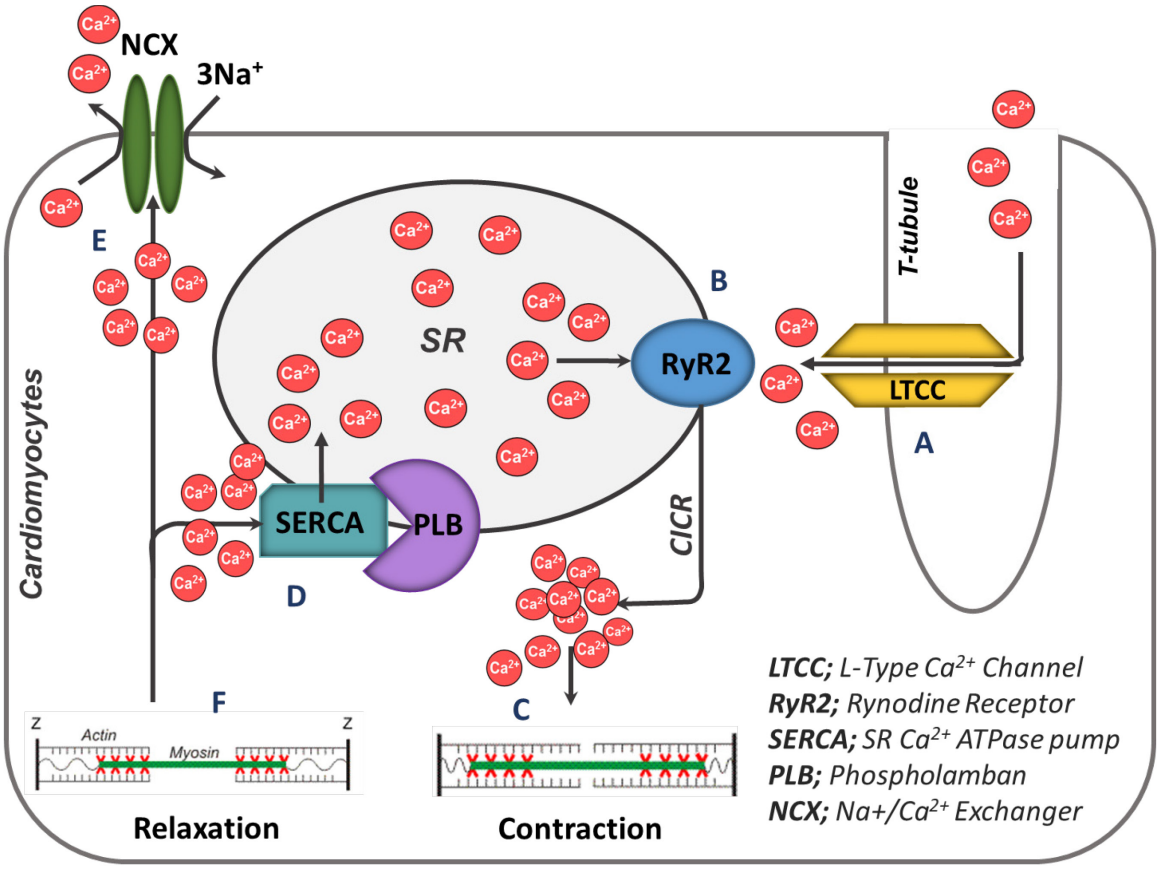

Figure 1.3 Excitation-contraction coupling in the cardiomyocyte. During systole, an action potential causes depolarization, allowing the entry of Ca^{2+} into the cytosol through LTCC (A). This results in massive Ca^{2+} release from the sarcoplasmic reticulum (SR) through RyR2 activation (B). The net result is increased cytosolic Ca^{2+} levels culminating in myocyte contraction (C). During diastole, rapid removal of Ca^{2+} from the cytosol to SR is facilitated by SERCA2a (D), and a small amount of Ca^{2+} also exits through NCX (E). Decreased cytosolic Ca^{2+} leads to cardiomyocyte relaxation (F).

which is phosphorylated and inhibited by protein kinase A (PKA) [166]. Defects in EC coupling due to abnormal expression and/or function of Ca^{2+}-handling proteins such as SERCA2a, PLB, RyR2 and NCX are a hallmark of cardiac dysfunction [161,167-169]. Although initial modifications of Ca^{2+} cycling can be beneficial, a sustained increase in LV pressure leads to compromised Ca^{2+} cycling, eventually progresses to HF pathology [170]. Compromised cardiomyocyte Ca^{2+} handling plays a vital role in causing diastolic cardiac dysfunction and is observed in several animal models of T1DM and T2DM [167,171-174]. For instance, streptozotocin (STZ)-induced T1DM mice and rats exhibit reduced Ca^{2+} transient amplitude, prolonged cytosolic Ca^{2+} clearance and a decline in SR Ca^{2+} load [172,175]. In *db/db* insulin-resistant mice with T2DM, lower systolic and diastolic Ca^{2+} levels are associated with a reduced decay rate of Ca^{2+} transient and increased Ca^{2+} leakage from the SR [171]. The molecular changes associated with abnormal Ca^{2+} handling in the obese and diabetic heart include lower SERCA2a and NCX activity, decreased SERCA2a protein levels, impaired RyR2 function and reduced PLN phosphorylation. Importantly, abnormal systolic and diastolic function normalizes after overexpression of SERCA2a in STZ-induced diabetic mouse heart [173]. These Ca^{2+} handling abnormalities are responsible for defective EC coupling associated with metabolic heart disease, which causes impairment in LV function [176].

1.4.2 Mitochondrial dysfunction and oxidative stress

In addition to altered energy metabolism, increased FAO and metabolism during diabetes are linked to oxidative stress and mitochondrial dysfunction. It is estimated that ~90% of ROS are generated within mitochondria of tissues with high respiration rates, such as cardiomyocytes [177]. Under high-fat or high-glucose conditions, there is an increase in electron transfer donors such as NADH and FADH2, which enhance the electron flux into the mitochondria through the electron transport chain (ETC) [178]. As a result, the mitochondrial membrane potential rises above a threshold value, leading to ROS overproduction, a process that can be blunted by detoxifying enzymes and uncoupling proteins [179]. In healthy myocardium, ROS production is tightly regulated at a low steady-state level by the concerted action of mitochondrial enzymes such as

superoxide dismutase, reduced glutathione and catalase [180]. An impairment in this antioxidant defense mechanism triggers ROS accumulation, which modifies and damages proteins, lipids and DNA. Excess ROS production inactivate ETC complexes and mitochondrial proteins, compromising oxidative phosphorylation and inducing mitochondrial dysfunction [141,181]. High ROS levels also activates NOGPs, which diverts glucose from glycolytic pathway into AGE formation, HBP, activation of HB, polyol and PKC pathways. Activation of these NOGPs cause glucotoxic signalling cascade in obese-diabetic heart; all of which could be ameliorated by normalizing levels of mitochondrial ROS [97,141-143].

1.4.3 Endoplasmic reticulum (ER) stress

Given the physical and functional interaction between mitochondria and the ER, numerous studies have also examined the contribution of ER dysfunction in cardiovascular complications during diabetes [182]. Since ER is the origin for the biosynthesis of luminal and transmembrane proteins, loss of ER function leads to an accumulation of misfolded or toxic proteins, a condition referred to as ER stress [183]. ER acutely activates unfolded protein response (UPR) to clear toxic protein accumulation [184,185]. In addition to mitochondrial dysfunction and cellular death, prior studies have reported that palmitate-induced lipotoxicity causes alteration in endoplasmic reticulum (ER) membrane phospholipids resulting in ER swelling, compromising ER membrane structure and integrity [186]. Dietary, pharmacological, and genetic rodent models of diabetes and patients with diabetes exhibit upregulation of UPR pathways in the heart [187]. Impairment in the ER stress response pathway yields terminally misfolded proteins, which then bind to distinct chaperones. Depending on the localization of misfolded proteins, they are retrogradely transported out of the ER and subjected to proteasomal degradation [184]. Failure of the proteasome during mild to moderate metabolic stress activates compensatory upregulation of lysosomal autophagy pathway to achieve maximal protein degradation to maintain cellular homeostasis [184]. Therefore, it is plausible that the disruption of lysosomal autophagy culminates in the accumulation of toxic protein aggregates, causing “proteotoxicity” and perturbing cellular homeostasis. A notable example of

proteotoxicity in obese and diabetic individuals is the accumulation of circulating amylin protein, leading to amylin deposition in the heart. Accumulation of amylin oligomers leads to proteotoxic stress and apoptosis in multiple organs, including remodeling of cardiomyocyte structure and function, causing cardiomyopathy [188]. Therefore, the pathogenesis of cardiomyopathy observed during obesity and diabetes is likely an outcome of glucolipotoxicity induced proteotoxicity triggered by mitochondrial dysfunction, ROS overload, ER stress. It is also plausible that changes in lysosome function impact mitochondrial, ER and nuclear function of the cardiomyocyte in obesity, insulin resistance and diabetes. However, limited studies have examined the molecular mechanisms by which glucolipotoxicity impacts inter-and intra-lysosomal signaling events.

1.4.4 Cardiomyocyte cell death

The heart maintains a critical balance between cell proliferation and cell death throughout its lifetime. A subtle increase in the rate of cardiomyocyte apoptotic cell death leads to detrimental consequences in the heart. Glucotoxic and lipotoxic stress induce cardiomyocyte apoptotic cell death in the obese and diabetic heart. Importantly, apoptotic cell death has profound cardiac consequences such as loss of myocytes that decrease the number of contractile units and remodels healthy cells, likely deteriorating cardiac function. A sequence of biochemical events during apoptosis includes activation of protein cleavage and cross-linking DNA breakdown, and phagocytic recognition. These events are followed by the activation of caspase, an intracellular apoptosis-associated protease expressed in an inactive proenzyme form in most cells. Once activated, it initiates protease cascade by activating pro-caspases mediated by two independent pathways, the “extrinsic” pathway, the death receptor-mediated pathway and the “intrinsic” pathway, the mitochondrion-mediated pathway [189]. Briefly, the extrinsic pathway involves the binding of apoptotic ligands to membrane-bound death receptors on the target myocytes. These receptors include the first apoptosis signal (Fas), tumor necrosis factor (TNF) receptor and TNF-related apoptosis-inducing ligand receptors (TNFR1). The next step involves the recruitment of Fas-associated death domain (FADD) of the adapter protein to the membrane along with pro-

caspase-8, which then triggers apoptosis by activating pro-caspase-3 protease to cleave target proteins. On the other hand, the intrinsic mitochondrial-mediated pathway involves a diverse array of non-receptor-mediated stimuli, such as DNA damage and heat shock [190]. The mitochondrial initiated events include the opening of mitochondrial permeability transition pore, loss of mitochondrial transmembrane potential and release of pro-apoptotic proteins from intermembrane space into the cytosol. The cascade is initiated by releasing cytochrome-c from the mitochondria by activating caspase-9 and caspase-3 to execute the apoptotic program **(Figure 1.2 G)** [148]. Importantly, the cell death pathway is regulated by Bcl2 family proteins (regulates cytochrome-c release), an inhibitor of apoptosis proteins (IAPs, inhibits caspase), and a second mitochondrial activator of caspases (Smac) [191].

During obesity and diabetes, chronic excessive caloric intake overwhelms adipocytes' ability to store TAG, leading to the uptake of systemic lipids by non-adipose tissues, including the heart [157,192,193]. The heart has a limited capacity to accommodate excess TAG, and hence, the TAG content of the heart is relatively low [157,192,193]. Prior studies demonstrate that lipid accumulation in the cardiomyocyte causes apoptosis and cardiac dysfunction. It is worth noting that TAG themselves are non-toxic or harmless; however, they become harmful once they hydrolyzed to fatty-acyl-CoA, which subsequently increases the synthesis of the pro-apoptotic sphingolipid ceramide [194-196]. Intracellular ceramide is synthesized through several pathways. De novo synthesis of ceramide occurs initially from palmitate and serine via the action of serine palmitoyltransferase (SPT) [197,198]. Ceramide is also synthesized from sphingomyelin that is hydrolyzed by sphingomyelinase [197]. Also, the salvage pathway from sphingosine-1-phosphate and the sphingomyelin pathway generate ceramide [197,199]. Ceramide accumulation upregulates protein phosphatase 2A, which dephosphorylates Akt at Ser473 and Thr308, inhibiting Akt, reducing GLUT4 mRNA expression and impairing glucose metabolism [195,196,200]. Increased intracellular ceramide levels also activate JNK1/2, which interacts with pro-apoptotic protein Bax on the mitochondrial membrane, resulting in the release of cytochrome-c and triggering myocyte

apoptosis [201]. Pharmacologic or genetic inhibition of ceramide synthesis or decreasing ceramide levels using SPT-I inhibitor, myriocin, improves cardiac structure, function and metabolism by increasing cardiac glucose utilization and protects against cardiac dysfunction [195]. Increased availability of glucose increases oxidative stress and decreases the production of antioxidants in the cardiomyocyte. Higher oxidative stress in the cardiomyocyte activates NOGPs such as the polyol pathway, HBP pathway, AGEs and PKC, which can further exacerbate ROS production **(Figure 1.2 H),** which eventually induces apoptosis and cell death [202].

1.5 Proteostasis: Balance between protein synthesis and protein degradation

Proteostasis plays an important role in maintaining cellular health. Intracellular and extracellular proteins are continuously turning over and hydrolyzed into their essential component amino acids to be replaced by newly synthesized proteins. Approximately 80-90% of cellular proteins, including short-lived, misfolded, native or damaged, are degraded by the ubiquitin-proteasome pathway (UPP) [203]. On the other hand, short- and long-lived proteins that reside on organelle membrane or protein aggregates or damaged organelles are subjected to degradation within the lysosome via autophagy [166]. An imbalance between protein synthesis and degradation triggers aggregation of misfolded proteins, cell death and organ dysfunction. Every cell has developed protein quality control machinery and complex mechanisms to overcome cellular proteotoxic stress. These mechanisms include, 1) activation of chaperones, which maintain and conserve protein's tertiary and quaternary structure and conformation, 2) activation of ER-associated degradation pathway to assist protein refolding, 3) activation of UPP to degrade misfolded proteins through proteasome and recycling amino acids and 4) degradation of misfolded protein through autophagy-lysosome pathway [166] **(Figure 1.4)**.

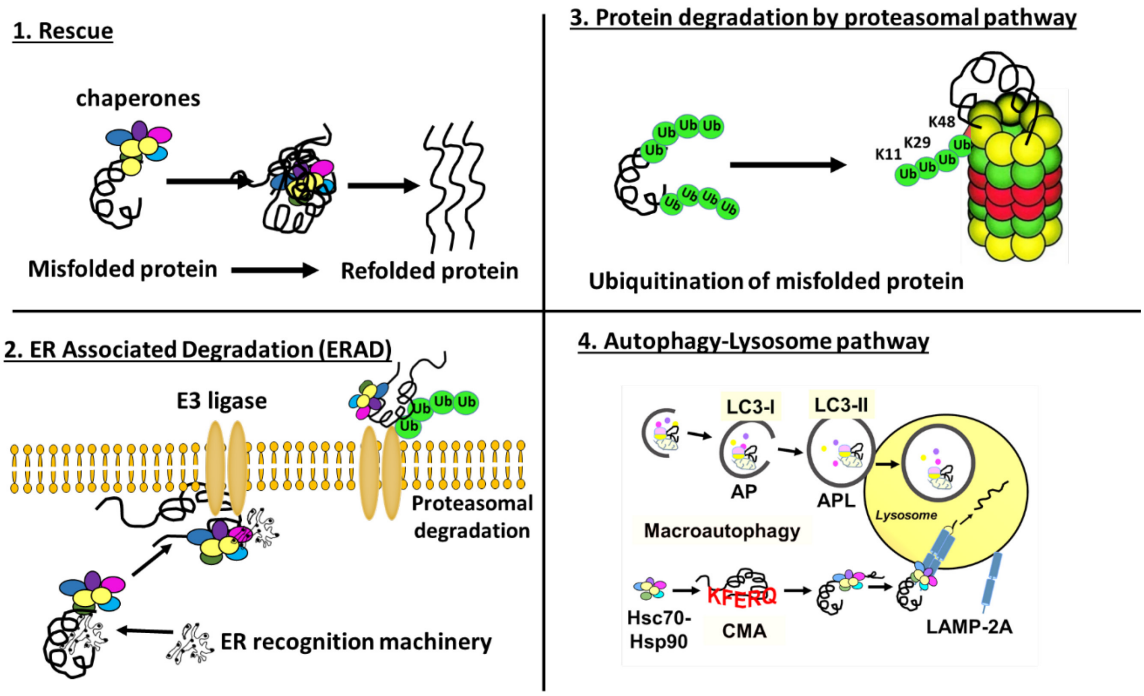

Figure 1.4 Cellular adaptation to maintain proteostasis in response to cellular stress. Perturbation in protein synthesis and degradation triggers the accumulation of misfolded proteins. This activates the cell's protein quality control machinery to overcome proteotoxic stress leading to the activation of 1) chaperones to refold proteins into their tertiary and quaternary structure, 2) ER-associated degradation pathway to assist protein folding, 3) UPP to degrade misfolded proteins, and 4) autophagy-lysosome pathway to sequester organelle and protein aggregates.

1.5.1 Ubiquitin proteasome pathway (UPP)

Proteins targeted for proteasomal degradation are conjugated to ubiquitin (Ub) by an ATP-dependent process, which involves the concerted action of three enzymes to tag proteins with polypeptide co-factor, Ub [204,205]. These Ub conjugated proteins are then recognized by the 26S proteasome, a large multi-catalytic proteasome complex that degrades ubiquitinated proteins to short peptides [206]. The first step in this cascade requires the activation of Ub at its C-terminus by the Ub-activating enzyme E1 that uses ATP to generate a highly reactive Ub thiolester [207]. Once activated, Ub bound to E1 via the thiolester linkage is transferred to a sulfhydryl group of Ub-carrier or conjugating proteins, E2s, which prepare Ub for conjugation [206]. The activated Ub is then transferred onto proteins via E3 Ub-protein ligase, critical for functional UPP. Generally, E3s are structurally homologous to either HECT (homologous to E6-AP carboxy-terminus) or RING finger domain [208].

Prior studies have demonstrated that glucolipotoxic milieu in the cardiomyocyte impairs protein quality control, induces ER stress, and activates the protein degradation pathway [209]. To counter the damaging effects of glucolipotoxicity, UPP-mediated degradation is acutely activated to clear the cellular proteotoxic load [210]. Indeed, Ub mRNA levels, caspase-3 and ATP-dependent proteasomal degradation are augmented acutely following T1DM, induced after a single dose of STZ injection (150 mg/kg body) [210]. However, sustained glucolipotoxicity exacerbates ER stress, saturating and impairing proteasomal protein degradation, causing toxic accumulation of misfolded proteins [180]. In agreement with this theory, failing hearts from chronically obese humans with type-2 diabetes display a significant accumulation of non-degraded proteins [188], suggesting that impaired proteasomal degradation in late stages of obesity and diabetes induces a maladaptive buildup of cytotoxic proteins, causing and/or exacerbating cardiomyopathy. Recent experimental evidence suggests that if the proteasome is impaired, then damaged proteins must be degraded by the lysosomal machinery via autophagy to maintain cellular homeostasis [211,212]. Interestingly,

increase in ER stress and cell death are observed in insulin-producing islet cells when *ob/ob* mice with impaired proteasomes are treated with lysosomal inhibitors [213].

1.5.2 Proteolysis by lysosomal autophagy

1.5.2.1 Macroautophagy

Lysosomal autophagy degrades short- and long-lived proteins either via macroautophagy, a non-selective degradation or via chaperone-mediated autophagy (CMA), a selective ATP-dependent degradation process occurring exclusively in the lysosome **(Figure 1.5)** [214]. Macroautophagy is initiated through an ER-derived double membrane-bound organelle, known as an autophagosome, which allows the bulk delivery of soluble and insoluble protein load, mid-body rings and organelles to lysosomes for degradation proteolysis. Autophagy-related (Atg) proteins organize and control various steps of macroautophagy [215,216]. The initiation of macroautophagy occurs via the de novo synthesis of an ER-derived isolation membrane known as the omegasome, resulting in a cup-shaped structure, termed preautophagosome [217]. This first step in the induction of autophagy is initiated by a protein complex consisting of unc-51 like kinase 1 (ULK1), FAK family kinase-interacting protein of 200kDa (FIP200) and Atg13 **(Figure 1.5 A)** [217]. During nutrient abundance, serine/threonine kinase mTOR (mammalian target of rapamycin) phosphorylates and inactivates ULK1/2 to inhibit autophagy, whereas following nutritional deprivation, inactivation of mTOR relieves inhibition on ULK1, leading to the induction of autophagy [217]. The class-III PI3K complex consisting of Beclin1, Atg14L, and vacuole protein sorting (Vps) 34-vps15 positively regulates PI3P-binding protein **(Figure 1.5 B)** and double FYVE domain-containing protein 1 (DFCP1) localized on the omegasome [217]. Subsequently, the isolation membrane elongates to engulf cytoplasmic cargoes by recruiting two parallel ubiquitin-like conjugation systems essential for autophagosome formation [218]. In mammals, Atg12-Atg5 conjugate interacts with Atg16L1 to form a multimeric complex of Atg12-Atg5-Atg16L1 **(Figure 1.5 C),** which localizes to the outer membrane of the preautophagosomal structure [214]. The second ubiquitin-like conjugation system is Atg8-LC3, which targets phospholipid,

phosphatidylethanolamine (PE), called Atg8/LC3 "lipidation" [214] **(Figure 1.5 D)**. LC3 is synthesized as proLC3, which is cleaved by cysteine protease Atg4B to form LC3I, primarily localized to the cytosolic (outer) side of the autophagosome. LC3I is then activated by Atg7 (an E1 like enzyme) and transferred to Atg3 (an E2 like enzyme) **(Figure 1.5 E)** and conjugates to PE to form LC3-PE conjugation, also referred to as LC3II. LC3II is localized to both the outer and the inner membrane of autophagosomes [214]. LC3II on the cytosolic side of autophagosome is de-lipidated by Atg4B to form LC3I, which is recycled for autophagosomal formation. Therefore, Atg4B acts as a de-conjugating enzyme controlling free LC3 content. Autophagosomal membrane localized LC3II is essential for the maturation of autophagosome and, therefore, is used as a measure of autophagosomal content. Additionally, adaptor proteins such as ubiquitin-binding protein p62 (also known as sequestosome 1) **(Figure 1.5 F)** and NBR1 (Neighbor of BRCA1 gene) are recruited to the developing autophagosomal membrane through an LC3-interaction binding domain, enabling partial selectivity of the autophagic process [219]. Upon completion and closure, the mature autophagosome eventually fuses with a lysosome to form an autolysosome. Autolysosomal formation is required for the degradation of protein cargo since autophagosomes lack proteases for degrading engulfed content. Following autolysosome formation, the lysosomal hydrolases degrade LC3-II and the intra-autophagosomal content [220,221]. This dynamic kinetics of autophagosome production and clearance by lysosomes is known as autophagic flux [222,223]. Unexpectedly, different models of diabetes exhibit dissimilar regulation of LC3-II content, which is influenced by the rate of fusion between autophagosome and lysosome. Notably, calmodulin overexpressing OVE26 type-1 diabetic mouse heart decreases LC3-II content, signifying reduced autophagosome formation and inhibition of macroautophagy [224]. However, macroautophagy is elevated with increases in LC3-II in hearts from fructose-fed insulin-resistant rats [225], Akita type-1 diabetic mice and STZ-treated mice. These dissimilarities in the regulation of LC3-II content are likely due to an outcome of altered autophagic flux, which is governed by the rate of fusion between autophagosomes and lysosomes. Indeed, our laboratory and others demonstrate that nutrient

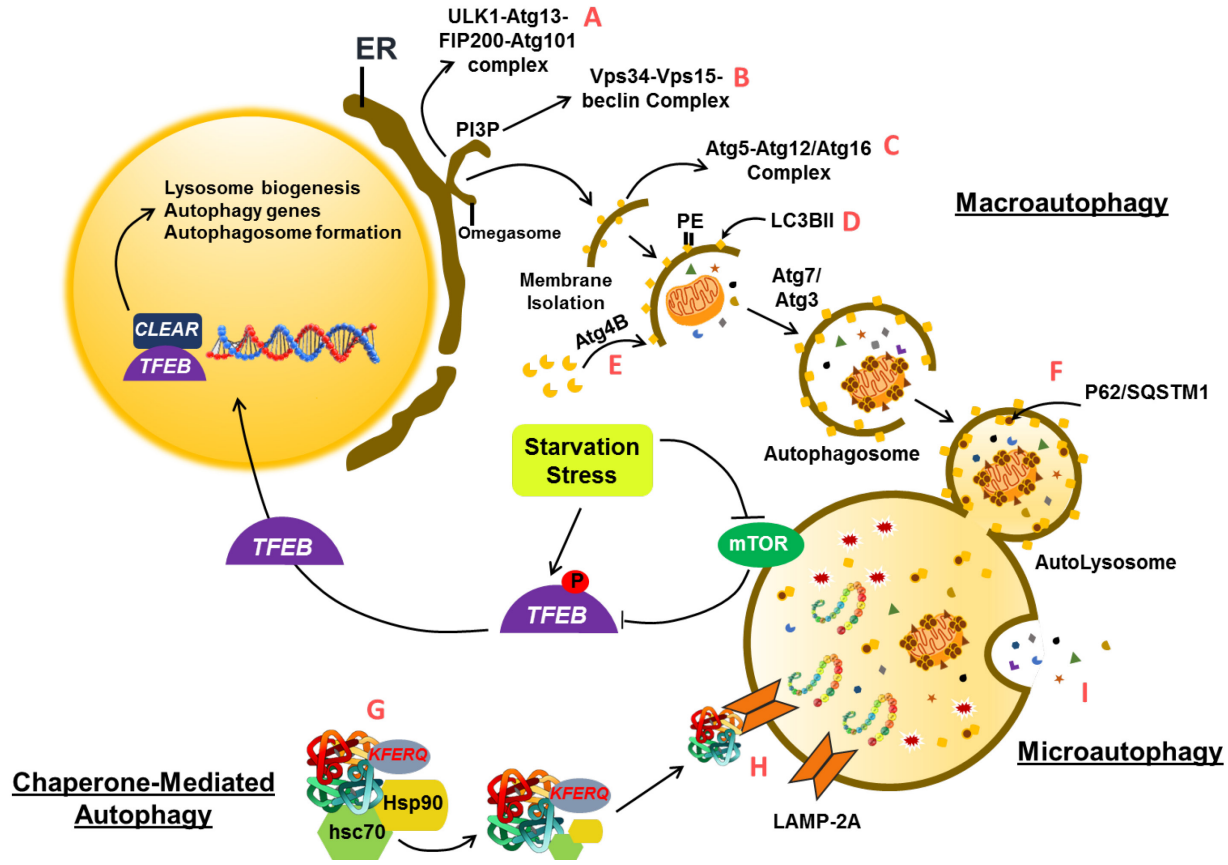

Figure 1.5 Proteolysis by lysosomal autophagy. Macroautophagy initiation from the ER occurs by de novo synthesis of a preautophagosome with ULK1-Atg13-Fip200-Atg101 protein complex (A), which is further propagated forward by the formation of Beclin1-Vps34-Vps15 protein complex (B). Recruitment and PE lipidation of LC3B on the developing autophagosomal membrane promotes autophagosomal maturation, elongation and closure (D). Cargo receptor P62 mediates autophagosomal targeting of proteotoxic and organelle load (F). Autophagosomes fuse with a lysosome to form an autolysosome, where lysosomal hydrolases induce proteolysis. CMA targets intracellular KFERQ-proteins utilizing the Hsc70-Hsp90 chaperone complex (G). Targeted protein cargo is transported to the lysosomal lumen through LAMP2A for its degradation within the lysosomal lumen (H). Microautophagy involves the sequestration of proteins by lysosomal membrane invagination (I).

overload in the heart of mice subjected to diet-induced obesity or in H9C2 cells or neonatal/adult rat cardiomyocytes significantly suppresses autophagic flux [226].

Lysosomal autophagy also plays an important role in breaking down lipid droplets (LDs) via a process referred to as "lipophagy" [227]. Lipophagy was first described in hepatocytes and is indispensable for TAG breakdown as $Atg7^{-/-}$ mice display dysfunctional autophagy, resulting in reduced β-oxidation, higher lipid accumulation and hepatic steatosis [40,227]. Additionally, macrophages isolated from $Atg5^{-/-}$ mice exhibit impairment in LD delivery to the lysosome for lysosomal acid lipase-mediated hydrolysis, suggesting that autophagy is crucial for the lipid catabolic process [228]. In addition to lipophagy, mitophagy ensures mitochondrial quality control by degrading dysfunctional mitochondria and maintaining functionally-active mitochondria [229,230]. Dysfunctional mitochondria that cannot handle ROS overload are targeted for mitophagy by a PTEN-induced putative kinase 1 (PINK1)- and Parkin-mediated mechanism [231]. Like mitochondria, damaged lysosomes are also subjected to repair or clearance, albeit with assistance from ESCRT (endosomal sorting complex required for transport) machinery-dependent sorting complex. The process of degrading damaged lysosomes via selective macroautophagy is termed as "lysophagy" [232,233].

1.5.2.2 Chaperone-mediated autophagy (CMA)

Physiological activation of autophagy is initiated ~ 30 min into starvation and does not last more than 8–10 hr. However, CMA begins after 10 h of starvation, and unlike macroautophagy, CMA promotes individual and selective degradation of proteins [234]. CMA targets intracellular proteins harboring a consensus KFERQ sequence (Lys-Phe-Glu-Asp-Glm) in their amino acid sequence, that are being targeted for lysosomal degradation [235]. KFERQ proteins are recognized and targeted by the concerted action of a chaperone complex consisting of heat shock cognate 70 (Hsc70), heat shock protein 90 (HSP90), HSP40, HIP, HOP, and Bag-1 [236] **(Figure 1.5 G)**. Transportation of the chaperone complex along intracellular scaffolds is an ATP-intensive process and upon arrival at the lysosome, the protein cargo is translocated to the lysosomal lumen via the

indispensable lysosome-associated membrane protein 2A (LAMP2A) [235,237] **(Figure 1.5 H)**. LAMP2A is the only receptor capable of binding and translocating, a characteristic absent in other LAMP isoforms [238]. Following the binding of the targeted proteins-chaperone complex to monomeric LAMP2A, LAMP2A is multimerized to a high molecular weight complex, a prerequisite for the substrate translocation to luminal side of the lysosome [238]. Once inside the lysosomal lumen, protein cargo is unfolded and rapidly degraded by a mixture of lysosomal luminal hydrolases [236]. Importantly, levels of LAMP2A at the lysosomal membrane are tightly regulated and directly correlate with CMA activity [239]. Furthermore, LAMP2A levels are regulated by alterations in its half-life, which rely on the redistribution of LAMP2A between the lysosomal membrane and the matrix [238].

Disruptions in lysosomal CMA are commonly observed in chronic pathologies such as aging, neurodegeneration, cancer and obesity [240-242]. Loss-of-function of cytosolic chaperones, Hsc70 and Hsp90 and lysosomal CMA receptor, LAMP2A perturb lysosomal homeostasis [243,244]. Notably, the heart from patients with Danon's disease carries a mutation in the gene that encodes for LAMP2, resulting in toxic accumulation of autophagic vacuoles and cardiomyopathy [240,245]. We previously reported the downregulation of lysosomal proteins (Hsc70, Hsp90, LAMP2A) in type-1 diabetes and diet-induced obesity and in cardiac cells subjected to glucolipotoxicity *ex-vivo* [226]. Short term exposure of macrophages [246] and more prolonged exposure of hepatocytes [241,242] to glucolipotoxic milieu impaired LAMP activity and lysosomal autophagy. During an ischemic injury, LAMP2A expression diminishes and sensitizes the myocardium to protein aggregation and ROS-induced cell death [247]. These findings suggest that LAMP2A expression and activity are crucial in regulating lysosomal autophagy. Since macroautophagy and CMA eventually culminate in the lysosome, lysosome content and lysosome function are critical in maintaining cellular proteostasis.

1.6 Structural and functional organization of the lysosome

Seminal studies by Duve Laboratory uncovered the lysosome as the cellular compartment for the degradation of biological macromolecules [248]. Endocytic [249], autophagic [250] and phagocytic [251] pathways facilitate macromolecule degradation within the lysosome. Acid hydrolases and lysosomal membrane proteins (LMPs) dictate lysosomal function [252]. The acidity of the lysosome stabilizes and mediates the activity of ~60 luminal hydrolytic enzymes. The lysosomal limiting membrane harbors ~25 LMPs, including transporters, tracking/fusion machinery, ion channels and structural proteins [253], which exert an indispensable role in regulating lysosomal pH and function [253].

Lysosomal ions and ion channel: Lysosomal ionic gradient is crucial for lysosome biogenesis, lysosome motility and membrane contact site formation with ER and mitochondria. The lysosomal lumen comprises of various ions, including Ca^{2+}, Na^{+}, K^{+}, Zn^{2+}, H^{+} and Fe^{2+}. Ionic movement is maintained by channels and transporters located on the lysosomal membrane, which is pertinent to ensuring proper ionic homeostasis within the lysosomal lumen. There are three lysosomal Ca^{2+} channels in mammals: TRPML1-3 (Transient Receptor Potential Cation Channel, Mucolipin subfamily), TPC1-2 (Two-Pore Channel) and P2X4, which play a key role in regulating lysosomal activity and function. TRPML belongs to the large superfamily of transient receptor potential that consists of three non-selective cation channels, TRMPL1, TRPML2 and TRPML3. TRPML channels are permeable to Ca^{2+}, Na^{+}, K^{+}, Fe^{2+} and Zn^{2+} [254]. Upon activation, the TRPML channel releases Ca^{2+} from the endo-lysosomal lumen to regulate various physiological processes such as endo-lysosomal membrane formation, phagocytosis, lysosome biogenesis, autophagy and exocytosis. Increases in reactive oxygen species (ROS) activate TRPML1 channel to facilitate lysosomal Ca^{2+} release, in turn inducing lysosomal autophagy to scavenge ROS [255]. Loss of TRPML1 function is reported in Mucolipidosis type IV [256] and Nieman-Pick disease (NP) [257].

Lysosomal hydrolase: Lysosomes have an abundance of hydrolytic enzymes such as proteases, sulfatases, nucleases, lipases, phosphatases, and glycosidases, which degrade complex

macromolecules. Lysosomal enzymes have optimal activity at pH 5. Among the sixty lysosomal hydrolases, serine cathepsins (A and G), aspartic cathepsins (D and E) and cysteine cathepsins are particularly important. Cathepsin cysteine proteases consist of 11 cathepsins (B, C/DPP1, F, H, L, K, O, S, V, W and X) [258]. Proteases play an integral role in proteolytic processing, protein modification and degradation of low-density lipoproteins [259]. Furthermore, mice with combined deficiency of cathepsin B and L display an accumulation of endo-lysosomes in the brain, leading to brain atrophy and death in the second and fourth week of life [260]. Cathepsin E assists in lysosomal autophagy by regulating lysosomal luminal pH [261]. Indeed, mouse macrophages deficient in Cathepsin E accumulate lysosomal membrane proteins with increased lysosomal pH [261], phenocopying lysosomal storage disorders. Together, these studies signify that cathepsin proteases are essential for structural integrity and the autophagy function of the lysosome. Lysosomal proteases such as Atg8, Atg7 and Atg3 also play a significant role in autophagosomal closure and maturation [262]. In addition to cathepsin proteases, lysosomal acid lipase plays a critical role in energy metabolism, signaling and cellular membrane integrity [263]. Lysosomal acid lipase is primarily responsible for hydrolyzing lipoprotein cholesteryl esters and TAG to free cholesterol and FAs, respectively. Lysosomal acid lipase hydrolyzes exogenous and endogenous neutral lipids delivered mainly to the lysosome either through endocytosis of lipoproteins or through autophagy [264].

1.7 Role of the lysosome in signalling and metabolism

1.7.1 The lysosome as a nutrient-sensing machinery

The lysosome is purported to be a singular organelle that receives cargo intracellularly and extracellularly, positioning them uniquely to sense nutrients and maintain cellular homeostasis. Lysosomal nutrient sensing fine-tunes cellular metabolism and growth by physical and functional association with the master growth regulator mammalian target of rapamycin complex 1 (mTORC1) [265]. mTORC1 is localized to the lysosome, where it receives information from nutrients or growth factors and activates downstream signaling programs to coordinate cell growth

or proliferation [265]. The availability of nutrients translocate mTORC1 to the lysosomal surface [265-267]. Growth factors, hormones, amino acids [268], glucose [267] and stress [269,270] are the major activators of mTORC1, which turn on anabolic programs such as protein translation and lipid biosynthesis [265-267]. The amino acid content of the lysosomal lumen dictates the docking of mTORC1 on the lysosomal surface [266]. Importantly, the surveillance of the lysosome nutrient content occurs via the lysosomal nutrient sensing machinery (LYNUS), a multi-protein complex that is recruited to the lysosomal surface **(Figure 1.6 A)** [52,271,272]. An important component of the LYNUS machinery is mTORC1 complex, which includes mTOR associated regulatory proteins such as RAPTOR (regulatory-associated protein of mTOR), mLST8 (mammalian lethal with SEC13 protein) and DEPTOR (DEP domain-containing mTOR-interacting protein) [268,271]. The LYNUS machinery senses the nutrient status of the lysosomal lumen and relays that information to the nucleus [268,273,274]. During nutrient abundance, mTORC1 binds to the LYNUS machinery on the lysosomal surface. On the lysosomal membrane, mTORC1 is activated by interacting with RAG GTPase (RAGA or RAGB and RAGC or RAGD), which is controlled by the agulator complex **(Figure 1.6 A)** [267,268,271,275]. mTORC1 on the lysosomal membrane is also activated by RHEB (growth factor-mediated upregulation of small GTPase RAS homologue enriched in brain) protein [276,277]. The second major component of LYNUS machinery is the vATPase complex, which senses the amino acid content of the lysosomal lumen. vATPase facilitates the interaction between the RAG channel and mTORC1 and participates in nutrient sensing on the lysosomal surface [278,279]. In the presence of nutrients, activation of mTORC1 suppresses the autophagy-lysosome pathway by direct phosphorylation of the ULK1 complex, resulting in the inhibition of catabolic processes [280,281]. However, during starvation, nutrient insufficiency inactivates mTORC1 by dissociating mTORC1 from the LYNUS machinery on the lysosomal membrane. The inactivation of mTORC1 relieves phosphorylation of the ULK1 complex leading to increases in autophagosome biogenesis and autophagy [280,281].

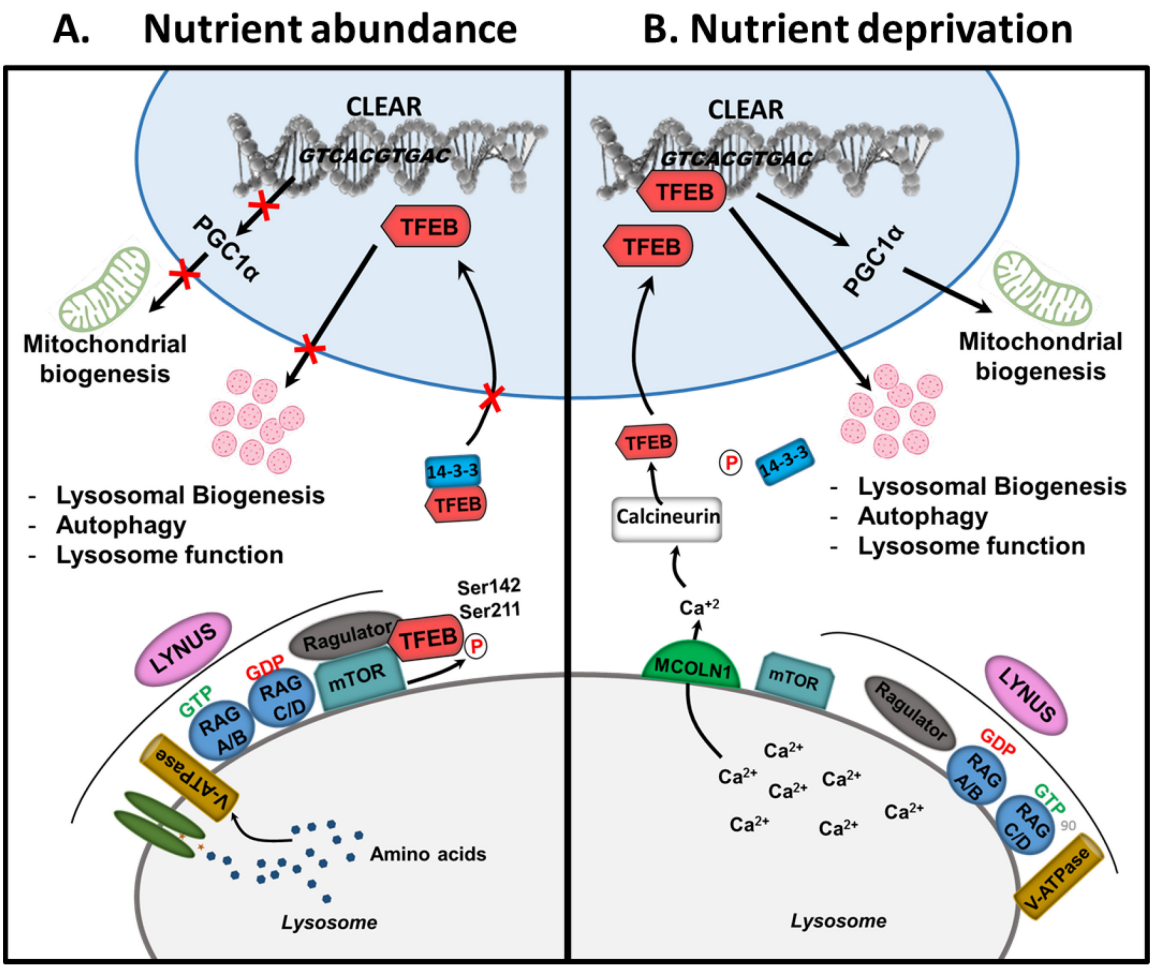

Figure 1.6 Nutrient-dependent regulation of TFEB. (A) During nutrient sufficiency, TFEB interacts with lysosome nutrient sensing (LYNUS) machinery that senses lysosomal nutrient content through the vATPase channel. This results in the activation of mTORC1 on the lysosomal membrane that phosphorylates TFEB at Ser142 and Ser211, which is recognized by 14-3-3 protein, restricting and inactivating TFEB in the cytoplasm. Cytosolic retention of TFEB decreases the nuclear content of TFEB, resulting in inhibition of TFEB-mediated regulation of lysosome biogenesis, lysosome function, autophagy and mitochondrial biogenesis. (B) During nutrient deprivation, mTORC1 moves away from the LYNUS machinery and releases Ca^{2+} from the lysosomal lumen through MCOLN1, which activates phosphatase calcineurin-mediated dephosphorylation of TFEB. Dephosphorylated TFEB dissociates from 14-3-3 protein, enabling translocation of TFEB to the nucleus to permit the transcriptional function of TFEB.

1.7.2 Transcriptional regulation of lysosomal autophagy and function

Several key proteins have been identified as critical transcriptional effectors and inhibitors of autophagy function in recent decades. Particular transcription factors are key regulators of proteins involved in the macroautophagy process, such as FOXO3a being a regulator of LC3 and nuclear factor erythroid 2-related factor 2 (Nrf2) being a regulator of p62 [282]. Other transcription factors implicated in autophagy regulation include hypoxia-inducible factor-1α (HIF-1α) and p53, which induce the expression of various genes involved in lysosomal autophagy [283,284]. Most importantly, two major transcription factors are critically involved in regulating a network of proteins indispensable for autophagic function. The zing finger family DNA-binding protein, ZKSCAN3 as the major repressor of autophagic functioning [285]. The microphthalmia-associated transcription factor (MiTF) superfamily comprised of TFEB and TFE3, as the major transcriptional activator of genes critical for autophagosomal, lysosomal functioning and lysosome biogenesis [286]. ZKSCAN3 negatively regulates lysosomal autophagy, biogenesis and function, a process sensitive to the nutrient status of the cell. During nutrient deprivation, ZKSCAN3 accumulates in the cytoplasm, leading to the inhibition of its activity, whereas nutrient availability promotes mTOR-dependent nuclear translocation of ZKSCAN3, allowing inhibition over autophagy [285]. On the other hand, the MiTF family of transcription factors, particularly TFEB and TFE3, are identified to be an important transcriptional influence over autophagy and lysosomal functioning [287]. In response to various stimuli such as starvation, lysosomal stress and pharmacological treatment, TFEB binds to the gene network called Coordinated Lysosomal Expression And Regulation (CLEAR) elements present in the promoter region of lysosomal and autophagy genes [288]. Upon binding to the CLEAR gene network, TFEB increases transcription of genes engaged in autophagy, lysosome biogenesis and lysosome function [288]. In addition to ZKSCAN3 and MiTF, post-translational modification of histones is implicated in regulating genes involved in autophagy. For instance, histone H4K16, demethylation of H3K9 and trimethylation of H3K27 influence autophagic activity [289]. G9a dimethylates H3K9 and represses autophagy genes,

whereas trimethylation of H3K27 inhibits autophagy by upregulating mTOR activity [289]. A recent study also identified Bromodomain and Extra-Terminal (BET) family protein Bromodomain containing 4 (BRD4), which represses autophagy and lysosomal genes by modifying histones [289].

1.8 Transcription factor EB (TFEB) and MiTF/TFE family

1.8.1 Members of MiTF/TFE family

The microphthalmia (MiTF)/TFE family of transcription factors include four members, namely Microphthalmia-associated transcription factor (MiTF), TFEB, TFE3 and TFEC [290]. They are a subfamily of basic/helix-loop-helix/leucine zipper (bHLH-LZ) transcription factors [291]. The common feature of MiTF/TFE proteins includes three critically important regions. The basic DNA-binding motif, while helix-loop-helix and leucine zipper motifs are critical for protein interaction and dimerization [292]. MiTF/TFE proteins bind to a palindromic DNA sequence (CACGTG) referred to as E-box, located in the proximal promoter region of its target gene [292,293]. MiTF/TFE family members heterodimerize with each other to trigger the expression of genes by binding to basic DNA-motif [290], whereas they do not heterodimerize with other members of HLH/leucine-zipper family such as MAX, USF and MYC [294]. Additionally, MITF, TFEB and TFE3 possess an activation domain (AD) required for their transcriptional activation. Conversely, TFEC does not contain AD, and therefore, rather than activation, TFEC inhibits the transcription of its downstream target genes **(Figure 1.7)** [295].

MiTF/TFE genes are present in all metazoan organisms. They are also conserved in vertebrates and primarily expressed in the retinal pigment epithelia, macrophages, osteoclasts, mast cells, melanocytes and natural killer cells [290]. However, invertebrates such as *Drosophila* and *Caenorhabditis elegans* only have a single family member of the MiTF/TFE family known as Mitf HLH-30, respectively [296,297]. The function and regulation of *Mitf* and HLH-30 appear to be similar to that of TFEB [296].

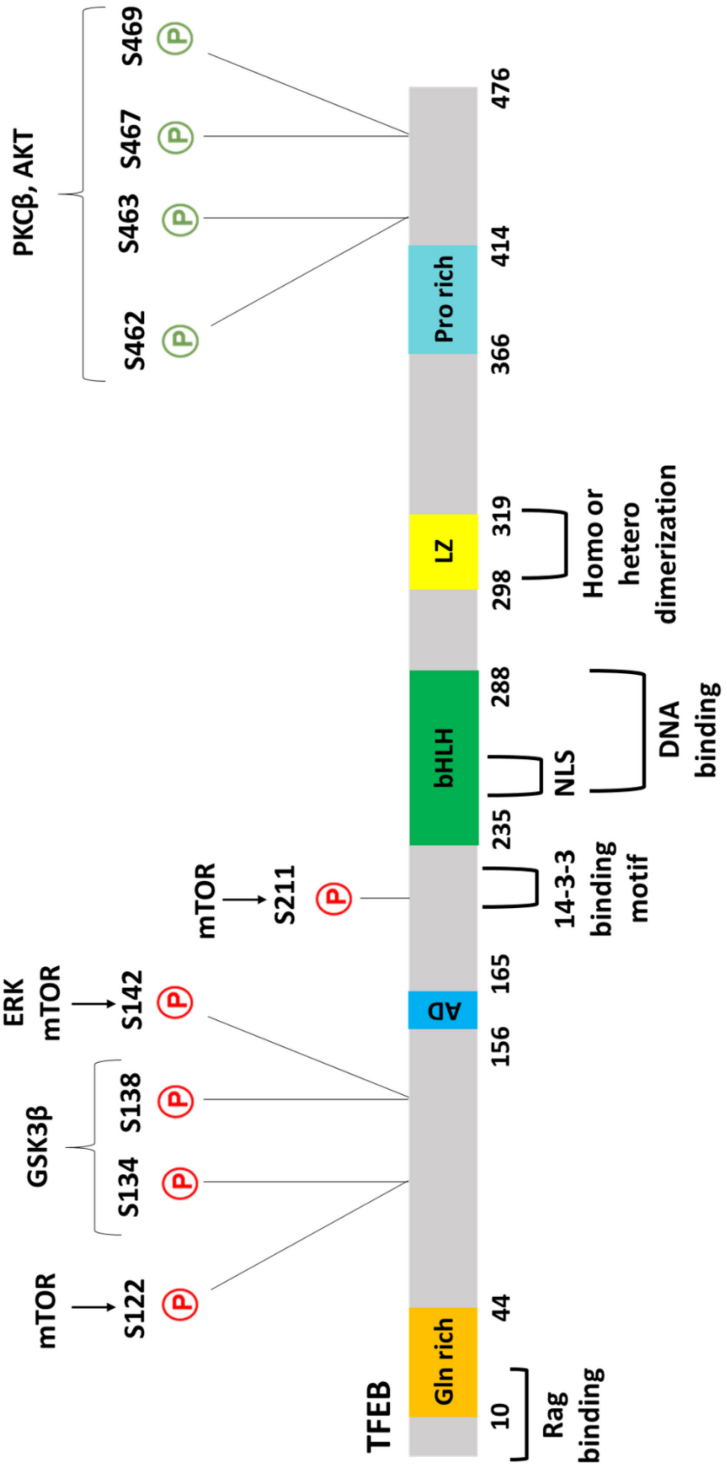

Figure 1.7 Relevant TFEB phosphorylation sites and their regulatory role. The various domains found in TFEB protein. Gln, glutamine-rich region; AD, acidic domain, bHLH, basic helix-loop-helix; LZ, leucine zipper domain; Pro-rich, proline-rich segment. Red P indicates TFEB nuclear translocation inhibition by inhibitory phosphorylation, and green P indicates TFEB stabilization and nuclear translocation with activating phosphorylation.

1.8.2 TFEB regulation of lysosomal biogenesis, autophagy and signalling

TFEB is a master transcriptional regulator of genes encoding proteins facilitating autophagosomal assembly, autophagosomal maturation, autophagosome-lysosome fusion and lysosomal biogenesis and lysosome function [298]. TFEB was not fully described until 2009, when Sardiello *et al*. elegantly characterized TFEB's ability and capacity to regulate cellular degradation processes, particularly those involving autophagy and lysosomal proteolysis [288]. Lysosomal genes are co-expressed and regulated by common factors leading to the identification of a ten palindromic motif (TCACGTGA) in the proximity of their transcription start site [288,299]. The DNA binding specificity for the HLH-LZ family is induced by sequences immediately flanking the E-box. The MiTF/TFE family favours the GTCACGTGAC consensus sequence known as the CLEAR gene network, which stands for coordinated lysosomal expression and regulation [288]. CLEAR promoter elements are repetitions of ten base pair motif located within the first 200 base pair of numerous lysosomal genes. TFEB-signaling generates more autophagosomes and accelerates their delivery to lysosomes by increasing lysosomal number, thereby facilitating protein degradation [299]. Upon nuclear entry, TFEB binds to CLEAR promoter sequences of various genes such as UVRAG, WIPI, MAP1LC3B, SQSTM1, VPS11, VPS18, Atg9B and vATPase that are involved in autophagosomal and lysosomal function [221,288]. TFEB-mediated action ultimately dictates autophagosomal assembly/degradation and lysosomal biosynthesis/function by directly regulating proteins involved in lysosomal acidification and autophagy.

1.9 Regulation of TFEB signalling and action

1.9.1 TFEB phosphorylation and subcellular localization

Since the primary site-of-action for any transcription factor is the nucleus, transcription factors are regulated by shuttling between cytoplasm and nucleus. The importation of transcription factors from the cytosol to the nucleus is facilitated by importin-dependent and importin-independent mechanisms [300]. The nuclear translocation of TFEB is triggered by a variety of stimuli such as nutrient deficiency, pharmacological treatment, chemical stressors and post-

translation modification. Notably, HeLa cells treated with sucrose induce translocation of TFEB from the cytosol to the nucleus, while TFEB remained in the cytosol in cells without sucrose treatment [288]. MEFs, Hepatocytes and HeLa cells subjected to amino acid-derived medium show increased nuclear translocation of TFEB as early as one-hour post-nutrient insufficiency **(Figure 1.6)** [288,299]. Re-feeding cells following starvation shuttles TFEB from the nucleus to the cytoplasm within a minute **(Figure 1.6)** [299]. Consistently, mice subjected to starvation for 24 hr increase nuclear localization of TFEB in the liver, muscle and kidney [299].

The subcellular localization of TFEB is also influenced by post-translational modification through its phosphorylation at serine residues. mTOR-mediated phosphorylation of TFEB is dependent on the nutrient status of the cell. During conditions of nutrient surplus, LYNUS machinery senses the increased intra-lysosomal amino acid content **(Figure 1.6 A)** [229,230,273]. This results in the localization and tethering of mTOR and TFEB on the lysosomal membrane. At the lysosomal membrane, mTOR phosphorylates TFEB at three different serine residues; Ser122, Ser142 and Ser211, resulting in the restriction and inactivation of TFEB in the cytosol **(Figure 1.6 A)** [286,298,301-303]. Whereas mutations of either Ser142 and Ser211 with alanine (S142A and S211A) result in resistance in phosphorylation by mTOR, leading to the constitutive nuclear localization of TFEB [302,304]. Additionally, extracellular receptor kinase (ERK) is activated during nutrient replete conditions and negatively regulates TFEB through its phosphorylation at Ser142, restraining and inactivating TFEB in the cytosol [302]. mTOR-mediated TFEB phosphorylation at Ser211 promotes binding of TFEB to YWHA (14-3-3) cytosolic adaptor proteins, which restricts mobilization of TFEB to the nucleus **(Figure 1.6 A)**. 14-3-3 proteins retain TFEB to the cytosol by masking TFEB's nuclear localization sequence [286]. While activation of mTOR activity promotes cytosolic restriction of TFEB, upregulation of mTORC1 activity in TSC1 (hamartin)/TSC2 (tuberin) deficient MEFs subjected to starvation promotes nuclear localization of TFEB [305]. TSC1/TSC2 complex tightly controls cellular growth and proliferation by inhibiting mTORC1 activity. Remarkably, mutation of C-terminal serine-rich motif includes

S462/463/466/467/469 with alanine causes cytoplasmic retention of TFEB, whereas mutation of aspartate induces constitutive nuclear mobilization of TFEB [305,306].

In addition to mTOR and ERK, other kinases such as PKCβ, GSK3, RIP1K and Akt regulate TFEB localization through its phosphorylation. A recent study demonstrated that serine-threonine kinase RIP1K negatively targets TFEB by activating ERK and regulates the autophagy-lysosome pathway in a breast cancer cell model [307]. RIP1K also plays an essential role in cellular pathways related to cell death, such as apoptosis and necroptosis [307]. Interestingly, PKCβ-mediated phosphorylation of TFEB at multiple serine residues located in the C-terminus in human TFEB (Ser462, Ser463, Ser467 and Ser469) does not induce nuclear localization but promotes TFEB cytosolic protein stability in osteoclasts **(Figure 1.7)** [306]. Phosphorylation by GSK3β at Ser134 and Ser138 promotes lysosomal localization and cytoplasmic retention of TFEB, whereas double mutation of S134A/S138A significantly increases nuclear translocation of TFEB **(Figure 1.7)** [308]. TFEB is also phosphorylated by Akt at Ser467, resulting in its cytoplasmic localization, whereas treating the cell with autophagy activator, trehalose, inhibits Akt and promotes nuclear retention of TFEB **(Figure 1.7)** [309]. Conversely, TFEB is localized in the nucleus upon dephosphorylation. A prior study demonstrates that upon nutrient deprivation, low levels of intra-lysosomal nutrients induce Ca^{2+}-mediated activation of calcineurin (CaN) phosphatase, which dephosphorylates and induces nuclear intrusion of TFEB and increases transcription of lysosomal genes **(Figure 1.6 B)** [310].

TFEB subcellular localization is not only regulated through its phosphorylation but also by acetylation at lysine residue 116, acting analogously to phosphorylation by confining TFEB to the cytosol [311]. Interestingly, TFEB is activated through deacetylation by sirtuin 1 (SIRT1), promoting the nuclear localization of TFEB. Pharmacological treatments such as chloroquine (which inhibits fusion of autophagosome and lysosome by neutralizing lysosomal acidity), bafilomycin or trehalose induce nuclear translocation of TFEB [301,302,309]. Infections [312], bacterial phagocytosis [313], lipopolysaccharide (LPS) treatment [314] and mitochondrial damage

[315] promote nuclear importation of TFEB. Remarkably, an increase in physical activity has a notable impact on the subcellular localization of TFEB. Mice subjected to progressive increases in exercise intensity show significant TFEB nuclear translocation with concomitant depletion in cytosolic TFEB content [316] in the muscle. Ubiquitin proteasome pathway (UPP) is also an important regulator of lysosomal autophagy through its ability to modulate TFEB functions. Indeed, the E3 ubiquitin ligase, STUB1 activates TFEB by directing phosphorylated TFEB for proteasomal degradation, thereby increasing nuclear content of TFEB in mouse embryonic fibroblasts (MEFs) [317], whereas the E3 ubiquitin ligases, SKP2 (S-phase kinase-associated protein 2) and MID1 (Midline1) inhibit nuclear localization of TFEB [318]. Interestingly, proteasomal inhibitor MG-132 significantly increases the nuclear mobilization of TFEB in hepatocytes [318]. Together, these findings highlight the complex regulation of TFEB by controlling its subcellular localization through various mechanisms **(Figure 1.8)**.

1.9.2 Transcriptional activators and inhibitors of TFEB

TFEB regulates its expression by binding to the CLEAR network on its promoter region as reported in nutrient-deprived MEFs, hepatocytes, HeLa and mouse tissues [299]. This enhanced positive feedback of TFEB on its expression during starvation was disrupted in nutrient replete conditions [299]. Interestingly, PGC1α and PPARα are direct targets of TFEB that regulate TFEB expression. Treating neuronal cells with Gemfibrozil, an agonist of PPARα upregulates TFEB mRNA and protein levels by recruiting PGC1α, PPARα and retinoid X receptor α (RXRα) to the PPAR-binding site on the TFEB promoter region [319]. TFEB expression is also regulated by transcriptional effectors through the recently described farnesoid X receptor (FXR)/cAMP response element-binding (CREB) transcription axis [320]. Hepatocytes subjected to starvation with HBSS media activate and induce nuclear inclusion of CREB protein, which increases expression of TFEB proteins to upregulate autophagy. However, during the nutrient-rich state, activation of FXR protein antagonizes CREB-mediated transcriptional activation of TFEB, resulting in inhibition of

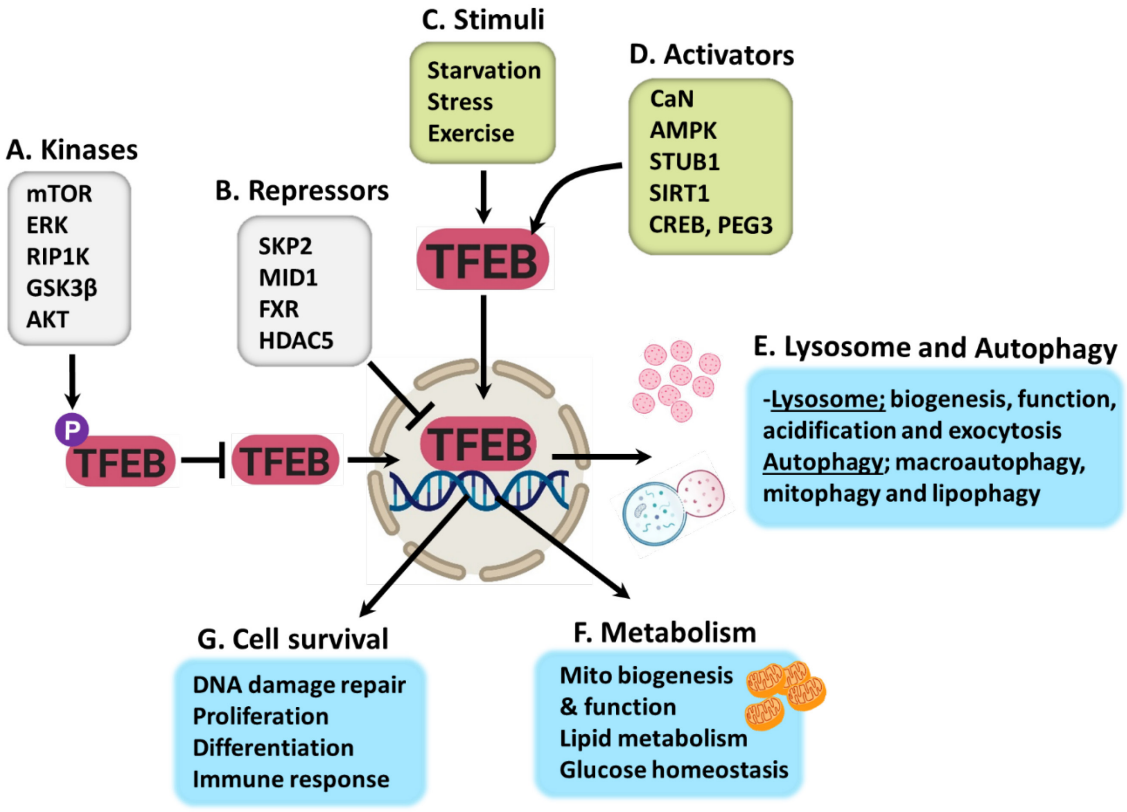

Figure 1.8 Cellular modifiers of TFEB action. (A) Kinases and (B) repressors that inhibit nuclear translocation of TFEB. (C) stimuli and (D) activators that activate and induce nuclear localization of TFEB. The primary role of TFEB includes regulating genes involved in (E) lysosome function, lysosome autophagy, (F) cellular metabolism such as mitochondrial biogenesis, function and (G) cellular survival, including DNA damage repair and immune response.

autophagic process [320]. Post-transcriptionally, TFEB mRNA is regulated by micro-RNA 128, which targets TFEB mRNA for Argonaut-mediated degradation [321]. A recent study also identified a new signaling axis of AMPK-SKP2 (an F-box protein of the SCF E3 ubiquitin ligase complex)-CARM1 (co-activator-associated arginine methyltransferase 1), which transcriptionally regulates TFEB expression [322]. During starvation, AMPK phosphorylates FOXO3a in the nucleus in MEFs, which represses E3 ubiquitin ligase SKP2, a negative regulator of CARM1. FOXO3a-mediated repression on SKP2 increases CARM1 levels, increasing the expression of TFEB and lysosomal genes **(Figure 1.8)** [322].

Nuclear TFEB is also inhibited by histone deacetylase 5 (HDAC5), through binding and inhibition of TFEB's transcription activity. However, protein kinase-D 1 (PKD1)-mediated phosphorylation of HDAC5 induces HDAC5 nuclear export in HEK293 cells, which relieves HDAC5-dependent inhibition of TFEB, allowing TFEB to activate the CLEAR network [323]. Together, these studies highlight the complex regulation of TFEB and its tight correlation with numerous other regulatory hubs controlling cell signalling and metabolism.

1.9.3 Cooperativity of TFEB with other MiTF family members

Both TFEB and TFE3 appear to regulate sets of genes and exhibiting similar biological effects in response to gain- and loss-function modifications. Like TFEB, the subcellular localization of TFE3 is regulated through its phosphorylation. During nutrient-rich conditions, mTORC1 phosphorylates TFE3, resulting in the cytosolic retention of TFE3 [287]. Furthermore, cell starvation with amino acid-deficient medium or treatment with Torin-1 (mTORC1 inhibitor) or cells incubated with chloroquine to induce lysosomal stress trigger nuclear translocation of TFE3. Like TFEB, TFE3 binds to the CLEAR gene network present in the promoter region of proteins involved in lysosome biogenesis [287]. Recent studies have investigated redundancy and cooperation between TFEB and TFE3 transcription factors using single and double knock-out (KO) mouse models. Interestingly, whole-body TFEBKO mice die during embryonic development, whereas TFE3KO mice exhibit no apparent phenotype [324]. Loss-of-function of TFE3 study

reveals that TFE3 plays a key role in regulating whole-body glucose homeostasis, glycogen homeostasis, lipid metabolism, mitochondrial function and metabolic homeostasis. Remarkably, TFE3 overexpression in TFEBKO mice abolishes the obese phenotype [324]. Liver-specific TFEB and TFE3 double KO mice exhibit exacerbation in obese phenotype compared to singular deletion of TFEB or TFE3 alone. These findings suggest that both TFEB and TFE3 play an important role in regulating lipid and glucose homeostasis and combined depletion of both transcription factors result into additive alterations in cellular metabolism and function.

TFEB is also implicated in regulating the innate immune response. Mice with conditional deletion of TFEB in macrophages exhibit decreased expression of genes encoding pro-inflammatory cytokines and chemokines. Furthermore, macrophage-specific TFEB deletion impairs autophagy and lysosome biogenesis, leading to defective anti-bacterial response [314]. The impairment in innate immune response due to the loss of TFEB in macrophages is exacerbated by the added depletion of TFE3. These findings collectively suggest that both TFEB and TFE3 regulate very similar genes and exhibit cooperativity in multiple tissues.

1.10 Physiological roles of TFEB

1.10.1 Role of TFEB in cellular proliferation and pro-survival

MiTF/TFE family of transcription factors regulate multiple cellular physiological processes, including organelle biogenesis, cell proliferation, cell differentiation and survival [306,325]. Additionally, TFEB also participates in regulating nutrient sensing, energy metabolism and cellular clearance [299,326]. Prior study has demonstrated that TFEB-mediated increases in lysosome biogenesis are crucial for osteoclast differentiation [306]. Mice with TFEB silencing exhibit defective bone resorption due to the suppression of lysosomal content and function [306]. TFEB is also involved with other physiological processes such as regulating the expression of genes encoding critical metabolic regulators [299,316] and activation of the innate immune system [314]. Additionally, TFEB is also essential for placental vascularization [325]. Notably, the aberrant expression of TFEB is associated with different types of human cancers, such as renal carcinomas

[327], breast cancer [328] and pancreatic ductal adenocarcinoma [329]. Recent evidence indicates that TFEB and TFE3 are activated in response to mitochondrial and ER stress, suggesting a more generic role while responding and adapting to stress to maintain cellular survival and homeostasis.

1.10.2 TFEB and cellular energy metabolism

In addition to its canonical role of regulating genes involved in autophagy, lysosome biogenesis and lysosome function, TFEB engages nutrient-sensing pathways to remodel cellular energy metabolism. In the liver, transcriptome analysis reveals that TFEB overexpression in the liver upregulates the expression of genes engaged in FA oxidation, lipophagy and ketogenesis [299]. Whereas TFEB overexpression downregulates genes associated with anabolic processes, including steroid, lipid and isoprenoid biosynthesis [299]. Furthermore, mice with liver-specific TFEB deletion, subjected to a high-fat diet, show excess accumulation of LDs in the liver, indicating defective lipid degradation during diet-induced obesity. Conversely, TFEB overexpression in the liver improves lipid catabolic profile and attenuates hepatic steatosis during diet-induced obesity. These findings further reveal that TFEB-mediated regulation of lipid metabolism in the liver also requires a functional lipophagy pathway. Notably, TFEB regulates genes involved in lipid metabolism through its effect on PGC1α and PPARα. Subsequent study also indicates that TFEB directly governs PGC1α gene expression by binding to the CLEAR sequence in its promoter [299].

In the skeletal muscle, loss of TFEB significantly impacts cellular metabolism [316]. Genome-wide analysis reveals that several genes involved in cellular metabolism, including glucose homeostasis, lipid homeostasis, mitochondrial biogenesis and oxidative phosphorylation, are upregulated in muscle-specific TFEB overexpressing mice and downregulated in skeletal muscle with TFEB deletion [316]. Gain- and loss-of-function studies in the skeletal muscle unveil that TFEB regulates mitochondrial biogenesis and glucose homeostasis independent of its effect on PGC1α. Interestingly, muscle-specific TFEB overexpression enhances high-intensity exercise training performance in mice, whereas TFEB-deficient muscle decreases metabolic flexibility and intolerance during exercise training [316]. Exercise-induced TFEB expression upregulates genes

associated with glucose transports (GLUT1 and GLUT4), hexokinase-I/II, TBC1D1 and GYS, leading to glycogen accumulation to sustain energy production.

In addition to liver and skeletal muscle, TFEB overexpression in adipocytes enhances metabolic rate and white adipose tissue browning by upregulating uncoupling protein 1 (UCP1), an essential protein for regulating thermogenesis [330]. As observed in skeletal muscle, metabolic phenotypes of TFEB overexpression in adipocytes are PGC1α dependent. Whereas TFEB overexpression in macrophages attenuates ventricular dysfunction by upregulating the lysosomal acid lipase gene to increase lipophagy, likely indicating TFEB's involvement in governing lipid metabolism through autophagy [330]. However, the exact role of TFEB in regulating cellular energy metabolism in the heart, specifically the cardiomyocyte, remained unexplored.

1.11 Adipostatic and anti-inflammatory role of TFEB

Liver-specific TFEB KO mice gain more weight compared to their control mice [298]. These mice also display an increase in peripheral adiposity, indicating that modulation of TFEB levels in the liver also affects peripheral fat metabolism. Conversely, TFEB overexpression by injecting mice with helper-dependent adenoviral vector (HDad) that expresses human TFEB (HDAd-TFEB) arrests the development of obesity phenotype and decreases peripheral adiposity, circulating leptin, TAG and cholesterol compared to mice with control virus injection. Similarly, viral-mediated delivery of TFEB in leptin-deficient *ob/ob* mice significantly reduces circulating TAG, cholesterol, improves glucose tolerance test and overall metabolic phenotype syndrome [298].

Like the liver, TFEB overexpression in adipocytes protects against diet-induced obesity. This protective effect of TFEB overexpression is attributed to reducing peripheral adiposity in both male and female mice [330]. These mice also exhibit decreased gonadal white adipose tissue and inguinal white adipose tissue weight compared to control mice; however, no change in brown adipose tissue weight is observed [330]. Furthermore, adipocyte-specific TFEB overexpression also improves glucose tolerance and insulin sensitivity and protects mice against hepatic steatosis,

indicating TFEB overexpression rescues metabolic complications in diet-induced obesity [330]. Together, these findings suggest that gain- or loss-of-function of TFEB in liver and adipose tissue protect against diet-induced obesity by influencing whole-body metabolism and peripheral fat metabolism.

Loss of TFEB is implicated in several cardiovascular diseases and in multiple cell types, given the hetero-cellularity of the heart. For instance, the autophagy-lysosome pathway within macrophages plays a vital role during atherosclerosis to clear dysfunctional proteins and organelles [331]. Macrophage-specific autophagy is also important for lipid clearance [331], whereas autophagy-deficient macrophages remodel to be atherogenic in murine and human atherosclerotic lesions [331,332]. Overexpressing TFEB or treatment with the natural sugar trehalose which activates TFEB, augments the lysosome-autophagy pathway in macrophages and reverses autophagic dysfunction, attenuating macrophage apoptosis and pro-inflammatory IL-1β levels [331,332]. Using a cell culture model of atherosclerosis, macrophages with high levels of oxidized-LDL and cholesterol crystals display an increase in lysosome pH, suppression of lysosomal proteolytic capacity and lysosomal dysfunction [333]. Macrophage-specific TFEB overexpressing transgenic mice exhibit increased lysosome biogenesis and proteolytic capacity in macrophages with atherogenic lipids [333]. Furthermore, mice with ischemia-reperfusion injury and in cardiac macrophages of humans with ischemic cardiomyopathy, loss of TFEB and dysfunction of lysosome-autophagy pathway is observed [334]. Transgenic mice with macrophage-specific TFE-B overexpression attenuate ventricular dysfunction and IL-1β secretion post-ischemia-reperfusion injury. This effect is attributed to increased lipophagy, secondary to the augmented expression of lysosomal acid lipase, a direct target of TFEB [334]. These findings emphasize that TFEB is a central coordinator of not only cellular energy metabolism but also functions as an adipostat and attenuates inflammation. However, it is still unclear whether TFEB modulates similar cellular metabolism pathways in the heart. Another group of disorders in which TFEB deficiency and suppression in the autophagy-lysosome pathway observed are neurodegenerative diseases,

including Parkinson's, Huntington's and Alzheimer's disease, as well as other tauopathies [335-337]. TFEB attenuation and defective lysosomal function are also observed in lysosomal storage disorders (LSDs) such as multiple sulfatase deficiency, mucopolysaccharidosis type-IIIA, Batten disease, Pompe disease, Gaucher disease, Tay–Sachs disease and cystinosis [338]. Whereas overexpression of TFEB in cellular and mouse models of LSDs is beneficial in reducing substrate accumulation by upregulating the autophagy-lysosome pathway and attenuating LSD complications [335,336]. These findings indicate that TFEB is beneficial in vast majority of diseases.

1.12 Regulation of TFEB by nutrients and metabolites

Recent studies indicate that cellular nutrients play a key role in regulating the transcriptional activity of TFEB. Cells such as MEFs, hepatocytes and HeLa cells deprived of amino acids induce nuclear translocation of TFEB, whereas supplementing cells with growth media induces cytosolic retention of TFEB [299]. Given that TFEB regulates genes associated with lipid metabolism and glucose homeostasis, it is plausible that glucose and lipid availability influence TFEB activity. Similar to amino acids, glucose deprivation in HT29 cells translocate TFEB to the nucleus and activate its target genes [326], whereas re-feeding cells export TFEB from the nucleus within 30 minutes [326]. A recent study also identified a glucose-mediated transcriptional regulation of TFEB mediated by AMPK-SKP2-CARM1 signaling axis in MEFs [322]. In addition to glucose, a non-reducing natural disaccharide, trehalose (α,α-1,1-glucoside), synthesized endogenously by non-mammalian organisms such as insects, crustaceans and plants, is implicated in regulating TFEB levels in macrophages [332]. Trehalose treatment increases TFEB content to the nucleus and augments its activity, reducing atherogenic lipid-induced polyubiquitinated protein accumulation in macrophages [332]. Furthermore, trehalose-induced augmentation of TFEB activity is also investigated *in-vivo*. ApoE-null mice subjected to high-fat diet for six weeks to develop atherosclerotic lesions, are given i.p. administration of trehalose for two-weeks. Splenic macrophages derived from trehalose-treated mice exhibit enhanced TFEB nuclear importation,

increases in transcription of genes involved in autophagy and lysosome pathway and protect mice from atherosclerosis compared to vehicle-treated mice [331,332]. On the contrary, non-reducing disaccharide sucrose and reducing disaccharide maltose do not affect TFEB activity compared to trehalose [331,332].

Notably, studies from our laboratory reported the role of different FAs-mediated regulation of TFEB. We demonstrated that saturated FA palmitate depletes TFEB and induces cell death in H9C2 cells and primary cells of neonatal or adult rat cardiomyocytes [226]. In contrast, monounsaturated FA, oleate does not affect cellular TFEB content and maintains cardiomyocyte viability. Similar to oleate, monosaccharide glucose does not affect cardiomyocyte TFEB content. However, a combination of glucose and palmitate treatment significantly reduces TFEB expression in the cardiomyocyte and suppresses cardiomyocyte viability. These findings collectively suggest that TFEB is a nutrient-sensitive target and its activity depends on the availability of types and carbon chain length of different nutrients.

Thesis hypothesis and objectives

The prevalence of CVD is increased among obese and diabetic patients. Current therapies for obesity- and diabetes-related CVD are limited to exerting glycemic control. However, merely controlling hyperglycemia is inadequate in improving cardiovascular function in obese and diabetic patients. Identifying and characterizing novel targets and pathogenic pathways contributing to obesity- and diabetes-induced cardiovascular complications are critical to developing new and effective therapies. TFEB-autophagy/lysosome pathway-cellular metabolism is a relatively novel signaling axis reported to be dysregulated in several metabolic disorders. Loss of TFEB has been implicated in numerous diseases like neurodegeneration, LSDs, cancer, obesity, and heart diseases such as ischemia-reperfusion injury, atherosclerosis, hypertrophy and DOX-induced cardiotoxicity. Since lysosomal autophagy enables cellular waste clearance and TFEB is a central coordinator of metabolism, inflammation and adiposity, selective targeting of cellular TFEB in the obese diabetic heart could prevent or ameliorate obesity- and diabetes-related metabolic heart disease. We reported that nutrient overload during obesity and diabetes decreases TFEB content with a concomitant reduction in lysosomal proteolytic activity and increased cardiomyocyte injury [226]. These findings highlight the pro-survival role of TFEB in influencing cardiomyocyte viability and function. However, the underlying mechanisms by which loss of TFEB engages in the nutrient-sensing pathway to remodel cardiac energy metabolism remain unanswered. In this thesis, I examined the central hypothesis that constitutive nuclear restoration of TFEB attenuates nutrient overload-induced cardiomyocyte injury, lysosomal dysfunction, impairment in cardiomyocyte energy metabolism and function. Chapters 2-5 contain experiments that investigate this hypothesis through the following objectives:

1. To examine how nutrient overload negatively targets TFEB in the heart and if TFEB levels are altered temporally in the heart of mice fed high-fat high sucrose (HFHS) diet
2. To elucidate whether TFEB inactivation is necessary and sufficient to disrupt lysosome integrity and autophagy causing injury in the obese and diabetic heart *in-vivo* and *ex-vivo*

3. To assess whether preventing the decline of TFEB ameliorate lipid overload-induced lysosome dysfunction and cardiomyocyte injury

4. To determine whether loss-of-function of TFEB in-vivo remodels cardiomyocyte metabolism, cell death, Ca^{2+} dynamics and contractile function

Chapter 2: Effect of fatty acid overload on TFEB content and lysosome function in the cardiomyocyte

This chapter contains materials (sections 2.4, figure 2.1 B, F, J, N and figure 2.3 A-D) originally published in:

Trivedi, P.C.; Bartlett, J.J.; Perez, L.J.; Brunt, K.R.; Legare, J.F.; Hassan, A.; Kienesberger, P.C.; Pulinilkunnil, T. Glucolipotoxicity diminishes cardiomyocyte TFEB and inhibits lysosomal autophagy during obesity and diabetes. Biochim Biophys Acta 2016, 1861, 1893-1910 [226].

Remaining figures and portions of the text present in this chapter have been reproduced with the copyright permission from Elsevier and edited as appropriate:

Trivedi, P.C.; Bartlett, J.J.; Mercer, A.; Slade, L.; Surette, M.; Ballabio, A.; Flibotte, S.; Hussein, B.; Rodrigues, B.; Kienesberger, P. C.; Pulinilkunnil, T. Loss of function of transcription factor EB remodels lipid metabolism and cell death pathways in the cardiomyocyte. Biochim Biophys Acta Mol Basis Dis 2020, 1866 (10):165832 [339].

Lipidomic analysis data (Table 2.1 and 2.2) was generated by Angella Mercer, Kienesberger lab.

2.1 Rationale and objectives

During obesity and diabetes, chronic nutrient overload inhibits cellular protein quality control and protein degradation precipitating ER stress in multiple tissues like the heart, adipose and liver [226,340,341]. Acute response to nutrient overload hyperactivates proteasomal machinery to clear cellular protein aggregates [342]. However, during sustained nutrient-overload, proteasomal insufficiency ensues, triggering activation of lysosomal autophagy to facilitate the clearance of proteotoxic load [342,343]. Experimental evidence suggests that if damaged proteins evade degradation by the proteasome, these proteins must be degraded by the process of lysosomal autophagy to maintain cellular homeostasis [343]. Genes encoding lysosomal structure and function are under the transcriptional control of TFEB [298]. Transcriptional activity of TFEB encodes genes

involved in autophagosome formation and accelerates its delivery and clearance by lysosomes via increases in lysosomal biogenesis [288,304]. It is plausible that changes in TFEB content and associated lysosomal dysfunction could significantly impact cellular function during obesity, insulin resistance and diabetes. Numerous studies have provided evidence that TFEB is necessary to maintain cardiomyocyte function. Notably, a prior study from our laboratory demonstrated cardiomyocytes exposed to doxorubicin (DOX) [344] and glucolipotoxic stress [226] diminish nuclear TFEB content, renders lysosome dysfunctional and induces cardiomyocyte death. For instance, the severity of ischemia-reperfusion injury is sensitive to TFEB action, as viral overexpression of TFEB in neonatal rat cardiomyocytes (NRCMs) protects against hypoxia-induced cell death [247]. Another study examined the role of TFEB in zebrafish and mouse hearts following amyloid deposition, wherein increases in TFEB expression improves cardiac outcome in zebrafish and mice hearts [345]. Despite the above studies highlighting the critical role of TFEB in influencing cardiomyocyte viability and function, how TFEB is inhibited remains unclear. Moreover, if bioactive metabolites, nutrients and inflammatory mediators directly target TFEB content, localization, and activity merits investigation. However, the mechanism by which the time-dependent changes in TFEB reprograms myocyte signaling, metabolism and function during obesity and diabetes remains unexplored. Therefore, the first objective of this thesis was to examine in rodents and humans if changes in myocyte TFEB content and action during nutrient overload are temporally associated with lysosomal dysfunction and abnormal lipid metabolism.

2.2 Materials and methods

2.2.1 Animal studies:

All protocols involving rodents were approved by the Dalhousie University, Institutional Animal Care and Use Committee (Protocol #18-114, #18-115, #18-116). Mice were maintained in a temperature- and humidity-controlled animal-care facility, with a 12 h light/dark cycle with food and water provided ad libitum.

Diet-induced obesity: Nine to ten weeks old male C57BL/6J mice (Jackson Laboratory: Stock number; 000664) were housed in a 12 h light-dark cycle. Mice were randomly assigned to groups fed either chow diet (5001; Lab diet, St Louis, MO, USA; with 13.5 kcal% from fat) or high fat-high sucrose (HFHS) diet (12451; Research Diets, New Brunswick, NJ, USA; with 45 kcal% from fat and 17 kcal% from sucrose) for 4, 8, 12 and 16 weeks. Bodyweight gain was recorded weekly by taking the differences in body weight before starting the diet and every week after starting the diet. After 4, 8, 12 and 16 weeks of chow and HFHS diet feeding, mice were subjected to 1 h food withdrawal before euthanasia. Tissues were collected and stored at - 80℃ for biochemical analysis.

2.2.2 Tissue homogenization

The frozen heart was powdered using pestle and mortar, followed by homogenization using polytron homogenizer in ice-cold buffer containing 20 mM Tris-HCl, pH 7.4, 5 mM EDTA, 10 mM $Na_4P_2O_7$ (567540; Calbiochem, EMD Chemicals, Gibbstown, NJ, USA), 100 mM NaF, 1% Nonidet P-40, 2 mM Na_3VO_4, 10 µl/ml of protease inhibitor (P8340, Sigma, St Louis, MO, USA; contains AEBSF - [4-(2-Aminoethyl)benzenesulfonyl fluoride hydrochloride], aprotinin, bestatin hydrochloride, E-64 – [N-(trans-Epoxysuccinyl)-L-leucine-4-guanidinobutylamide], leupeptin hemisulfate salt and pepstatin A) and 10 µl/ml of phosphatase inhibitor (524628, Calbiochem; contains bromotetramisole oxalate, cantharidin and calyculin A, Discodermia calyx). Homogenate was centrifuged at 1000 x g for 10 min at 4℃ to obtain a '1000 x g pellet', which is composed of nuclear membrane proteins. The supernatant obtained was then transferred to another microfuge tube, consisting of soluble proteins in the cytosolic compartment. The 1000 x g pellet was sonicated using nucleus extraction buffer containing 1 mM EGTA, 1 mM EDTA, 10 mM HEPES, 1.25 g glycerol, 412 mM NaCl, 1.5 mM $MgCl_2$, 1mM DTT (0281; Amresco, OH, USA), a protease inhibitor (P8340, Sigma, St Louis, MO, USA; 10 µl/ml) and phosphatase inhibitor (524628, Calbiochem, EMD Chemicals, Gibbstown, NJ, USA; 20 µg/ml) and pH was adjusted to 7.5. The resulting lysate was then centrifuged at 10,000 x g for 10 min at 4℃, and supernatant (consisting of nuclear membrane proteins) was collected in a microfuge tube. The protein concentration of the

lysate for the cytosolic compartment was determined using the BCA protein assay kit (23255; Pierce, Thermo Fisher Scientific, Waltham, MA, USA), and protein concentration from the nuclear membrane was determined using Bradford protein assay reagent (500205; Quick Start Bradford Dye Reagent, BioRad, Mississauga, Ontario, Canada). Lysates were stored at -80℃ for subsequent biochemical analysis.

2.2.3 Cardiac lipidomic analysis

For targeted lipidomic analysis in the heart, total lipids of weighed heart tissue (10–15 mg) were spiked with 10 µl of 100 µM internal standards (ISTD, DG 14:0/14:0, TAG 15:0/15/0/15:0 and TAG 17:0/17:0/17:0 Avant Polar Lipids) per sample. Heart tissues were homogenized in methanol using polytron homogenizer. Homogenate was transferred into a glass tube filled with UPLC grade methanol. Extraction was performed using 5 mL of meth-tert-butyl ether (MTBE) [346] with continuous shaking for 60 min at room temperature (RT). Following the addition of 1.2 mL ddH_2O, samples were vortexed and spun at 1000 ×g for 10 min on RT to establish phase separation. The upper organic phase was collected. MTBE, methanol and ddH_2O were added to the remaining aqueous phase, and samples were vortexed and spun to establish phase separation. Combined organic phases of the double-extraction were dried under a stream of nitrogen, and lipids were reconstituted in 1:1 of $CHCl_3$: MeOH. The extract was re-suspended and diluted 20× using 2:1:1 isopropanol:acetonitrile:ddH_2O for UPLC-MS ESI+ analysis. The interphase was dried, lysed using 300–500 µl NaOH/SDS (0.3 N/0.1%), and proteins were quantified using BCA assay. Chromatographic separation was modified [347] using an AQUITY-UPLC system (Waters Corporation) and XEVO TQSµ Tandem Mass Spectrometer equipped with a Waters CSH (2.1 × 100 mm, 1.7 µm; CSH pre-column). The extract was diluted (For phase A; 10 mM ammonium formate and 0.1% formic acid (40:60, ddH_2O:acetonitrile) and for phase B; 10 mM ammonium formate and 0.1% formic acid (10:90, actetonitrile:isopropanol)) and injected for quantification as shown previously [347]. Lipid species/groups were analyzed by using multiple reaction monitoring (DG: [MNH_4] + to [RCOO+58] + of the respective esterified fatty acid; TAG: [MNH_4] + to [DG-

H_2O] + of the respective DG). Data were acquired with Target Lynx Software. Data were normalized for recovery, extraction, and ionization efficacy by calculating analyte/ISTD ratios (AU) and expressed as AU/mg tissue protein.

2.2.4 Obesity Post-Operative Surgical Outcome (OPOS) trial Study

Patients participating in this study were scheduled to undergo elective, first-time cardiac surgery at the New Brunswick Heart Centre in Saint John, NB and the Maritime Heart Centre (MHC) in Halifax, NS. Patients of normal weight and BMI of 18.5–24.9 kg/m^2 were considered as the control group (N-O; non-obese), BMI 25.0-29.9 kg/m^2 as pre-obese (P-O) and BMI 30.0–34.9 kg/m^2 as obese class-I (OC-I). To eliminate the effect of age, patients who were older than 75 years of age were not included in this study to exclude the effect of frailty on the physical ability for recovery. We are currently amending OPOS studies to account for frailty as an important variable to incorporate this variable into a comprehensive and complete assessment of surgical fitness. Patients who fulfilled the criteria were approached by the research coordinator and consented before surgery. During the surgery, right atrial appendage cardiac tissues were isolated by clean-cut punch of the atria and stored in -80℃ freezer for further analysis. Atrial appendages were homogenized and processed for western blot analysis. All protocols involving human subjects were approved by the Ethics Review Board of the Saint John Regional Hospital, New Brunswick (Protocol # 2014-2006) and the Ethics Review Board of the Dalhousie University, Nova Scotia.

2.2.5 Cell Culture

2.2.5.1 H9C2 cardiomyoblast culture

H9C2 rat embryonic cardiomyoblast (CRL-1446; ATCC) cells were cultured at a cell density of 4 x 10^5 in 60 mm plates and maintained in Dulbecco's modified Eagle's high-glucose medium (SH30243.01; DMEM-HG; Hyclone Laboratories, UT, USA) supplemented with 10% fetal bovine serum (1400-500; FBS, Seradigm) for 48 hr. H9C2 cardiomyoblasts were allowed to differentiate for 48 h in DMEM-1X medium (11966025; Thermo Fisher Scientific, MA, USA) supplemented with 0.5% FBS and 5 mM glucose. After 48 h of differentiation, cells were exposed

to high concentrations of glucose, palmitate and a combination of glucose and palmitate as described in section 2.2.5.4. Cells were then harvested in phosphate-buffered saline (0780; Amresco), followed by centrifugation at 10,000g for 10 min at 4˚C to pellet down the cells. Cell pellets were sonicated using lysis buffer (composition as described in tissue homogenization section 2.2.2., followed by centrifugation at 1500 x g for 10 min at 4˚C. The supernatant was transferred to another microfuge tube and protein concentrations were determined using the BCA protein assay kit (23255; Pierce, Thermo Fisher Scientific, Waltham, MA, USA). Lysates were stored at -80˚C for subsequent analysis.

2.2.5.2 Adult mouse cardiomyocyte isolation

Adult mouse cardiomyocytes (AMCMs) were isolated from male C57BL/6 mice anaesthetized using sodium pentobarbital 65 mg/kg as described previously [226,344]. Isolated hearts were perfused retrogradely by the non-circulating Langendorff method using the perfusion buffer (113 mM NaCl, 4.7 mM KCl, 0.6 mM KH_2PO_4, 0.6 mM Na_2HPO_4, 1.2 mM $MgSO_4.7H_2O$, 12 mM $NaHCO_3$, 10 mM $KHCO_3$, 10 mM HEPES, 30 mM Taurine, 10 mM BDM and 5.5 mM glucose, pH 7.4). The isolated ventricular myocytes were exposed to increasing concentrations of Ca^{2+} (100 μM, 400 μM and 900 μM) to render myocytes Ca^{2+} tolerant. Cardiomyocytes were plated on laminin-coated plates at a density of 40-60 x 10^3 cells/plate and incubated at 37°C. The media was changed to cardiomyocyte culture media (Minimum Essential Media containing 0.1% BSA, 10 mM BDM, 100 U/ml penicillin, 2 mM glutamine and 2 mM ATP) after 3 h of plating.

2.2.5.3 Preparation of bovine serum albumin complexed fatty acid

Bovine serum albumin (BSA, 68700-100, Proliant Biologicals) complexed fatty acid (FA) solution was prepared in DMEM-1X media using the BSA/fatty acid molar ratio of 3.9. 120 mM stock solution of sodium oleate (O7501; Sigma) and sodium palmitate (P9767; Sigma) was prepared separately in DMEM-1X media. For preparing the stock solution of 120 mM FA: briefly, 250.5 mg of palmitate or oleate was added to 15 ml of DMEM-1X media. Palmitate or oleate media was then placed into a boiling water bath. After five minutes, palmitate and oleate media were

vortexed and aliquoted into 1.5 ml Eppendorf tube and stored at -80℃. BSA and FA complexation involved: preparing 2% FA free-BSA in pre-warmed DMEM-1X media at 37℃. BSA media was dissolved by centrifuging the media at 2000 g for 5 min and warming the media at 50℃ for 15 mins. The resulting stock solution of FAs was mixed with 2% FA free-BSA (126575; Sigma Aldrich) solution to achieve the desired FA concentration. Subsequently, FA and BSA solutions were kept at 37˚C dry bath for 30 min to form complex. After 30 min, the media was sterile filtered using a 2 μm filter to treat cells. Polyunsaturated fatty acids (PUFA; arachidonic acid (AA), eicosapentaenoic acid (EPA) and linoleic acid (LA) were dissolved in 95% ethanol to prepare a stock concentration of 50 mM. PUFAs at a final concentration of 50 μM and 0.1% ethanol as vehicle control were complexed with 2% BSA prior to cell treatment. PUFAs were purchased from Nu-Check Prep (Elysian, MN) and were stored at -80℃ under nitrogen gas phase.

2.2.5.4 Cell culture treatment and harvesting

H9C2 cells were incubated with either 2% BSA (68700-100, Proliant Biologicals), glucose (G; 30 mM; DX0145; EMD Chemicals), palmitate (P; 1.2 mM) or fructose (F; 5, 30 and 50 mM, F3510, Sigma), a combination of fructose/palmitate (FP; 30/0.8 and 30/1.2 mM), a combination of glucose/palmitate (GP; 30/1.2 mM) or polyunsaturated fatty acids (AA, EPA or LA; 50 μM) for 16 h. Following 16 h of incubation with different substrates, cells were harvested in cold 1 X phosphate-buffered saline (20-031-CV, Corning), followed by centrifugation at 10,000 g for 10 min at 4˚C to pellet down cells. The cell pellet was sonicated using a lysis buffer and centrifuged at 1500 g for 15 min at 4˚C. Subsequently, the supernatant was collected, and protein concentrations were determined using the BCA protein assay kit (23255; Pierce, Thermo Fisher Scientific, Waltham, MA, USA). Lysates were stored at -80℃ for subsequent biochemical analysis.

2.2.6 Immunoblot analysis

Heart lysates containing 20-30 μg of proteins were subjected to sodium dodecyl sulfate-polyacrylamide (SDS) gel electrophoresis. Proteins were transferred onto a nitrocellulose membrane. Blotted proteins were visualized using reversible Coomassie stain (24580; MemCode

Reversible protein Stain, Pierce, Thermo Fisher Scientific, Waltham, MA, USA) and targets probed using the primary antibodies: anti-LC3B (2775S; Cell Signaling, Beverly, MA, USA), anti-LAMP-2A (18528; Abcam, Toronto, ON, Canada), anti-Cleaved Caspase-3 (9664; Cell Signaling), anti-Bcl2 (SC-7351; Santa Cruz Biotechnology), anti-TFEB (A303-673a-T; Bethyl Labs), anti-HA (2362; Cell Signaling), anti-MYC (132500; Life Technologies.), anti-KLF15 (NBP2-24635; Novus Biologicals), anti-PPARα (P0369; Sigma Aldrich), anti-CD36 (NB400-144; Novus Biologicals), anti-Pan Actin (sc-1616; Santa Cruz Biotechnology, TX, USA), anti-JNK Thr^{183}/Tyr^{185} (9251; Cell Signaling), anti-p62 (03-GP62-C; American Research), anti-RAN GTPase and anti-Atg7 (2631; Cell Signaling.). Immunoblots were developed using the Western Lightning Plus-ECL to enhance chemiluminescence substrate (NELI05001EA; Perkin Elmer, Waltham, MA). Densitometric analysis was performed using Image Lab software (Bio-Rad), and protein levels were corrected to protein stain.

2.2.7 Cathepsin B Activity

Cathepsin B is a lysosomal cysteine proteases enzyme that hydrolyzes proteins and cleaves substrates at the carboxyl side of the Arg-Arg bond. The substrate N-Suc-Leu-Leu-Val-Tyr-7-AMC (S6510; Sigma, MA, USA) was used for the fluorometric detection of cathepsin B activity. The fluorescence of the free aminomethyl coumarin released was measured. Cathepsin B activity was measured in tissue or cellular lysates. A standard curve was prepared in the range of 300 nM to 12.5 nM using 7-Amino-4-Methylcoumarin (26093-31-2; Enzo, Alfa Aesar). Briefly, standards, samples and cathepsin B enzyme (BML-SE198-0025; Enzo life sciences, NY, USA) were added into 96 well microtiter plates. Following the addition of standards, samples and cathepsin B, activation buffer L-Cysteine (prepared in a buffer containing 352 mM potassium phosphate monobasic, 48 mM sodium phosphate dibasic and 4.0 mM EDTA at 40° C, pH 6.0) was added to get the final concentration of 8.0 mM. The volume of each well was made up to 150 µl by adding 0.1% of Brij 35 solution (0281; Amresco, OH, USA, 0.1% V/V of 30% w/v Brij solution in water). Lastly, the fluorogenic substrate at a final concentration of 0.006 mM was added into the sample

and control wells, and the plate was mixed immediately using thermo mixture. The intensity of fluorescence was measured in triplicate using the Synergy H4 fluorescence plate reader at the excitation wavelength of 360 nm and the emission wavelength of 440 nm from 0-60 min time point at 37℃. Data are presented as RFU/min/µg of proteins.

2.2.8 Statistical Analysis

Results are expressed as mean ± SEM. A pairwise comparison between groups was performed using unpaired two-tailed Student's t-test. Comparisons between multiple groups were performed using one- or two-way ANOVA followed by a Bonferroni or Tukey post hoc test, as appropriate. All statistical analysis was performed using Prism (GraphPad Software). P-values of less than 0.05 were considered statistically significant. For animal studies, "n" refers to the number of mice used, unless otherwise specified. For cell culture studies, experiments were performed in triplicates and data are from at least three independent experiments.

2.3 Results

2.3.1 Time-dependent decline in nuclear TFEB content in the heart from high-fat high-sucrose (HFHS)-fed mice

Using a murine mouse model of diet-induced obesity, previously, our laboratory demonstrated a significant depletion of nuclear TFEB content in the heart of mice fed HFHS diet at 16 weeks [226]. However, the onset of TFEB depletion during the progressive feeding of the HFHS diet and whether changes in TFEB content were associated with altered lysosome function were not ascertained. To assess the longitudinal changes in cardiac TFEB levels, we subjected C57BL6J mice subjected to progressive feeding of HFHS diet for 4, 8, 12 and 16 weeks**.**

Cellular lipid content and type of lipids are crucial for the lysosomal membrane lipid composition, necessary for the stability of lysosomal membrane proteins such as lysosome-associated membrane protein 2A (LAMP-2A), an indicator of lysosomal abundance and function [348]. We first examined if diet-induced obesity negatively affected proteins involved in lysosome-

dependent proteolysis. We observed that LAMP-2A protein content was significantly increased 4 (1.5 fold) and 8 weeks (1.6 fold) post-HFHS diet-feeding compared to chow-fed mouse heart, whereas this increase was modest post 12 weeks (1.2 fold) of HFHS-feeding **(Figure 2.1 A, C, D and E).** Furthermore, LAMP-2A content was significantly decreased in mice hearts after 16 weeks (-0.43 fold) of HFHS-feeding [226] **(Figure 2.1 B and F)**. Progressive decline in cardiac LAMP-2A abundance during diet-induced obesity also corresponded with changes in the lysosomal proteolytic capacity as examined by measuring cathepsin B activity, a readout of lysosomal function **(Figure 2.1 G-J).** We observed a robust increase in cathepsin B activity in mice heart post 4 (1.35 fold) and 8 weeks (2.26 fold) of HFHS diet-feeding compared to chow-fed mice heart, while a negligible increase in the activity was observed post 12 weeks (1.01 fold) of HFHS diet-feeding **(Figure 2.1 G, H and I).** Importantly, cathepsin B activity was significantly suppressed at 16 weeks (-0.71 fold) post-HFHS diet-feeding compared to chow diet-feeding [226] **(Figure 2.1 J)**. Surprisingly, despite the early increase in myocardial lysosomal content and function following exposure to HFHS diet, nuclear TFEB content decreased progressively from 8 (-0.87 fold), 12 (-0.78 fold) and 16 weeks (-0.71 fold) in HFHS diet-fed mouse heart when compared to the corresponding chow-fed group **(Figure 2.2 A, B, K, L, M and N).** These findings indicate that lysosomes adapt to an acute nutrient overload (4 weeks) by augmenting lysosomal content and function independently of changes in TFEB levels. However, prolonged nutrient overload (8-16 weeks) precipitates a decline in TFEB levels, leading to loss of lysosomal adaptation to augment lysosome content and function in the mouse heart **(Figure 2.2)**.

2.3.2 Increased myocardial triacylglycerol accumulation in the heart of mice fed HFHS diet

We next examine whether the gradual decline in TFEB level is associated with changes in lipid utilization in mice hearts with chronic nutrient overload. We performed the lipidomic analysis

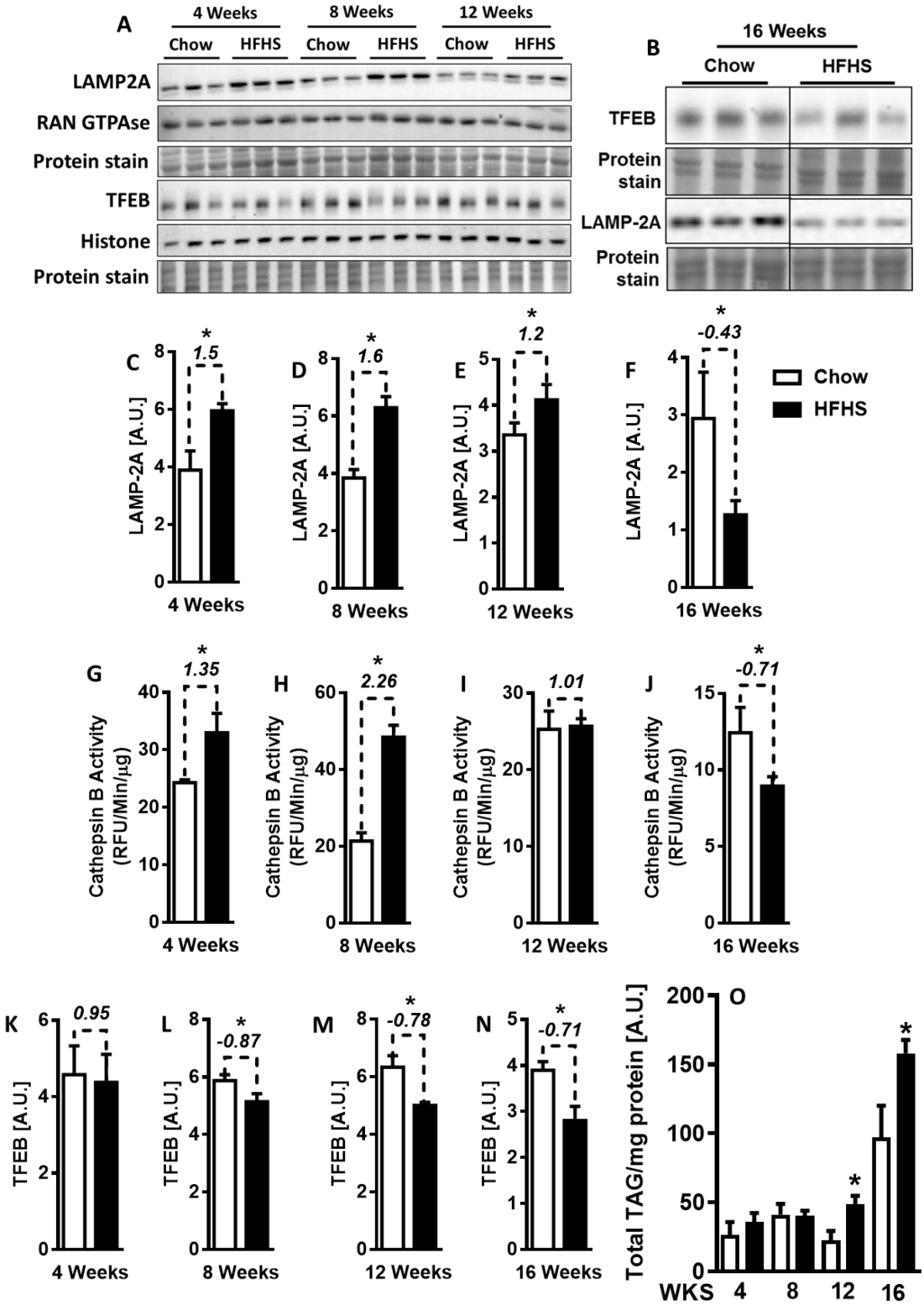
A
4 Weeks
8 Weeks
12 Weeks
Chow
HFHS
LAMP2A
RAN GTPAse
Protein stain
TFEB
Histone
Protein stain
B
16 Weeks
Chow
HFHS
TFEB
Protein stain
LAMP-2A
Protein stain
C
D
E
F
LAMP-2A [A.U.]
1.5
1.6
1.2
-0.43
4 Weeks
8 Weeks
12 Weeks
16 Weeks
Chow
HFHS
G
H
I
J
Cathepsin B Activity (RFU/Min/μg)
1.35
2.26
1.01
-0.71
4 Weeks
8 Weeks
12 Weeks
16 Weeks
K
L
M
N
TFEB [A.U.]
0.95
-0.87
-0.78
-0.71
4 Weeks
8 Weeks
12 Weeks
16 Weeks
O
Total TAG/mg protein [A.U.]
WKS 4 8 12 16

Figure 2.1. Progressive decline in nuclear TFEB content of the heart of mice fed high-fat high sucrose (HFHS)-fed diet. (A and B) Immunoblot and densitometric analysis of protein expression of cytosolic (C, D, E and F) LAMP-2A and (G, H, I and J) cathepsin B activity in the heart from C57BL6J male mice fed either chow or HFHS diet for 4, 8, 12 and 16 weeks. (A and B) Immunoblot and densitometric analysis of protein expression of nuclear (K, L, M and N) TFEB and (O) total TAG levels in the heart from C57BL6J male mice fed either chow or HFHS diet for 4, 8, 12 and 16 weeks. Graph represents mean ± S.E.M., n = 3 to 5 to 5, *P < 0.05 Vs Chow diet was performed using Student's t-test. A.U.; arbitrary unit, P Stain; Protein stain.

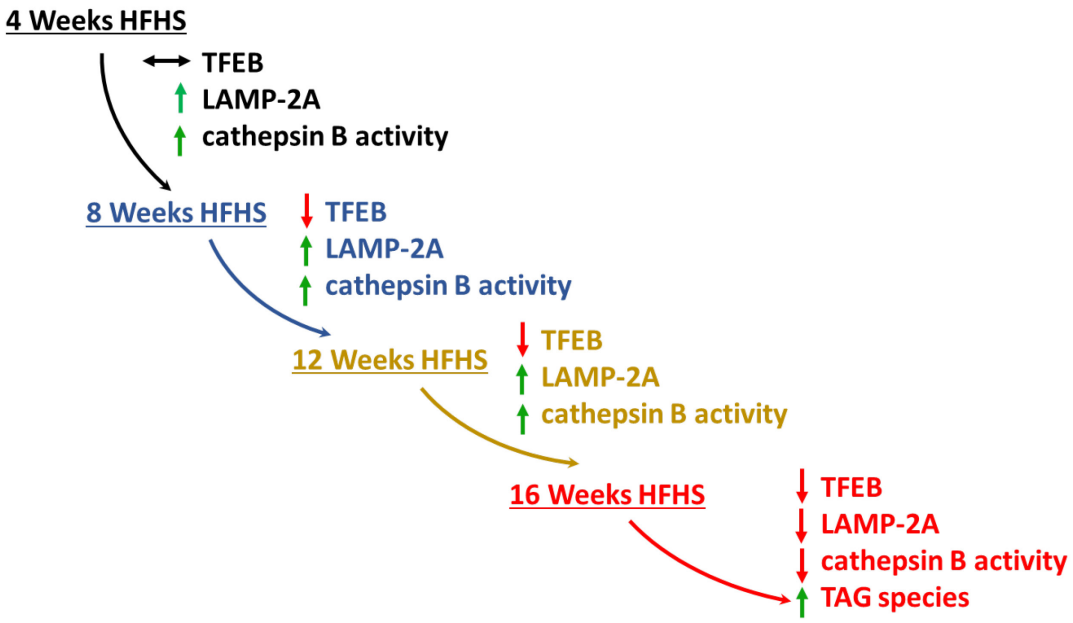

Figure 2.2. Progressive decline in nuclear TFEB content in the heart of mice fed high-fat high sucrose (HFHS)-fed diet.

to evaluate the lipid utilization in the mouse heart during DIO. Cardiac lipidomic analysis revealed a global increase across most triacylglycerol (TAG) species (50:3 (18:1), 52:2, 52:4, 54:3 and 56:5, 52:3, 54:4 (18:1), 54:4 (18:2), 50:3 (16:0), 54:2 (18:1)) post 16 weeks of HFHS-feeding compared to chow-fed diet **(Table 2.1).** Furthermore, the heart from 12 weeks of HFHS diet-fed mice exhibited significantly increased levels of TAG acyl chains such as 50:3 (18:1), 52:2, 52:4, 54:3 and 56:5 **(Table 2.1).** Not only distinct species of TAG but also total TAG content in the mouse heart were significantly increased post 12 and 16 weeks of HFHS diet feeding compared to chow-fed mouse heart **(Figure 2.1 O)**. Notably, most diacylglycerol (DAG) species were significantly decreased in the heart of the mouse fed HFHS diet for 4 and 8 weeks compared to chow-fed mouse heart **(Table 2.2).** Whereas DAG species with acyl chain length of 32:1, 36:1 and 38:5 were significantly increased in 16 weeks of HFHS diet-fed mouse heart compared to chow-fed **(Table 2.2)**. These data suggest an accumulation of distinct species of TAG and DAG in the mouse heart at different times following HFHS diet-feeding. Furthermore, these data reveal that in the obese mouse heart, a decline in nuclear TFEB content and impaired lysosomal function are associated with marked elevation of specific lipid species questioning the causal or effector role of TFEB in regulating cardiac lipid metabolism.

2.3.3 TFEB content is decreased in hearts of Class-I Obese patients

We next determined if our preclinical data extended to the human population, specifically in obese and diabetic patients with CVD. We measured TFEB protein expression in atrial appendages from patients with increased severity of obesity and diabetes. All patients involved in OPOS (Impact of **O**besity on **P**rospective **O**utcomes following cardiac **S**urgery, TCPS-2–2014) trial study were registered to undergo cardiac surgery [349]. Patients scheduled to undergo cardiac surgery were stratified as per their body mass index (BMI) as non-obese (N-O, BMI 18.5-24.9 kg/m^2), pre-obese (P-O, BMI 25-29.9 kg/m^2) and obese class-I (OC-I, BMI 30-34.9 kg/m^2) **(Figure 2.3 A).** We observed a significant decline in TFEB expression in atrial appendages from OC-I patients compared to both N-O and P-O patients **(Figure 2.3 B-C).** Furthermore, the decrease

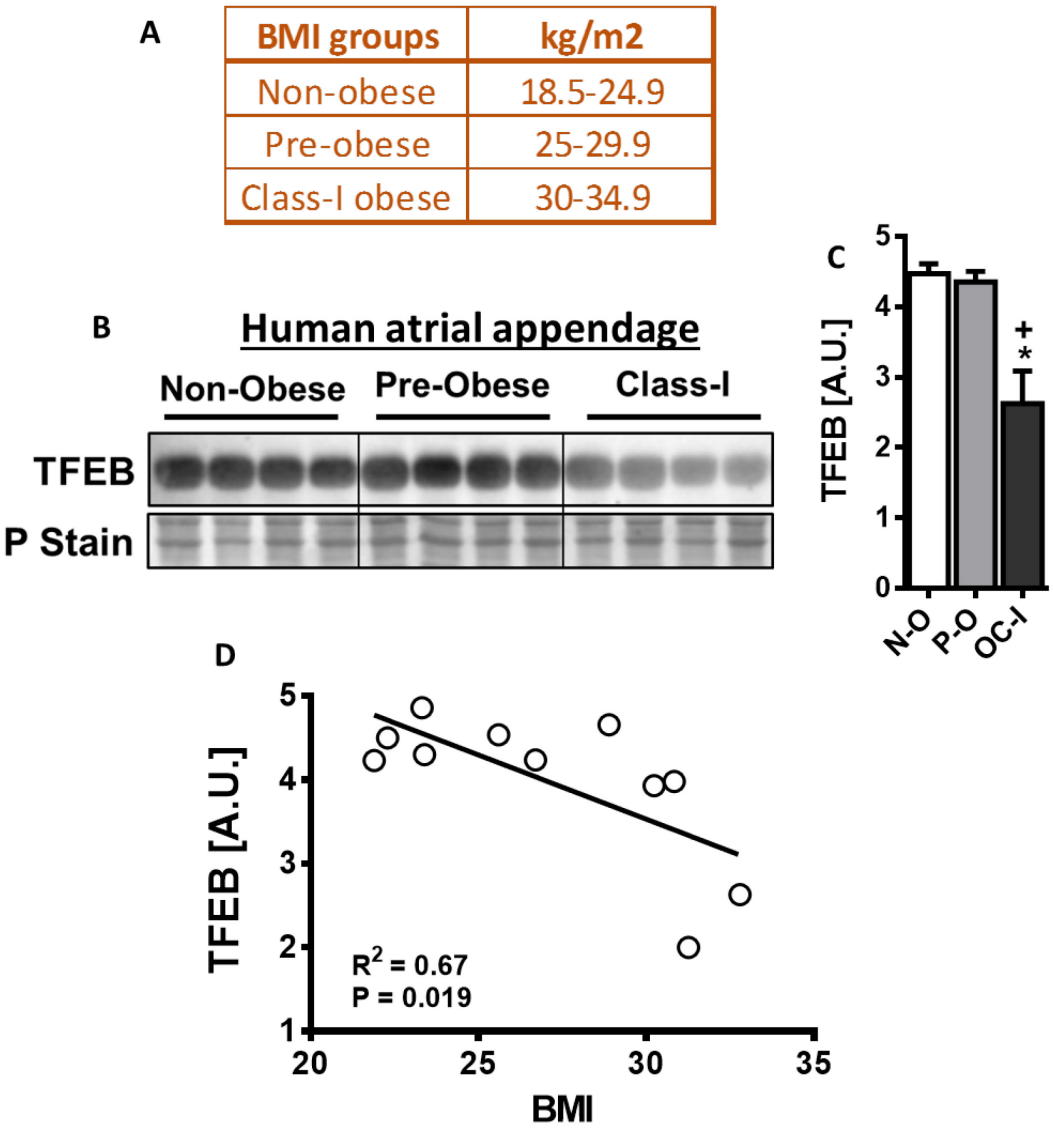

Figure 2.3 TFEB expression in atrial appendage from obese class-I patients negatively correlates with BMI. (A) Classification of body mass index (BMI). (B) Immunoblot and densitometric analysis of protein expression of (C) TFEB from total lysate in atrial appendage from non-obese (N-O), pre-obese (P-O) and obese class-I (OC-I) individuals. (D) Linear regression curve of TFEB protein expression vs BMI of N-O, P-O and OC-I individuals. Graph represents mean ± S.E.M., n=3 to 4 patients per group, *P<0.05 vs non-obese (N-O) and +P<0.05 vs pre-obese (P-O); one-way ANOVA; A.U.; arbitrary unit.

in TFEB expression was inversely correlated with the patient's BMI **(Figure 2.3 D).** These findings from our clinical study suggested that, as the severity of obesity and diabetes progresses, TFEB levels decrease in the human heart.

2.3.4 The saturated fatty acid palmitate depletes TFEB and suppresses proteolytic activity in a concentration- and time-dependent manner in H9C2 cells

Previously our laboratory demonstrated that cardiomyocytes exposed to 1.2 mM palmitate decreased cellular TFEB protein content with a marked reduction in the lysosomal function [226]. We next tested whether palmitate declines TFEB content in a time- and concentration-dependent manner. Treatment of H9C2 cells with 0.8 mM palmitate for 16 h decreased cellular TFEB levels compared to the BSA control group, whereas 1.2 mM significantly decreased TFEB levels compared to BSA, 0.2 mM and 0.4 mM palmitate **(Figure 2.4 A and B)**. Since TFEB is a master regulator of lysosomal content and function, we then assessed the lysosomal function by measuring the lysosomal proteolytic activity of the cathepsin B enzyme. We observed that a decrease in cellular TFEB content was associated with suppression in cathepsin B activity in a concentration-dependent manner at 0.4 mM, 0.6 mM, 0.8 mM and 1.2 mM palmitate treatment compared to 0.2 mM palmitate and BSA control group **(Figure 2.4 C)**. We next sought to determine the concentration of palmitate, which was sufficient to induce activation of stress and cell death pathways in H9C2 cells. We observed concentration-dependent activation of stress-activated protein kinase Jun amino-terminal kinase (JNK) 1 and 2 by 0.4 mM, 0.6 mM, 0.8 mM and 1.2 mM palmitate compared to the BSA control group, demonstrated by increased phosphorylation of JNK1/2 at Thr183 and Tyr185 residues **(Figure 2.4 A, D)**. Since activation of JNK has been reported to initiate apoptotic cellular death processes [350], we examined the protein expression of cleaved caspase-3, an executor of cellular apoptosis [351]. Indeed, the expression of cleaved caspase-3 was significantly increased with palmitate treatment at concentrations of 0.6 mM, 0.8 mM and 1.2 mM when compared with 0.2 mM palmitate and BSA control group **(Figure 2.4 A, E)**. Furthermore, 1.2 mM palmitate treatment significantly increased cleaved to total caspase-3

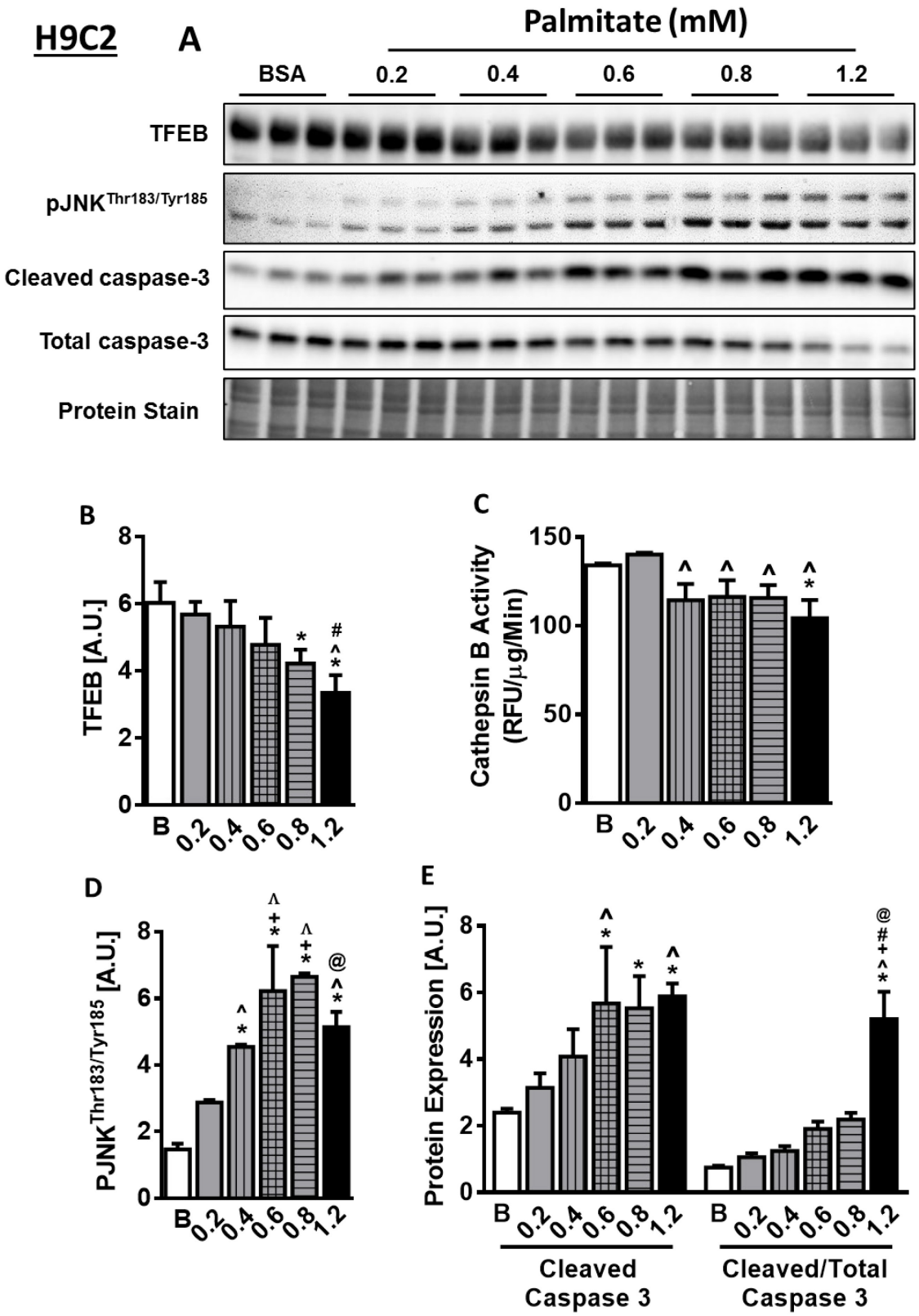
H9C2
A
Palmitate (mM)
BSA
0.2
0.4
0.6
0.8
1.2
TFEB
pJNK Thr183/Tyr185
Cleaved caspase-3
Total caspase-3
Protein Stain
B
TFEB [A.U.]
C
Cathepsin B Activity (RFU/μg/Min)
D
PJNK Thr183/Tyr185 [A.U.]
E
Protein Expression [A.U.]
Cleaved Caspase 3
Cleaved/Total Caspase 3

Figure 2.4 Saturated fatty acid palmitate depletes TFEB content in a concentration-dependent manner in H9C2 cells. H9C2 cells were incubated with either BSA or 0.2 mM, 0.4 mM, 0.6 mM, 0.8 mM and 1.2 mM palmitate for 16 h. (A) Immunoblot and densitometric analysis of protein expression of (B) TFEB and cathepsin B activity (C) in H9C2 cells treated with different concentrations of palmitate. (A) Immunoblot and densitometric analysis of (D) phosphorylated $JNK^{Thr183/Tyr185}$, (E) cleaved caspase-3 and (E) cleaved/total caspase-3 ratio in H9C2 cells treated with different concentrations of palmitate. Graph represents mean ± S.E.M., n = 3, *P < 0.05 vs BSA, ^P < 0.05 vs 0.2 mM palmitate, +P < 0.05 vs 0.4 mM palmitate and #P < 0.05 vs 0.6 mM palmitate and @P < 0.05 vs 0.8 mM palmitate, one-way ANOVA; A.U.; arbitrary unit.

ratio compared to BSA control and 0.2 mM, 0.4 mM, 0.6 mM and 0.8 mM palmitate **(Figure 2.4 A, E)**.

Furthermore, to assess if palmitate's effect on regulating TFEB is species-specific, we utilized HL-1 cells, an atrial tumor cell line derived from adult female mice [352,353]. Unlike H9C2 cells, HL-1 cells exhibit augmented sensitivity to the effects of palmitate. We noticed that palmitate treatment at a concentration as low as 0.4 mM to 0.6, 0.8 and 1.2 mM for 16 h decreased TFEB levels and increased cleaved to total caspase-3 ratio compared to BSA control and 0.2 mM palmitate **(Figure 2.5 A-B)**. Our laboratory previously reported a comparable reduction in TFEB content in neonatal rat ventricular cardiomyocytes (NRCMs) following treatment with 0.4 mM palmitate for 16 hr [226]. Furthermore, in HL-1 cells, despite a reduction in TFEB levels after 0.4 mM palmitate treatment, cathepsin-B activity was suppressed only at 0.8 mM and 1.2 mM concentration of palmitate **(Figure 2.5 D)**, suggesting that a decrease in TFEB primes the myocyte to suppress proteolytic activity. In addition to cell lines, we also recapitulated in vitro data in a primary cell culture model of adult mouse cardiomyocytes (AMCM), wherein AMCM exposed to 1.2 mM palmitate for 12 h decreased TFEB levels, an effect not observed at 8 h **(Figure 2.5 E-F)**. Together, these data using in vitro and *ex-vivo* cell culture models definitively establish that palmitate decreases TFEB content in a concentration- and time-dependent manner.

2.3.5 Polyunsaturated fatty acids and fructose do not alter TFEB content in H9C2 cells

Since glucose, oleate, and palmitate exerted differential effects on TFEB levels, autophagy induction and cellular viability [226], we also determined the effect of polyunsaturated fatty acids (PUFAs) such as arachidonic acid (AA), eicosapentaenoic acid (EPA) and linoleic acid (LA) on TFEB levels and autophagy induction. Given that PUFAs play a pivotal role in cellular signaling more so than metabolism, we chose a concentration of 50 μM PUFA that is reported to trigger a myriad of biological effects [354]. To examine the impact of PUFA on myocyte autophagy and autophagic flux, we examined the conversion of pre-autophagosome bound microtubule protein LC3B-I to the autophagosome-bound lipidated form of LC3B-II in the presence or absence of

lysosomal de-acidifier, CQ. Unlike palmitate [226], we observed that H9C2 rat embryonic cardiomyoblast cells treated with AA, EPA and LA for 16 h did not alter baseline autophagy compared to its BSA control group **(Figure 2.6 A-B, E-F and I-J)**. We observed that in the absence of autophagy inhibitor chloroquine (CQ), LC3BII/I ratio did not change in response to AA, EPA and LA exposure for 16 h compared to their respective BSA control group **(Figure 2.6 A-B, E-F and I-J)**. Furthermore, CQ treatment elicited a higher response of autophagosome accumulation in cells treated with AA (9.66 vs 7.67 fold, **Figure 2.6 A-B)** and EPA (6.9 vs 5.91 fold, **(Figure 2.6 E-F)** as measured by an increase in LC3BII/I ratio at 16h post-PUFA exposure. Unlike AA and EPA, LA did not potentiate autophagosome accumulation following CQ treatment (4.89 vs 4.86 fold, **Figure 2.6 I-J)** when compared to the BSA group. Notably, EPA treatment significantly increased caspase-3 cleavage in H9C2 cells **(Figure 2.6 G-H)**. In contrast to EPA, AA and LA treatment did not increase cleaved caspase-3 content in H9C2 cells **(Figure 2.6 C-D and K-L)**. Since TFEB transcriptionally regulates proteins involved in autophagy flux, we next ascertained whether PUFA treatment for 16 h alters TFEB protein levels in H9C2 cells. Strikingly, H9C2 cells treated with PUFA did not display alterations in cellular TFEB content **(Figure 2.6 C-D, G-H and K-L)**, suggesting that PUFA-induced changes in myocyte autophagy is likely independent of TFEB action and fatty acid's effect to downregulate TFEB is likely specific to saturated FA, palmitate. In addition to FAs, we also assessed whether different carbohydrates alter TFEB protein content. We have previously demonstrated that monosaccharide, glucose did not alter TFEB levels, lysosomal autophagy and lysosome function compared to the control group [226]. In the present study, similar to glucose, fructose alone or in combination with glucose did not alter cellular TFEB content **(Figure 2.7 A-B)**. Whereas fructose, in conjunction with palmitate exacerbated palmitate-induced decrease in TFEB levels, similar to the effect observed with a combination of glucose and palmitate treatment **(Figure 2.7 C-D)**. Together, these data suggest that unlike palmitate, TFEB content is unaltered when myocytes are exposed to either PUFA or fructose alone.

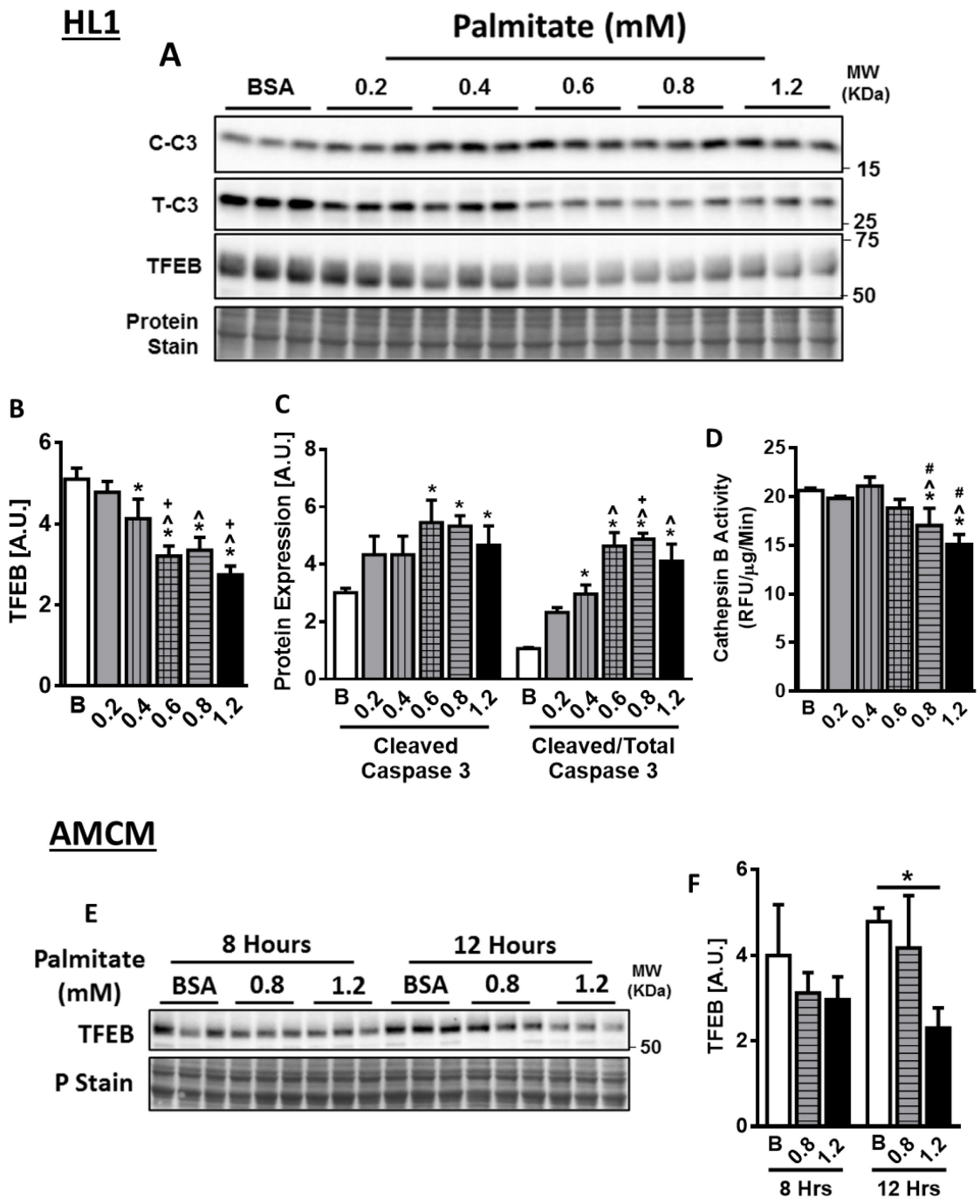

Figure 2.5 Saturated fatty acid, palmitate depletes TFEB content in a concentration-dependent manner in HL1 cells and adult mouse cardiomyocytes. HL1 cells were incubated with either BSA or 0.2 mM, 0.4 mM, 0.6 mM, 0.8 mM and 1.2 mM palmitate for 16 h. (A) Immunoblot and densitometric analysis of protein expression of (B) TFEB, (C) cleaved caspase-3, (C) cleaved/total caspase-3 ratio and (D) cathepsin B activity in HL1 cells treated with different concentrations of palmitate. Graph represents mean ± S.E.M., n = 3, *P < 0.05 vs BSA, ^P < 0.05 vs 0.2 mM palmitate, +P < 0.05 vs 0.4 mM palmitate and #P < 0.05 vs 0.6 mM palmitate, one-way

ANOVA; A.U.; arbitrary unit. Adult mouse cardiomyocytes treated with either BSA, 0.8 mM or 1.2 mM palmitate for 8 h or 12 h. (E) Immunoblot and densitometric analysis of (F) TFEB protein expression. Graph represents mean ± S.E.M., n = 3, *P < 0.05 vs BSA and 0.8 mM palmitate was performed using one-way ANOVA; A.U.; arbitrary unit.

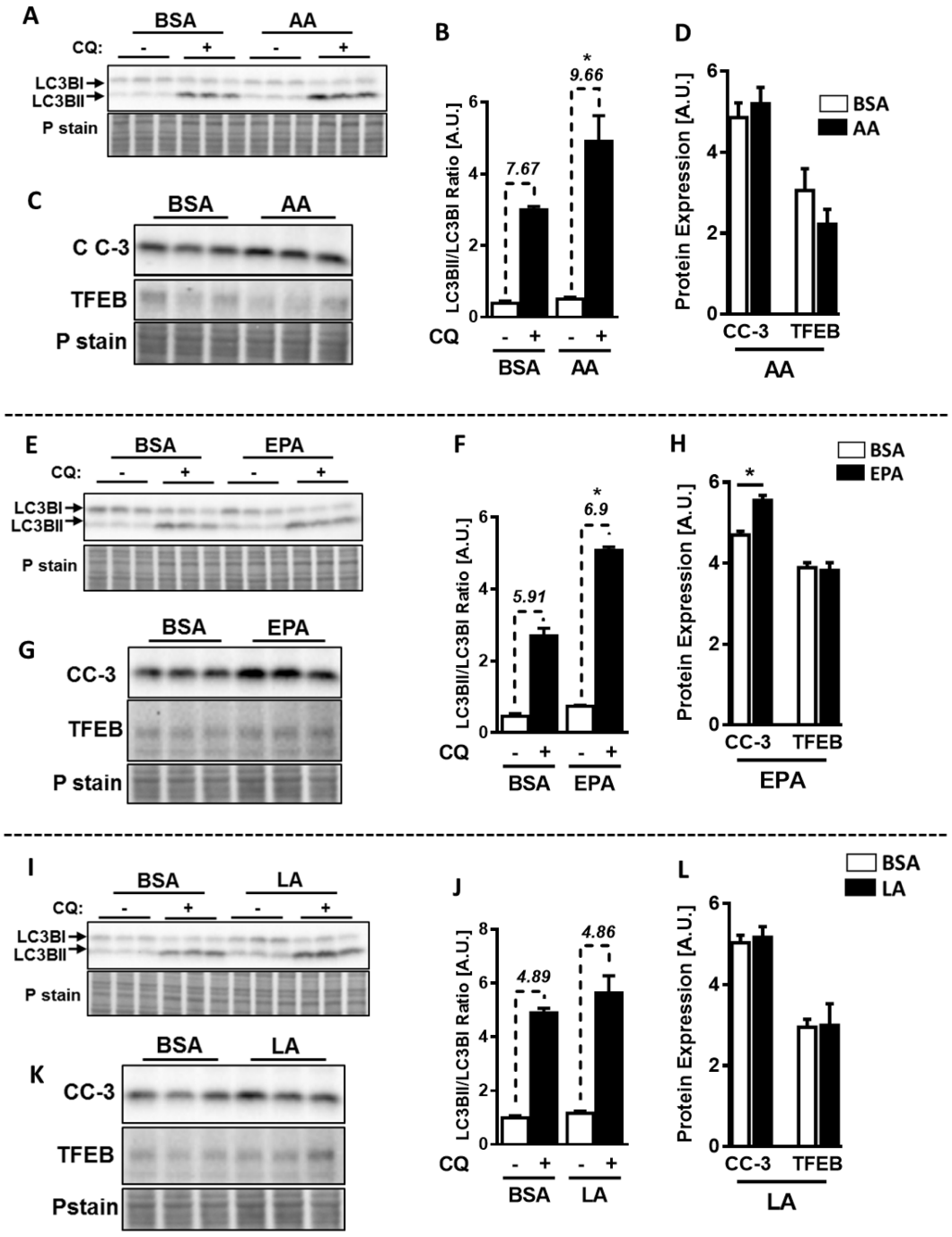

Figure 2.6 AA and EPA but not LA increase autophagic flux in H9C2 cardiomyoblasts independent of changes in TFEB content. H9C2 cells were incubated with either BSA, arachidonic acid (AA, 50 μM), eicosapentaenoic acid (EPA, 50 μM) or linoleic acid (LA, 50 μM) for 16 h. After 16 h, cells were treated with either vehicle or chloroquine (CQ; 200 μM) for 3 h in the presence of nutrient-deprived media, EBSS to assess autophagic flux. (A, C, E, G, I and K) Immunoblot and densitometric analysis of protein expression of (B, F and J) LC3B, (D, H and L) cleaved caspase-3 (CC-3) and (D, H and L) TFEB. *P<0.05 performed using student's t-test; A.U.; arbitrary unit, P Stain; protein stain.

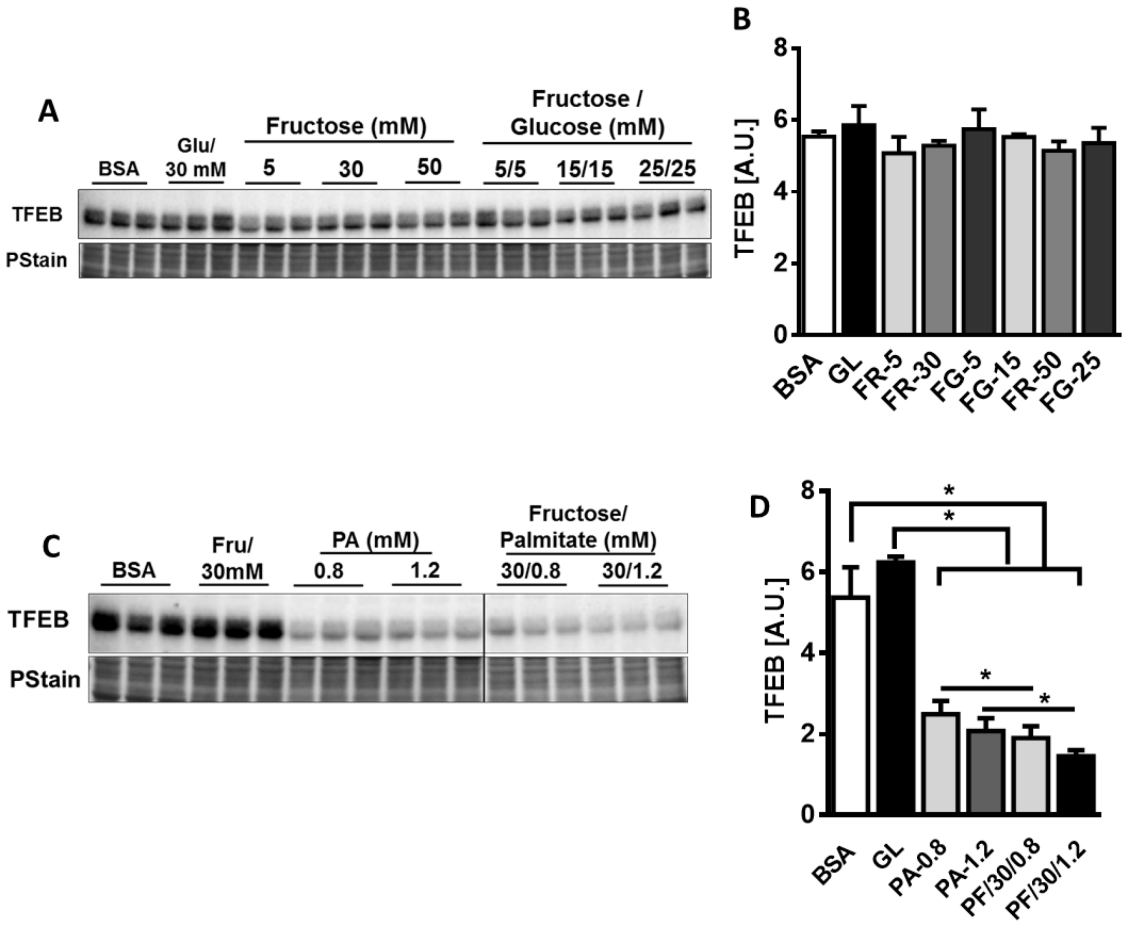

Figure 2.7 TFEB protein expression is unaltered by fructose in H9C2 cells. H9C2 cells incubated with either BSA, glucose (GL; 30 mM), fructose (FR; 5, 30, 50 mM), palmitate (PA; 0.8 or 1.2 mM), a combination of fructose/glucose (FG; 5/5, 15/15 or 25/25 mM) or a combination of palmitate/fructose (PF; 30/0.8 or 30/1.2 mM) for 16 h. (A and C) Immunoblot and densitometric analysis of protein expression of (B and D) TFEB. Graph represents mean ± S.E.M., n = 3, *P<0.05 performed using one-way ANOVA; A.U.; arbitrary unit.

2.4 Discussion

Nutrients exhibit a distinct effect on proteins involved in the autophagy machinery in the heart [226,355], skeletal muscle and liver [354,356]. We reported decreased autophagic flux and lysosome function in the cardiomyocyte exposed to palmitate [226], which is in contrast to a prior study, wherein, palmitate augments autophagy in U2OS (osteosarcoma) cells [354,357]. However, our findings on PUFA (AA and EPA) in cardiomyoblasts agree with previous reports, wherein PUFA increased autophagic flux upon chloroquine incubation in U2OS cells [354,357]. Furthermore, saturated fatty acid, palmitate alone downregulated TFEB in cardiomyoblasts and cardiomyocytes in a concentration- and time-dependent manner. Moreover, the suppression in TFEB levels was associated with concentration-dependent augmentation of stress and cell death pathways. We did not observe changes in TFEB levels upon exposure to unsaturated fatty acid, oleate [226] and PUFA such as AA, EPA and LA. In contrast to our finding, in U2OS (osteosarcoma) cells, AA and palmitate increased nuclear TFEB levels [357]. Not only fatty acids and amino acids but also carbohydrate exerts (monosaccharide vs disaccharide) a distinct effect on autophagy and TFEB. In the cardiomyocytes, monosaccharide sugars such as glucose and fructose had a negligible impact on the autophagic process and TFEB content in the absence of fatty acid co-incubation. Unlike monosaccharides, disaccharide sugar trehalose increased TFEB protein content in macrophages [332]. The heterogeneity of autophagic responses to nutrients across different studies can be attributed to the type, concentration and duration of carbohydrate and FA treatment and the cell type employed in the study. These inconsistencies are also compounded due to the lack of information on lysosomal content and proteins in regulating lysosome signaling, metabolism and function. Our data also imply that different FAs, depending on their carbon chain length, exhibit distinct effects on lysosomal autophagy and function, an effect dependent or independent of TFEB.

Accumulating evidence supports a robust association between increased accumulation of myocardial lipids and cardiac dysfunction in rodents and humans [358-360]. We examined whether

the alteration in TFEB levels *in-vivo* is dependent on progressive changes in myocyte lipidome. Lipidomic analysis revealed a significant increase in DAG and TAG species in the mouse heart following chronic nutrient overload (16 weeks), but not after acute fat feeding (4 weeks). Sustained nutrient overload for 16 weeks revealed an abundance of acyl TAG species with 54 carbons (54:2, 54:3, 54:4 (18:1) and 54:4 (18:2)) and DAG species (32:0, 32:1, 36:1 and 38:5). A prior study from Bruneck cohort identified plasma TAG 54:2 as a strong predictor for cardiovascular disease [360]. In addition to DAG and TAG, acylcarnitine [361,362], ceramides [363], phosphatidylcholine (PC), phosphatidylethanolamine (PE) and sphingomyelin (SM) species are among the lipid classes identified as potential biomarkers associated with changes in cardiac function during obesity and diabetes [364,365]. Strikingly, following the short-term feeding of HFHS diet, lysosomal content and proteolytic activity were augmented in the mouse heart, changes preceding the onset of cardiac dysfunction. However, long-term feeding of HFHS diet suppressed lysosomal function and downregulated TFEB in the heart. In support of our finding, a prior study showed altered lysosomal membrane lipid composition and autophagosome-lysosome fusion in the liver of mice subjected to chronic high-fat-diet (60% Kcal fat) [366], highlighting the impact of excess intracellular lipid loading in perturbing lysosome function. Furthermore, our preclinical findings were recapitulated in the heart from patients with class-I obesity, suggesting that TFEB levels are negatively correlated with cardiovascular comorbidity progression during obesity and diabetes. Collectively, our data suggest that during acute nutrient overload, lysosome function is upregulated to accommodate the increasing burden of myocyte nutrient intake; however, following chronic caloric surplus, downregulation of TFEB and ensuing lysosomal dysfunction render cardiomyocytes susceptible to metabolic remodeling and failure.

Impaired proteostasis and resulting proteotoxicity is a hallmark of the failing heart [188]. In agreement with our findings, a prior study demonstrated decreases in TFEB protein expression and defective lysosome function in heart from patients with amyloid cardiomyopathy [345]. We theorize that impaired protein degradation within the lysosome in the early stages of obesity and

diabetes could initiate maladaptive buildup of cytotoxic proteins precipitating cardiac dysfunction. Indeed, lysosomal dysfunction and inhibition of autophagy are observed in ischemia-reperfusion injury [247], obesity and diabetes-related cardiomyopathy [226,355,367], doxorubicin-induced cardiotoxicity [344] and in hearts from patients with mutations in proteins regulating protein quality control [345,368]. Our laboratory [226] and others [369,370] demonstrated that injury to cardiomyocytes via nutrient overload or hypoxic stress decreases nuclear TFEB content, increases inhibitory phosphorylation of TFEB with a concomitant decline in lysosomal content and proteolytic activity. We also demonstrated that loss of TFEB and lysosomal insufficiency are among the earliest insults to cardiomyocytes following metabolic stress, which results in ER stress, dysregulation of autophagy, cell death, causing myocyte dysfunction.

2.5 Tables

Table 2.1:

TAG species	Chow-4W	HFHS-4W	CHow-8W	HFHS-8W	Chow-12W	HFHS-12W	Chow-16W	HFHS-16W
50:1(16:0)	3.084 ± 1.607	3.012 ± 0.517	3.530 ± 0.766	3.564 ± 0.422	2.220 ± 0.693	3.970 ± 0.763	6.68 ± 3.314	9.825 ± 1.174
50:2(16:0)	3.026 ± 1.548	2.272 ± 0.385	3.446 ± 0.795	2.652 ± 0.334	2.160 ± 0.635	3.160 ± 0.644	7.350 ± 3.156	10.065 ± 1.951
52:2(16:0)	3.478 ± 1.726	3.718 ± .680	3.814 ± 0.790	4.436 ± 0.481	2.334 ± 0.659	5.4775 ± 0.649*	4.895 ± 1.689	14.175 ± 1.881*
52:3(16:0)	4.532 ± 1.880	3.892 ± .646	4.720 ± 0.926	4.694 ± 0.503	3.018 ± 0.765	4.778 ± 0.852	7.925 ± 2.507	14.900 ± 2.068*
54:3(18:1)	6.098 ± 2.767	6.872 ± 1.373	5.962 ± 1.222	7.348 ± 0.682	3.702 ± 0.955	7.960 ± 1.402*	7.820 ± 3.345	27.900 ± 4.482*
54:4(18:1)	7.914 ± 2.821	6.678 ± 1.314	7.082 ± 1.323	7.010 ± 0.632	4.714 ± 0.992	6.948 ± 1.103	7.780 ± 2.219	26.150 ± 4.939*
54:4(18:2)	4.546 ± 1.561	3.480 ± 0.694	4.020 ± 0.721	3.618 ± 0.273	2.782 ± 0.571	3.644 ± 0.539	4.880 ± 1.351	14.800 ± 1.946*
54:5(18:1)	3.570 ± 1.063	2.222 ± 0.453	2.942 ± 0.508	2.326 ± 0.190	2.084 ± 0.751	2.182 ± 0.311	8.610 ± 3.418	8.340 ± 1.795
54:6(18:2)	3.366 ± 0.847	1.360 ± 0.318	2.378 ± 0.366	1.422 ± 0.124	1.890 ± 0.278	1.240 ± 0.150	7.850 ± 1.837	4.950 ± 1.334
50:3(16:0)	0.606 ± 0.376	0.468 ± 0.075	0.676 ± 0.179	0.532 ± 0.084	0.394 ± 0.125	0.724 ± 0.158	0.810 ± 0.224	3.646 ± 0.715*
50:3(18:1)	0.500 ± 0.296	0.418 ± 0.074	0.512 ± 0.124	0.496 ± 0.070	0.318 ± 0.094	0.660 ± 0.137*	0.730 ± 0.224	2.652 ± 0.600*
50:4(18:2)	0.388 ± 0.203	0.234 ± 0.036	0.354 ± 0.081	0.296 ± 0.040	0.230 ± 0.059	0.376 ± 0.081	0.890 ± 0.248	1.487 ± 0.329*
52:1(18:1)	0.578 ± 0.319	0.504 ± 0.113	0.634 ± 0.136	0.626 ± 0.077	0.414 ± 0.140	0.692 ± 0.153	0.852 ± 0.498	1.222 ± 0.107
52:4(16:1)	0.676 ± 0.399	0.576 ± 0.098	0.672 ± 0.166	0.662 ± 0.105	0.382 ± 0.105	0.908 ± 0.192*	1.115 ± 0.393	3.902 ± 0.693*
52:5(18:2)	0.632 ± 0.298	0.416 ± 0.068	0.572 ± 0.133	0.482 ± 0.061	0.354 ± 0.079	0.602 ± 0.120	1.757 ± 0.575	2.417 ± 0.418
54:2(18:1)	1.580 ± 0.781	1.492 ± 0.328	1.646 ± 0.363	1.670 ± 0148	1.028 ± 0.316	1.780 ± 0.315	1.305 ± 0.478	4.582 ± 0.845*
56:4(18:1)	0.852 ± 0.214	0.640 ± 0.149	0.764 ± 0.095	0.578 ± 0.034	0.562 ± 0.101	0.576 ± 0.055	0.937 ± 0.270	1.400 ± 0.353
56:5(18:1)	0.364 ± 0.088	0.524 ± 0.113	0.346 ± 0.038	0.482 ± 0.038	0.268 ± 0.038	0.514 ± 0.055*	0.382 ± 0.100	1.277 ± 0.331*

Table 2.1 Levels of triacylglycerol (TAG) species in the heart of mice fed HFHS or chow diet for 4, 8, 12 and 16 weeks. Graph represents mean ± S.E.M., n = 5 to 8, ⁎P < 0.05 Vs Chow diet was performed using Student's t-test.

Table 2.2:

DAG species	Chow-4W	HFHS-4W	CHow-8W	HFHS-8W	Chow-12W	HFHS-12W	Chow-16W	HFHS-16W
34:1 (18:1/16:0)	1.796 ± 0.396	0.786 ± 0.098*	1.130 ± 0.224	0.850 ± 0.078	0.566 ± 0.070	0.774 ± 0.058	1.676 ± 0.249	1.190 ± 0.103
34:2 (16:0/18:2)	2.158 ± 0.494	0.494 ± 0.064*	1.252 ± 0.297	0.616 ± 0.056	0.560 ± 0.079	0.650 ± 0.061	0.186 ± 0.038	0.344 ± 0.087
36:2 (18:1/18:1)	2.290 ± 0.220	0.630 ± 0.107*	1.786 ± 0.525	0.762 ± 0.072	0.534 ± 0.095	0.840 ± 0.063	1.750 ± 0.404	2.145 ± 0.031
36:2 (18:0/18:2)	0.984 ± 0.227	0.266 ± 0.028*	0.680 ± 0.087	0.240 ± 0.015*	0.446 ± 0.039	0.264 ± 0.015	0.712 ± 0.117	0.468 ± 0.033
36:3 (18:1/18:2)	3.345 ± 0.326	0.506 ± 0.103*	2.308 ± 0.688	0.570 ± 0.052*	0.664 ± 0.123	0.636 ± 0.039	3.602 ± 0.535	2.980 ± 0.474
36:4 (18:2/18:2)	2.492 ± 0.243	0.178 ± 0.038*	1.546 ± 0.503	0.224 ± 0.022*	0.426 ± 0.099	0.274 ± 0.020	2.815 ± 0.374	0.998 ± 0.145*
38:4 (18:0/20:4)	3.515 ± 0.125	2.904 ± 0.355	3.720 ± 0.167	2.392 ± 0.223*	3.856 ± 0.295	2.574 ± 0.118*	3.315 ± 0.204	4.050 ± 0.339
32:0 (16:0/16:0)	0.464 ± 0.087	0.260 ± 0.029	0.332 ± 0.057	0.366 ± 0.038	0.214 ± 0.033	0.356 ± 0.044*	0.6475 ± 0.090	0.684 ± 0.070
36:1 (18:0/18:1)	0.394 ± 0.095	0.104 ± 0.013*	0.252 ± 0.060	0.124 ± 0.007	0.110 ± 0.015	0.138 ± 0.011	0.165 ± 0.010	0.334 ± 0.027*
38:5 (18:1/20:4)	0.376 ± 0.061	0.174 ± 0.025*	0.276 ± 0.040	0.174 ± 0.014*	0.196 ± 0.016	0.222 ± 0.007	0.265 ± 0.026	0.466 ± 0.034
38:5 (16:0/22:5)	0.318 ± 0.056	0.076 ± 0.009*	0.194 ± 0.045	0.076 ± 0.002*	0.100 ± 0.011	0.132 ± 0.012	0.2275 ± 0.016	0.198 ± 0.014
38:6 (16:0/22:6)	0.472 ± 0.078	0.086 ± 0.010*	0.300 ± 0.058	0.068 ± 0.005*	0.166 ± 0.015	0.11 ± 0.010*	0.200 ± 0.014	0.164 ± 0.015
40:6 (18:0/22:6)	0.344 ± 0.063	0.026 ± 0.005*	0.208 ± 0.069	0.030 ± 0.004*	0.054 ± 0.011	0.044 ± 0.004	0.125 ± 0.017	0.130 ± 0.019
32:1 (14:0/18:1)	0.078 ± 0.013	0.03 ± 0.003*	0.056 ± 0.014	0.034 ± 0.002	0.020 ± 0.004	0.046 ± 0.006	0.0475 ± 0.003	0.126 ± 0.020*
32:1 (16:0/16:1)	0.062 ± 0.011	0.032 ± 0.003*	0.044 ± 0.013	0.028 ± 0.005	0.028 ± 0.008	0.036 ± 0.002	0.0875 ± 0.017	0.132 ± 0.037
32:2 (14:0/18:2)	0.118 ± 0.021	0.026 ± 0.004*	0.078 ± 0.021	0.032 ± 0.002	0.034 ± 0.006	0.046 ± 0.006	0.085 ± 0.005	0.104 ± 0.015
34:2 (16:1/18:1)	0.130 ± 0.027	0.050 ± 0.007*	0.096 ± 0.026	0.044 ± 0.007	0.042 ± 0.008	0.064 ± 0.009	0.186 ± 0.038	0.190 ± 0.017
36:1 (16:0/20:1)	0.096 ± 0.024	0.018 ± 0.002*	0.058 ± 0.015	0.020 ± 0.001*	0.022 ± 0.004	0.018 ± 0.002	0.052 ± 0.009	0.032 ± 0.003

Table 2.2 Levels of diacylglycerol (DAG) species in the heart of mice fed HFHS or chow diet for 4, 8, 12 and 16 weeks. Graph represents mean ± S.E.M., n = 5 to 8, ⁎P < 0.05 Vs Chow diet was performed using Student's t-test.

Chapter 3: Ventricular transcriptome analysis of mice with constitutive cardiomyocyte-specific TFEB deletion

All figures and portions of the text present in this chapter have been reproduced with the copyright permission from Elsevier (Appendix 1) and edited as appropriate:

Trivedi, P.C.; Bartlett, J.J.; Mercer, A.; Slade, L.; Surette, M.; Ballabio, A.; Flibotte, S.; Hussein, B.; Rodrigues, B.; Kienesberger, P. C.; Pulinilkunnil, T. Loss of function of transcription factor EB remodels lipid metabolism and cell death pathways in the cardiomyocyte. Biochim Biophys Acta Mol Basis Dis 2020, 1866 (10):165832 [339].

RNA Sequencing and transcriptome analysis for cardiomyocyte-specific TFEB$^{-/-}$ mice colony were performed by Dr. Rodrigues laboratory and Stephane Flibotte.

3.1 Rationale and objectives

TFEB promotes transcription by binding to the CLEAR motif in the promoter region of genes involved in the lysosomal biogenesis and function [288,304] and metabolism [298,316]. Loss of TFEB action, impaired autophagy, and increased proteotoxicity are observed in numerous diseases like neurodegeneration [371], cancer [372], renal diseases [373], non-alcoholic fatty liver diseases [374], obesity and more importantly, heart disease [247,344,369,370,375]. It was demonstrated that TFEB gain- or loss-of-function influences liver function and whole-body energy metabolism; however, a similar role of TFEB in the heart was never explored prior [299]. In chapter 2, I demonstrated that nutrient overload-induced depletion in TFEB content is associated with suppressed lysosomal proteolytic activity in the mouse heart. Furthermore, saturated fatty acid, palmitate downregulated TFEB in the cardiomyocyte in a time- and concentration-dependent manner. Despite these findings from other laboratories and ours highlighting the critical role of TFEB in influencing cardiomyocyte viability and function, underlying mechanisms by which loss of TFEB engages nutrient-sensing pathways to remodel cardiac energy metabolism and function remain unclear. Outstanding questions I tested in this thesis chapter include; 1) elucidating

signaling pathway networks impacted by TFEB specifically in the cardiomyocyte by employing cardiomyocyte transcriptome analysis in a mouse model of TFEB deletion and 2) examining whether constitutively activating TFEB or preventing loss of TFEB in the cardiomyocyte improves lysosome function and survival under a lipotoxic stress challenge.

3.2 Materials and methods

3.2.1 Generation of constitutive cardiomyocyte-specific TFEB$^{-/-}$ mice

Mice bearing TFEB-floxed alleles (TFEB$^{fl/fl}$, Stock # 400102) provided by Dr. Andrea Ballabio were crossbred with transgenic mice expressing Cre under the control of myosin heavy chain promoter (αMHC-Cre, Stock: 009074) to generate cardiomyocyte-specific *Tcfeb* knockdown (TFEB$^{-/-}$) mice. Genomic DNA isolated from TFEB$^{fl/fl}$ and MHC-Cre mice was subjected to PCR analysis using the primers as listed in Table 3.1. All mice were male and maintained on a C57BL/6J background strain. For all experiments involving TFEB$^{-/-}$ mice, the control mice were TFEB$^{fl/fl}$ mice that did not carry αMHC-Cre transgene and are referred to as wild-type (WT) mice. Mice were maintained in a temperature- and humidity-controlled animal-care facility, with a 12 h light/dark cycle with food and water provided ad libitum.

3.2.2 Cell culture

3.2.2.1 Adult mouse cardiomyocyte isolation

Adult mouse cardiomyocytes were isolated as described in section 2.2.5.2.

3.2.2.2 H9C2 cardiomyoblast culture

H9C2 cardiomyoblast cells were cultured as described in section 2.2.5.1.

3.2.2.3 Neonatal rat ventricular cardiomyocyte isolation

Neonatal rat ventricular cardiomyocytes (NRCMs) were isolated from 2-day old Sprague-Dawley rat pups. Briefly, hearts were excised, RBC and atria were discarded, and ventricles were collected. Ventricles were then minced into small pieces and thoroughly washed with ice-cold 1X PBS. Minced ventricles then digested repeatedly using proteolytic enzymes collagenase- type 2

(2% W/V; LS004176; Worthington Biochemical Corporation), Deoxyribonuclease-I (0.5% W/V; LS002007; Worthington Biochemical Corporation) and trypsin (2% W/V; LS003707; Worthington Biochemical Corporation) (Worthington Biochemical Corporation) with gentle stirring to dissociate tissues into single cells. Following digestion, cells were collected and centrifuged to obtain a cell pellet. After the digestion, the cell pellet was re-suspended using plating media which composed of DMEM/F12 HAM (D6421; Sigma), 10% FBS, 15 % horse serum, 1% penicillin-streptomycin (30-002-CI, Corning, NY, USA) and 50 µg/ml gentamycin (30-005-CR; Corning) and subjected to differential plating for 2 h to eliminate non-cardiomyocytes such as fibroblasts. Supernatant from differential plating containing cardiomyocytes was collected and suspended in a growth medium containing DMEM/F12 HAM (D6421; Sigma), 10% FBS, 10 µM cytosine-β-D-arabinofuranoside (C1768; ARAC, Sigma), Insulin-Transferrin-Selenium (25800-CR, ITS, Corning), 1% penicillin-streptomycin (30-002-CI, Corning, NY, USA) and 50 µg/ml gentamycin (30-005-CR; Corning) and plated at a density of 5 x10^4 using 35 mm primaria cell culture plates. The following day, cells were washed in DMEM 1X media and cultured in serum-free DMEM-1X medium containing 10 µM ARAC, 50 µg/ml gentamycin, 1% penicillin-streptomycin and 10 mM glucose for 24 h. After 24 h, cells were treated with low and high concentrations of different substrates, as described in section 2.2.5.4.

3.2.2.4 Adenoviral transduction

H9C2 cells or neonatal rat cardiomyocytes were transduced with either HA-tagged human TFEB (SKU: ADV-225358, Lot:20140903T9) or Myc-tagged human phosphorylation-resistant mutant TFEB (S142A) (courtesy of Dr. Shawn Ferguson laboratory) or FLAG-tagged human phosphorylation-resistant mutant TFEB (S211A) or CMV-mCherry (SKU: 1060, Lot: 20161220T5), CMV-GFP (20160126T6) or Scramble-RNAi (SKU: 1122, Lot: 20150210T14) or rat TFEB-ShRNA (shADV-294304, Lot: 20140930T3) for 48 hr. All adenoviral vectors were obtained from Vector Biolab, unless specified. Following adenoviral transduction, cells were

treated with different substrates such as BSA (B), glucose (G), palmitate (P) and a combination of glucose/palmitate (GP) as described in section 2.2.5.4.

3.2.2.5 Preparation of bovine serum albumin (BSA) complexed fatty acid

BSA complexed fatty acids media were prepared as described in section 2.2.5.3.

3.2.3 RNA sequencing and analysis

RNA sequencing and analysis were performed as described previously [376]. Total RNA from 12 to 14 weeks old $TFEB^{fl/fl}$ and $TFEB^{-/-}$ adult mouse cardiomyocytes were isolated using TRIzol. Sequencing libraries were prepared from 400 ng total RNA using the TruSeq Stranded mRNA Sample Preparation kit (Illumina, San Diego, CA). Samples were assessed for quality using a Bioanalyzer (Agilent, Paulo Alto) and quantified using a Qubit fluorometer. Libraries were then multiplexed and sequenced over one rapid run lane on the NextSeq 500 Sequencing System (Illumina), collecting a total of 409 million read pairs (2 x 75 bases). The number of read pairs per sample ranged from 14-75 million (median 21). Multiple analysis pipelines (STAR-DESeq2, kallisto-DESeq2, salmon-DESeq2 and hisat2-stringtie-DESeq2) were applied, and results combined. Briefly, for reading alignment, we used both STAR and HISAT2. We also used the pseudo aligners kallisto and Salmon. Quantification was performed directly with STAR, kallisto and Salmon or with RSEM and StringTie for the pipelines producing real alignments. The mouse reference genome and transcriptome from version GRCm38 were downloaded from the Ensembl web site (http://www.ensembl.org). In-house Perl scripts were used to sum the read counts at the transcript level for each gene and create a matrix comprising the read counts for all of the genes for all of the samples.

Statistical analysis of differential gene expression: Differential expression analysis was performed on the matrix data using the R package DESeq2 and edgeR. Each sample was assessed using the quality-control software RSeQC and the PtR script from the trinity suite. The output for each pipeline was a list of genes ranked by the p-value for differential expression after correction for multiple testing. A combined list was obtained by ranking the genes according to their median

rank from the various analysis pipelines. Genes with differential expression with inconsistent values between different analysis pipelines were eliminated from that combined list. P-value adjustment for multiple comparisons was made with the FDR of Benjamini Hochberg. The threshold for statistical significance chosen was FDR 0:05; further filtering was performed by selecting genes with an absolute fold change_1:5 for both increased (upregulated genes) and decreased (downregulated genes) expression levels. The ventricular transcriptome data from $TFEB^{-/-}$ mice have been deposited in NCBI's Gene Expression Omnibus (GEO) and are accessible through accession number GSE138470.

3.2.4 Quantitative polymerase chain reaction

RNA was extracted from adult mouse cardiomyocytes using RIBOZOL (N580-CA; Amresco) and chloroform (C2432; Sigma Aldrich) according to the manufacturer's instruction. The RNA pellet was re-suspended in 20-50 µl of nuclease-free water (10977-015; Life Technologies). The RNA integrity and quantity of RNA were assessed using Qiaxel Advanced system. cDNA was synthesized using qScript cDNA supermix (CA101414-104; Quanta Biosciences) from 1 µg of RNA. qPCR reactions were carried out in 96-well plates on a ViiA7 Real-time PCR machine (Thermo Fisher Scientific). Each well contained 2 µl of cDNA template, 5µL of SYBR green Low ROX PCR supermix (AB1323A, Thermo Fisher Scientific), 0.25 µl of each forward and reverse primer and nuclease-free water in a total of 10 µl per reaction mixture. Primer sequences are summarized in Table 3.1. mRNA levels were determined using Biogazelle qbase+ software and normalized to two reference genes and presented as fold change.

3.2.5 Immunoblot analysis

Immunoblot analysis was performed as described in section 2.2.7.

3.2.6 Cathepsin B activity

Cathepsin B activity in $TFEB^{-/-}$ and $TFEB^{fl/fl}$ cardiomyocytes was performed as described in section 2.2.8.

3.2.7 Immunostaining

Cells were plated on sterile coverslips. Following differentiation, adenoviral transduction and treatment, cells were fixed using 4% paraformaldehyde (PX0055-3; EMD) at room temperature for 15 minutes and then washed with PBS. Cells were permeabilized/blocked by incubating them in blocking buffer (3% BSA in 1X-PBS-0.1%-Triton-X) for 60 mins at room temperature. Subsequently, cells were incubated with the primary antibody, anti-TFEB at room temperature for 1 hr in a humidified chamber. Following incubation, cells were then washed 3X with PBS and incubated with Alexa conjugated secondary antibody Alexa 488 (A11008; Life Technologies) or Alexa 564 (A21428; Life Technologies) in a dark, humidified chamber for 1 h. After the incubation with secondary antibody, cells were again washed 3X with PBS. Eventually, coverslips were mounted on slides in the dark using Vectashield with DAPI (H-1200; Vector Laboratories) in PBS to stain the nuclei for 15 minutes. Cell images were captured using the ZEISS microscope with filter sets for DAPI, Alexa 488 or Alexa 564.

3.2.8 Statistical Analysis

Results are expressed as mean ± SEM. Pairwise comparison between groups was performed using unpaired two-tailed Student's t-test. Comparisons between multiple groups were performed using one- or two-way ANOVA followed by a Bonferroni or Tukey post hoc test, as appropriate. All statistical analysis was performed using Prism (GraphPad Software). P-values of less than 0.05 were considered statistically significant. For animal studies, "n" refers to the number of mice used, unless otherwise specified. For cell culture studies, experiments were performed in triplicates, and data are from at least three independent experiments.

3.3 Results

3.3.1 Cardiomyocyte-specific transcriptome analysis in mice with constitutive cardiomyocyte-specific TFEB deletion

Prior study from our laboratory demonstrated depletion of TFEB content in response to *ex-vivo* and *in-vivo* glucolipotoxic stress in the cardiomyocyte and in the mouse heart, respectively [226]. Furthermore, loss of TFEB impairs lysosomal proteolysis to degrade cellular waste, rendering cardiomyocytes susceptible to cell death and toxicity. However, the identity of underlying pathways that are engaged following the loss of TFEB in the heart and the mechanisms by which these pathways signal and reprogram cardiac metabolism and function during obesity and diabetes remains unclear.

To ascertain the network of metabolic, signaling and functional pathways following the loss of TFEB *in-vivo*, we used a loss-of-function approach based on a knockdown mouse model to explore the physiological role of TFEB. By breeding TFEB floxed mice with CRE expressing mice under the control of cardiomyocyte-specific α-myosin heavy chain (Myh6) promoter, we generated mice with cardiomyocyte-specific TFEB deletion ($TFEB^{-/-}$) **(Figure 3.1 A)**. TFEB deletion in the cardiomyocyte was first confirmed by measuring TFEB mRNA expression using qPCR **(Figure 3.1 B)**. Alternately, we confirmed TFEB deletion both in cytosol and nucleus of cardiomyocytes from $TFEB^{-/-}$ mice compared to their $TFEB^{fl/fl}$ mice **(Figure 3.1 C, D, E and F)**. To decipher the signaling pathways impacted by the loss of TFEB, we performed a transcriptome analysis in cardiomyocytes isolated from $TFEB^{-/-}$ and $TFEB^{fl/fl}$ mice. Transcriptome analysis revealed that of ~ 45,000 transcripts analyzed, approximately 25% of differentially expressed genes (DEGs) were enriched in myocytes lacking TFEB. Following TFEB deletion in cardiomyocytes, 70% (1122/1606 genes) genes were upregulated, and 30% (484/1606 genes) were downregulated **(Figure 3.2 A)**. To gain an understanding of the possible effects of transcriptomic changes on biological processes in $TFEB^{-/-}$ mice, we clustered DEGs according to their function using a threshold for statistical significance (false discovery rate (FDR<0:05) **(Figure 3.2 B)**. We observed

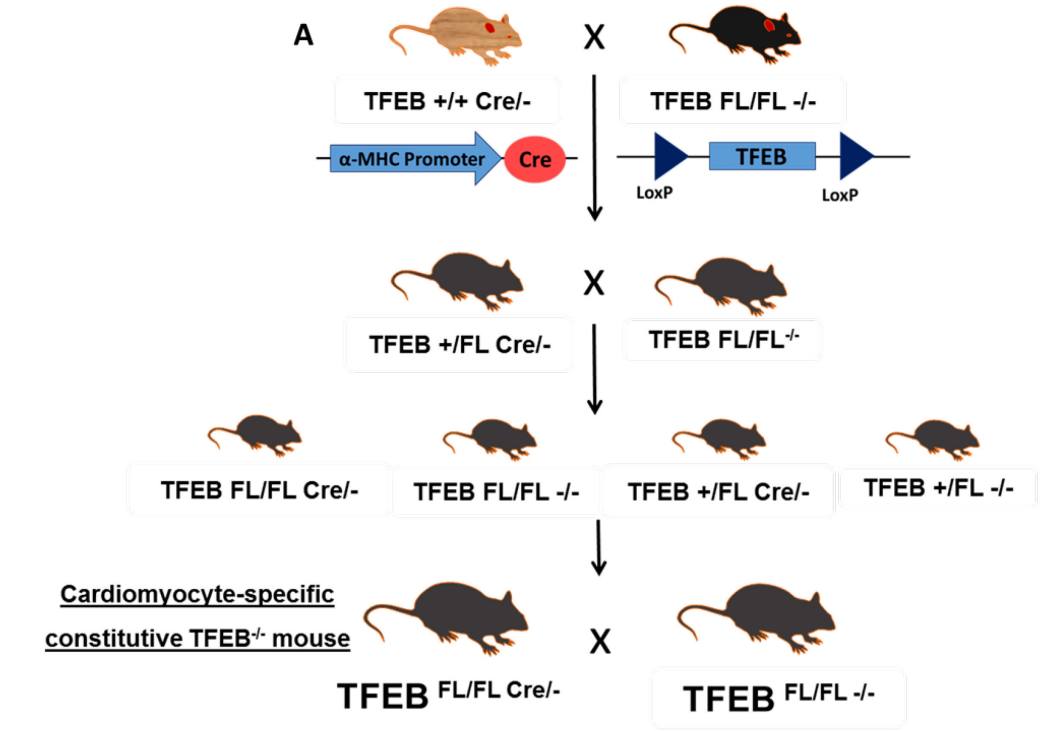
A
X
TFEB +/+ Cre/-
TFEB FL/FL -/-
α-MHC Promoter
Cre
TFEB
LoxP
LoxP
X
TFEB +/FL Cre/-
TFEB FL/FL-/-
TFEB FL/FL Cre/-
TFEB FL/FL -/-
TFEB +/FL Cre/-
TFEB +/FL -/-
Cardiomyocyte-specific
constitutive TFEB-/- mouse
X
TFEB FL/FL Cre/-
TFEB FL/FL -/-

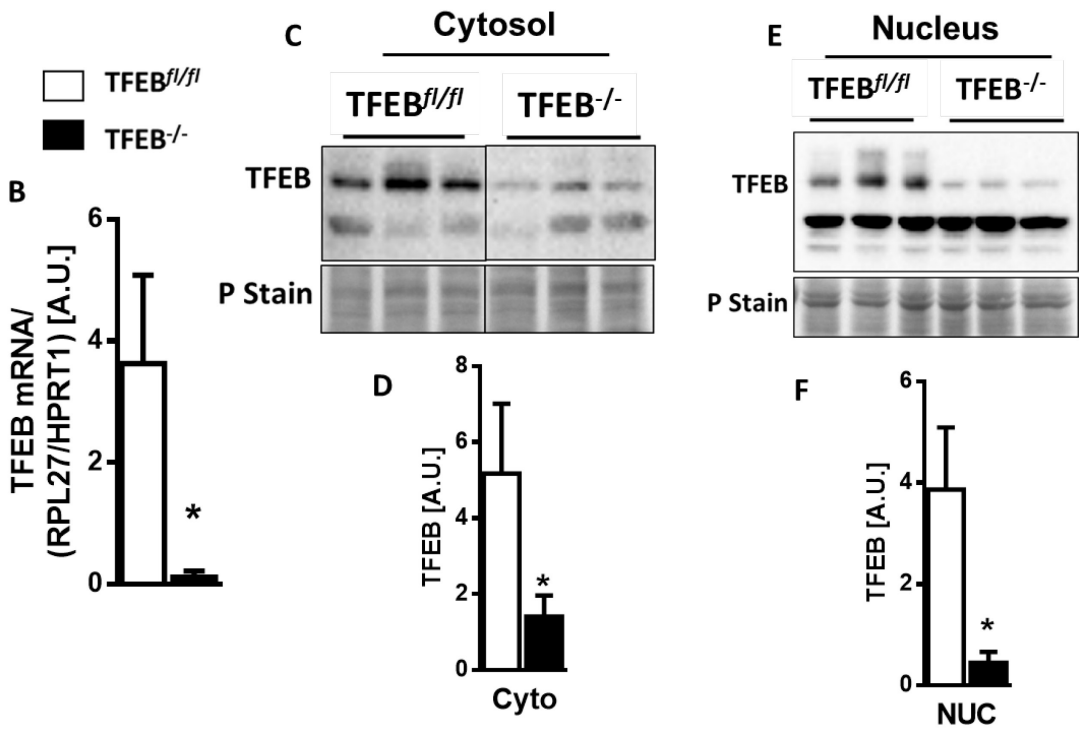
TFEBfl/fl
TFEB-/-
B
TFEB mRNA/
(RPL27/HPRT1) [A.U.]
6
4
2
0
*
C
Cytosol
TFEBfl/fl
TFEB-/-
TFEB
P Stain
D
TFEB [A.U.]
8
6
4
2
0
*
Cyto
E
Nucleus
TFEBfl/fl
TFEB-/-
TFEB
P Stain
F
TFEB [A.U.]
6
4
2
0
*
NUC

Figure 3.1 Cardiomyocyte-specific constitutive TFEB deletion mouse model. (A) Breeding strategy to generate cardiomyocyte-specific $TFEB^{-/-}$ mouse. (B) Quantification of TFEB mRNA from adult cardiomyocytes isolated from $TFEB^{-/-}$ and $TFEB^{fl/fl}$ mice. TFEB mRNA expression was corrected to reference genes HPRT1 and RPL27, and data presented as fold change. Graph represents mean ± S.E.M., n = 3, *P<0.05 was performed using Student's t-test. (C and E) Immunoblot and densitometric analysis of protein expression of (D and F) TFEB from cytosolic soluble protein fraction and nuclear membrane protein fraction in cardiomyocytes from $TFEB^{-/-}$ or $TFEB^{fl/fl}$ mice. Graph represents mean ± S.E.M., n = 3, *P<0.05 vs $TFEB^{fl/fl}$ was performed using Student's t-test.

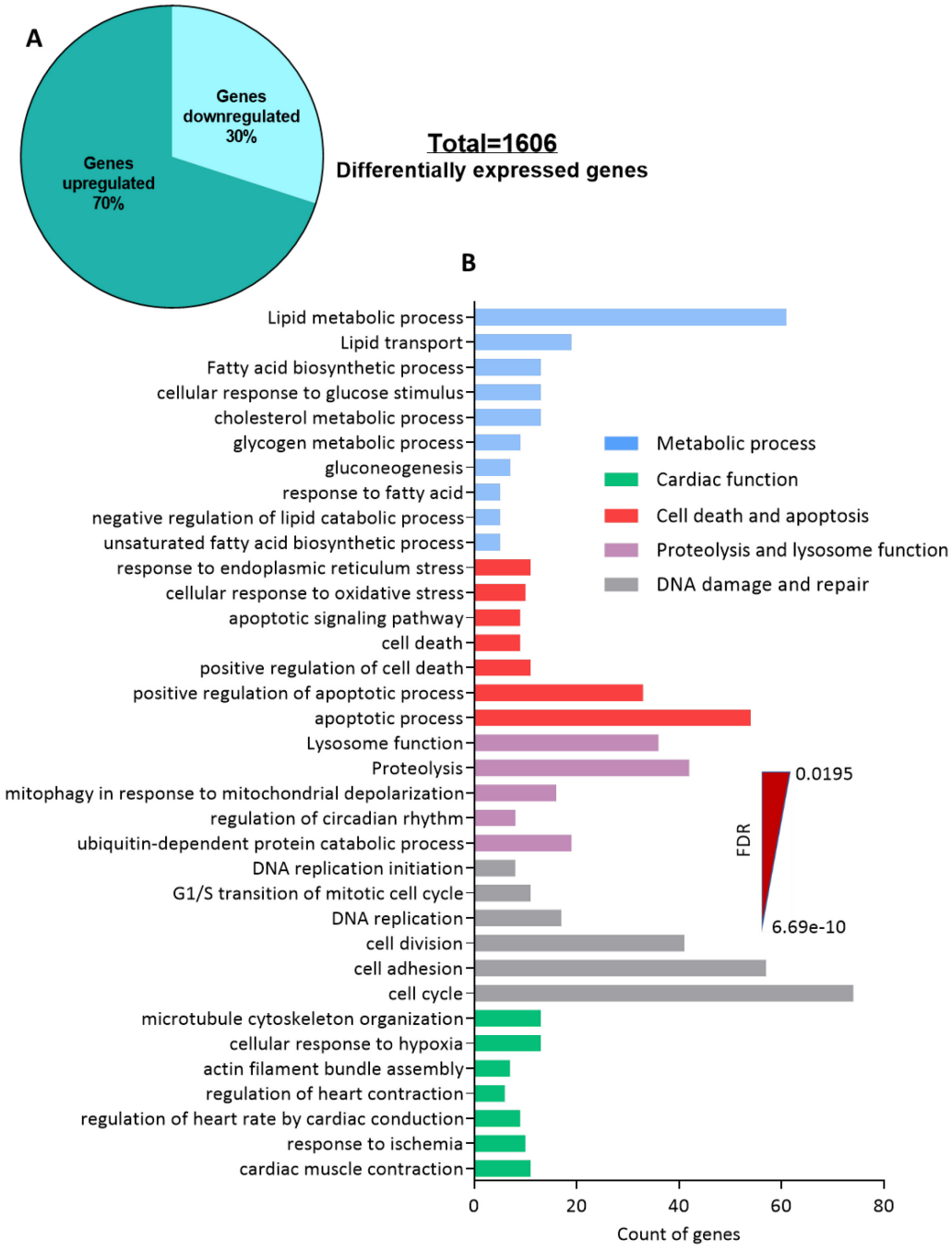

Figure 3.2 Ventricular myocyte transcriptome analysis in the mice with cardiomyocyte-specific constitutive TFEB deletion. (A) The inset describes the percentage of differentially expressed genes that were up-or down-regulated from RNA-Seq analysis of cardiomyocytes isolated from TFEB$^{fl/fl}$ and TFEB$^{-/-}$ mice. (B) Cardiomyocyte RNA from TFEB$^{fl/fl}$ and TFEB$^{-/-}$ mice were sequenced, and differentially regulated genes (padj < 0.05 and significant in at least 5 out of the 10 analysis pipelines used) were clustered according to the function and ranked based on FDR. n=3, the expression level of genes involved in pathways is indicated as a log2 fold change.

alterations in several pathways involved in cellular metabolism (220 genes), ER stress, apoptosis/cell death (140 genes), DNA replication (20 genes)/cell cycle (90 genes), proteolysis/lysosome function (62 genes) and cardiac function (35 genes) in TFEB$^{-/-}$ mice **(Figure 3.2 B)**.

3.3.2 Influence of TFEB deletion on lysosome function and autophagy in the cardiomyocyte

Given the role of TFEB in governing lysosome biogenesis and function pathways [288,304], we next analyzed the impact of TFEB ablation on genes encoding lysosomal function, lysosome biogenesis and autophagy in the cardiomyocyte.

Transcriptome analysis revealed 66 genes involved in macroautophagy, mitophagy and lysosome function **(Figure 3.3 A)**, which constituted a small portion (total 4 % of genes) of DEGs in TFEB$^{-/-}$ cardiomyocytes. Strikingly, 73.6 % of genes related to lysosome function were upregulated, and 26.3 % were down-regulated in TFEB$^{-/-}$ cardiomyocytes (as indicated by $ mark in **Figure 3.3 B)**. Glycosidases, *Hexb* and proteases, *Ctsc*, which are a direct target of TFEB [288], were downregulated in cardiomyocytes lacking TFEB **(Figure 3.3 B)**. Contrary to our expectation, lysosomal hydrolases such as cathepsin proteases (*Ctsz, Ctsk* and *Ctsh*), beta glycosidases (*Gba* and *Gba2*) and lipase (*Lipa*) were significantly upregulated in TFEB$^{-/-}$ cardiomyocytes **(Figure 3.3 B and C)**. We next examined genes related to vATPase activity, which is crucial in governing lysosomal luminal acidification and important for regulating lysosomal proteolytic activity [288,377]. We observed the upregulation of lysosomal function genes such as those involved in vATPase activity, including *Atp6v0a1, Atp6v1d* and *Atp6v0e2* **(Figure 3.3 C)**. Strikingly, 71.5 % of genes responsible for fusion machinery and autophagy were upregulated (*Sqstm1, Atg13, Vps53* and *Map1a*), whereas 28.5 % were downregulated by loss of TFEB in the cardiomyocyte **(Figure 3.3 C)**. These findings are reflected in increased p62/SQSTM1 protein content in the cardiomyocytes from TFEB$^{-/-}$ mice **(Figure 3.3 D and E)**. Concurrent with the transcriptome data, Cathepsin B proteolytic activity, an indicator of lysosomal function, remained unchanged in

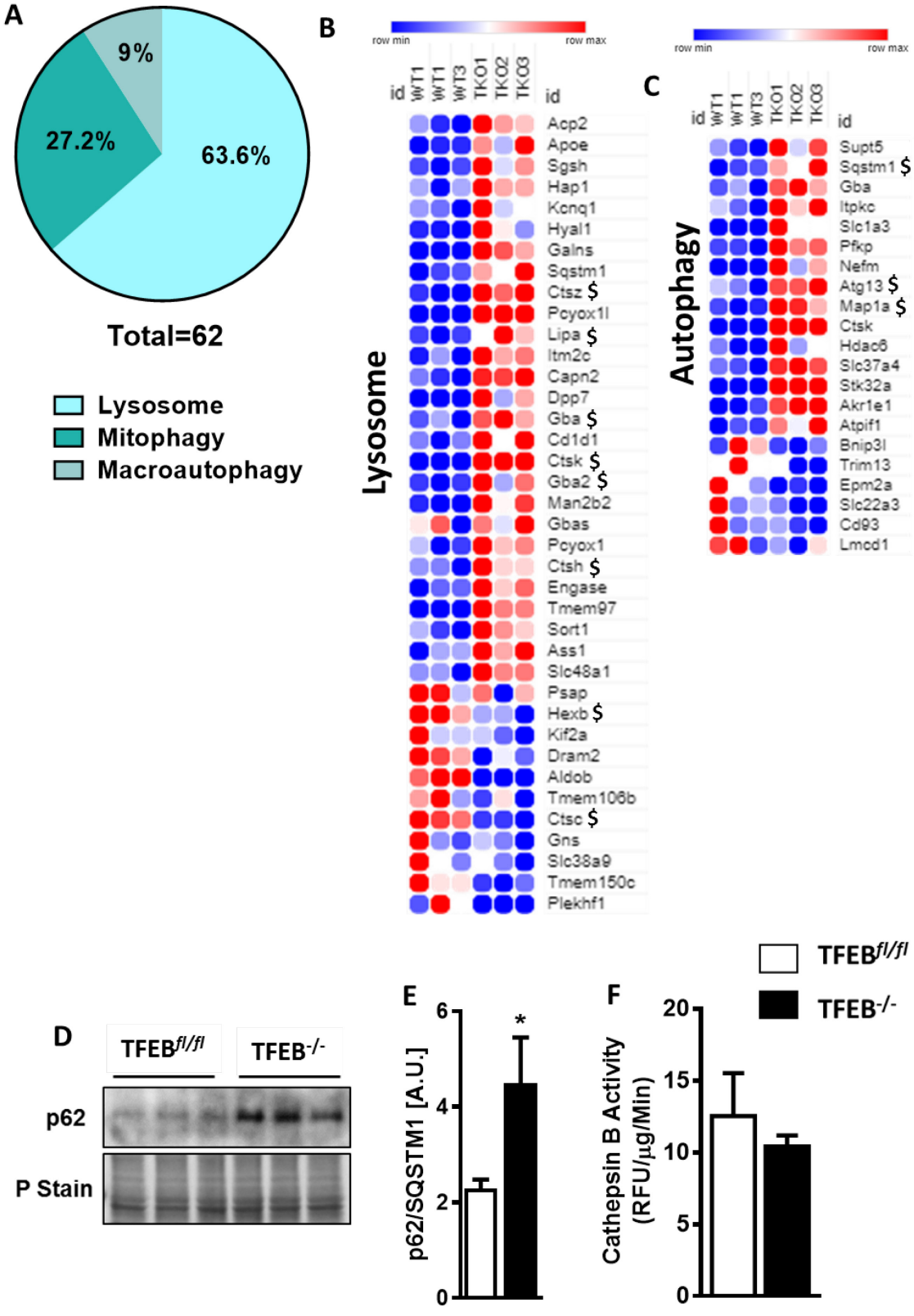
A
9%
27.2%
63.6%
Total=62
Lysosome
Mitophagy
Macroautophagy
B
row min
row max
id
WT1
WT1
WT3
TKO1
TKO2
TKO3
id
Lysosome
Acp2
Apoe
Sgsh
Hap1
Kcnq1
Hyal1
Galns
Sqstm1
Ctsz $
Pcyox1l
Lipa $
Itm2c
Capn2
Dpp7
Gba $
Cd1d1
Ctsk $
Gba2 $
Man2b2
Gbas
Pcyox1
Ctsh $
Engase
Tmem97
Sort1
Ass1
Slc48a1
Psap
Hexb $
Kif2a
Dram2
Aldob
Tmem106b
Ctsc $
Gns
Slc38a9
Tmem150c
Plekhf1
C
row min
row max
id
WT1
WT1
WT3
TKO1
TKO2
TKO3
id
Autophagy
Supt5
Sqstm1 $
Gba
Itpkc
Slc1a3
Pfkp
Nefm
Atg13 $
Map1a $
Ctsk
Hdac6
Slc37a4
Stk32a
Akr1e1
Atpif1
Bnip3l
Trim13
Epm2a
Slc22a3
Cd93
Lmod1
D
TFEBfl/fl
TFEB-/-
p62
P Stain
E
p62/SQSTM1 [A.U.]
0
2
4
6
*
F
Cathepsin B Activity (RFU/μg/Min)
0
5
10
15
20
TFEBfl/fl
TFEB-/-

Figure 3.3 Impact of TFEB deletion on autophagy genes and lysosomal proteolytic activity in the cardiomyocyte. (A) The inset describes the percentage of differentially expressed genes involved in lysosome function and autophagy from RNA-Seq analysis of cardiomyocytes isolated from $TFEB^{fl/fl}$ (n=3) and $TFEB^{-/-}$ (n=3) mice. (B and C) Heatmap of differentially expressed genes involved in lysosome function and autophagy in cardiomyocytes from $TFEB^{fl/fl}$ and $TFEB^{-/-}$ mice. (D) Immunoblot and densitometric analysis of protein expression of (E) p62 in cardiomyocytes from $TFEB^{-/-}$ or $TFEB^{fl/fl}$ mice. Graph represents mean ± S.E.M., n = 3, *P<0.05 was performed using Student's t-test. (F) Cathepsin B activity in cardiomyocytes isolated from $TFEB^{-/-}$ and $TFEB^{fl/fl}$ mice. Graph represents mean ± S.E.M., n = 3, *P<0.05 vs $TFEB^{fl/fl}$ was performed using Student's t-test.

in TFEB$^{-/-}$ cardiomyocytes compared to TFEB$^{fl/fl}$ cardiomyocytes **(Figure 3.3 F)**. Despite prior studies demonstrating that lysosomal proteolytic machinery is significantly impacted by the loss of TFEB action in the liver [299], skeletal muscle [316], pancreas [378] and brain [379], our studies in the cardiomyocyte did not yield similar findings. Together, our results suggest that loss of TFEB in the cardiomyocyte differentially affected subsets of genes in pathways of lysosome function and autophagy.

3.3.3 Constitutive localization of nuclear TFEB content attenuates palmitate-induced suppression of lysosomal proteolytic activity

We previously demonstrated that doxorubicin- and glucolipotoxicity-induced cardiomyocyte injury resulted in depletion of TFEB content, impaired lysosome biogenesis and function in the cardiomyocyte [226]. Therefore, we next examined if preventing TFEB decline in cardiomyocytes attenuate glucolipotoxicity-induced impairment in lysosome content and function.

To ascertain the physiological importance of TFEB, we employed an *in-vitro* model of differentiated H9C2 cardiomyoblast cells. H9C2 cells are derived from embryonic rat heart and are one of the preferred cell types for myocyte experiments, as it simulates signaling profile and functionality of a primary cardiomyocyte [380]. H9C2 cells were transduced with adenovirus overexpressing either wild type (WT) human TFEB or constitutively active phosphorylation resistant human TFEB (S142A and S211A) followed by treatment with different substrates such as glucose (G), palmitate (P), glucose/palmitate (GP) combination or BSA control. We first assessed the subcellular localization of TFEB post adenovirus transduction using immunostaining analysis. We found that H9C2 cells transduced with S142A or S211A adenoviruses revealed a robust increase in nuclear translocation of TFEB as indicated with white arrows **(Figure 3.4)**. Next, we determined the effect of constitutive nuclear localization of TFEB on lysosome content by measuring LAMP2A protein levels. We observed an increase in LAMP-2A content upon treatment

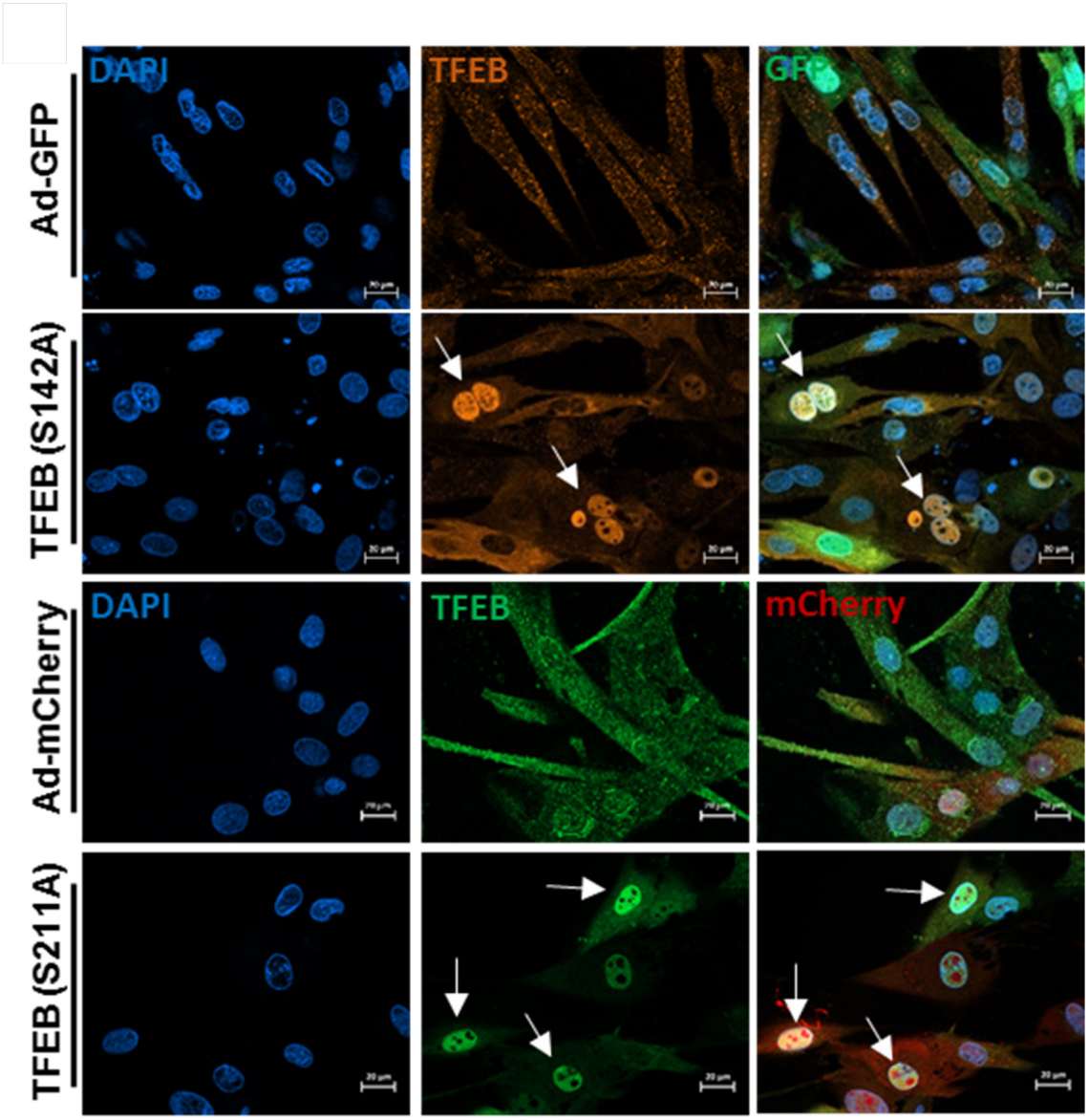

Figure 3.4 Constitutive nuclear localization of TFEB in H9C2 cells. Immunofluorescence image showing TFEB (Green or Orange), GFP (Green) or mCherry (Red) and nuclei stained with Hoechst 33342 (Blue) in H9C2 cells transduced with adenoviruses overexpressing either human phosphorylation resistant mutant TEFB (S142A or S211A) or viral control GFP/mCherry. White arrow showing TFEB localization in the nucleus.

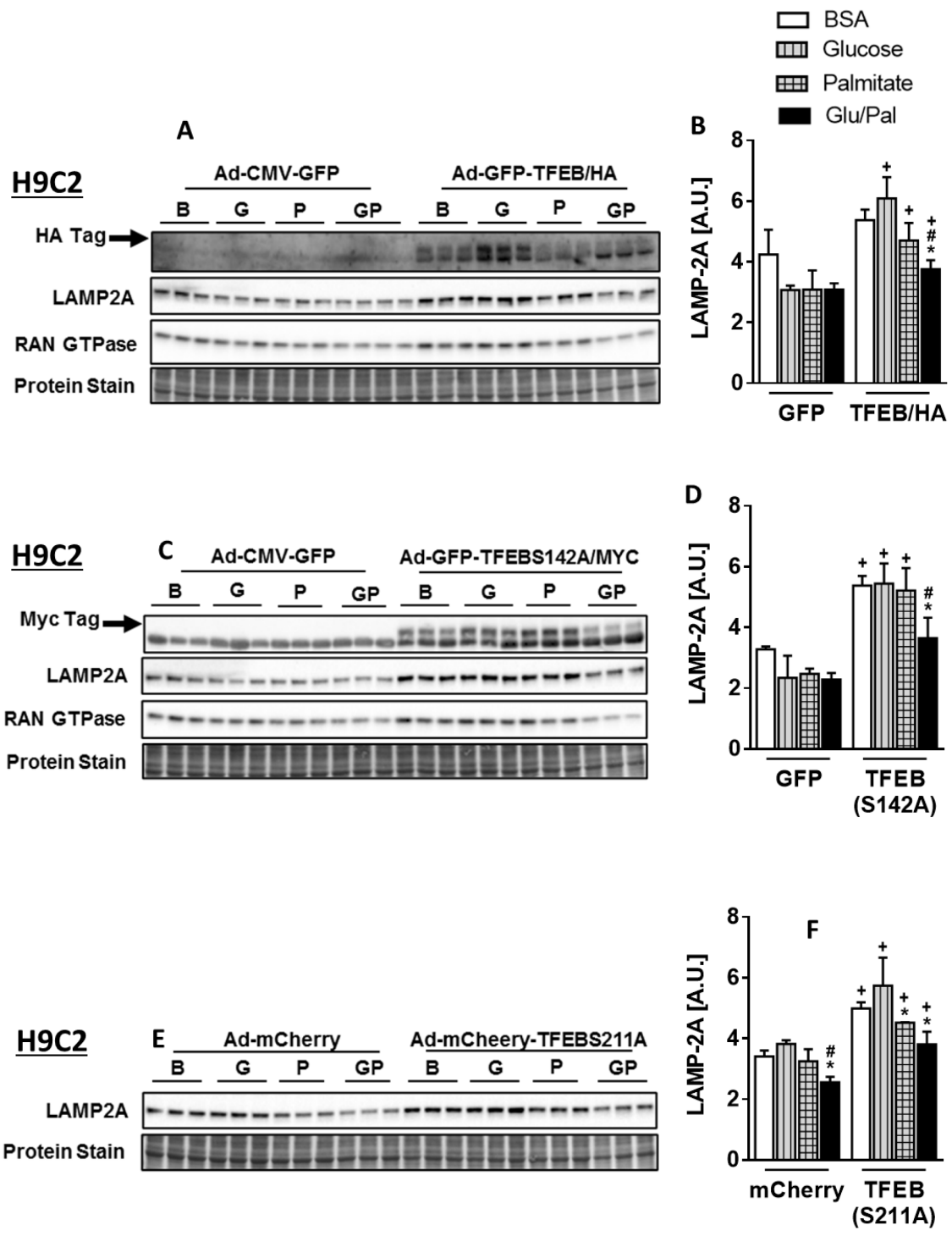

Figure 3.5 Increased nuclear TFEB localization and content attenuate nutrient overload-induced suppression of lysosomal proteolytic activity in H9C2 cells. H9C2 cells transduced with adenovirus overexpressing either human WT TFEB, mutant TFEB (S142A or S211A) or viral control GFP/mCherry, followed by treatment with BSA, glucose (G; 30mM), palmitate (P; 1.2 mM) or a combination of glucose/palmitate (GP; 30/1.2 mM) for 16 h. (A, C and E) Immunoblot

and densitometric analysis of protein expression of (B, D and F) LAMP-2A. Graph represents mean ± S.E.M., n = 3 from three independent sets of experiments, *P<0.05 vs BSA, #P<0.05 vs G and +P<0.05 vs respective viral control was performed using two-way ANOVA; A.U.; arbitrary unit, P Stain; protein stain.

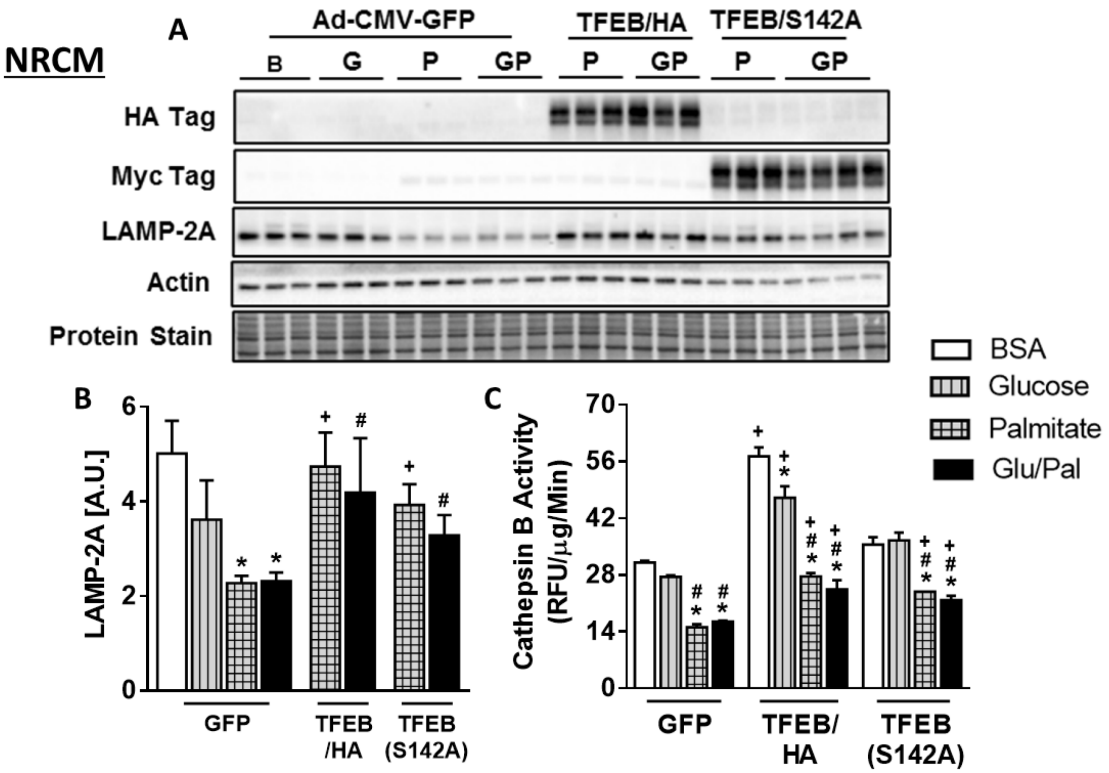

Figure 3.6 Increased nuclear TFEB localization and content attenuate nutrient overload-induced suppression of lysosomal proteolytic activity in neonatal rat cardiomyocytes. Neonatal rat cardiomyocytes transduced with adenovirus overexpressing either human WT TFEB, mutant phosphorylation resistant TEFB (S142A) or viral control GFP followed by treatment with BSA, glucose (G; 30 mM), palmitate (P; 1.2 mM) or a combination of glucose/palmitate (GP; 30/1.2 mM) for 16 h. (A) Immunoblot and densitometric analysis of protein expression of (B) LAMP-2A and (C) cathepsin B activity in neonatal rat cardiomyocytes. Graph represents mean ± S.E.M., n = 3 from three independent sets of experiments, *P<0.05 vs BSA, #P<0.05 vs G and +P<0.05 vs respective viral control was performed using two-way ANOVA; A.U.; arbitrary unit, P Stain; protein stain.

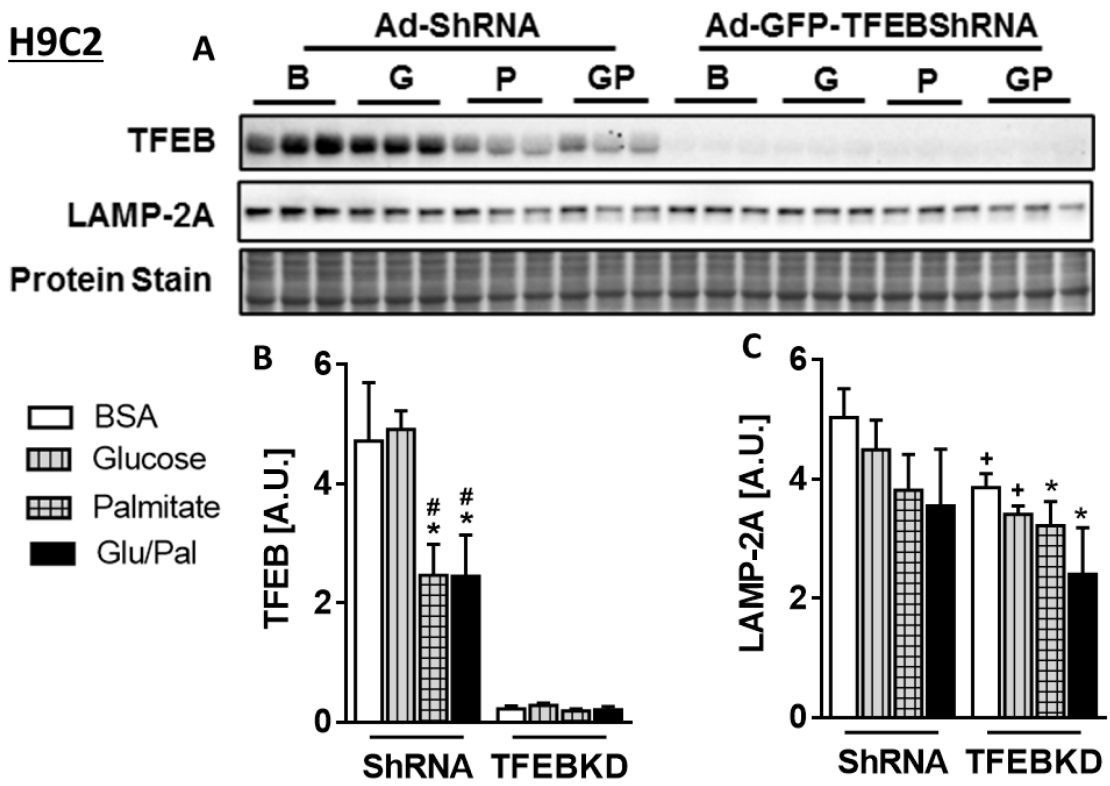

Figure 3.7 Silencing TFEB did not exacerbate nutrient overload-induced suppression in lysosomal content. H9C2 cells transduced with adenoviruses overexpressing TFEB-ShRNA or ShRNA control followed by the treatment with BSA, glucose (G; 30mM), palmitate (P; 1.2 mM) or a combination of glucose/palmitate (GP; 30/1.2 mM) for 16 h. (A) Immunoblot and densitometric analysis of protein expression of (B) TFEB and (C) LAMP-2A. Graph represents mean ± S.E.M., n = 3 from three independent sets of experiments, *P<0.05 vs BSA, #P<0.05 vs G and +P<0.05 vs respective viral control was performed using two-way ANOVA; A.U.; arbitrary unit, P Stain; protein stain.

with different substrates such as BSA, glucose, palmitate and a combination of glucose/palmitate when H9C2 cells were transduced with WT TFEB or mutant TFEB (S142A and S211A) compared to their respective viral control **(Figure 3.5 A-B, C-D and E-F)**. Findings in H9C2 cells were recapitulated in neonatal rat cardiomyocytes (NRCM), wherein WT or phosphorylation-resistant TFEB (S142A) overexpression attenuated palmitate- and GP-induced decrease in LAMP-2A levels compared to the GFP control group **(Figure 3.6 A and B)**. We further assessed the effect of TFEB restoration on lysosomal proteolytic capability by measuring the activity of the cysteine protease enzyme, cathepsin B. We reconfirmed our prior findings that NRCMs treated with either palmitate or a combination of GP significantly suppressed cathepsin B activity compared to cells treated with either BSA or glucose **(Figure 3.6 C**). Furthermore, cathepsin B activity was significantly increased in BSA or glucose incubated NRCMs transduced with either WT or phosphorylation resistant TFEB (S142A) compared to viral control GFP **(Figure 3.6 C**). TFEB restoration in NRCMs also attenuated palmitate- or GP-induced suppression in cathepsin B activity **(Figure 3.6 C**). Alternatively, we examined the effect of TFEB silencing on lysosomal content. In contrast to our finding from *in-vivo* $TFEB^{-/-}$ cardiomyocyte, we observed that acute silencing of TFEB in H9C2 cells using short hairpin RNA (shRNA)-TFEB (TFEBKD) significantly decreased LAMP-2A levels following treatment with all substrates compared to their shRNA control group **(Figure 3.7 A, B and C**). These data suggest that the impact of acute (cell culture-short term genetic manipulation of TFEB) versus chronic (constitutive TFEB deletion in mouse cardiomyocytes) loss of TFEB might have distinct effects on lysosomal signaling and function. Furthermore, in the cardiomyocytes, profound effects on lysosomal proteolytic machinery are more evident following overexpression of TFEB than compared to TFEB silencing.

3.4 Discussion

Prior report from our laboratory demonstrated that simulating nutrient overload in *in-vivo, ex-vivo* and *in-vitro* negatively targets TFEB to suppress autophagy, lysosome function and proteolytic activity in the cardiomyocyte [226]. TFEB-mediated regulation of lysosome biogenesis, lysosome autophagy and lysosome function are tested in several cellular and mouse models of human diseases, especially resulting from the accumulation of non-degraded proteotoxic aggregates [288,299,304]. Mice with TFEB overexpression in the liver and macrophages positively regulates the expression of genes involved in lysosome function and autophagy [299] [333,334]. Conversely, both skeletal muscle- and adipocytes-specific TFEB overexpressing mice did not upregulate lysosome and autophagy-related genes [316,330]. Remarkably, in the current study, transcriptome analysis in the cardiomyocyte from mice with constitutive cardiomyocyte specific TFEB deletion revealed that loss of TFEB did not exert expected inhibition on lysosomal and autophagic pathways. In fact, lack of TFEB in the cardiomyocyte rather induced a striking upregulation of genes required for lysosome function (*Ctsz, Ctsk, Ctsh, Gba* and *Gba2*), autophagosome formation and fusion machinery (*Sqstm1, Atg13* and *Map1a*), findings distinct from prior published models of genetic inactivation of TFEB [298,299].

In addition to *in-vivo* mouse model with cardiomyocyte-specific TFEB$^{-/-}$, we employed the *ex-vivo* model to modulate TFEB levels and examine its role in regulating lysosome function and biogenesis. Interestingly, the gain-of-function of TFEB increases lysosome content and proteolytic activity, whereas loss-of-function of TFEB yielded the opposite outcome in an *ex-vivo* model of cardiomyocytes. Our data agree with the prior finding, which suggests that TFEB regulates lysosome function and biogenesis in the cardiomyocyte. Indeed, forced expression of TFEB in the cardiomyocyte increases lysosome biogenesis and autophagosome processing and attenuates BNIP3-induced cell death [369]. In a separate study, myocardial TFEB signaling is impaired in cardiac proteinopathy, whereas TFEB overexpression improves the autophagic-lysosomal pathway

and protects against proteotoxicity in the cardiomyocyte [381]. Likewise, TFEB overexpression in HUVEC cells induces transcription of lysosome and autophagy genes.

Disparate findings on the role of TFEB in regulating lysosome function and lysosome biogenesis could likely be time-dependent. For instance, an *in-vivo* mouse model with constitutive (since birth) deletion of TFEB in the cardiomyocyte versus an acute loss of TFEB *ex-vivo*. Importantly, the impact of lack of TFEB *in-vivo* on lysosome function and autophagy in the cardiomyocyte was investigated at baseline or in unchallenged mice. It is also likely any residual TFEB in $TFEB^{-/-}$ cardiomyocytes will promote transcription of TFEB targeted genes involved in autophagy and lysosome pathway. Since TFEB and TFE3 share overlapping functions, it is unclear in the current study whether TFE3 compensates for the loss-of-function of TFEB in the cardiomyocyte and upregulates genes associated with lysosome function. It is plausible that pathways of autophagy and lysosome function are upregulated in the cardiomyocyte to compensate for the loss-of-action of genes involved in other pathways and help promote the survival of mice at birth. We speculate that subjecting $TFEB^{-/-}$ mice to metabolic stress can lead to loss of the compensatory upregulation of lysosome pathways in the cardiomyocyte and likely triggering cardiac remodeling and hypertrophy.

3.5 Tables

Table 3.1: List of mouse primers and sequences

Primer	Primer Sequence (5' to 3')
Mouse-TFEB F (Genotyping)	GTAGAACTGAGTCAAGGCATACTGG
Mouse-TFEB R (Genotyping)	GGGTCCTACCTACCACAGAGCC
Mouse-LoxP	CTTCGTATAATGTATGCTATACGAAG
Mouse-LAR3	CAACGGGTTCTTCTGTTAGTCC
Mouse-ET-188 F	GCC CTGGAAGGGATTTTTGAAGCA
Mouse-ET-189 R	ATGGCTAATCGCCATCTTCCAGCA
Mouse-ET-190 F	GATCTCCAGCTCCTCCTCTGTC
Mouse-ET-191 R	GGTCAGCCTAATTAGCTCTGT
Mouse-TFEB F	GTCTAGCAGCCACCTGAACGT
Mouse-TFEB R	ACCATGGAGGCTGTGACCTG
Mouse-HPRT1 F	CAGTCCCAGCGTCGTGATTA
Mouse-HPRT1 R	GGCCTCCCATCTCCTTCATG
Mouse-RPL27 F	ACGGTGGAGCCTTATGTGAC
Mouse-RPL27 R	TCCGTCAGAGGGACTGTCTT

Chapter 4: Loss of TFEB remodels lipid metabolism and cell death pathways in the cardiomyocyte

All figures and portions of the text present in this chapter have been reproduced with the copyright permission from Elsevier (Appendix 1) and edited as appropriate:

Trivedi, P.C.; Bartlett, J.J.; Mercer, A.; Slade, L.; Surette, M.; Ballabio, A.; Flibotte, S.; Hussein, B.; Rodrigues, B.; Kienesberger, P. C.; Pulinilkunnil, T. Loss of function of transcription factor EB remodels lipid metabolism and cell death pathways in the cardiomyocyte. Biochim Biophys Acta Mol Basis Dis 2020, 1866 (10):165832 [339].

4.1 Rationale and objectives

Prior research has demonstrated that autophagy is activated during starvation to perform a lysosome-dependent catabolic process and resulting break down products are used as the source of energy to ensure cell survival and homeostasis. On the other hand, increased TAG and lipid droplet content are observed when autophagy is inhibited, highlighting a critical role of autophagy in regulating lipid metabolism [382]. Furthermore, autophagy is also important in shuttling lipid droplets to the lysosome, where they are hydrolyzed into free FAs and glycerol through the action of lysosomal acid lipase [383]. These observations indicate the close relationship between intracellular lipid metabolism and the lysosomal-autophagic pathway. Interestingly, in chapter 3, our transcriptome data in the cardiomyocyte from $TFEB^{-/-}$ mice revealed that among DEGs, majority of genes are associated with cellular metabolism pathways. However, the process by which TFEB-autophagy-lipid metabolism is coordinated in cardiomyocytes to reprogram metabolism remained to be examined.

In addition to cellular metabolism, transcriptome analysis also indicated alteration of genes involved in cell death and cell survival pathways due to the loss of TFEB in the cardiomyocyte. Indeed, numerous studies have established the role of TFEB in influencing cardiomyocyte viability and function. Ischemia-reperfusion and hypoxic injuries in the heart are exacerbated following the

loss of TFEB function, an effect dependent on BNIP3-induced cell death [369,370]. Data from our laboratory showed that cardiomyocytes exposed to doxorubicin (DOX) [344] and glucolipotoxicity [226] diminish nuclear TFEB content and concomitantly induces cell death.

Despite the above studies highlighting the critical role of TFEB in influencing cardiomyocyte viability and function, underlying mechanisms by which loss of TFEB engages nutrient-sensing pathways to remodel cardiac energy metabolism remain unclear. Therefore, the objective of this thesis chapter is to examine 1) the metabolic pathways remodeled in response to the loss of TFEB action and whether this metabolic switch impacts cardiac energy metabolism, 2) whether TFEB-dependent regulation of cardiac metabolism requires autophagy, 3) whether cell death and cell survival pathways impacted due to the cardiomyocyte TFEB depletion, 4) whether an alteration in TFEB levels ameliorate or exacerbate glucolipotoxicity-induced cardiomyocyte injury and 5) putative upstream regulators of TFEB in the cardiomyocyte.

4.2 Materials and Methods

4.2.1 Cell culture

4.2.1.1 Adult mouse cardiomyocyte isolation

Adult mouse cardiomyocytes were isolated as described in section 2.2.5.2.

4.2.1.2 H9C2 cardiomyoblast culture

H9C2 cardiomyoblast cells were cultured as described in section 2.2.5.1.

4.2.1.3 Neonatal rat ventricular cardiomyocyte isolation

Neonatal rat ventricular cardiomyocytes (NRCMs) were isolated as described in section 3.2.2.3.

4.2.1.4 Adenoviral transduction

Adenoviral transduction of Myc-tagged human KLF15 (SKU: ADV-213183, Lot: 20161122T3), HA-tagged human TFEB (SKU: ADV-225358, Lot:20140903T9), Myc-tagged human phosphorylation-resistant mutant TFEB (S142A) (courtesy of Dr. Shawn Ferguson

laboratory), FLAG-tagged human phosphorylation-resistant mutant TFEB (S211A), CMV-GFP (20160126T6), Scramble-RNAi (SKU: 1122, Lot: 20150210T14), rat TFEB-ShRNA (shADV-294304, Lot: 20140930T3) or CMV-mCherry (SKU: 1060, Lot: 20161220T5) were performed as described in section 3.2.2.3.

4.2.1.5 Cell transfection

H9C2 cells were plated at a density of 0.25 x 10^6 in 35 mm plates. Cells were transfected in a serum-free medium of DMEM 1X (1196600-025, Thermo Fisher Scientific) at a confluency of 80% after the plating. For transfection, 9 µl of Lipofectamine RNAiMAX reagent (13778150; Thermo Fisher Scientific) was diluted in Opti-MEM medium (31985-062; Gibco by Life Technologies). In a separate set of tubes, SiRNA against Atg7 (259550; Thermo Fisher Scientific) and SiRNA negative control (4390844; Thermo Fisher Scientific) Opti-MEM medium were diluted. In a ratio of 1:1, diluted SiRNA was mixed with diluted Lipofectamine RNAiMAX reagent. The mixture was incubated for five minutes to form SiRNA-lipid complex. Finally, 250 µl of SiRNA-lipid complex was added to cells with a concentration of 10 nM of SiRNA per plate. After 24 hr of cell transfection, medium serum-free medium was replaced with H9C2 growth medium. 24 hr following the medium replacement, cells were treated with different substrates as described in section 2.2.5.4.

4.2.1.6 Preparation of bovine serum albumin (BSA) complexed fatty acid

BSA complexed fatty acids media was prepared as described in section 2.2.5.3.

4.2.2 Immunoblot analysis

Immunoblot analysis was performed as described in section 2.2.6.

4.2.3 Immunostaining

Immunostaining for KLF15 (NBP2-24635; Novus Biologicals) and TFEB (A303-673a-T; Bethyl Laboratories) was performed as described in section 3.2.7.

4.2.4 Oil Red O staining

H9C2 cells were plated on 60 mm plates with a coverslip at a density of 0.5 x 10^6 and treated with BSA or 1.2 mM oleate for 20 h to induce lipid droplet formation. Oil Red O stock solution was prepared by dissolving 300 mg of Oil Red O powder (O0625; Sigma Aldrich) in 100 ml of 100% isopropanol. Oil Red O working solution was prepared by adding 3 parts of Oil Red O stock solution to 2 parts of water, following which the solution was filtered through Whatman filter paper (1001-150; Whatman Filter Papers). Cells were washed 2X with PBS and fixed using 10% formalin for 30 mins. After fixing, cells were washed twice with PBS and incubated with 60% isopropanol for 5 mins. After 5 mins, isopropanol was discarded, and cells were covered evenly with the Oil Red O working solution for 20 mins. Cells were then washed with water carefully to discard the excess stain and incubated with hematoxylin (72704; Thermo Fisher Scientific) for 1 min to stain the nuclei. Following hematoxylin staining, cells were washed and cover with water to view under the ZEISS microscope with brightfield view. The area of lipid droplets from 80 to 150 images (300 to 400 nuclei) was quantified using Image J software. In the Image J software, lipid droplets were separated using the Threshold color from the Adjust program. Lipid droplets were analyzed from the Analyze Particles menu, and lipid droplets size was restricted from 20 to 30 infinity. Results were exported to an excel file and presented as %Area/Nuclei.

4.2.5 Caspase-3 activity

H9C2 cells were plated in 24 well plates. Cells were differentiated for 48 h and transfected using adenoviruses for 48 h. Subsequently, cells were treated with either BSA, glucose, palmitate or a combination of glucose/palmitate for 16 h and caspase-3 activity was measured using a caspase-3 activity assay kit (5723, Cell Signaling). Briefly, following treatment, the cell plate was spun at 300g for 10 min, media was removed, and cells were rinsed with ice-cold PBS by spinning the plate at 300g for 10 min. Lysis buffer was added, and the plate was left on ice for 5 min. In a separate 96 black well plate appropriate for fluorescent assay, 25 µl of AMC (7-amino-4-methylcoumarin) and 200 µl of assay buffer was added, which served as a positive control. For

samples, 200 µl of Ac-DEVD-AMC fluorescent substrate and 25 µl of lysate solution was added. The plate was incubated at 37°C in the dark, at least for 1h. The relative fluorescence unit (RFU) was measured by using the Synergy H4 fluorescence plate reader with the excitation wavelength of 380 nM and the emission wavelength of 420– 460 nM.

4.2.6 Statistical Analysis

Results are expressed as mean ± SEM. Pairwise comparison between groups was performed using unpaired two-tailed Student's t-test. Comparisons between multiple groups were performed using one- or two-way ANOVA followed by a Bonferroni or Tukey post hoc test, as appropriate. All statistical analysis was performed using Prism (GraphPad Software). P-values of less than 0.05 were considered statistically significant. For animal studies, "n" refers to the number of mice used, unless otherwise specified. For cell culture studies, experiments were performed in triplicates and data are from at least three independent experiments.

4.3 Results

4.3.1 Differential expression of energy metabolism pathway genes in cardiomyocyte with TFEB deletion

In addition to TFEB's canonical role in governing the autophagy-lysosome pathway, it remains unclear which other pathways have been remodeled due to the loss of TFEB in the cardiomyocyte. Transcriptome data depicted the modulation of genes engaged in cellular metabolism in $TFEB^{-/-}$ cardiomyocytes.

We first analyzed genes associated with carbohydrate metabolism. Transcriptome analysis depicted that from DEGs associated with cellular metabolism, ~20% were related to carbohydrate metabolic processes in $TFEB^{-/-}$ cardiomyocytes **(Figure 4.1)**. Amongst these, ~ 8% and ~ 3% genes represented pathways related to glucose metabolism and gluconeogenesis, respectively **(Figure 4.1 A)**. Genes involved in processing glucose through glycolysis such as *Pfkp, Gpd1, slc37a4, hk1,*

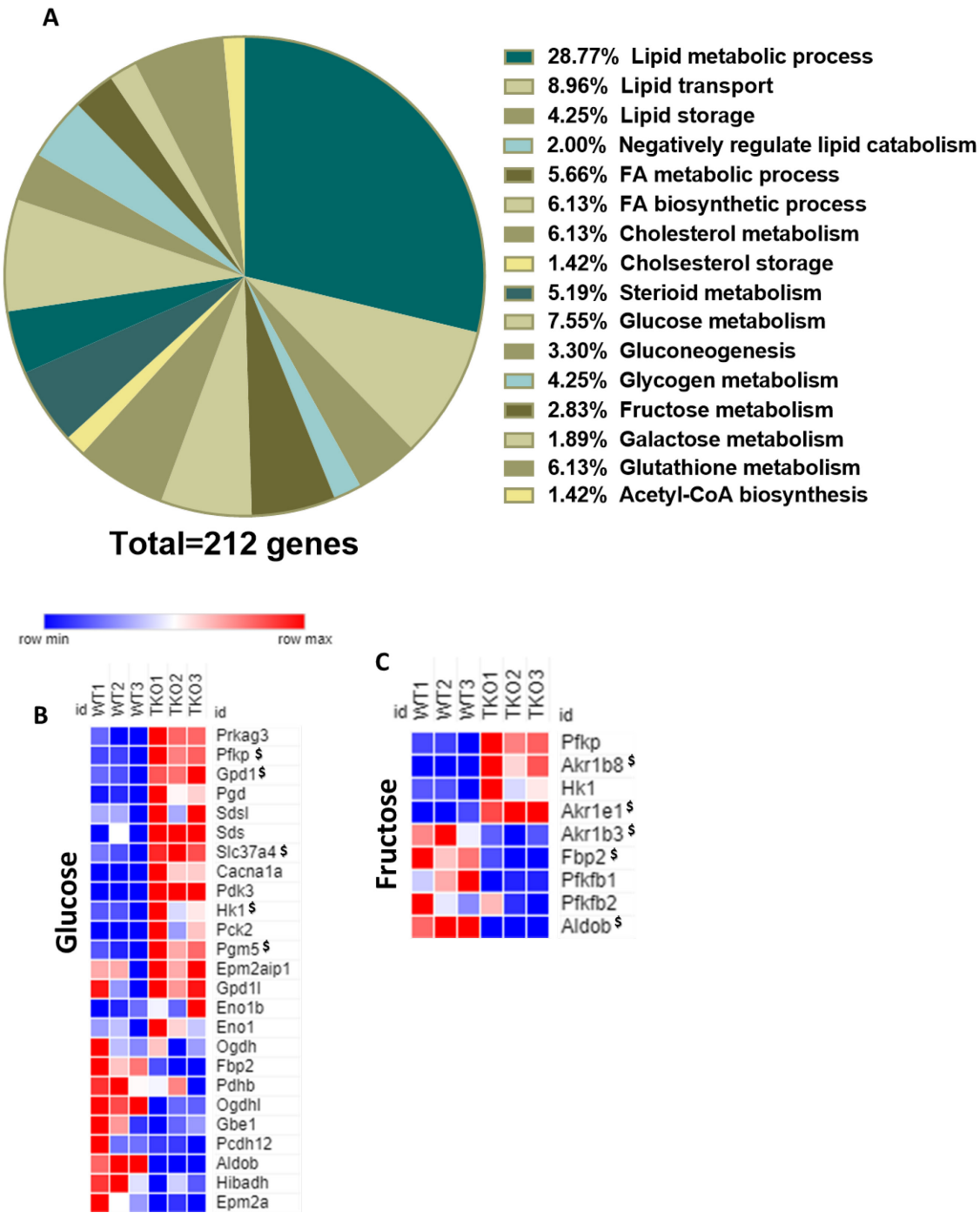

Figure 4.1 TFEB regulates genes involved in energy metabolism pathways in the cardiomyocyte. (A) The inset describes the percentage of differentially expressed genes involved in cellular metabolic processes from RNA-Seq analysis in cardiomyocytes from TFEB$^{fl/fl}$ (n=3) and TFEB$^{-/-}$ (n=3) mice. (B and C) Heatmap of differentially expressed genes involved in glucose metabolism and fructose metabolism from RNA-Seq analysis in cardiomyocytes from TFEB$^{fl/fl}$ (n=3) and TFEB$^{-/-}$ (n=3) mice.

Pdk3 and *Pgm5* were significantly upregulated in TFEB$^{-/-}$ cardiomyocytes **(Figure 4.1 B)**. Additionally, genes involved in processing fructose and aldehyde sugars such as *Akr1b8, Akr1b3, Akr1e1, Aldob*, and *Fbp2* were differentially expressed in TFEB$^{-/-}$ cardiomyocytes **(Figure 4.1 C)**. Among genes associated with metabolic processes, ~72% were involved in pathways related to lipid, phospholipid, and cholesterol transport, lipid storage and metabolism and fatty acid metabolism and biosynthesis **(Figure 4.1 A)**. Additionally, genes essential for processing lipid intermediates (cholesterol, phospholipid, sphingolipid) such as *Decr2, Acsf2, Lipa and Stard3 w*ere significantly upregulated in cardiomyocytes lacking TFEB **(Figure 4.2 A and B)**. Surprisingly, lipid transport and metabolism gene such as *Cd36* were downregulated in TFEB$^{-/-}$ cardiomyocytes **(Figure 4.2 D-E)**. Additionally, the decrease in CD36 transcript was also confirmed by immunoblot analysis wherein CD36 protein levels were significantly decreased in cardiomyocytes from TFEB$^{-/-}$ mice **(Figure 4.2 B)**. Transcriptional regulator of lipid metabolism, PPARα, was also decreased in myocytes lacking TFEB **(Figure 4.2 C and D)**, suggesting that fatty acid oxidation processes are dampened in TFEB$^{-/-}$ cardiomyocytes. Genes that are located on the surface of the LD and regulate LD accumulation such as *Plin2* and *Plin5* were upregulated and downregulated, respectively **(Figure 4.2 B)**. Whereas genes involved in fatty acid biosynthesis (*Fasn, Mlycd)* and TG hydrolysis (*Lpl*) were upregulated **(Figure 4.2 A and B)**, signifying a plausible flux of FA from oxidation into storage in myocytes lacking TFEB.

4.3.2 Loss of TFEB action increases lipid deposition in the cardiomyocyte

Our transcriptome data suggested that loss of TFEB in the cardiomyocyte upregulates genes involved in lipid storage processes, suggesting that TFEB is crucial in regulating lipid metabolism in the cardiomyocyte. Therefore, we next examined the potential impact of the loss of TFEB on lipid droplet formation in cardiomyocytes.

To examine the effect of TFEB on lipid droplet (LD) formation, we first modulated TFEB levels by transducing H9C2 cells with adenoviruses that overexpress either human TFEB mutated at Ser211 (S211A) or silence TFEB using short hairpin RNA or their respective viral control.

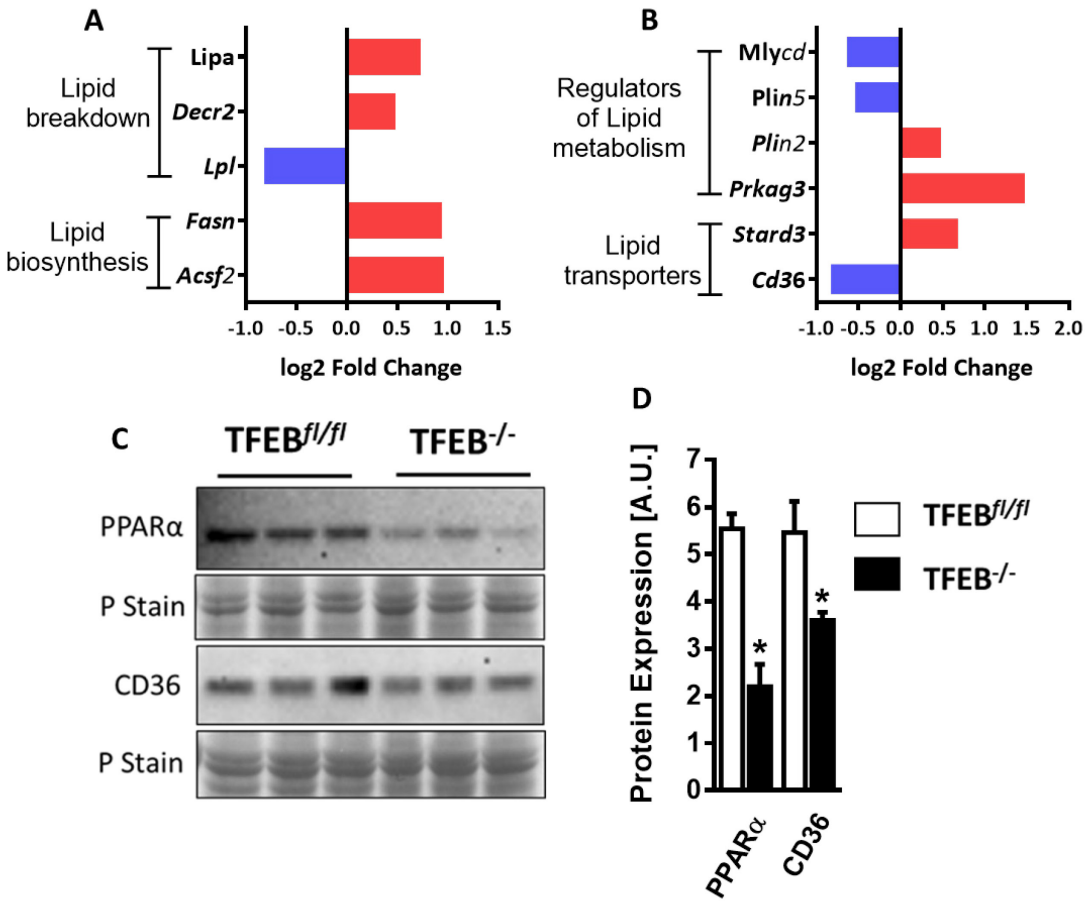

Figure 4.2 TFEB alters genes involved in lipid metabolism pathways in the cardiomyocyte. Log2 fold change of differentially expressed genes of (A) lipid breakdown, (A) lipid biosynthesis, (B) lipid metabolism regulators and (B) lipid transporters. (F) Immunoblot and densitometric analysis of protein expression of nuclear and cytosolic (G) PPARα and CD36, respectively, in adult mouse cardiomyocytes isolated from $TFEB^{-/-}$ and $TFEB^{fl/fl}$ mice. Graph represents mean ± S.E.M., n = 3, *P<0.05 vs $TFEB^{fl/fl}$ was performed using Student's t-test. A.U.; arbitrary unit, P Stain; Protein stain.

Subsequently, cells were treated with oleate or BSA control for 24 hr to induce LD formation. Following oleate treatment, LDs were stained with Oil Red O and the area of LD formation was examined. We found that in oleate treated H9C2 cells, adenoviral-mediated TFEB knockdown (TFEBKD) not only resulted in higher LD accumulation but also enlarged LD size compared to shRNA control **(Figure 4.3 A and B)**. Alternatively, TFEB overexpression (S211A) resulted in decreased LD formation compared to mCherry viral control **(Figure 4.3 A and C)**. Since autophagy plays an important role in lipid catabolism, we next assessed whether TFEB-mediated lipid breakdown requires the macroautophagy pathway. To examine whether lysosomal autophagy is required for lipid breakdown in the cardiomyocyte, we inhibited autophagy by targeting Atg7. Atg7 is essential in forming two ubiquitin-like conjugation complex such as Atg12-Atg5 and LC3II-PE conjugation, which are important for the maturation of autophagosome [214]. We transfected H9C2 cells with Atg7 SiRNA (Atg7KD) or siRNA control to inhibit macroautophagy, followed by treatment with oleate to induce LD formation. Atg7 silencing was confirmed using immunoblot analysis **(Figure 4.4 A-B)**. Atg7KD significantly increased LD formation in H9C2 cells compared to its SiRNA control **(Figure 4.4 C-D)**. Importantly, the decrease in oleate-induced LD formation following TFEB overexpression persisted in cells lacking Atg7 **(Figure 4.4 C-D)**. These data suggest that TFEB-dependent regulation of cardiomyocyte lipid utilization is largely independent of the macroautophagy pathway. Furthermore, TFEB exerts a non-canonical role in regulating lipid metabolism by affecting FA delivery, transport, oxidation and storage, and plausibly remodeling glucose utilization **(Figure 4.5).**

4.3.3 TFEB regulates cell death pathways and viability in the cardiomyocyte

Studies from our laboratory have demonstrated that loss of TFEB during glucolipotoxic stress increases caspase-3 cleavage and induces cell death in the cardiomyocyte [226]. Analysis of the transcriptome data revealed that in addition to genes involved in cellular metabolism, genes associated with cell death and apoptotic processes **(Figure 4.6 A)** were differentially enriched in cardiomyocytes with TFEB deficiency. Genes involved in the apoptotic process (*Sgpl1, Tnfrsf1a*

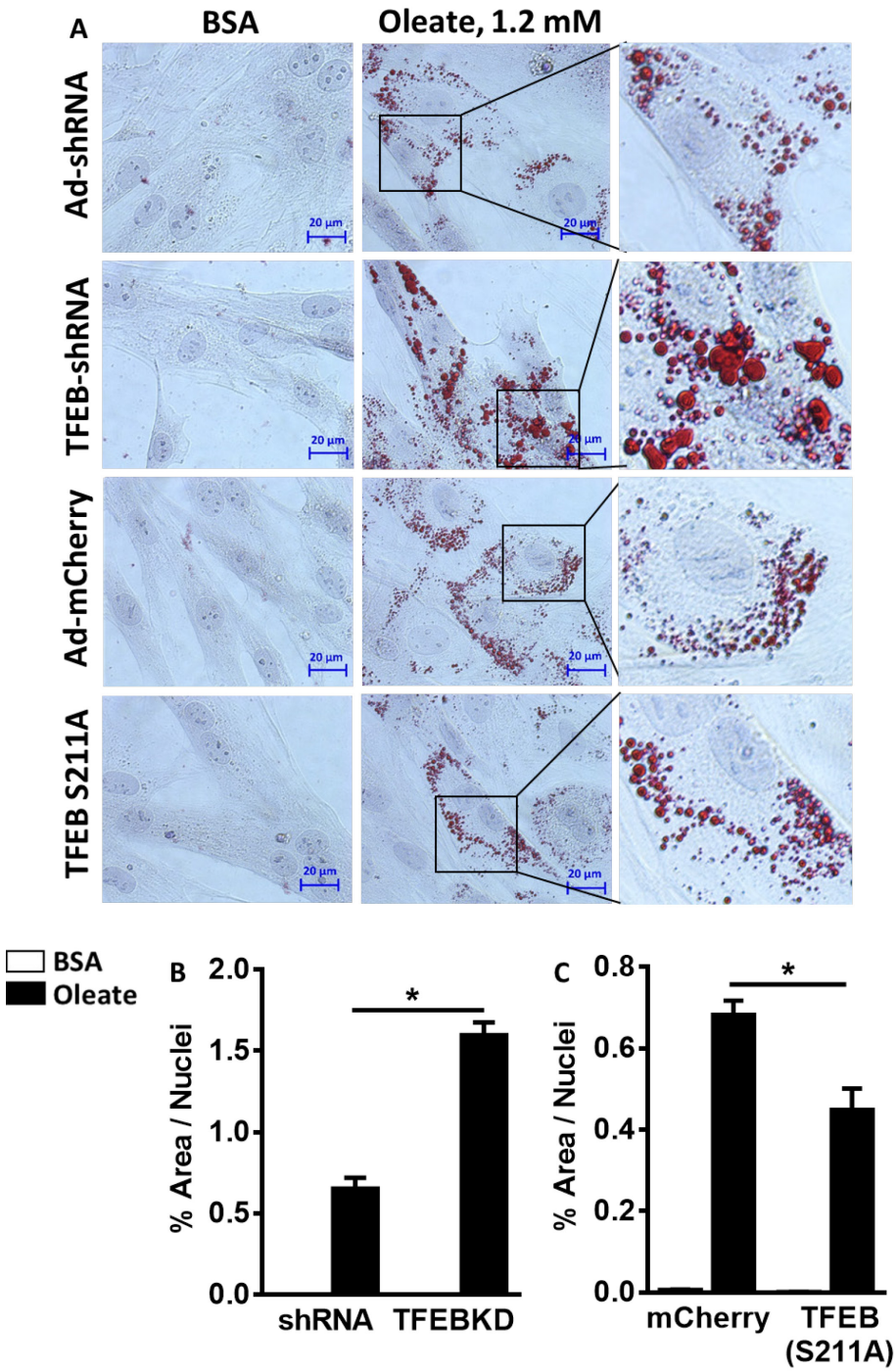

Figure 4.3 Oleate-induced lipid droplet formation is increased following TFEB silencing in H9C2 cells. (A, B and C) Lipid droplet staining using Oil Red O in H9C2 cells transduced with adenoviruses either overexpresses human mutant TFEB (S211A), rat TFEB shRNA or their respective control viruses, following their treatment with oleate (1.2 mM) or BSA for 16 hr. Graph represents mean ± S.E.M., n = 300 to 400 (80 to 100 images per group) nuclei from five technical replicates, *P<0.05 performed using one-way ANOVA.

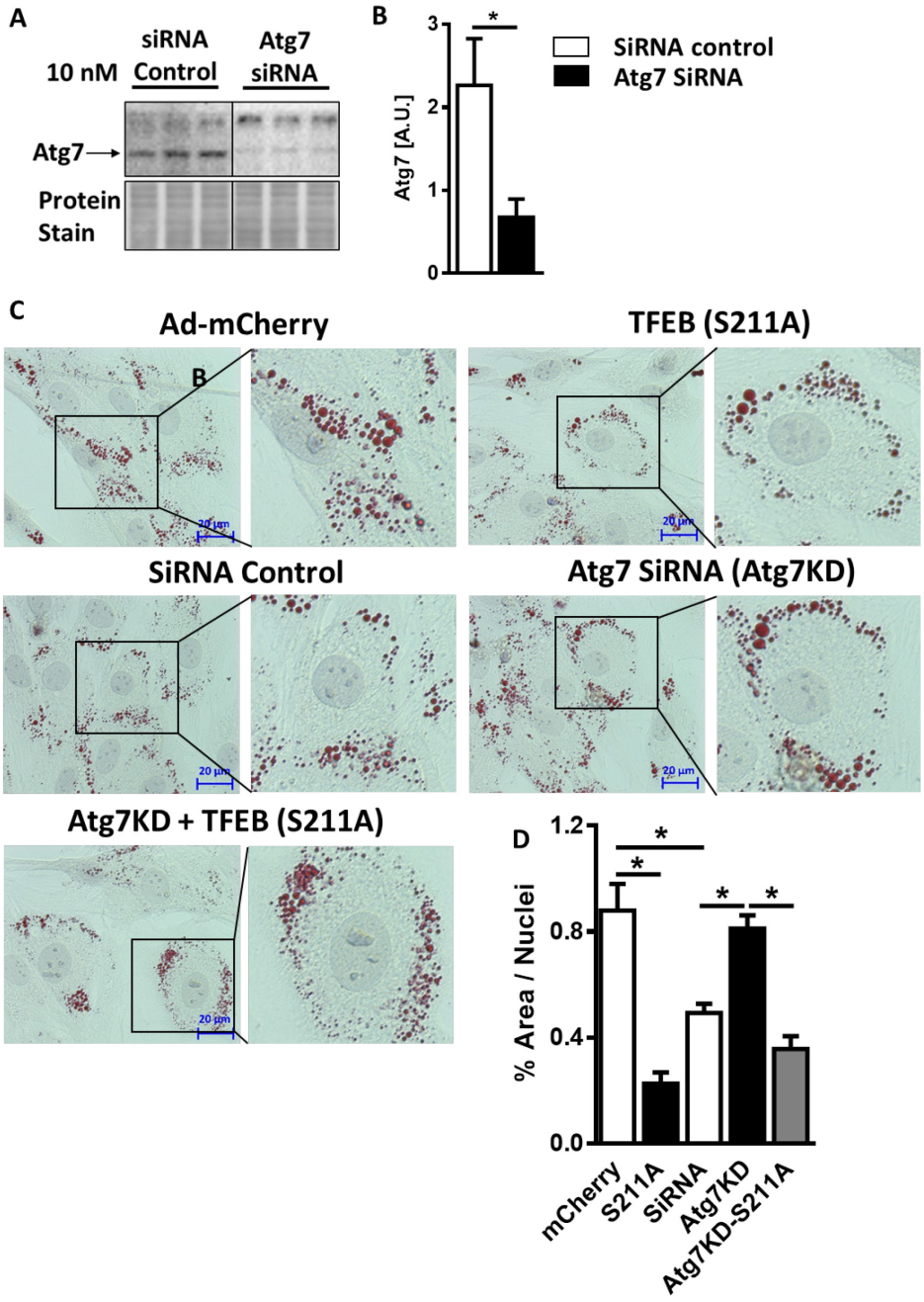

Figure 4.4 TFEB-mediated effect on lipid metabolism is independent of macroautophagy in the cardiomyocyte. (A) Immunoblot and densitometric analysis of protein expression of (B) Atg7 in H9C2 cells transfected with Atg7 siRNA or siRNA control for 48 h. Graph represents mean ± S.E.M., n = 3, *P < 0.05 was performed using Student's t-test. (C-D) Lipid droplet staining using Oil Red O in H9C2 cells transduced with adenoviruses overexpressing human mutant TFEB-S211A, rat TFEB shRNA or their respective viral controls and transfected with Atg7 siRNA or siRNA control following their treatment with oleate (1.2 mM) or BSA for 16 h. Graph represents mean ± S.E.M., n = 300 to 400 (80 to 100 images per group) nuclei from five technical replicates, *P < 0.05 was performed using One-Way ANOVA.

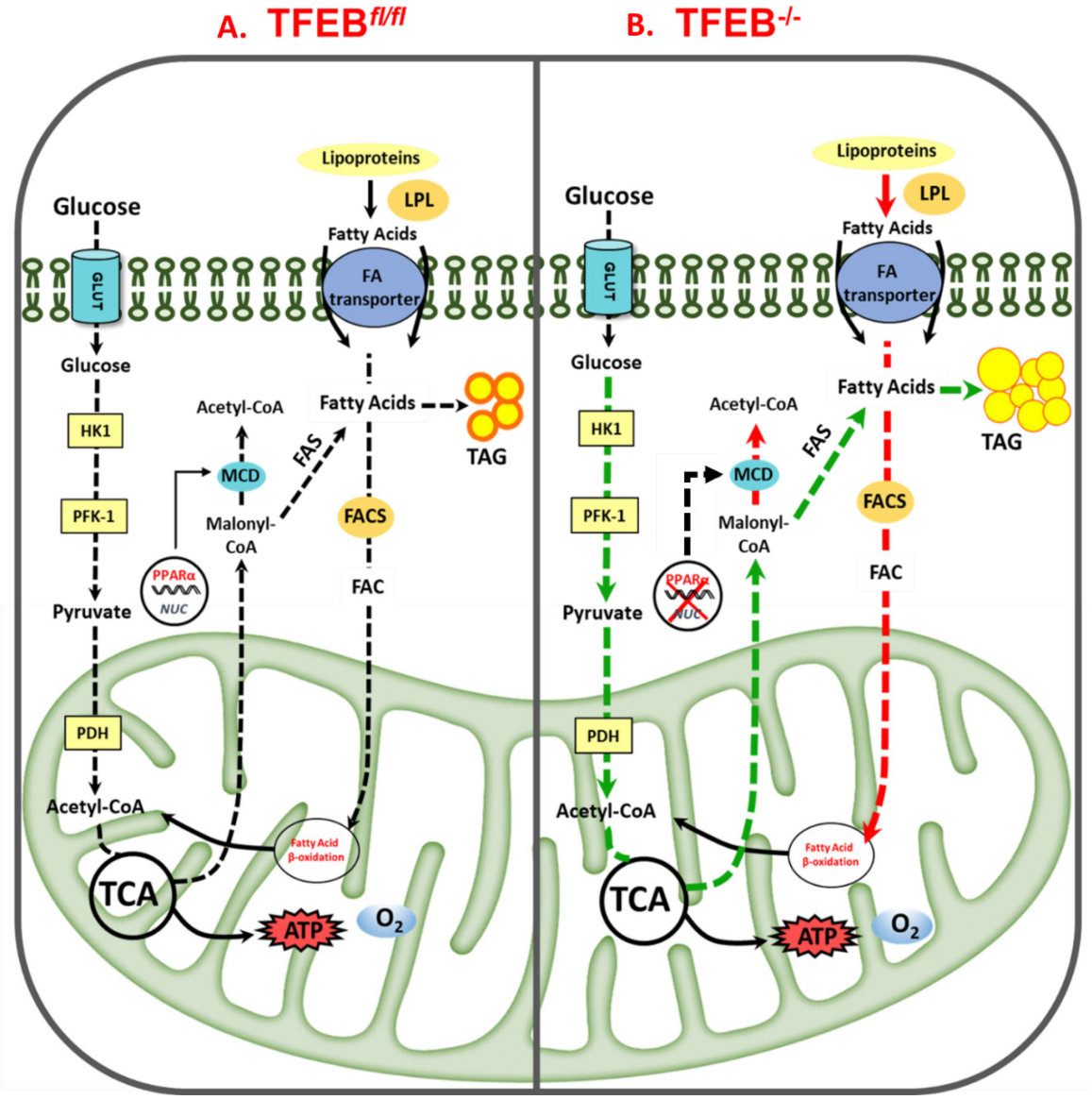

Figure 4.5 A probable mechanism for TFEB-dependent regulation of lipid and glucose metabolism in cardiomyocytes. (A) Intracellularly, glucose is processed to its end-product pyruvate through the sequential action of hexokinase 1 (HK1) and phosphofructokinase-1 (PFK-1) enzymes. The glycolytic end-product pyruvate is transported into the mitochondrial matrix and converted by PDH complex to form acetyl-CoA, which is processed via the TCA cycle to generate ATP. Within the mitochondria, citrate generated during the TCA cycle translocates to the cytosol to form malonyl-CoA, which is eventually converted back into acetyl-CoA by the action of malonyl-CoA decarboxylase (MCD) enzyme. LPL-derived FAs enter the myocardium via the concerted action of FA transporters. Intracellular FAs are processed by fatty acyl-CoA synthetase (FACS), generating intermediate fatty-acylcarnitine (FAC) that is further processed via a mitochondrial β-oxidation pathway to generate ATP through the TCA cycle. Activation of PPARα upregulates genes involved in FA oxidation. Additionally, activation of PPARα increases the MCD enzyme activity and decreases malonyl-CoA levels, augmenting FA oxidation. An increase in

malonyl-CoA levels can inhibit mitochondrial β-oxidation of FAs, redirecting FA incorporation into TAG. (B) Low levels of TFEB in the cardiomyocyte augment glucose utilization through the glycolytic pathway, as shown with the green dotted line. Furthermore, TFEB depletion in the cardiomyocytes decreases PPARα levels and MCD expression, likely increasing malonyl-CoA levels. Consequently, increases in malonyl CoA inhibits FA utilization, as shown in dotted red dotted lines and diverts FAs to TAG formation. The green dotted line signifies an upregulated pathway, and the red dotted line indicates the downregulated pathway due to the loss of TFEB in the cardiomyocytes.

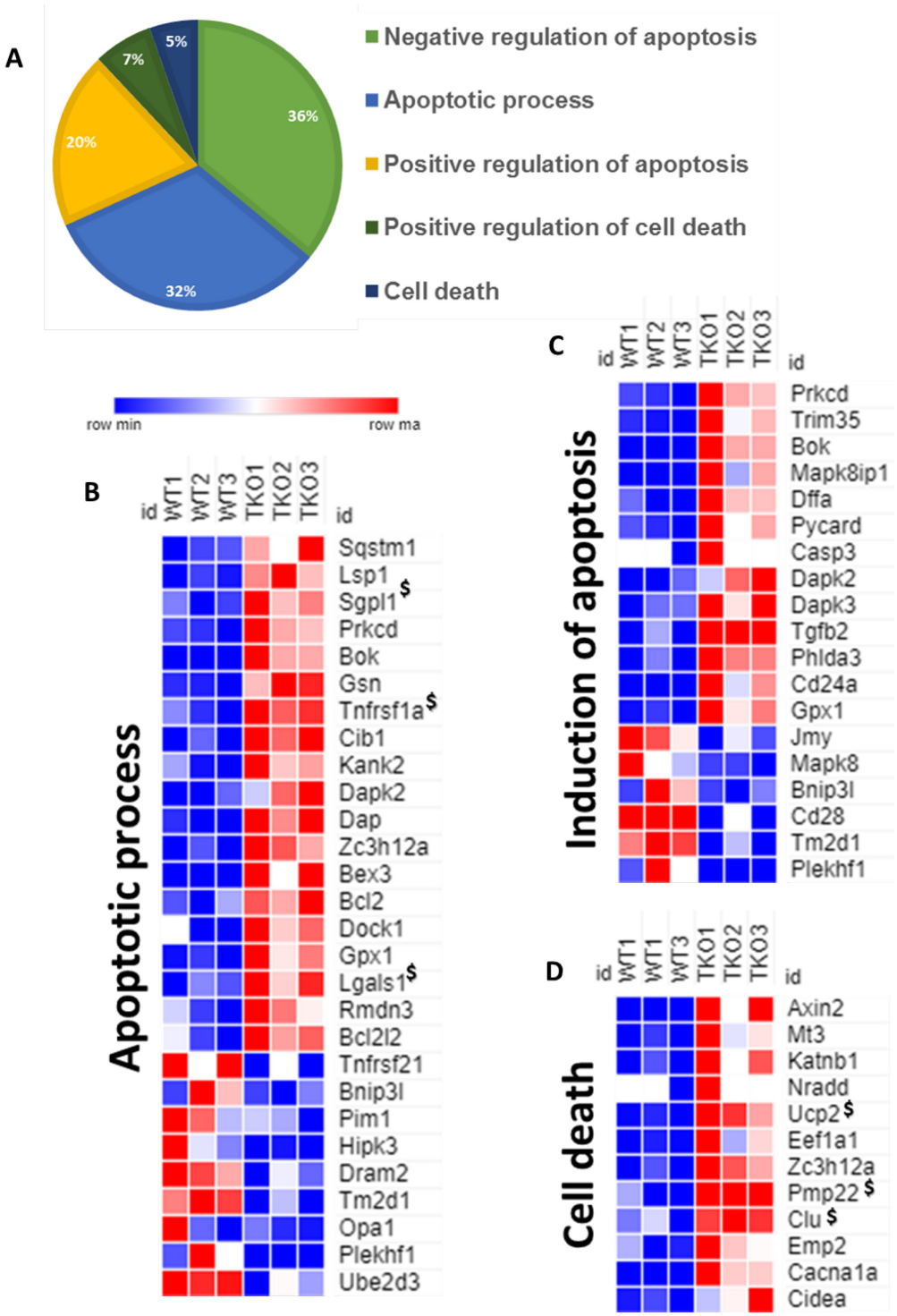

Figure 4.6 TFEB regulates the cell death pathway in the cardiomyocyte. (A) The inset describes the percentage of differentially expressed genes involved in apoptosis and cell death processes from RNA-Seq analysis in cardiomyocytes from TFEB$^{fl/fl}$ (n = 3) and TFEB$^{-/-}$ (n = 3) mice. Heatmap of differentially expressed genes in cardiomyocytes encoding (B) apoptotic process, (C) induction of apoptosis and (D) cell death.

and *Lgals1*) and cell death (*UCP2, Clu* and *Pmp22*) were upregulated in the cardiomyocyte lacking TFEB **(Figure 4.6 B, C and D)**. Since genes engaged in apoptosis and cell death pathways were increased in response to TFEB deficiency in cardiomyocytes, we postulated that TFEB is essential for cardiomyocyte survival. We further assessed the role of TFEB in regulating cell survival and whether preventing TFEB decline resisted glucolipotoxicity-induced cell death in the cardiomyocyte. We next ascertain whether gain- or loss-of-function of TFEB prevent or exacerbate glucolipotoxicity-induced cellular stress. We transduced H9C2 cells with adenoviruses overexpressing human WT TFEB or phosphorylation resistant mutant TFEB (S142A and S211A) or TFEB short hairpin RNAi or GFP/mCherry/ShRNA control viruses. Subsequently, H9C2 cells were treated with different substrates. We first reconfirmed our prior findings and observed that H9C2 cells treated with palmitate or a combination of glucose/palmitate (GP) augmented caspase-3 cleavage compared to BSA control and glucose alone **(Figure 4.7 A-B, D-E and G-H)**. Importantly, WT TFEB or constitutively active phosphorylation resistant mutant TFEB (S142A and S211A) attenuated palmitate- or GP-induced increase in caspase-3 cleavage **(Figure 4.7 A-B, D-E and G-H)**. Next, we also ascertained whether anti-apoptotic proteins were involved in TFEB-mediated suppression of palmitate- and GP-induced caspase-3 activation. We did not observe a significant alteration in expression of anti-apoptotic protein B-cell lymphoma 2 (Bcl2) in response to palmitate and GP treatment in H9C2 cells **(Figure 4.7 A, C and D, F and G, I)**. Importantly, TFEB overexpression augmented Bcl2 content in H9C2 cells treated with all different substrates compared to their respective viral control group **(Figure 4.7 A, C and D, F and G, I)**.

We further examined whether TFEB knock-down exacerbates or attenuate caspase-3 cleavage. We first confirmed TFEB deletion using western blot analysis when H9C2 cells were transduced with adenovirus overexpressing TFEB ShRNA **(Figure 4.8 A and B).** Furthermore, TFEBKD significantly increased caspase-3 cleavage in H9C2 cells treated with palmitate or GP compared to BSA control and glucose alone **(Figure 4.8 A and C)**. Notably, TFEBKD did not exacerbate caspase-3 cleavage when H9C2 cells were treated with palmitate and GP compared to

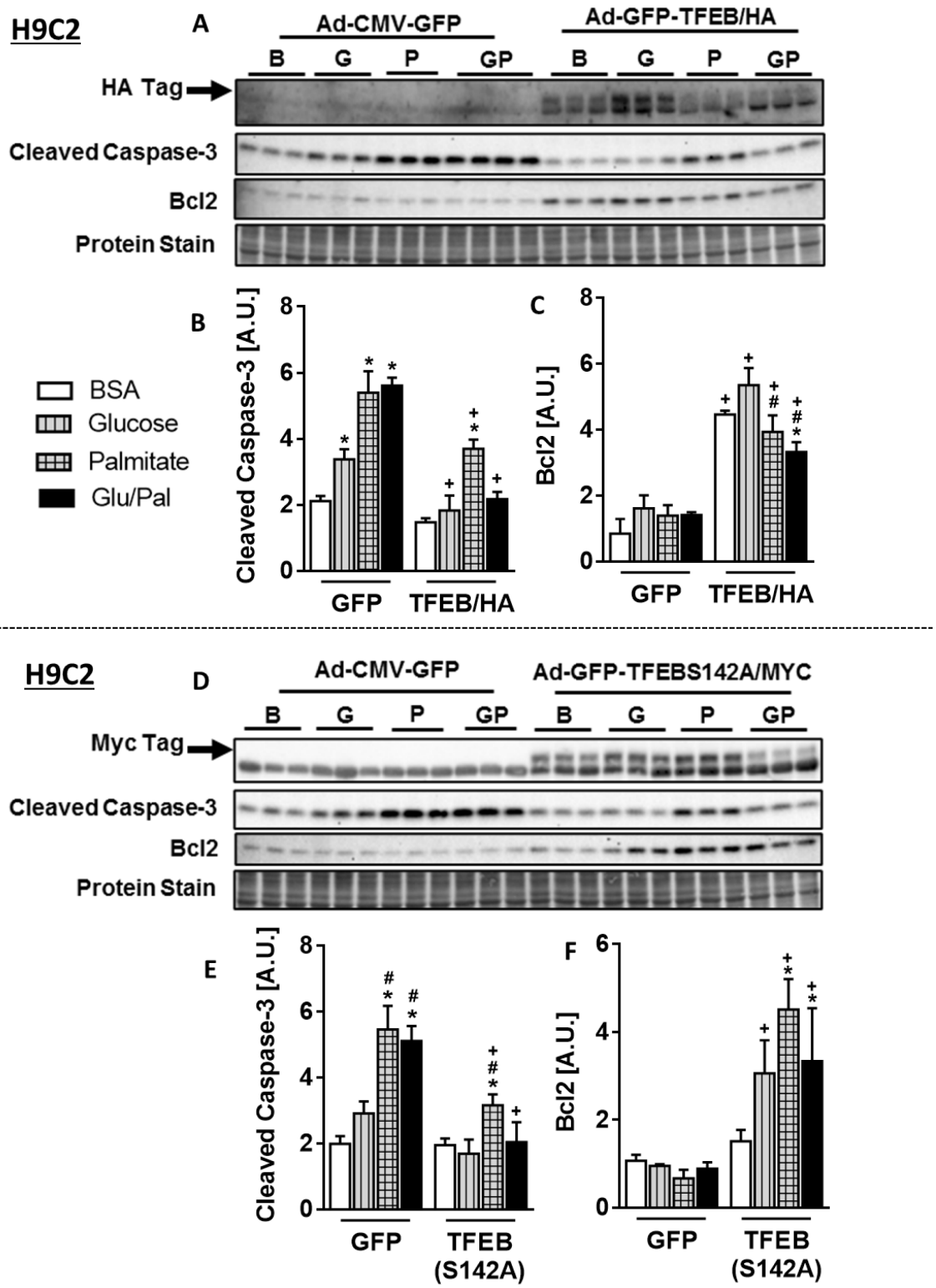

Figure 4.7 is continued on the next page

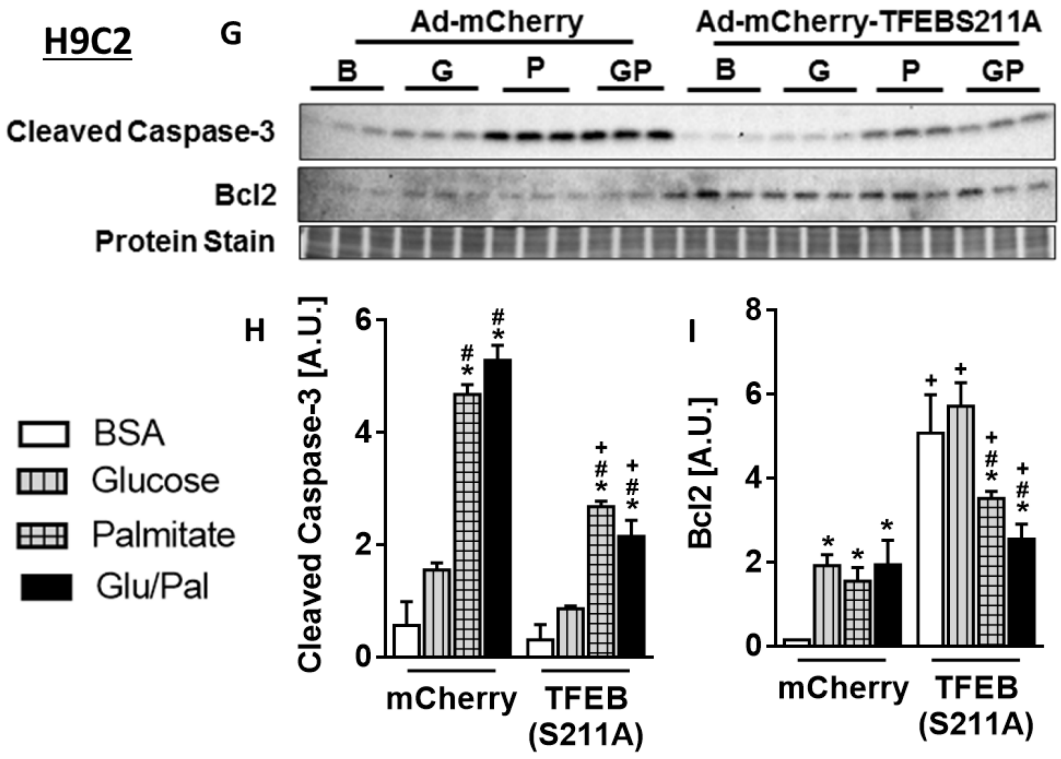

Figure 4.7 Preventing TFEB decline attenuates the nutrient overload-induced increase in caspase-3 cleavage and activity. H9C2 cells transduced with adenoviruses overexpressing either human WT-TFEB, phosphorylation-resistant mutant TFEB (S142A and S211A) or control GFP/mCherry virus, followed by treatment with BSA (B), glucose (G; 30 mM), palmitate (P; 1.2 mM) or a combination of glucose and palmitate (GP; 30/1.2 mM) for 16 h. (A, D and G) Immunoblot and densitometric analysis of protein expression of (B, E and H) cleaved caspase-3 and (C, F and I) Bcl2. Graph represents mean ± S.E.M., n = 3 from three independent sets of experiments, *P < 0.05 vs BSA, #P < 0.05 vs G and +P < 0.05 vs their respective control virus, two-way ANOVA; A.U.; arbitrary unit, P Stain; protein stain.

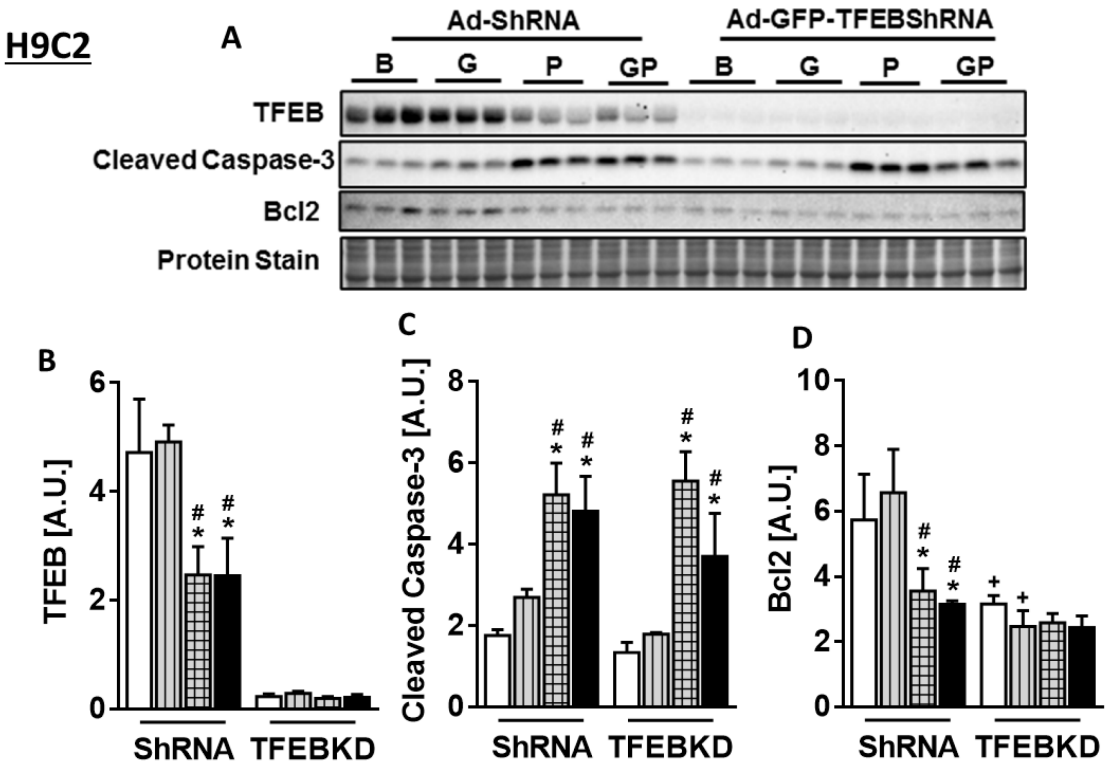

Figure 4.8 TFEB silencing did not exacerbate caspase-3 cleavage following nutrient overload in H9C2 cells. H9C2 cells transduced with adenoviruses overexpressing TFEB-ShRNA or ShRNA control followed by the treatment with BSA, glucose (G; 30mM), palmitate (P; 1.2 mM) or a combination of glucose/palmitate (GP; 30/1.2 mM) for 16 h. (A) Immunoblot and densitometric analysis of protein expression of (B) TFEB, (C) cleaved caspase-3 and (D) Bcl2. Graph represents mean ± S.E.M., n = 3 from three independent sets of experiments, *P<0.05 vs BSA, #P<0.05 vs G and +P<0.05 vs respective viral control was performed using two-way ANOVA; A.U.; arbitrary unit, P Stain; protein stain.

their respective ShRNA viral control group **(Figure 4.8 A and C)**. We next assessed the effect of TFEBKD on Bcl2 protein expression. We observed that TFEBKD significantly decreased Bcl2 levels in H9C2 cells treated with BSA, glucose, palmitate or a combination of glucose/palmitate compared to their respective ShRNA control group **(Figure 4.8 A and D)**. We further recapitulated our findings from the *ex-vivo* H9C2 model in the primary cell culture of neonatal rat cardiomyocytes (NRCMs). We demonstrated that NRCMs treated with palmitate, and a combination of glucose/palmitate significantly increased cleaved to total caspase-3 ratio **(Figure 4.9 A and B).** NRCMs transduced with WT-TFEB or mutant-TFEB (S142A) adenoviruses ameliorated the palmitate- and GP-induced increase in cleaved to total caspase-3 ratio **(Figure 4.9 A and B).** Additionally, overexpression of phosphorylation-resistant TFEB (S142A) ameliorated palmitate- or GP-induced increase in caspase-3 activity in H9C2 cells **(Figure 4.9 C)**. These data infer that glucolipotoxicity adversely affects TFEB's action, rendering cardiomyocytes susceptible to cellular stress and injury, an effect reversed by restoring TFEB content in the nucleus **(Figure 4.9 D)**.

4.3.4 Intramyocellular TFEB is modulated by changes in KLF15 expression

TFEB plays an essential role in regulating lipid metabolism through its effects on PPARα in the liver and skeletal muscle [299,316]. In the current study, we have provided evidence that TFEB remodels lipid metabolism in the cardiomyocyte. Kruppel-like family (KLF15) of transcription factors are also master regulators of FA and glucose metabolism [384-386]. Recently, a link between KLF4 and autophagy was reported in *C. elegans* [387]. Since both TFEB and KLF15 govern lipid metabolic processes through the common axis of PPARα [299,316,385], we hypothesized if TFEB and KLF15 regulate each other to alter myocyte metabolism. H9C2 cells were transduced with adenovirus overexpressing either human KLF15 or its viral control mCherry followed by treatment with different substrates. KLF15 overexpression increased TFEB content and prevented palmitate-induced depletion of TFEB levels in H9C2 cells compared to the viral control cells

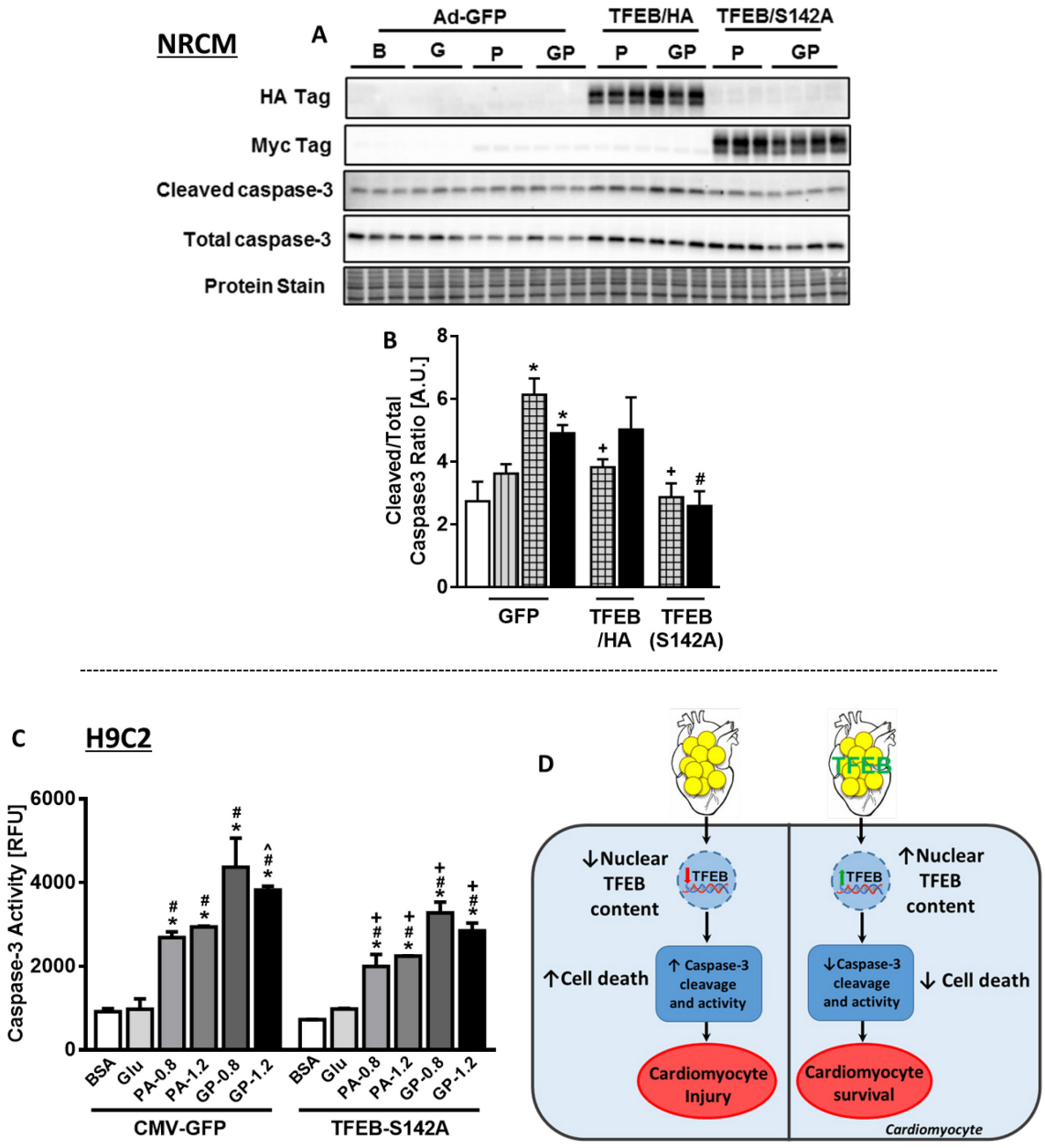

Figure 4.9 TFEB restoration ameliorates nutrient overload-induced increase in caspase-3 cleavage in neonatal rat cardiomyocytes (NRCMs). NRCMs transduced with adenovirus overexpressing either human WT-TFEB, mutant TFEB-S142A or control GFP adenovirus, followed by treatment with different substrates for 16 h. (A) Immunoblot and densitometric analysis of protein expression of (B) cleaved/total caspase-3 ratio. Graph represents mean ± S.E.M., n=3 from three independent sets of experiments, *P<0.05 vs BSA, +P<0.05 vs P-GFP and #P<0.05 vs GP-GFP was performed using Student's t-test. A.U.; arbitrary unit. (C) Caspase-3 activity in H9C2 cells transduced with adenoviruses overexpressing either human phosphorylation-resistant TFEB (S142A) or CMV-GFP control followed by the treatment with BSA, glucose (GLU; 30 mM), palmitate (PA; 0.8 or 1.2 mM) or a combination of glucose/palmitate (GP; 30/0.8 or 30/1.2 mM) for 16 h. Graph represents mean ± S.E.M., n = 3 from three independent sets of experiments,

*P<0.05 vs BSA, #P<0.05 vs glucose, ^P<0.05 vs 0.8 palmitate and +P<0.05 vs respective viral control was performed using two-way ANOVA. (D) Possible molecular mechanism of nutrient overload-induced myocyte injury. Nutrient overload decreases nuclear TFEB content in the cardiomyocyte, leading to an increase in caspase-3 cleavage and activity, causing cardiomyocyte injury. Restoration of TFEB in cardiomyocytes increases the nuclear translocation of TFEB and attenuates the nutrient overload-induced increase in cell death, offering protection from cellular injury.

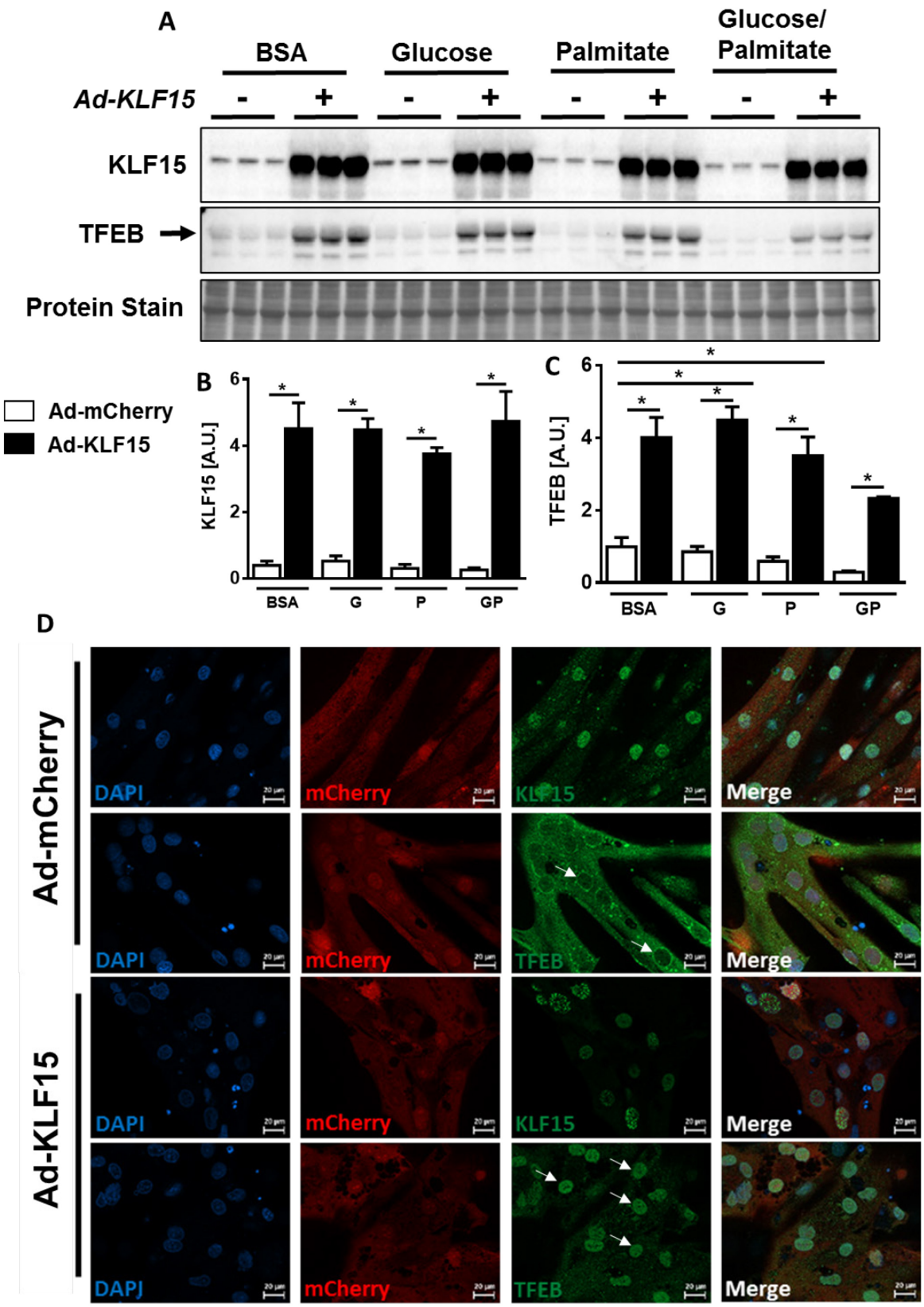
A
BSA
Glucose
Palmitate
Glucose/
Palmitate
Ad-KLF15
- + - + - + - +
KLF15
TFEB
Protein Stain
Ad-mCherry
Ad-KLF15
B
KLF15 [A.U.]
BSA G P GP
C
TFEB [A.U.]
BSA G P GP
D
Ad-mCherry
Ad-KLF15
DAPI
mCherry
KLF15
TFEB
Merge

Figure 4.10 KLF15 alters TFEB protein content in the cardiomyocyte. H9C2 cells transduced with adenoviruses either overexpressing human KLF15 or control mCherry, followed by treatment with BSA, glucose (G; 30 mM), palmitate (P; 1.2 mM) or a combination of glucose/palmitate (GP; 30/1.2 mM) for 16 h. (A) Immunoblot and densitometric analysis of protein expression of (B) KLF15 and (C) TFEB. (D) Immunofluorescence image showing TFEB (green) and KLF15 (green), mCherry (red) and nuclei stained with Hoechst 33342 (blue) in H9C2 cells transduced with adenoviruses overexpressing either human KLF15 or mCherry. The white arrow indicates TFEB localization. Graph represents mean ± S.E.M., n = 3 from three independent sets of experiments, *P < 0.05 performed using two-way ANOVA; A.U.; arbitrary unit.

(Figure 4.10 A, B and C). Additionally, high glucose did not significantly alter TFEB content; however, high glucose combined with palmitate exacerbated TFEB decline compared to the BSA control group **(Figure 4.10 A, B and C)**. Alternatively, KLF15 overexpression abrogated glucose/palmitate-induced decline in TFEB expression **(Figure 4.10 A, B and C)**. Immunostaining analysis revealed a marked increase in nuclear translocation of TFEB in H9C2 cells transduced with human KLF15 adenovirus compared to mCherry viral control **(Figure 4.10 D)**. Our data support the role of KLF15 in augmenting TFEB and nuclear translocation in the cardiomyocyte.

4.4 Discussion

Transcriptome analysis was performed to interrogate the role of TFEB in engaging metabolic and signaling networks in the cardiomyocyte. Ventricular transcriptome data from constitutive cardiomyocyte-specific TFEB$^{-/-}$ mice indicated that TFEB regulates a network of genes involved in glucose (*Pfkp, Gpd1, slc37a4, hk1, Pdk3* and *Pgm5*) and fructose (*Akr1b8, Akr1b3, Akr1e1, Aldob*, and *Fbp2)* metabolism. Notably, acute overexpression of fructose-bisphosphatase 2 (Fbp2; a bifunctional enzyme catalyzing the synthesis and degradation) in the cardiomyocytes countered detrimental effects of hypoxia by augmenting glycolysis. Whereas chronic Fbp2 overexpression caused cardiac dysfunction [388], signifying that in myocyte with TFEB deletion, perturbations in fructose flux could likely precipitate cardiac dysfunction. Furthermore, a notable decrease in malonyl CoA decarboxylase (*Mlycd*) gene expression was observed in TFEB$^{-/-}$ cardiomyocytes, implying reduced malonyl CoA degradation. Malonyl CoA inhibits CPT1 and directs fatty acids away from oxidation towards triacylglycerol formation and concomitantly relieving inhibition of fatty acids on glucose metabolism [389]. Indeed, Mlycd silencing in human skeletal muscle myotube, rodent and porcine hearts increase malonyl CoA levels and stimulates glucose uptake and glucose oxidation and simultaneously inhibits FA oxidation [389-391]. In contrast to our findings from TFEB$^{-/-}$ cardiomyocytes, in a murine model of skeletal muscle-specific TFEB overexpression, glucose metabolizing genes, GLUT1, GLUT4, hexokinase I and II

and TBC1 domain family member 1 (TBC1D1) were significantly increased [316], suggesting that TFEB regulation of energy metabolism is not comparable between cardiac and skeletal muscle. Since the expression of glycolytic genes (*Pfkp, Gpd1, Hk1 and Pgm5*) were also increased in TFEB deficient cardiomyocytes, we theorized that lipid utilizing genes in TFEB depleted cardiomyocytes might be remodeled or impaired and hence, likely activating pathways using glucose through glycolysis.

Besides glucose and fructose metabolism, TFEB deletion affected several steps of lipid metabolic processes, such as lipid transport (*Cd36*), lipid storage (*Plin2, Plin5 and Mlycd*), FA biosynthesis (*Fsn*) and FA metabolism (*Lpl*). Importantly, TFEB overexpression in liver upregulated genes involved in monocarboxylic acid, fatty acid and cellular ketone metabolic processes and downregulated several gene categories related to lipid biosynthesis [299]. Furthermore, a study in the liver also suggests that PGC-1α mediates the TFEB function of regulating lipid metabolism by controlling the activity of PPARα [299]. Conversely, TFEB acts independently of PGC-1α to regulate glucose homeostasis and mitochondrial functions in skeletal muscle [316]. In cardiomyocytes, TFEB-dependent regulation of lipid metabolism was evident by depletion in PPARα protein expression. However, in cardiomyocytes, it remains to be determined whether TFEB is directly engaged in governing lipid metabolism independently from PGC-1α. On the other hand, TFEB overexpression in macrophage upregulates lysosomal lipid metabolizing genes, notably lysosomal acid lipase, to attenuate ischemia reperfusion-induced remodeling in the mouse heart [334]. Furthermore, loss of TFEB action led to a significant accumulation of LD, while TFEB overexpression decreased LD size and accumulation. Our finding was in agreement with the prior study, wherein mice with liver-specific TFEB deletion, when subjected to high-fat diet, exhibit large, pale and lipid vacuoles, filled hepatocytes, whereas livers from TFEB overexpressed mice show reddish-brown oxidative phenotype with markedly reduced lipid content [299]. Additionally, livers from adipocyte-specific TFEB overexpressed mice fed a western diet showed reduced TAG content [330]. Together, these findings suggest that TFEB plausibly remodel lipid

metabolism in the cardiomyocyte. Furthermore, these observations also indicate that networks of genes regulated by TFEB are stimuli- and tissue-specific, supporting distinct metabolic functions.

Increasing evidence also suggests that autophagy is important in maintaining the homeostasis of intracellular LD by either regulating the biogenesis, FAs mobilization or degradation in *in-vivo* and *ex-vivo* studies. In a murine genetic model of obesity such as *ob/ob* mice, excessive lipid overload inhibits autophagy, whereas enhancing liver autophagy ameliorates their metabolic phenotype [392]. The role of autophagy in governing lipid metabolism was further demonstrated in liver-specific Atg7 or Atg5 knockdown mice, which display an increase in lipid droplet, cholesterol and TAG formation in the liver [382,393]. Since TFEB is a key player in controlling autophagy by directly regulating lysosomal and autophagy genes, we next determined whether TFEB dependent regulation in lipid metabolism in the cardiomyocyte involves macroautophagy. Despite Atg7 deficiency in cardiomyocytes, TFEB overexpression significantly reduced lipid droplet formation. Unlike the observation from the liver studies, in which TFEB overexpression with Atg7 deficient liver did not rescue hepatic steatosis [299], the finding in cardiomyocytes yielded the opposite outcome. Our data in the cardiomyocyte demonstrate that TFEB-mediated regulation of lipid metabolism is largely independent of the macroautophagy pathway to degrade lipids. Moreover, it is likely that TFEB's regulation on lipid storage or lipid catabolism is mediated through its effect on PGC1α and PPARα in the cardiomyocyte.

In addition to TFEB's role in governing cellular energy metabolism in the cardiomyocyte, our transcriptome analysis identified upregulation of genes encoding apoptosis (*Tnsfrsf1a, Sgpl1, Cib1 and Lgals1*) and cell death (*UCP2, Clu and Pmp22*) pathways in response to the loss of TFEB in the cardiomyocyte. Indeed, a recent report demonstrated that TNFα-induced activation of receptor-interacting protein 1 (RIP-1) and necroptosis in cardiomyocytes was abolished by RIP-1 inhibitor, necrostatin in a TFEB-dependent manner [394]. Alternatively, augmenting nuclear localization of TFEB rescued lipotoxicity-induced increase in caspase-3 activity and protein levels, indicating that cardiomyocyte deficient in TFEB is triggering molecular events leading to cell

death. Our finding agrees with a pro-survival role of TFEB. Indeed, activation of TFEB protects cardiomyocyte from ischemia-reperfusion-induced cell death. The pro-survival role of TFEB has also been confirmed in the cardiomyocyte model of proteinopathy [381]. Forced overexpression of TFEB in neonatal rat cardiomyocytes expressing mutant αβ-crystallin (missense (R120G) CryABR^{120G}) blunted proteotoxicity by attenuating CryABR^{120G}-induced accumulation of ubiquitinated proteins, caspase 3 cleavage and cell death [381]. Indeed, using a Dox-induced cardiotoxicity model, a prior study from our laboratory reported that DOX exposure in cardiomyocytes resulted in the loss of TFEB content, lysosomal dysfunction and associated cell death, whereas constitutive localization of nuclear TFEB ameliorated DOX-induced cytotoxicity [344]. Collectively, our findings indicate that TFEB is critical for regulating cardiomyocyte cell survival and protects against stress-induced cardiac injury.

Given the central role of TFEB in regulating cellular metabolism and survival, numerous tissue-specific upstream regulators have been characterized. STUB1 (E3 ubiquitin ligase) targets phosphorylated TFEB for proteasomal degradation and induces nuclear translocation of non-phosphorylated TFEB in HEK293 cells and mouse embryonic fibroblast [317]. Paternally Expressed Gene 3 (PEG3) is required for TFEB nuclear translocation via VEGFR2- and AMPK-dependent manner in HUVEC cells [395]. In the current study, we found that overexpression of KLF15 not only increases TFEB protein content but also induces nuclear translocation of TFEB. Recently, a link between KLFs and autophagy was uncovered, wherein nematode lifespan control by KLF3 and vascular aging by KLF4 [387] were observed to be dependent on autophagy. Our findings suggest that the effects of KLF15 on metabolism and autophagy most likely involves modulation of myocyte TFEB, mechanisms for which still merits investigation.

In summary, data from this thesis chapter definitively established 1) TFEB as a key player in regulating genes involved in lipid metabolism in the cardiomyocyte, 2) loss of TFEB in cardiomyocytes impairs lipid catabolism, 3) TFEB engages pathways of cellular survival in the cardiomyocyte and 4) increase in cardiomyocyte TFEB attenuates glucolipotoxicity-induced

cardiomyocyte injury. Together, our findings suggest that TFEB alterations reprogram lipid metabolism and cell survival pathways in the cardiomyocyte. However, whether the loss of TFEB-mediated changes in lipid breakdown and cell death signaling pathways impacts the cardiomyocyte function remained unexplored. Therefore, we next assessed the functional importance of TFEB alterations in the cardiomyocyte.

Chapter 5: Cardiomyocyte Ca^{2+} dynamics is altered in mice with constitutive cardiomyocyte-specific TFEB deletion

5.1 Rationale and objectives

Our transcriptome data from chapter 3 revealed that amongst the differentially expressed genes following the loss of TFEB in the cardiomyocyte included genes associated with cardiomyocyte Ca^{2+} signaling and function. Furthermore, prior studies also demonstrated that overexpression of TFEB protected against amyloidogenic immunoglobulin light chain (AL-LC)-induced cardiomyocyte contractile dysfunction and decreased Ca^{2+} transient amplitude in zebrafish [345]. A separate study demonstrated that adeno-associated virus-mediated transduction of TFEB in transgenic mice with αβcrystallin R120G mutant attenuates the progression of the fatal cardiomyopathic manifestations and improves LV ejections performance, reduced LV end-systolic diameter and hypertrophy [368]. In macrophages, overexpression of TFEB rescues ventricular dysfunction after ischemia/reperfusion injury [247]. However, if the loss of TFEB impacts contractile function and Ca^{2+} signaling in the cardiomyocyte was unexplored. Therefore, the objective of this chapter is to examine whether the loss of TFEB in the cardiomyocyte alters 1) contractile properties and 2) Ca^{2+} dynamics and signaling.

5.2 Materials and methods

5.2.1 Sarcomere length measurement

Adult mouse cardiomyocytes (AMCM) were isolated, as described in section 2.2.5.2. Sarcomere length was measured using a cell shortening analysis system from HORIBA. Inc. Briefly, cells were mounted in the stage of an inverted microscope with a buffer containing: 131 mM NaCl, 4 mM KCl, 1 mM $CaCl_2$, 1 mM $MgCl_2$, 10 mM glucose, 10 mM HEPES, at pH 7.4. The cells were field stimulated with a suprathreshold voltage at a frequency of 0.5, 1, 1.5 and 2 Hz, for 30 sec duration, using a pair of platinum wires placed on the side of the chamber connected to

a Myopacer (Myopacer Field Stimulator, Ion Optix). The myocyte being studied was displayed on the computer monitor using Grabber camera (ZEISS microscope), which rapidly scans the image area at every 8.3 msec. The amplitude and velocity of contraction and relaxation is recorded with good fidelity. The FelixGX software was used to capture changes in cell length during contraction and relaxation. Cardiomyocyte contraction and relaxation were assessed using the following indices: Min represents contraction (shortening), Max represents relaxation (relengthening) and SL represents sarcomere length. Min SL (peak shortening) which indicates sarcomere length during peak ventricular contractility; Max SL (peak relengthening) indicates sarcomere length during peak ventricular relaxation; ΔSL which indicates a change in sarcomere length from the peak of contraction to the peak of relaxation; ΔSL (%) which indicates % change in sarcomere length from peak ventricular contraction to peak relaxation; $-dSL/dt_{min}$ and $+dSL/dt_{max}$ indicate the rate of velocity of a peak contraction and relaxation, respectively; Time to Min SL indicates time to reach peak ventricular contractility. After altering stimulus frequency (from 0.5 - 2 Hz), the steady-state contraction of myocyte was achieved (usually after the first five to six beats) before sarcomere length was recorded. Myocytes with obvious sarcolemmal blebs or spontaneous contractions were excluded from mechanical recording. All measurements were performed at 25–27℃. Sarcomere length was analyzed using Matlab software.

5.2.2 Intracellular Ca^{2+} transient measurement

Both intracellular Ca^{2+} and sarcomere length were measured simultaneously in the same set of myocytes. Myocytes were loaded with Fura-2AM (1 mM) for 15 min at room temperature in the dark, and fluorescence measurements were recorded with a dual-excitation fluorescence photomultiplier system. In brief, AMCM was placed on a ZEISS inverted microscope equipped with a temperature-controlled Warner chamber and imaged through a Fluor640 oil objective. Myocytes were exposed to light emitted by a 75W lamp and passed through either a 360 or a 380 nm filter while being electrically paced at 0.5, 1, 1.5 and 2 Hz. Fluorescence emissions were detected between 480–520 nm by a photomultiplier tube after first illuminating the cardiomyocytes

at 360 nm then at 380 nm for 30 sec. The qualitative changes in intracellular Ca^{2+} ($[Ca^{2+}]i$) concentration was inferred from the ratio of the fluorescence intensity at two wavelengths (360/380). Intracellular Ca^{2+} was measured using the following indices: min indicates relaxation; max indicates contraction; $[Ca^{2+}]i_{min}$ indicates $[Ca^{2+}]i$ during ventricular relaxation; $[Ca^{2+}]i_{max}$ indicates $[Ca^{2+}]i$ during ventricular contraction; $\Delta[Ca^{2+}]i$ indicates Ca^{2+} transient amplitude (change in intracellular Ca^{2+} from peak of relaxation to peak of contraction); $+dCa/dt_{max}$ indicates maximum rate of Ca^{2+} transient; $-dCa/dt_{min}$ indicates maximum rate of Ca^{2+} removal, 50% Ca^{2+} Tau and 80% Ca^{2+} Tau indicate time to 50% and 80% Ca^{2+} decay, respectively and time constant (T) of $[Ca^{2+}]i$ decay.

5.2.3 Statistical Analysis

Results are expressed as mean ± SEM. Pairwise comparison between groups was performed using unpaired two-tailed Student's t-test. A comparison between multiple groups was performed using analysis of variance one-way ANOVA or Two-way ANOVA followed by Tukey test using GraphPad Prism software. P values of less than 0.05 were considered statistically significant.

5.3 Results

5.3.1 Loss of TFEB increased Ca^{2+} transient amplitude in the cardiomyocyte

Transcriptome analysis from cardiomyocytes lacking TFEB revealed alterations in genes associated with cardiomyocyte Ca^{2+} signaling and cardiomyocyte contractility. Therefore, we first investigated the impact of the loss of TFEB on cardiomyocyte Ca^{2+} dynamic.

We first analyzed genes associated with cardiomyocyte contraction. Genes involved in cardiomyocyte contraction such as *Myh7* and *Tnnc1* were upregulated, whereas *Tpm2* was downregulated due to the loss of TFEB in the cardiomyocyte **(Figure 5.1 A and B)**. Additionally, genes associated with cardiomyocyte Ca^{2+} cycling such as Ca^{2+} channel genes (*Cacna1s, Cacnb1),*

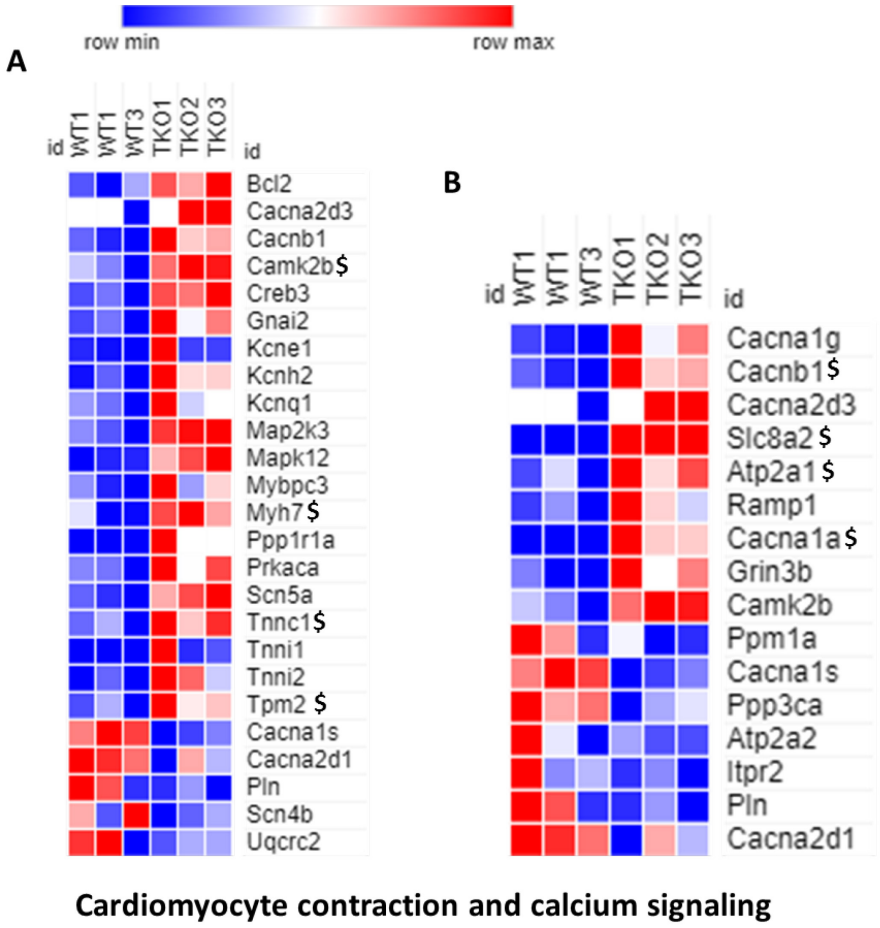

Figure 5.1 Loss of TFEB modulates genes associated with cardiomyocyte Ca^{2+} signaling and contraction. (A and B) Heatmap of differentially expressed genes involved in cardiomyocyte Ca^{2+} signaling and contraction from $TFEB^{fl/fl}$ and $TFEB^{-/-}$ mice.

Na^+/Ca^{2+} exchanger (NCX) channel *(Slc8a2),* and SR Ca^{2+} ATPase pump 1 (*Atp2a1)* were upregulated in $TFEB^{-/-}$ cardiomyocytes **(Figure 5.1 A and B)**. Notably, the *Camk2b* gene, which has been implicated in cardiac hypertrophy and heart failure [396,397], was upregulated in $TFEB^{-/-}$ cardiomyocytes **(Figure 5.1 A and B)**.

We next examined the impact of the loss of TFEB on cardiomyocyte Ca^{2+} transient. We used membrane-permeable intracellular Ca^{2+} fluorescent dye Fura-2AM to evaluate intracellular Ca^{2+} homeostasis in $TFEB^{-/-}$ and $TFEB^{fl/fl}$ cardiomyocytes **(Figure 5.2 A and B)**. Intracellular Ca^{2+} was measured by electrically stimulating cardiomyocytes at 0.5, 1, 1.5 and 2 Hz and representative tracing of Ca^{2+} transient amplitude is shown in **Figure 5.2 C.** Our results depicted a decrease in intracellular Ca^{2+} during relaxation at 0.5, 1, 1.5 and 2 Hz compared to $TFEB^{fl/fl}$ cardiomyocytes, whereas intracellular Ca^{2+} levels were unchanged during contraction **(Figure 5.3 A and B),** implying lower diastolic Ca^{2+} in TFEB deficient cardiomyocytes. Furthermore, there was a significant increase in Ca^{2+} transient amplitude (rise in intracellular Ca^{2+} from the peak of relaxation to peak of contraction) in cardiomyocytes from $TFEB^{-/-}$ mice compared with those from $TFEB^{fl/fl}$ mice **(Figure 5.3 C).** This data indicates that despite lower diastolic Ca^{2+}, $TFEB^{-/-}$ cardiomyocytes achieved peak Ca^{2+} levels similar to that observed in $TFEB^{fl/fl}$ cardiomyocytes during contraction. An increase in Ca^{2+} transient amplitude was further associated with an increase in peak rate of rise and rate of removal of $[Ca^{2+}]i$ during contraction and relaxation, respectively, in $TFEB^{-/-}$ cardiomyocytes compared to $TFEB^{fl/fl}$ cardiomyocytes **(Figure 5.3 D and E)**. Furthermore, time to 50% Ca^{2+} decay (which indicates a decrease in Ca^{2+} concentration resulting from Ca^{2+} sequestration into SR via SERCA), time to 80% Ca^{2+} decay (which indicates Ca^{2+} removal from the cytoplasm to the extracellular space through the NCX during the late part of the relaxation) and time constant of $[Ca^{2+}]i$ transients were significantly lower in $TFEB^{-/-}$ cardiomyocytes, indicating rapid Ca^{2+} decay compared to $TFEB^{fl/fl}$ cardiomyocytes **(Figure 5.3 F-H).** These findings collectively suggest that despite having low diastolic Ca^{2+}, $TFEB^{-/-}$ cardiomyocytes efficiently increase peak Ca^{2+} level during contraction and rapidly remove intracellular Ca^{2+} during relaxation.

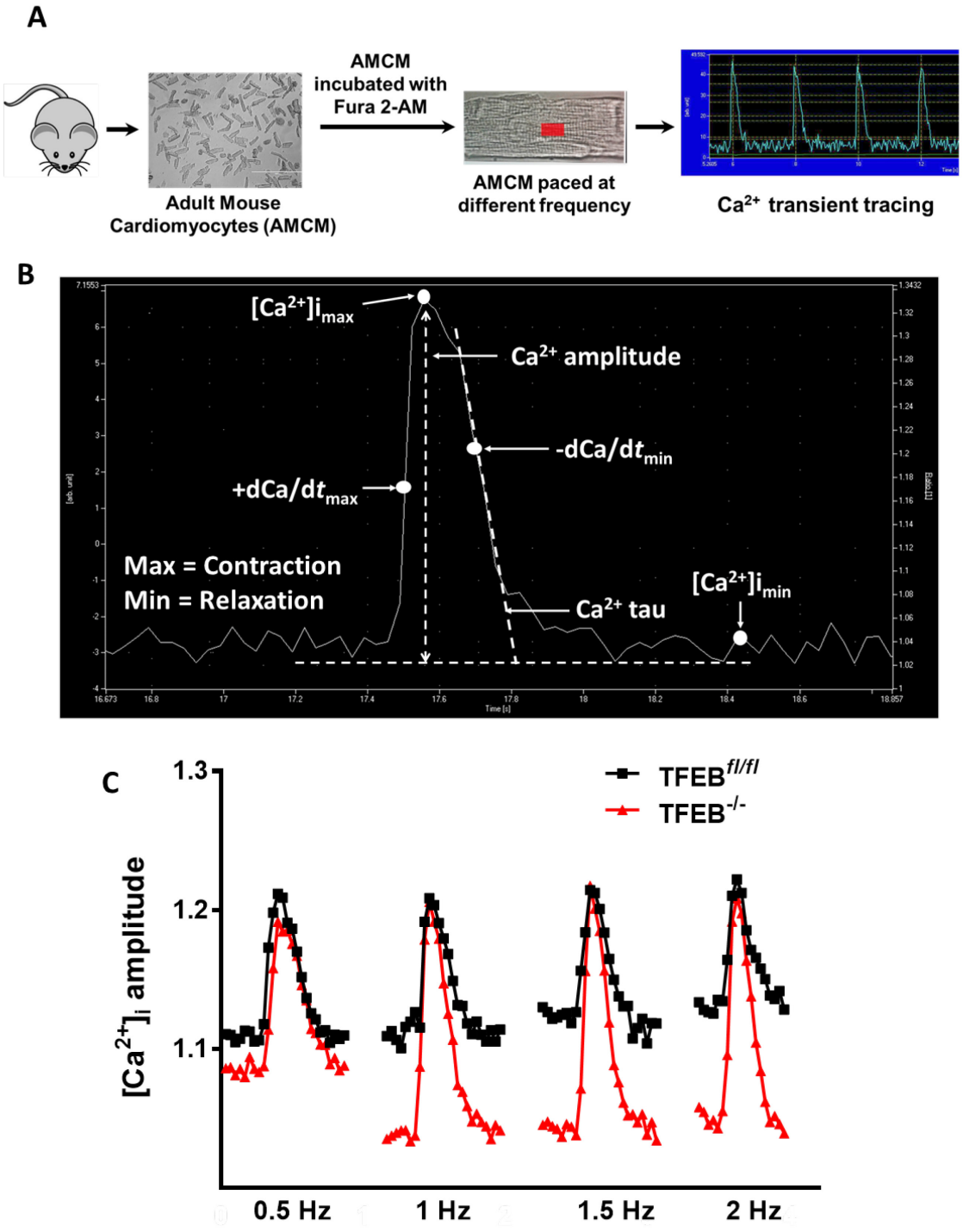

Figure 5.2 Intracellular Ca^{2+} transient measurement in isolated adult mouse cardiomyocytes. (A) Experimental layout of intracellular Ca^{2+} transient measurement. (B) Ensemble of Ca^{2+} transient tracing. (C) Representative tracing of the amplitude of intracellular Ca^{2+} transient evaluated in isolated cardiomyocytes paced at 0.5, 1, 1.5 and 2 Hz.

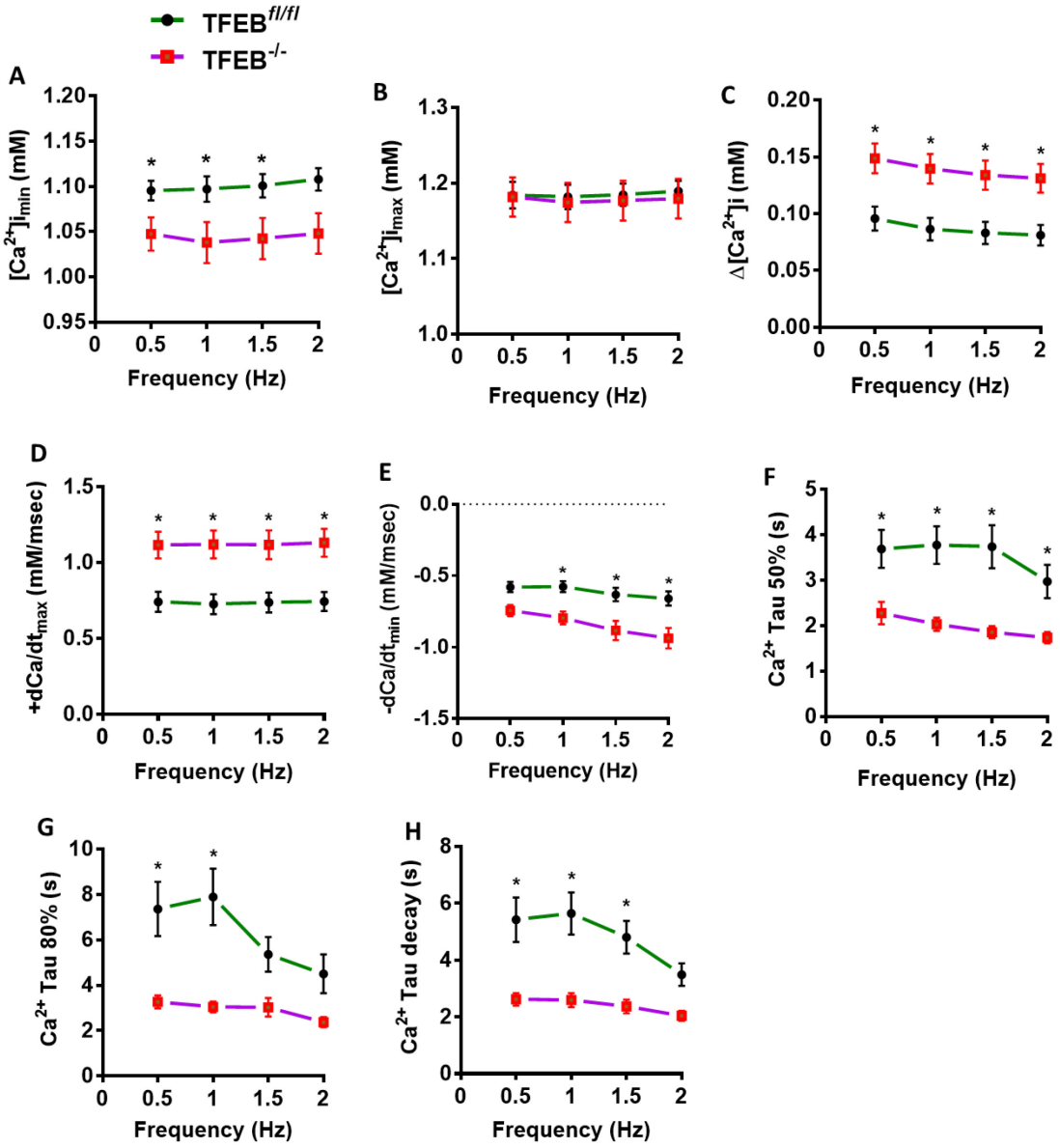

Figure 5.3 Intracellular Ca^{2+} transient is altered in the cardiomyocyte with TFEB deletion. (A) Intracellular Ca^{2+} during relaxation, (B) intracellular Ca^{2+} during contraction, (C) change in intracellular Ca^{2+} from the peak of relaxation to the peak of contraction, (D) rate of maximum Ca^{2+} transient, (E) rate of maximum Ca^{2+} decay, (F) time to 50% and (G) time to 80% Ca^{2+} removal decay and (H) time constant of intracellular Ca^{2+} decay in isolated cardiomyocytes. Graph represents mean ± S.E.M., n = 3 mice and 6-8 cardiomyocytes were analyzed per mouse (n=21 to 24 cardiomyocytes). *P<0.05 vs $TFEB^{fl/fl}$ cardiomyocyte performed using Two-way ANOVA.

5.3.2 Cardiomyocyte sarcomere length is unaltered in TFEB$^{-/-}$ mice

Transcriptome analysis from TFEB deficient cardiomyocytes revealed alteration in genes involved in cardiomyocyte contraction **(Figure 5.1)**. We also found that loss of TFEB increased Ca^{2+} transient amplitude in the cardiomyocyte compared to TFEB$^{fl/fl}$ cardiomyocytes, as detailed in section 5.3.1. Therefore, we next investigated whether an increase in Ca^{2+} transient is associated with changes in cardiomyocyte contractile properties.

We measured cardiomyocyte contractility using a sarcomere shortening analysis system. Adult mouse cardiomyocytes were isolated, electrically paced using a myopacer at 0.5, 1, 1.5, and 2 Hz **(Figure 5.4 A and B)** to record sarcomere length. **Figure 5.4 C** shows representative tracing of sarcomere length. Contrary to our expectation, alterations in Ca^{2+} transient amplitude did not alter sarcomere length during contraction and relaxation in TFEB$^{-/-}$ cardiomyocytes compared to TFEB$^{fl/fl}$ cardiomyocytes **(Figure 5.5 A and B)**. Similarly, the change in sarcomere length from the peak relaxation to peak contraction (ΔSL) was not altered between TFEB$^{fl/fl}$ and TFEB$^{-/-}$ cardiomyocytes **(Figure 5.5 C)**. Furthermore, % change in ΔSL was decreased when TFEB$^{-/-}$ cardiomyocytes were paced at 0.5 Hz compared to TFEB$^{fl/fl}$ cardiomyocytes **(Figure 5.5 D)**, whereas no change in % ΔSL was observed when cardiomyocytes were paced at 1, 1.5 and 2 Hz between two groups **(Figure 5.5 D)**. Similarly, the rate of velocity of the cardiomyocyte contraction ($-dSL/dt_{min}$) was significantly decreased at 0.5 Hz, while no change in the rate of velocity of cardiomyocyte contraction was observed at 1, 1.5 and 2 Hz between two groups **(Figure 5.5 E and F)**. Moreover, the rate of velocity of cardiomyocyte relaxation ($+dSL/dt_{max}$) and time to reach peak contraction (Time to Min SL) was no different between TFEB$^{fl/fl}$ and TFEB$^{-/-}$ cardiomyocytes **(Figure 5.5G)**. Together, these findings suggest that despite exhibiting higher Ca^{2+} transient amplitude, TFEB$^{-/-}$ cardiomyocytes did not display a change in contractile properties and were able to contract as efficiently as TFEB$^{fl/fl}$ cardiomyocytes.

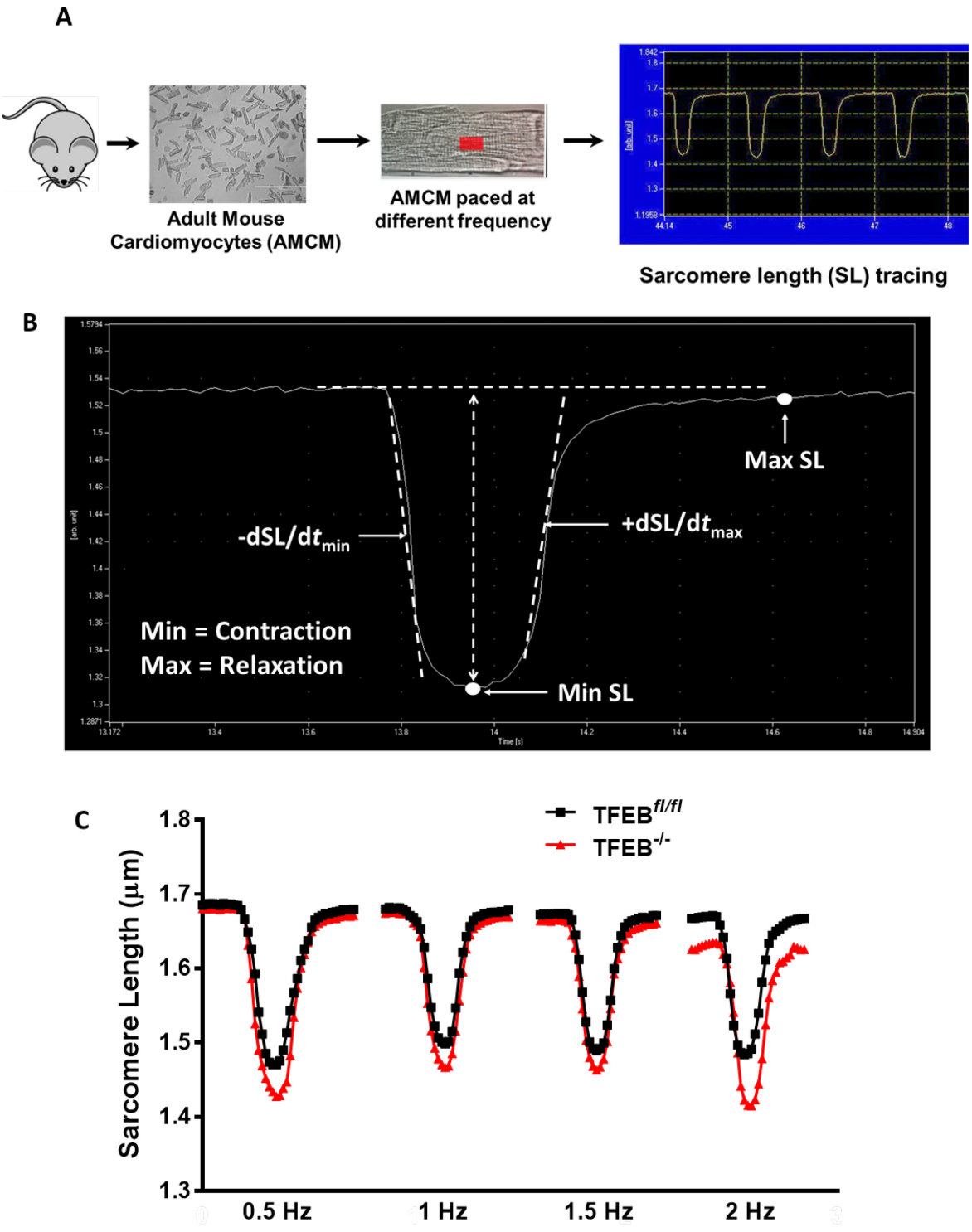

Figure 5.4 Sarcomere length measurement in isolated adult mouse cardiomyocytes. (A) Experimental layout of sarcomere length measurement in isolated cardiomyocytes. (B) Ensemble of contractility tracing and (C) representative tracing of sarcomere length from TFEB$^{-/-}$ and TFEB$^{fl/fl}$ cardiomyocytes electrically paced at 0.5, 1, 1.5 and 2 Hz.

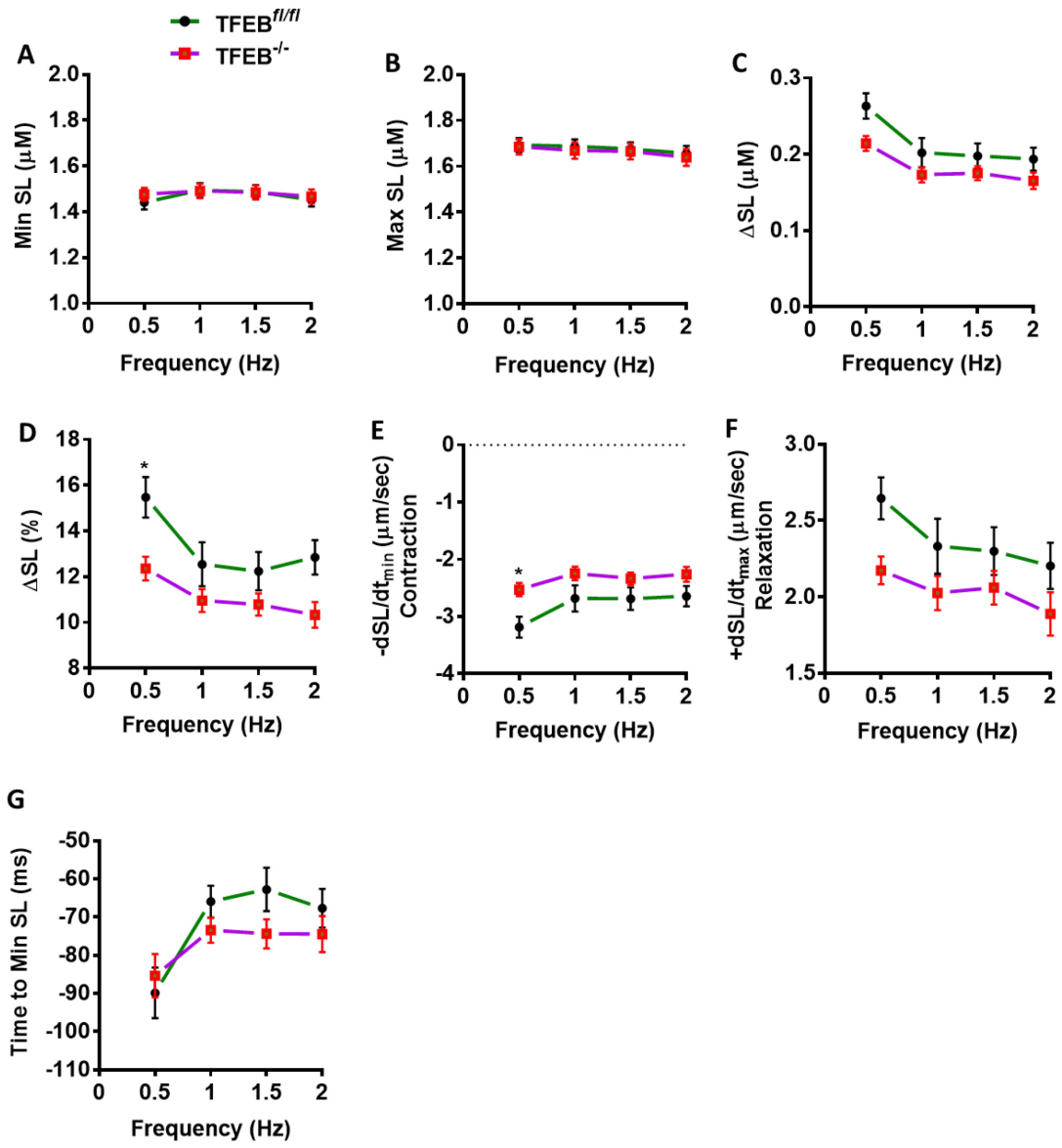

Figure 5.5 Loss of TFEB did not alter cardiomyocyte sarcomere length. Cardiomyocyte contractility was evaluated from TFEB$^{-/-}$ and TFEB$^{fl/fl}$ mice. (A) Sarcomere length (SL) during contraction, (B) SL during relaxation, (C) change in SL from the peak of contraction to the peak of relaxation, (D) % change in SL from peak ventricular contraction to peak relaxation, (E) rate of velocity of cardiomyocyte contraction, (F) rate of velocity of cardiomyocyte relaxation and (G) time to reach peak contraction in isolated cardiomyocytes. Graph represents mean ± S.E.M., n = 3 mice and 6-8 cardiomyocytes were analyzed per mouse (n=21 to 24 cardiomyocytes). *P<0.05 vs TFEB$^{fl/fl}$ cardiomyocyte performed using Two-way ANOVA.

5.4 Discussion

Transcriptome analysis was performed to interrogate the role of TFEB in engaging Ca^{2+} signaling networks and contractile properties in the cardiomyocyte. Ventricular transcriptome data from constitutive cardiomyocyte-specific $TFEB^{-/-}$ mice indicated that TFEB alters genes involved in cardiomyocyte contraction and Ca^{2+} signaling. Our Ca^{2+} transient analysis revealed low diastolic Ca^{2+} levels, while systolic Ca^{2+} levels were unchanged. This data suggests that despite having low Ca^{2+} levels during relaxation, $TFEB^{-/-}$ cardiomyocytes achieved the peak Ca^{2+} level during contraction similar to that observed in $TFEB^{fl/fl}$ cardiomyocytes. Importantly, transcriptome data indicated the upregulation of *Atp21a* (SERCA1) and *Slc8a2* (NCX, Na^{+}/Ca^{2+} exchanger) genes, which play an important role in regulating SR Ca^{2+} content by removing intracellular Ca^{2+} following cardiomyocyte contraction. Indeed, a prior study has revealed that adenoviral-mediated gene transfer of SERCA1a into isolated rabbit ventricular cardiomyocytes increases Ca^{2+} transient amplitude [398]. The increase in Ca^{2+} transient amplitude due to the loss of TFEB is likely a consequence of increases in the SERCA1a level, suggesting an increased capacity of SR Ca^{2+} storage or an increase in SR Ca^{2+} leak. Cardiac contraction occurs because of the influx of Ca^{2+} through L-type Ca^{2+} channel, which triggers SR Ca^{2+} release that binds to myofilaments proteins to initiate contraction. Given that loss of TFEB increases Ca^{2+} transient amplitude with no effect on cardiomyocyte contractility, it is possible that TFEB-mediated increases in Ca^{2+} amplitude modulate myofilament Ca^{2+} sensitivity. The upregulation of SERCA1a and NCX gene expression in $TFEB^{-/-}$ cardiomyocytes coincided with rapid intracellular Ca^{2+} decay. Together, Ca^{2+} transient analysis indicates that TFEB plays an important role in regulating Ca^{2+} dynamic in the cardiomyocyte, likely by altering the expression of genes involved in Ca^{2+} cycling in the heart, however, the intracellular molecular mechanism of this regulation merit further investigation.

Importantly, the link between TFEB and Ca^{2+} was reported in a prior study, wherein lysosomal Ca^{2+} regulates TFEB activity. This study showed that lysosomal Ca^{2+} release through mucolipin 1 (MCOLN1) activates calcineurin phosphatase, which dephosphorylates TFEB and

promotes its nuclear translocation [310]. Moreover, prior studies highlighted the importance of ER and lysosome membrane contract site formation in regulating Ca^{2+} signaling between these organelles [399,400]. Interestingly, a recent study showed that TFEB silencing in HeLa cells increases Ca^{2+} re-uptake rate in the ER through its effect on lysosome activity [401]. Whether lysosomal Ca^{2+} likely contributes to higher intracellular Ca^{2+} transient $TFEB^{-/-}$ cardiomyocytes remain unanswered. Contrary to our expectation, the observed alteration in Ca^{2+} signaling in the $TFEB^{-/-}$ cardiomyocytes did not reflect an alteration in cardiomyocyte contractile properties. Cardiomyocyte contractile measurement in $TFEB^{-/-}$ mice revealed no change in sarcomere length during contraction or relaxation. Additionally, the rate of velocity of cardiomyocyte contraction or relaxation was comparable to $TFEB^{fl/fl}$ cardiomyocytes. The possible explanation for the disconnect between Ca^{2+} dynamic and contractility is that these studies were performed in unchallenged conditions in $TFEB^{-/-}$ mice. It is likely that challenging these mice with different stressors such as metabolic stress-induced by feeding high-fat diet or angiotensin II infusion or DOX treatment to cause cardiac dysfunction would exacerbate impairment in contractile properties due to higher Ca^{2+} transient amplitude in $TFEB^{-/-}$ cardiomyocytes.

Chapter 6: General discussion and conclusion

6.1 Overview:

Metabolic remodeling is one of the early biochemical events that take place in the obese and diabetic heart. One of the underlying causes of metabolic dysfunction in the heart is either loss of insulin content or insulin function, leading to fatty acid overutilization and hyperglycemia, culminating in glucolipotoxic stress [22,97,142]. Glucolipotoxicity triggers cardiovascular complications such as left ventricular stiffness, myocardial fibrosis and Ca^{2+} mishandling [97]. Prior studies have shown that glucolipotoxicity pathologically remodels the heart by increasing endoplasmic reticulum (ER) stress, mitochondrial dysfunction, and perturbing cellular proteostasis [75,76,152,183,209,210,229,402].

Cardiomyocyte glucolipotoxicity impairs protein quality control, causing ER stress and activating the protein degradation pathway [209,229,402]. To counter the damaging effects of glucolipotoxicity, proteasomal degradation pathway is upregulated to clear the proteotoxic load. However, sustained glucolipotoxic stress exacerbates ER stress and impairs proteasomal protein degradation causing toxic accumulation of misfolded proteins [209,229,402]. Previous studies suggest that impairment in the proteasomal system is compensated by the upregulation of lysosomal machinery in order to clear damaged intracellular proteins via lysosomal autophagy [211,212]. We [226] and others [226,355,403,404] have previously shown that glucolipotoxicity impairs autophagic flux and suppresses lysosome biogenesis and function, causing cardiomyocyte injury and cellular stress in obese and diabetic hearts. These studies suggest that lysosome dysfunction in the stressed heart is central to inducing cardiac injury. Importantly, TFEB is a master regulator of autophagy, lysosomal biogenesis and lysosomal function [288,301,405]; however, its regulation in the cardiometabolic disease was unknown. Preliminary studies from our laboratory showed that cardiomyocytes exposed to the lipotoxic [226] or chemotoxic (DOX) [344] environment *in-vitro, ex-vivo* and *in-vivo* exhibited a significant decrease in the nuclear content of TFEB. Moreover, ischemic-reperfusion and hypoxic injuries in the heart exacerbated BNIP3-induced cell death

following the deficiency of TFEB function [369,370]. Augmenting TFEB action reversed amyloid deposit-induced proteotoxicity in zebrafish and mouse hearts [345], signifying the cardioprotective role of TFEB. A plethora of studies has now definitively shown that loss of TFEB action renders the heart susceptible to dysfunction. However, the underlying mechanism by which loss of TFEB engages pathological pathway networks to remodel cardiomyocyte signaling, metabolism and function remained unexplored.

The goal of this thesis was to investigate the role of TFEB signaling in regulating cellular metabolism and function in obese and diabetic. Here, we sought to elucidate 1) metabolic pathways that are remodeled in response to the loss of TFEB action in the cardiomyocyte and 2) physiological importance of TFEB in regulating cardiomyocyte viability and function.

By utilizing *in-vitro, ex-vivo* and *in-vivo* model of lipid overload, my thesis work revealed that 1) palmitate decreases TFEB content *ex-vivo* in a time- and concentration-dependent manner, 2) nutrient overload *in-vivo* exhibited an early-onset and time-dependent decline in nuclear TFEB content and lysosome function, 3) adenoviral expression of constitutively active TFEB rescued cardiomyocytes from glucolipotoxicity-induced lysosomal dysfunction and cell death, 4) Kruppel-like factor (KLF15) was identified as an upstream modulator of TFEB protein expression, 5) cardiomyocyte transcriptome data provided evidence for a non-canonical role of TFEB in governing lipid metabolism and cell death pathways and 6) loss of TFEB altered intracellular Ca^{2+} transient in cardiomyocytes with no change in contractility in an unchallenged state. Given that activation of lysosomal autophagy enables cellular waste clearance, selective targeting of cellular TFEB in obese and diabetic hearts is anticipated to prevent or ameliorate cardiomyopathy.

6.2 Nutrient-dependent regulation of TFEB in the cardiomyocyte

Chronic glucotoxicity and lipotoxicity during obesity and diabetes cause ER stress, mitochondrial dysfunction, Ca^{2+} mishandling, and proteotoxicity, negatively impacting cellular homeostasis [150,178,188,192,406]. Impairment of lysosomal protein degradation induces accumulation of damaged proteins and organelles, resulting in cellular proteotoxicity observed in

cancer, diabetes, neurodegeneration and heart failure. Several studies have previously shown that metabolic maladaptation is associated with perturbed action of TFEB, a master regulator of lysosomal genes and function [325,336,371]. During nutrient excess, phosphorylation of TFEB by mTOR at Ser211 and ERK at Ser142 restricts TFEB within the cytosol to promote its degradation, preventing TFEB translocation into the nucleus to induce CLEAR genes [288,377]. However, it was unclear if specific nutrients exhibit a distinct effect on TFEB activity and autophagy-lysosome signaling in the heart. Our data demonstrated that glucolipotoxicity in the *in-vivo* and *ex-vivo* triggers the loss of TFEB action by altering TFEB phosphorylation and localization. We showed that palmitate alone or and a combination of palmitate/glucose depletes TFEB content, reduces lysosome content, suppresses proteolytic activity and increases cell death, an effect not sensitive to glucose alone, oleate alone or PUFAs per se. Moreover, hepatocytes, HeLa cells and MEFs subjected to starvation with amino acid-deficient and growth factor-deficient media induce nuclear translocation of TFEB, increasing the transcription of genes involved in the lysosomal-autophagy pathway [299]. These findings strongly support the theory that cellular nutrients exert a distinct effect on regulating TFEB activity.

Several mechanisms are proposed by which an overload of specific nutrients impairs autophagy and lysosome function. For instance, in pancreatic β-cells, palmitate treatment decreases ATP levels and impairs lysosomal acidification and proteolytic function [407,408]. Lipid overload *in-vivo* or *ex-vivo* modulates lysosomal membrane lipid content, directly impacting autophagosome and lysosome fusion [355]. Similarly, palmitate treatment impairs lysosomal acidification and lysosome function in H9C2 cells by activating the PKC-Nox2 signaling axis [355]. Here, we uncovered nutrient-specific effects on TFEB regulation in the cardiomyocyte. Specifically, TFEB is negatively regulated by palmitate [226], an effect insensitive to mono- or poly-unsaturated FAs and carbohydrates. Consistently, mice subject to HFHS diet revealed a temporal decline in nuclear TFEB protein expression with the associated elevation of TAG species in the heart.

However, mechanisms by which nutrient overload *in-vivo* and *ex-vivo* deplete TFEB levels are still unclear. Since TFEB mRNA expression is unaltered in glucolipotoxicity both *in-vivo* and *ex-vivo* [226], we propose that TFEB levels are dysregulated at the level of protein synthesis, post-translational modification or through yet uncharacterized signaling mechanisms. It is also possible that glucolipotoxicity-induced loss of TFEB content is an outcome of impaired TFEB mRNA translation since TFEB regulates ribosome biogenesis [288].

6.3 The role of TFEB in regulating the autophagy-lysosome pathway

Findings from this thesis demonstrated that nutrient overload in the cardiomyocyte depletes TFEB expression with concomitant reduction in lysosome content and lysosomal proteolytic ability. Notably, TFEB silencing *ex-vivo* did not significantly impact lysosome function; however, constitutive nuclear localization of TFEB in the cardiomyocyte partially attenuated nutrient overload-induced impairment in the autophagy-lysosomal pathway.

Remarkably, transcriptome analysis from mouse cardiomyocytes lacking TFEB aligned with the *ex-vivo* data showing that loss of TFEB in the myocyte minimally impacted genes engaged in autophagy and lysosome function. Loss of TFEB upregulated majority of autophagy and lysosome genes in the cardiomyocyte. Notably, the transcriptome analysis was performed in a non-challenged condition, wherein cardiomyocyte-specific $TFEB^{-/-}$ mice were not subjected to metabolic stress, such as feeding mice with HFHS diet. Similar to the cardiomyocyte findings, adipose-specific TFEB overexpression or knock-down did not alter autophagy and lysosome genes [330]. In contrast, genome-wide analysis from liver- and skeletal muscle-specific TFEB overexpressing mice demonstrated alteration in genes related to autophagy and lysosome pathway [299,316]. The disparity in our observation of TFEB-mediated regulation of lysosome function *ex-vivo* (acute modulation of TFEB in cell culture) versus *in-vivo* (chronic knockdown of TFEB in mice heart) model is likely a tissue-specific and a context-specific effect.

6.4 The role of TFEB in regulating apoptosis/cell death

Our data is in agreement with prior findings that TFEB is not only important to regulate lysosome biogenesis and lysosome function in the cardiomyocyte but also promotes cardiomyocyte survival, which is compromised in response to glucolipotoxic stress [247,334,369,370]. We demonstrated that nuclear restoration of TFEB in the cardiomyocyte attenuated glucolipotoxicity-induced cell death. This finding was further supported by transcriptome analysis, which unveiled that TFEB deficiency in the cardiomyocyte upregulated majority of genes associated with apoptosis and cell death pathway. Our data highlight that TFEB plays an important role in regulating cardiomyocyte viability and function.

Several studies have demonstrated the pro-survival role of TFEB in different disease models such as LSDs, neurodegenerative diseases, neurotoxicity, ischemia-reperfusion injury, proteinopathy and metabolic disorders [247,345,368,409]. TFEB overexpression in HEK293 cells attenuated palmitate- and LPS-induced cell death by upregulating lysosome biogenesis and function [246]. Similarly, cadmium increases cell death via suppressing lysosome function and autophagosome-lysosome fusion in Neuro-2a cells (mouse neuroblastoma cell line), an effect which is reversed in the presence of TFEB overexpression [410]. The involvement of TFEB in promoting cell survival is also demonstrated in proteotoxic cardiomyopathy. For instance, the formation of protein aggregates in both amyloid cardiomyopathy and desmin-related cardiomyopathy exhibit mitochondrial structural abnormalities and cell death [368]. TFEB overexpression during proteotoxic cardiomyopathy attenuates mitochondrial abnormalities, decreases cell death and improves cardiovascular function [368]. Given that TFEB plays an important role in regulating mitochondrial biogenesis and function [299], TFEB plausible ameliorates glucolipotoxicity-induced cell death by facilitating mitochondrial quality control in the cardiomyocyte. A prior study from our research group reported that TFEB overexpression in the cardiomyocyte increases lysosome biogenesis and function and attenuates DOX-induced cardiotoxicity by reducing ROS production [344], highlighting that TFEB is crucial for

cardiomyocyte survival and function. Another study recently reported that TFEB is negatively regulated by serine-threonine kinase, RIP1K, which plays multiple roles in signals that regulate the inflammatory response, cell death and cell growth [411]. RIP1K inhibits TFEB action by activating ERK, which negatively targets TFEB through its phosphorylation at Ser142 [307,394]. Thus, it can be theorized that glucolipotoxic stress may induce cardiomyocyte depletion of TEFB levels and lysosome function by upregulating the RIP1K-ERK signaling axis, rendering cardiomyocytes more susceptible to injury and cell death.

A recent study from our laboratory indicates that TFEB is hypophosphorylated and constitutively active in triple-negative breast cancer (TNBC) cells upon DOX treatment [328]. TFEB knock-down in TNBC cells increases caspase-3-dependent apoptosis and decreases cell survival [328]. In a separate study by Brady *et al*., TFEB and TFE3 were shown to control cell cycle in response to genotoxic stress in a p53- and mTORC1-dependent manner [412]. It has been reported that TFE3 overexpression allows cells to escape from Rb-induced cell cycle arrest [413]. Whereas depletion of TFEB reduces the proliferation of pancreatic and prostate cancer cells [329], indicating the oncogenic role of these transcription factors. Notably, our transcriptome analysis from $TFEB^{-/-}$ cardiomyocytes showed alterations in genes involved in DNA damage and repair pathways **(Figure 3.2 B)**. However, it remains to be determined whether TFEB restoration-dependent increase in cardiomyocyte survival is mediated by its effect on DNA damage and repair pathway in the heart. Whether double knock-down or overexpression of TFEB and TFE3 exhibit synergistic or antagonistic effect on cardiomyocyte survival in response to glucolipotoxic stress also merits investigation.

6.5 TFEB-mediated regulation of lipid metabolism in the cardiomyocyte

In addition to TFEB's canonical role in promoting lysosome biogenesis and function and promoting cellular survival, TFEB has also emerged as an important regulator of cellular metabolism. Indeed, several studies have demonstrated that TFEB is crucial in regulating cellular metabolism in the liver, skeletal muscle, adipocytes and macrophages [299,316,330]. In the

cardiomyocyte, we have shown an increase in nuclear TFEB content or silencing TFEB decreased lipid droplet (LD) formation or accumulated LDs, respectively. This finding implies that TFEB is a key player in regulating lipid metabolism, specifically regulating FA processing such as FA storage into TAG or FA catabolism. Our transcriptome analysis from cardiomyocyte-specific $TFEB^{-/-}$ mice suggested upregulation of genes involved in lipid biosynthesis and storage, whereas genes associated with lipid catabolism were downregulated. Findings from the liver and adipocyte studies suggest that TFEB-dependent regulation on cellular metabolism is driven by its effect on PGC1α and PPARα signaling axis [330]. Whereas in the skeletal muscle, TFEB regulates glucose homeostasis and mitochondrial biogenesis independent of its effect on PGC1α [316]. Interestingly, we observed a significant reduction in PPARα protein expression in $TFEB^{-/-}$ cardiomyocytes compared to WT cardiomyocytes, indicating that PGC1α and PPARα are possibly direct targets of TFEB in controlling lipid metabolism in the myocyte. Given that autophagy has been implicated in regulating lipid catabolism via lipophagy, we also investigated whether TFEB activated lipid breakdown by lipophagy in the cardiomyocyte. We observed that a viral-mediated increase in nuclear TFEB accelerated LD breakdown even in the presence of Atg7KD-mediated autophagy inhibition, implying that TFEB does not require a functional autophagy pathway to regulate lipid catabolism in the cardiomyocyte, whereas the opposite is true in the liver.

Prior studies have demonstrated that the gain- or loss-of-function of TFEB in mouse liver or adipose tissue influenced whole-body energy metabolism. For example, liver-specific TFEB knock-down mice display an increase in peripheral adiposity [299], whereas adipocyte-specific TFEB knock-down causes hepatic steatosis [330]. However, whether gain- or loss-of-function of TFEB in the liver, skeletal muscle or adipocytes exacerbate or attenuate diet-induced cardiac dysfunction remains undetermined. Overexpression of TFEB in the liver or adipocytes influence whole-body metabolism and protected mice against diet-induced metabolic dysfunction [299,330]. Interestingly, a recent study by Song *et al.* demonstrated that autophagy deficiency in mice with cardiomyocyte-specific inducible knock-down of Atg7 impaired whole-body glycemic control and

insulin sensitivity and increased fat storage in subcutaneous and adipose tissue [414]. However, it has yet to be determined whether cardiomyocyte-specific TFEB$^{-/-}$ mice influence cellular energy metabolism in other tissues such as the liver, adipocytes and skeletal muscle and protects against diet-induced obesity.

6.6 TFEB regulation in the heart

A longstanding query in the field of TFEB biology is to interrogate mechanisms by which TFEB is regulated within the cell. The nuclear translocation of TFEB has been observed in response to a variety of stimuli such as starvation [299], lysosomal stress [301,302,309] and oxidative stress [415,416]. TFEB nuclear translocation is also modulated by posttranslational modification through its phosphorylation by several kinases [405]. Emerging studies have identified that TFEB and TFE3 display cooperativity rather than redundancy in regulating cellular metabolism in the liver [314,324]. A recent study indicated that TFE3 compensates for TFEB deficiency and *vice versa* to regulate whole-body metabolism, innate immune responses and cell stress responses [314]. Further studies are warranted to ascertain whether TFEB and TFE3 exhibit cooperativity or redundancy in regulating cellular energy metabolic processes in the heart. Additionally, both Akt and GSK3β have been implicated in regulating TFEB subcellular localization through its phosphorylation [308,309,326]. In MCF7 cells, GSK3β phosphorylates TFEB at Ser134 and Ser138, resulting in inhibition of TFEB action by causing its cytoplasmic sequestration [308,326]. Akt is also reported to suppress the nuclear translocation of TFEB by phosphorylating TFEB at Ser467, a process independent of mTOR action [309]. Increased expression and activity of GSK3β has been reported in T2DM and obese animal models. Therefore, it is likely that glucolipotoxic stress activates GSK3β signaling to negatively targets TFEB through its phosphorylation and impairs lysosome function in the cardiomyocyte. Future studies are warranted to evaluate the impact of nutrient overload on GSK3-mediated TFEB subcellular localization of TFEB by examining the phosphorylation of serine residues of 134 and 138.

In the current study, we identified KLF15 as an upstream regulator of TFEB protein expression in the cardiomyocyte. Additional studies are warranted to investigate the underlying mechanisms by which KLF15 drives upregulation of TFEB protein expression in the cardiomyocyte. Given that KLF15 induces nuclear translocation of TFEB, it is plausible that KLF15 directly binds to the promoter region of the TFEB gene to trigger its nuclear intrusion. Whether KLF15 modulates autophagy and lysosome genes in a TFEB-dependent or -independent manner remains to be answered. Notably, a recent study identified a link between autophagy and KLF3 and KLF4. In this study, rapamycin (autophagy activator)-treated HEK293 cells upregulated KLF3 and KLF4, suggesting a KLF3/4-mediated regulation of autophagy pathway [387]. However, whether KLF3- and KLF4-dependent regulation of autophagy is mediated by their effects on TFEB remains unclear. Using gain- or loss-of-function of KLF15, it is also demonstrated that KLF15 plays a vital role in regulating genes related to lipid transport, lipid catabolism and FA oxidation in the heart [385,417], whereas genes associated with glucose transport and glycolysis are unaltered [385,417]. These findings suggest that KLF15 and TFEB share overlapping functions in governing lipid metabolism in the cardiomyocyte. Since KLF15 induces nuclear translocation of TFEB, it is possible that KFL15 regulates lipid metabolism in the heart via its effect on TFEB. Whether KLF15 and TFEB display cooperativity or redundancy in regulating lipid metabolism in the heart is not yet explored.

6.7 Therapeutic potential of TFEB

TFEB represents an appealing therapeutic target for many human diseases, including LSDs, neurodegenerative diseases and liver disease [338,418]. Many of these diseases are characterized by dysfunctional lysosomes and autophagy, resulting in the accumulation of protein aggregates [338]. Given that TFEB plays an important role in regulating autophagy, lysosome biogenesis and lysosome function, several attempts have been made to enhance cellular clearance of macromolecules by inducing TFEB expression. TFEB overexpression in mouse and cell culture models of LSDs, attenuated disease phenotype by reducing the accumulation of substrates [338].

Furthermore, impairment in lysosome function and autophagy have been implicated in neurodegenerative diseases such as Parkinson's (PD), Huntington's (HD) and Alzheimer's disease (AD), as well as other tauopathies [371]. Pharmacological or genetic activation of TFEB improves lysosome function and autophagy pathway and attenuates neuronal deposition of α-synuclein in a mouse model of PD [371]. These findings suggest that activation of TFEB can potentiate the effects of the recombinant therapeutic enzymes [336]. However, the underlying molecular mechanisms by which TFEB rescue lysosomal function in LSD merits further investigation.

The beneficial effects of TFEB expression or TFEB induction have also been reported in cardiovascular diseases. A prior study demonstrated that overexpression of TFEB protected against amyloidogenic immunoglobulin light chain (AL-LC, amyloid cardiomyopathy)-induced cardiomyocyte contractile dysfunction and impairment in Ca^{2+} transient amplitude in zebrafish [345]. In a separate study, AAV-mediated transduction of TFEB in transgenic mice with αβcrystallin R120G mutation attenuates the progression of fatal cardiomyopathic manifestations by increasing cell viability and improving LV ejections performance, reducing LV end-systolic diameter and hypertrophy [368,381]. The upregulation of TFEB is also beneficial in obesity-related diseases. TFEB overexpression in both liver and adipocytes protected against diet-induced obesity and obesity-related complications [299,330]. Although the exact mechanism by which TFEB upregulation reduces obesity is not known, it is likely that its regulation of lipid metabolism pathway mediates TFEB's effects.

In this thesis, I have demonstrated that TFEB plays an important role in regulating lipid catabolic processes in cardiomyocytes. Pathological intramyocardial lipid accumulation is a hallmark of heart diseases related to obesity and diabetes. It is possible that TFEB overexpression in the cardiomyocyte increases lipid catabolism and decreases intramyocardial lipid accumulation, likely improves cardiovascular outcome and protects against impaired systolic and diastolic heart function. These observations raise confidence in a therapeutic strategy targeting TFEB activation

to slow or reverse CVD pathogenesis. Therefore, TFEB is a potential therapeutic target to enhance lysosome function and autophagy to provide benefits in metabolic diseases.

6.8 Perspectives and Concluding Remarks

Our study demonstrated the nutrient-specific effect of TFEB regulation in the cardiomyocyte. Nutrient overload-induced accumulation of lipid species is associated with a decline in nuclear TFEB content and lysosomal proteolytic activity in the murine heart. Furthermore, transcriptome analysis revealed a non-canonical role of TFEB in governing lipid metabolism and cell death pathways in the cardiomyocyte as opposed to its canonical role in regulating lysosomal signaling and function **(Figure 6.1)**. This study sheds light on the tight linkages between TFEB and metabolism within cardiomyocytes, given the high nutrient and mitogenic demand of the heart to maintain functional homeostasis. Probing intramyocellular mechanisms regulating TFEB and identifying pathways targeted by TFEB offers promising therapeutic options for treating patients at risk for metabolic heart failure.

However, some of the outstanding questions that will advance the field of TFEB and its therapeutic utility include, 1) despite different nutrients exhibit differential effect on regulating TFEB in the cardiomyocyte, molecular mechanisms and the identity of the signaling players that regulate TFEB in the cardiomyocyte remains unclear, 2) Investigating factors that cause MiT/TFE proteins to regulate autophagy or other processes will be important in understanding their role in development and disease, 3) TFEB is regulated through phosphorylation by several kinases, whether regulation of TFEB function and subcellular localization in the cardiomyocyte is phosphorylation-dependent or -independent remains unexplored, 4) given the heterogeneity of the heart, how TFEB is regulated distinctly within different cells of the myocardium such as fibroblasts, adipocytes, macrophages, myocytes, endothelial cells is paramount to advancing TFEB biology and lastly, 6) interrogating TFEB cooperativity or redundancy with other MiTF family members or other transcriptional modifiers is a critical step in understanding the orchestration of metabolism and autophagy to maintain functional homeostasis in multiple tissues, including the heart.

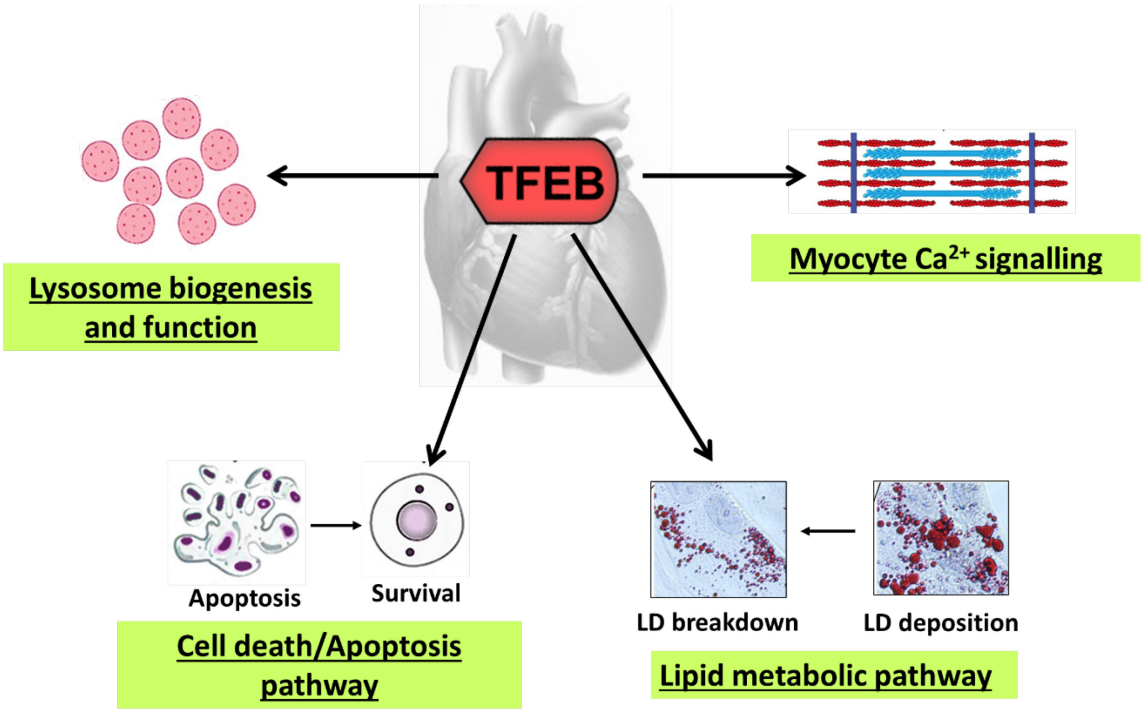

Figure 6.1 Cardiomyocyte-specific role of TFEB. TFEB plays an important role in regulating lysosome biogenesis and function (autophagy), cell death and survival, lipid metabolism and calcium dynamics in cardiomyocytes, which likely influences cardiac function.

References

1. Trivedi, P.C.; Bartlett, J.J.; Pulinilkunnil, T. Lysosomal Biology and Function: Modern View of Cellular Debris Bin. *Cells* **2020**, *9*, doi:10.3390/cells9051131.

2. Twells, L.K.; Gregory, D.M.; Reddigan, J.; Midodzi, W.K. Current and predicted prevalence of obesity in Canada: a trend analysis. *CMAJ Open* **2014**, *2*, E18-26, doi:10.9778/cmajo.20130016.
3. Canada, S. Health Fact Sheets - Overweight and Obese adults, 2018. **2019**, 1-8.

4. Canada, P.H.A.o. OBESITY IN CANADA, A JOINT REPORT FROM THE PUBLIC HEALTH AGENCY OF CANADA AND THE CANADIAN INSTITUTE FOR HEALTH INFORMATION. **2011**.

5. Steele, C.; Hagopian, W.A.; Gitelman, S.; Masharani, U.; Cavaghan, M.; Rother, K.I.; Donaldson, D.; Harlan, D.M.; Bluestone, J.; Herold, K.C. Insulin secretion in type 1 diabetes. *Diabetes* **2004**, *53*, 426-433, doi:10.2337/diabetes.53.2.426.

6. Brorsson, C.A.; Pociot, F.; Type 1 Diabetes Genetics, C. Shared Genetic Basis for Type 1 Diabetes, Islet Autoantibodies, and Autoantibodies Associated With Other Immune-Mediated Diseases in Families With Type 1 Diabetes. *Diabetes Care* **2015**, *38 Suppl 2*, S8-13, doi:10.2337/dcs15-2003.

7. Pi-Sunyer, X. The medical risks of obesity. *Postgrad Med* **2009**, *121*, 21-33, doi:10.3810/pgm.2009.11.2074.

8. Jaacks, L.M.; Siegel, K.R.; Gujral, U.P.; Narayan, K.M. Type 2 diabetes: A 21st century epidemic. *Best Pract Res Clin Endocrinol Metab* **2016**, *30*, 331-343, doi:10.1016/j.beem.2016.05.003.

9. Canada, S. Health Fact Sheets Diabetes, 2017.

10. American Diabetes, A. Diagnosis and classification of diabetes mellitus. *Diabetes Care* **2013**, *36 Suppl 1*, S67-74, doi:10.2337/dc13-S067.

11. Cerf, M.E. Beta cell dysfunction and insulin resistance. *Front Endocrinol (Lausanne)* **2013**, *4*, 37, doi:10.3389/fendo.2013.00037.

12. Araujo, L.S.; da Silva, M.V.; da Silva, C.A.; Borges, M.F.; Palhares, H.; Rocha, L.P.; Correa, R.R.M.; Rodrigues Junior, V.; Dos Reis, M.A.; Machado, J.R. Analysis of serum inflammatory mediators in type 2 diabetic patients and their influence on renal function. *PLoS One* **2020**, *15*, e0229765, doi:10.1371/journal.pone.0229765.

13. Wang, X.; Bao, W.; Liu, J.; Ouyang, Y.Y.; Wang, D.; Rong, S.; Xiao, X.; Shan, Z.L.; Zhang, Y.; Yao, P., et al. Inflammatory markers and risk of type 2 diabetes: a systematic review and meta-analysis. *Diabetes Care* **2013**, *36*, 166-175, doi:10.2337/dc12-0702.

14. Al-Huseini, I.; Harada, M.; Nishi, K.; Nguyen-Tien, D.; Kimura, T.; Ashida, N. Improvement of insulin signalling rescues inflammatory cardiac dysfunction. *Sci Rep* **2019**, *9*, 14801, doi:10.1038/s41598-019-51304-8.

15. Ghosh, S.; An, D.; Pulinilkunnil, T.; Qi, D.; Lau, H.C.; Abrahani, A.; Innis, S.M.; Rodrigues, B. Role of dietary fatty acids and acute hyperglycemia in modulating cardiac cell death. *Nutrition* **2004**, *20*, 916-923, doi:10.1016/j.nut.2004.06.013.

16. Pulinilkunnil, T.; Rodrigues, B. Cardiac lipoprotein lipase: metabolic basis for diabetic heart disease. *Cardiovasc Res* **2006**, *69*, 329-340, doi:10.1016/j.cardiores.2005.09.017.

17. Kolb, R.; Sutterwala, F.S.; Zhang, W. Obesity and cancer: inflammation bridges the two. *Curr Opin Pharmacol* **2016**, *29*, 77-89, doi:10.1016/j.coph.2016.07.005.

18. Must, A.; McKeown, N.M. The Disease Burden Associated with Overweight and Obesity. In *Endotext*, Feingold, K.R., Anawalt, B., Boyce, A., Chrousos, G., de Herder, W.W., Dungan, K., Grossman, A., Hershman, J.M., Hofland, H.J., Kaltsas, G., et al., Eds. South Dartmouth (MA), 2000.

19. Pepin, J.L.; Timsit, J.F.; Tamisier, R.; Borel, J.C.; Levy, P.; Jaber, S. Prevention and care of respiratory failure in obese patients. *Lancet Respir Med* **2016**, *4*, 407-418, doi:10.1016/S2213-2600(16)00054-0.

20. Thomas, M.C. Type 2 Diabetes and Heart Failure: Challenges and Solutions. *Curr Cardiol Rev* **2016**, *12*, 249-255, doi:10.2174/1573403x12666160606120254.

21. Miki, T.; Yuda, S.; Kouzu, H.; Miura, T. Diabetic cardiomyopathy: pathophysiology and clinical features. *Heart Fail Rev* **2013**, *18*, 149-166, doi:10.1007/s10741-012-9313-3.

22. Lehrke, M.; Marx, N. Diabetes Mellitus and Heart Failure. *Am J Cardiol* **2017**, *120*, S37-S47, doi:10.1016/j.amjcard.2017.05.014.

23. Iribarren, C.; Karter, A.J.; Go, A.S.; Ferrara, A.; Liu, J.Y.; Sidney, S.; Selby, J.V. Glycemic control and heart failure among adult patients with diabetes. *Circulation* **2001**, *103*, 2668-2673, doi:10.1161/01.cir.103.22.2668.

24. Tomova, G.S.; Nimbal, V.; Horwich, T.B. Relation between hemoglobin a(1c) and outcomes in heart failure patients with and without diabetes mellitus. *Am J Cardiol* **2012**, *109*, 1767-1773, doi:10.1016/j.amjcard.2012.02.022.

25. Kannel, W.B.; Hjortland, M.; Castelli, W.P. Role of diabetes in congestive heart failure: the Framingham study. *Am J Cardiol* **1974**, *34*, 29-34, doi:10.1016/0002-9149(74)90089-7.

26. Devereux, R.B.; Roman, M.J.; Paranicas, M.; O'Grady, M.J.; Lee, E.T.; Welty, T.K.; Fabsitz, R.R.; Robbins, D.; Rhoades, E.R.; Howard, B.V. Impact of diabetes on cardiac structure and function: the strong heart study. *Circulation* **2000**, *101*, 2271-2276, doi:10.1161/01.cir.101.19.2271.

27. Bertoni, A.G.; Hundley, W.G.; Massing, M.W.; Bonds, D.E.; Burke, G.L.; Goff, D.C., Jr. Heart failure prevalence, incidence, and mortality in the elderly with diabetes. *Diabetes Care* **2004**, *27*, 699-703, doi:10.2337/diacare.27.3.699.

28. DiMenna, F.J.; Arad, A.D. Exercise as 'precision medicine' for insulin resistance and its progression to type 2 diabetes: a research review. *BMC Sports Sci Med Rehabil* **2018**, *10*, 21, doi:10.1186/s13102-018-0110-8.

29. Teixeira de Lemos, E.; Pinto, R.; Oliveira, J.; Garrido, P.; Sereno, J.; Mascarenhas-Melo, F.; Pascoa-Pinheiro, J.; Teixeira, F.; Reis, F. Differential effects of acute (extenuating) and chronic (training) exercise on inflammation and oxidative stress status in an animal model of type 2 diabetes mellitus. *Mediators Inflamm* **2011**, *2011*, 253061, doi:10.1155/2011/253061.

30. Ventura-Clapier, R.; Mettauer, B.; Bigard, X. Beneficial effects of endurance training on cardiac and skeletal muscle energy metabolism in heart failure. *Cardiovasc Res* **2007**, *73*, 10-18, doi:10.1016/j.cardiores.2006.09.003.

31. de Lemos, E.T.; Reis, F.; Baptista, S.; Pinto, R.; Sepodes, B.; Vala, H.; Rocha-Pereira, P.; Silva, A.S.; Teixeira, F. Exercise training is associated with improved levels of C-reactive protein and adiponectin in ZDF (type 2) diabetic rats. *Med Sci Monit* **2007**, *13*, BR168-174.

32. Grajower, M.M.; Horne, B.D. Clinical Management of Intermittent Fasting in Patients with Diabetes Mellitus. *Nutrients* **2019**, *11*, doi:10.3390/nu11040873.

33. Hammer, S.; Snel, M.; Lamb, H.J.; Jazet, I.M.; van der Meer, R.W.; Pijl, H.; Meinders, E.A.; Romijn, J.A.; de Roos, A.; Smit, J.W. Prolonged caloric restriction in obese patients with type 2 diabetes mellitus decreases myocardial triglyceride content and improves myocardial function. *J Am Coll Cardiol* **2008**, *52*, 1006-1012, doi:10.1016/j.jacc.2008.04.068.

34. Stratton, I.M.; Adler, A.I.; Neil, H.A.; Matthews, D.R.; Manley, S.E.; Cull, C.A.; Hadden, D.; Turner, R.C.; Holman, R.R. Association of glycaemia with macrovascular and microvascular complications of type 2 diabetes (UKPDS 35): prospective observational study. *BMJ* **2000**, *321*, 405-412, doi:10.1136/bmj.321.7258.405.

35. Collyer, M.E. Resolving conflicts: leadership style sets the strategy. *Nurs Manage* **1989**, *20*, 77-80.

36. Nassif, M.; Kosiborod, M. Effect of glucose-lowering therapies on heart failure. *Nat Rev Cardiol* **2018**, *15*, 282-291, doi:10.1038/nrcardio.2017.211.

37. Paneni, F.; Luscher, T.F. Cardiovascular Protection in the Treatment of Type 2 Diabetes: A Review of Clinical Trial Results Across Drug Classes. *Am J Cardiol* **2017**, *120*, S17-S27, doi:10.1016/j.amjcard.2017.05.015.

38. Husain, M.; Birkenfeld, A.L.; Donsmark, M.; Dungan, K.; Eliaschewitz, F.G.; Franco, D.R.; Jeppesen, O.K.; Lingvay, I.; Mosenzon, O.; Pedersen, S.D., et al. Oral Semaglutide and Cardiovascular Outcomes in Patients with Type 2 Diabetes. *N Engl J Med* **2019**, *381*, 841-851, doi:10.1056/NEJMoa1901118.

39. Marso, S.P.; Daniels, G.H.; Brown-Frandsen, K.; Kristensen, P.; Mann, J.F.; Nauck, M.A.; Nissen, S.E.; Pocock, S.; Poulter, N.R.; Ravn, L.S., et al. Liraglutide and Cardiovascular Outcomes in Type 2 Diabetes. *N Engl J Med* **2016**, *375*, 311-322, doi:10.1056/NEJMoa1603827.

40. Zinman, B.; Wanner, C.; Lachin, J.M.; Fitchett, D.; Bluhmki, E.; Hantel, S.; Mattheus, M.; Devins, T.; Johansen, O.E.; Woerle, H.J., et al. Empagliflozin, Cardiovascular Outcomes, and Mortality in Type 2 Diabetes. *N Engl J Med* **2015**, *373*, 2117-2128, doi:10.1056/NEJMoa1504720.

41. Cholesterol Treatment Trialists, C.; Baigent, C.; Blackwell, L.; Emberson, J.; Holland, L.E.; Reith, C.; Bhala, N.; Peto, R.; Barnes, E.H.; Keech, A., et al. Efficacy and safety of more intensive lowering of LDL cholesterol: a meta-analysis of data from 170,000 participants in 26 randomised trials. *Lancet* **2010**, *376*, 1670-1681, doi:10.1016/S0140-6736(10)61350-5.

42. Mega, J.L.; Stitziel, N.O.; Smith, J.G.; Chasman, D.I.; Caulfield, M.; Devlin, J.J.; Nordio, F.; Hyde, C.; Cannon, C.P.; Sacks, F., et al. Genetic risk, coronary heart disease events, and the clinical benefit of statin therapy: an analysis of primary and secondary prevention trials. *Lancet* **2015**, *385*, 2264-2271, doi:10.1016/S0140-6736(14)61730-X.

43. Adeghate, E.; Singh, J. Structural changes in the myocardium during diabetes-induced cardiomyopathy. *Heart Fail Rev* **2014**, *19*, 15-23, doi:10.1007/s10741-013-9388-5.

44. Falcao-Pires, I.; Leite-Moreira, A.F. Diabetic cardiomyopathy: understanding the molecular and cellular basis to progress in diagnosis and treatment. *Heart Fail Rev* **2012**, *17*, 325-344, doi:10.1007/s10741-011-9257-z.

45. Franssen, C.; Gonzalez Miqueo, A. The role of titin and extracellular matrix remodelling in heart failure with preserved ejection fraction. *Neth Heart J* **2016**, *24*, 259-267, doi:10.1007/s12471-016-0812-z.

46. Zile, M.R.; Baicu, C.F.; Ikonomidis, J.S.; Stroud, R.E.; Nietert, P.J.; Bradshaw, A.D.; Slater, R.; Palmer, B.M.; Van Buren, P.; Meyer, M., et al. Myocardial stiffness in patients with heart failure and a preserved ejection fraction: contributions of collagen and titin. *Circulation* **2015**, *131*, 1247-1259, doi:10.1161/CIRCULATIONAHA.114.013215.

47. Fang, Z.Y.; Prins, J.B.; Marwick, T.H. Diabetic cardiomyopathy: evidence, mechanisms, and therapeutic implications. *Endocr Rev* **2004**, *25*, 543-567, doi:10.1210/er.2003-0012.

48. Battiprolu, P.K.; Gillette, T.G.; Wang, Z.V.; Lavandero, S.; Hill, J.A. Diabetic Cardiomyopathy: Mechanisms and Therapeutic Targets. *Drug Discov Today Dis Mech* **2010**, *7*, e135-e143, doi:10.1016/j.ddmec.2010.08.001.

49. Eguchi, K.; Manabe, I. Toll-like receptor, lipotoxicity and chronic inflammation: the pathological link between obesity and cardiometabolic disease. *J Atheroscler Thromb* **2014**, *21*, 629-639, doi:10.5551/jat.22533.

50. Alpert, M.A.; Omran, J.; Mehra, A.; Ardhanari, S. Impact of obesity and weight loss on cardiac performance and morphology in adults. *Prog Cardiovasc Dis* **2014**, *56*, 391-400, doi:10.1016/j.pcad.2013.09.003.

51. Blaha, M.J.; DeFilippis, A.P.; Rivera, J.J.; Budoff, M.J.; Blankstein, R.; Agatston, A.; Szklo, M.; Lakoski, S.G.; Bertoni, A.G.; Kronmal, R.A., et al. The relationship between insulin resistance and incidence and progression of coronary artery calcification: the Multi-Ethnic Study of Atherosclerosis (MESA). *Diabetes Care* **2011**, *34*, 749-751, doi:10.2337/dc10-1681.

52. Kim, M.; Oh, J.K.; Sakata, S.; Liang, I.; Park, W.; Hajjar, R.J.; Lebeche, D. Role of resistin in cardiac contractility and hypertrophy. *J Mol Cell Cardiol* **2008**, *45*, 270-280, doi:10.1016/j.yjmcc.2008.05.006.

53. Ormazabal, V.; Nair, S.; Elfeky, O.; Aguayo, C.; Salomon, C.; Zuniga, F.A. Association between insulin resistance and the development of cardiovascular disease. *Cardiovasc Diabetol* **2018**, *17*, 122, doi:10.1186/s12933-018-0762-4.

54. Shimizu, M.; Umeda, K.; Sugihara, N.; Yoshio, H.; Ino, H.; Takeda, R.; Okada, Y.; Nakanishi, I. Collagen remodelling in myocardia of patients with diabetes. *J Clin Pathol* **1993**, *46*, 32-36, doi:10.1136/jcp.46.1.32.

55. Gherasim, L.; Tasca, C.; Havriliuc, C.; Vasilescu, C. A morphological quantitative study of small vessels in diabetic cardiomyopathy. *Morphol Embryol (Bucur)* **1985**, *31*, 191-195.

56. Nunoda, S.; Genda, A.; Sugihara, N.; Nakayama, A.; Mizuno, S.; Takeda, R. Quantitative approach to the histopathology of the biopsied right ventricular myocardium in patients with diabetes mellitus. *Heart Vessels* **1985**, *1*, 43-47, doi:10.1007/BF02066486.

57. Vainio, L.E.; Szabo, Z.; Lin, R.; Ulvila, J.; Yrjola, R.; Alakoski, T.; Piuhola, J.; Koch, W.J.; Ruskoaho, H.; Fouse, S.D., et al. Connective Tissue Growth Factor Inhibition Enhances Cardiac Repair and Limits Fibrosis After Myocardial Infarction. *JACC Basic Transl Sci* **2019**, *4*, 83-94, doi:10.1016/j.jacbts.2018.10.007.

58. Szabo, Z.; Magga, J.; Alakoski, T.; Ulvila, J.; Piuhola, J.; Vainio, L.; Kivirikko, K.I.; Vuolteenaho, O.; Ruskoaho, H.; Lipson, K.E., et al. Connective tissue growth factor inhibition attenuates left ventricular remodeling and dysfunction in pressure overload-induced heart failure. *Hypertension* **2014**, *63*, 1235-1240, doi:10.1161/HYPERTENSIONAHA.114.03279.

59. Aronson, D. Cross-linking of glycated collagen in the pathogenesis of arterial and myocardial stiffening of aging and diabetes. *J Hypertens* **2003**, *21*, 3-12, doi:10.1097/00004872-200301000-00002.

60. Brunvand, L.; Heier, M.; Brunborg, C.; Hanssen, K.F.; Fugelseth, D.; Stensaeth, K.H.; Dahl-Jorgensen, K.; Margeirsdottir, H.D. Advanced glycation end products in children with type 1 diabetes and early reduced diastolic heart function. *BMC Cardiovasc Disord* **2017**, *17*, 133, doi:10.1186/s12872-017-0551-0.

61. Frunza, O.; Russo, I.; Saxena, A.; Shinde, A.V.; Humeres, C.; Hanif, W.; Rai, V.; Su, Y.; Frangogiannis, N.G. Myocardial Galectin-3 Expression Is Associated with Remodeling of the Pressure-Overloaded Heart and May Delay the Hypertrophic Response without Affecting Survival, Dysfunction, and Cardiac Fibrosis. *Am J Pathol* **2016**, *186*, 1114-1127, doi:10.1016/j.ajpath.2015.12.017.

62. Li, A.H.; Liu, P.P.; Villarreal, F.J.; Garcia, R.A. Dynamic changes in myocardial matrix and relevance to disease: translational perspectives. *Circ Res* **2014**, *114*, 916-927, doi:10.1161/CIRCRESAHA.114.302819.

63. Martinez-Martinez, E.; Calvier, L.; Fernandez-Celis, A.; Rousseau, E.; Jurado-Lopez, R.; Rossoni, L.V.; Jaisser, F.; Zannad, F.; Rossignol, P.; Cachofeiro, V., et al. Galectin-3 blockade inhibits cardiac inflammation and fibrosis in experimental hyperaldosteronism and hypertension. *Hypertension* **2015**, *66*, 767-775, doi:10.1161/HYPERTENSIONAHA.115.05876.

64. Bella, J.N.; Palmieri, V.; Roman, M.J.; Liu, J.E.; Welty, T.K.; Lee, E.T.; Fabsitz, R.R.; Howard, B.V.; Devereux, R.B. Mitral ratio of peak early to late diastolic filling velocity as a predictor of mortality in middle-aged and elderly adults: the Strong Heart Study. *Circulation* **2002**, *105*, 1928-1933, doi:10.1161/01.cir.0000015076.37047.d9.

65. Wang, M.; Yip, G.W.; Wang, A.Y.; Zhang, Y.; Ho, P.Y.; Tse, M.K.; Lam, P.K.; Sanderson, J.E. Peak early diastolic mitral annulus velocity by tissue Doppler imaging adds independent and incremental prognostic value. *J Am Coll Cardiol* **2003**, *41*, 820-826, doi:10.1016/s0735-1097(02)02921-2.

66. Brooks, B.A.; Franjic, B.; Ban, C.R.; Swaraj, K.; Yue, D.K.; Celermajer, D.S.; Twigg, S.M. Diastolic dysfunction and abnormalities of the microcirculation in type 2 diabetes. *Diabetes Obes Metab* **2008**, *10*, 739-746, doi:10.1111/j.1463-1326.2007.00803.x.

67. Ozasa, N.; Furukawa, Y.; Morimoto, T.; Tadamura, E.; Kita, T.; Kimura, T. Relation among left ventricular mass, insulin resistance, and hemodynamic parameters in type 2 diabetes. *Hypertens Res* **2008**, *31*, 425-432, doi:10.1291/hypres.31.425.

68. Shivalkar, B.; Dhondt, D.; Goovaerts, I.; Van Gaal, L.; Bartunek, J.; Van Crombrugge, P.; Vrints, C. Flow mediated dilatation and cardiac function in type 1 diabetes mellitus. *Am J Cardiol* **2006**, *97*, 77-82, doi:10.1016/j.amjcard.2005.07.111.

69. Aasum, E.; Belke, D.D.; Severson, D.L.; Riemersma, R.A.; Cooper, M.; Andreassen, M.; Larsen, T.S. Cardiac function and metabolism in Type 2 diabetic mice after treatment with BM 17.0744, a novel PPAR-alpha activator. *Am J Physiol Heart Circ Physiol* **2002**, *283*, H949-957, doi:10.1152/ajpheart.00226.2001.

70. Aasum, E.; Hafstad, A.D.; Severson, D.L.; Larsen, T.S. Age-dependent changes in metabolism, contractile function, and ischemic sensitivity in hearts from db/db mice. *Diabetes* **2003**, *52*, 434-441, doi:10.2337/diabetes.52.2.434.

71. Dong, F.; Zhang, X.; Yang, X.; Esberg, L.B.; Yang, H.; Zhang, Z.; Culver, B.; Ren, J. Impaired cardiac contractile function in ventricular myocytes from leptin-deficient ob/ob obese mice. *J Endocrinol* **2006**, *188*, 25-36, doi:10.1677/joe.1.06241.

72. Russell, J.C.; Proctor, S.D. Small animal models of cardiovascular disease: tools for the study of the roles of metabolic syndrome, dyslipidemia, and atherosclerosis. *Cardiovasc Pathol* **2006**, *15*, 318-330, doi:10.1016/j.carpath.2006.09.001.

73. Semeniuk, L.M.; Kryski, A.J.; Severson, D.L. Echocardiographic assessment of cardiac function in diabetic db/db and transgenic db/db-hGLUT4 mice. *Am J Physiol Heart Circ Physiol* **2002**, *283*, H976-982, doi:10.1152/ajpheart.00088.2002.

74. Christoffersen, C.; Bollano, E.; Lindegaard, M.L.; Bartels, E.D.; Goetze, J.P.; Andersen, C.B.; Nielsen, L.B. Cardiac lipid accumulation associated with diastolic dysfunction in obese mice. *Endocrinology* **2003**, *144*, 3483-3490, doi:10.1210/en.2003-0242.

75. Boudina, S.; Sena, S.; O'Neill, B.T.; Tathireddy, P.; Young, M.E.; Abel, E.D. Reduced mitochondrial oxidative capacity and increased mitochondrial uncoupling impair myocardial energetics in obesity. *Circulation* **2005**, *112*, 2686-2695, doi:10.1161/CIRCULATIONAHA.105.554360.

76. Boudina, S.; Sena, S.; Theobald, H.; Sheng, X.; Wright, J.J.; Hu, X.X.; Aziz, S.; Johnson, J.I.; Bugger, H.; Zaha, V.G., et al. Mitochondrial energetics in the heart in obesity-related diabetes: direct evidence for increased uncoupled respiration and activation of uncoupling proteins. *Diabetes* **2007**, *56*, 2457-2466, doi:10.2337/db07-0481.

77. Scognamiglio, R.; Avogaro, A.; Casara, D.; Crepaldi, C.; Marin, M.; Palisi, M.; Mingardi, R.; Erle, G.; Fasoli, G.; Dalla Volta, S. Myocardial dysfunction and adrenergic cardiac innervation in patients with insulin-dependent diabetes mellitus. *J Am Coll Cardiol* **1998**, *31*, 404-412, doi:10.1016/s0735-1097(97)00516-0.

78. Stolen, T.O.; Hoydal, M.A.; Kemi, O.J.; Catalucci, D.; Ceci, M.; Aasum, E.; Larsen, T.; Rolim, N.; Condorelli, G.; Smith, G.L., et al. Interval training normalizes cardiomyocyte function, diastolic Ca2+ control, and SR Ca2+ release synchronicity in a mouse model of diabetic cardiomyopathy. *Circ Res* **2009**, *105*, 527-536, doi:10.1161/CIRCRESAHA.109.199810.

79. Woodiwiss, A.J.; Libhaber, C.D.; Majane, O.H.; Libhaber, E.; Maseko, M.; Norton, G.R. Obesity promotes left ventricular concentric rather than eccentric geometric remodeling and hypertrophy independent of blood pressure. *Am J Hypertens* **2008**, *21*, 1144-1151, doi:10.1038/ajh.2008.252.

80. Sola, S.; Mir, M.Q.; Lerakis, S.; Tandon, N.; Khan, B.V. Atorvastatin improves left ventricular systolic function and serum markers of inflammation in nonischemic heart failure. *J Am Coll Cardiol* **2006**, *47*, 332-337, doi:10.1016/j.jacc.2005.06.088.

81. Bouthoorn, S.; Gohar, A.; Valstar, G.; den Ruijter, H.M.; Reitsma, J.B.; Hoes, A.W.; Rutten, F.H.; Queen of Hearts, C. Prevalence of left ventricular systolic dysfunction and heart failure with reduced ejection fraction in men and women with type 2 diabetes mellitus: a systematic review and meta-analysis. *Cardiovasc Diabetol* **2018**, *17*, 58, doi:10.1186/s12933-018-0690-3.

82. Hoit, B.D.; Castro, C.; Bultron, G.; Knight, S.; Matlib, M.A. Noninvasive evaluation of cardiac dysfunction by echocardiography in streptozotocin-induced diabetic rats. *J Card Fail* **1999**, *5*, 324-333, doi:10.1016/s1071-9164(99)91337-4.

83. Joffe, II; Travers, K.E.; Perreault-Micale, C.L.; Hampton, T.; Katz, S.E.; Morgan, J.P.; Douglas, P.S. Abnormal cardiac function in the streptozotocin-induced non-insulin-dependent diabetic rat: noninvasive assessment with doppler echocardiography and contribution of the nitric oxide pathway. *J Am Coll Cardiol* **1999**, *34*, 2111-2119, doi:10.1016/s0735-1097(99)00436-2.

84. Wold, L.E.; Relling, D.P.; Colligan, P.B.; Scott, G.I.; Hintz, K.K.; Ren, B.H.; Epstein, P.N.; Ren, J. Characterization of contractile function in diabetic hypertensive cardiomyopathy in adult rat ventricular myocytes. *J Mol Cell Cardiol* **2001**, *33*, 1719-1726, doi:10.1006/jmcc.2001.1431.

85. Malhotra, A.; Sanghi, V. Regulation of contractile proteins in diabetic heart. *Cardiovasc Res* **1997**, *34*, 34-40, doi:10.1016/s0008-6363(97)00059-x.

86. Tisdale, R.L.; Haddad, F.; Kohsaka, S.; Heidenreich, P.A. Trends in Left Ventricular Ejection Fraction for Patients With a New Diagnosis of Heart Failure. *Circ Heart Fail* **2020**, *13*, e006743, doi:10.1161/CIRCHEARTFAILURE.119.006743.

87. Pfeffer, M.A.; Shah, A.M.; Borlaug, B.A. Heart Failure With Preserved Ejection Fraction In Perspective. *Circ Res* **2019**, *124*, 1598-1617, doi:10.1161/CIRCRESAHA.119.313572.

88. Margonato, D.; Mazzetti, S.; De Maria, R.; Gorini, M.; Iacoviello, M.; Maggioni, A.P.; Mortara, A. Heart Failure With Mid-range or Recovered Ejection Fraction: Differential Determinants of Transition. *Card Fail Rev* **2020**, *6*, e28, doi:10.15420/cfr.2020.13.

89. van Heerebeek, L.; Hamdani, N.; Handoko, M.L.; Falcao-Pires, I.; Musters, R.J.; Kupreishvili, K.; Ijsselmuiden, A.J.; Schalkwijk, C.G.; Bronzwaer, J.G.; Diamant, M., et al. Diastolic stiffness of the failing diabetic heart: importance of fibrosis, advanced glycation end products, and myocyte resting tension. *Circulation* **2008**, *117*, 43-51, doi:10.1161/CIRCULATIONAHA.107.728550.

90. Huynh, T.; Harty, B.J.; Claggett, B.; Fleg, J.L.; McKinlay, S.M.; Anand, I.S.; Lewis, E.F.; Joseph, J.; Desai, A.S.; Sweitzer, N.K., et al. Comparison of Outcomes in Patients With Diabetes Mellitus Treated With Versus Without Insulin+Heart Failure With Preserved Left Ventricular Ejection Fraction (from the TOPCAT Study). *Am J Cardiol* **2019**, *123*, 611-617, doi:10.1016/j.amjcard.2018.11.022.

91. Poulsen, M.K.; Henriksen, J.E.; Dahl, J.; Johansen, A.; Gerke, O.; Vach, W.; Haghfelt, T.; Hoilund-Carlsen, P.F.; Beck-Nielsen, H.; Moller, J.E. Left ventricular diastolic function in type 2 diabetes mellitus: prevalence and association with myocardial and vascular disease. *Circ Cardiovasc Imaging* **2010**, *3*, 24-31, doi:10.1161/CIRCIMAGING.109.855510.

92. Sanders-van Wijk, S.; van Empel, V.; Davarzani, N.; Maeder, M.T.; Handschin, R.; Pfisterer, M.E.; Brunner-La Rocca, H.P.; investigators, T.-C. Circulating biomarkers of distinct pathophysiological pathways in heart failure with preserved vs. reduced left ventricular ejection fraction. *Eur J Heart Fail* **2015**, *17*, 1006-1014, doi:10.1002/ejhf.414.

93. Santhanakrishnan, R.; Chong, J.P.; Ng, T.P.; Ling, L.H.; Sim, D.; Leong, K.T.; Yeo, P.S.; Ong, H.Y.; Jaufeerally, F.; Wong, R., et al. Growth differentiation factor 15, ST2, high-sensitivity troponin T, and N-terminal pro brain natriuretic peptide in heart failure with preserved vs. reduced ejection fraction. *Eur J Heart Fail* **2012**, *14*, 1338-1347, doi:10.1093/eurjhf/hfs130.

94. Yap, J.; Tay, W.T.; Teng, T.K.; Anand, I.; Richards, A.M.; Ling, L.H.; MacDonald, M.R.; Chandramouli, C.; Tromp, J.; Siswanto, B.B., et al. Association of Diabetes Mellitus on Cardiac Remodeling, Quality of Life, and Clinical Outcomes in Heart Failure With Reduced and Preserved Ejection Fraction. *J Am Heart Assoc* **2019**, *8*, e013114, doi:10.1161/JAHA.119.013114.

95. Bugger, H.; Abel, E.D. Rodent models of diabetic cardiomyopathy. *Dis Model Mech* **2009**, *2*, 454-466, doi:10.1242/dmm.001941.

96. Peterson, L.R.; Herrero, P.; Schechtman, K.B.; Racette, S.B.; Waggoner, A.D.; Kisrieva-Ware, Z.; Dence, C.; Klein, S.; Marsala, J.; Meyer, T., et al. Effect of obesity and insulin resistance on myocardial substrate metabolism and efficiency in young women. *Circulation* **2004**, *109*, 2191-2196, doi:10.1161/01.CIR.0000127959.28627.F8.

97. An, D.; Rodrigues, B. Role of changes in cardiac metabolism in development of diabetic cardiomyopathy. *Am J Physiol Heart Circ Physiol* **2006**, *291*, H1489-1506, doi:10.1152/ajpheart.00278.2006.

98. Rodrigues, B.; Cam, M.C.; McNeill, J.H. Myocardial substrate metabolism: implications for diabetic cardiomyopathy. *J Mol Cell Cardiol* **1995**, *27*, 169-179, doi:10.1016/s0022-2828(08)80016-8.

99. Randle, P.J. The biochemical basis of the relation between glucose and fatty acid metabolism. *Acta Chir Scand Suppl* **1980**, *498*, 111-114.

100. Khan, R.S.; Lin, Y.; Hu, Y.; Son, N.H.; Bharadwaj, K.G.; Palacios, C.; Chokshi, A.; Ji, R.; Yu, S.; Homma, S., et al. Rescue of heart lipoprotein lipase-knockout mice confirms a role for triglyceride in optimal heart metabolism and function. *Am J Physiol Endocrinol Metab* **2013**, *305*, E1339-1347, doi:10.1152/ajpendo.00349.2013.

101. Yagyu, H.; Chen, G.; Yokoyama, M.; Hirata, K.; Augustus, A.; Kako, Y.; Seo, T.; Hu, Y.; Lutz, E.P.; Merkel, M., et al. Lipoprotein lipase (LpL) on the surface of cardiomyocytes increases lipid uptake and produces a cardiomyopathy. *J Clin Invest* **2003**, *111*, 419-426, doi:10.1172/JCI16751.

102. Luiken, J.J.; Coort, S.L.; Willems, J.; Coumans, W.A.; Bonen, A.; van der Vusse, G.J.; Glatz, J.F. Contraction-induced fatty acid translocase/CD36 translocation in rat cardiac myocytes is mediated through AMP-activated protein kinase signaling. *Diabetes* **2003**, *52*, 1627-1634, doi:10.2337/diabetes.52.7.1627.

103. Luiken, J.J.; Schaap, F.G.; van Nieuwenhoven, F.A.; van der Vusse, G.J.; Bonen, A.; Glatz, J.F. Cellular fatty acid transport in heart and skeletal muscle as facilitated by proteins. *Lipids* **1999**, *34 Suppl*, S169-175, doi:10.1007/BF02562278.

104. Luiken, J.J.; Turcotte, L.P.; Bonen, A. Protein-mediated palmitate uptake and expression of fatty acid transport proteins in heart giant vesicles. *J Lipid Res* **1999**, *40*, 1007-1016.

105. Knudsen, J.; Neergaard, T.B.; Gaigg, B.; Jensen, M.V.; Hansen, J.K. Role of acyl-CoA binding protein in acyl-CoA metabolism and acyl-CoA-mediated cell signaling. *J Nutr* **2000**, *130*, 294S-298S, doi:10.1093/jn/130.2.294S.

106. Lopaschuk, G.D.; Ussher, J.R.; Folmes, C.D.; Jaswal, J.S.; Stanley, W.C. Myocardial fatty acid metabolism in health and disease. *Physiol Rev* **2010**, *90*, 207-258, doi:10.1152/physrev.00015.2009.

107. Doenst, T.; Nguyen, T.D.; Abel, E.D. Cardiac metabolism in heart failure: implications beyond ATP production. *Circ Res* **2013**, *113*, 709-724, doi:10.1161/CIRCRESAHA.113.300376.

108. Murthy, M.S.; Pande, S.V. Mechanism of carnitine acylcarnitine translocase-catalyzed import of acylcarnitines into mitochondria. *J Biol Chem* **1984**, *259*, 9082-9089.

109. Steinberg, G.R.; Kemp, B.E. AMPK in Health and Disease. *Physiol Rev* **2009**, *89*, 1025-1078, doi:10.1152/physrev.00011.2008.

110. Brownsey, R.W.; Boone, A.N.; Elliott, J.E.; Kulpa, J.E.; Lee, W.M. Regulation of acetyl-CoA carboxylase. *Biochem Soc Trans* **2006**, *34*, 223-227, doi:10.1042/BST20060223.

111. Finck, B.N.; Lehman, J.J.; Leone, T.C.; Welch, M.J.; Bennett, M.J.; Kovacs, A.; Han, X.; Gross, R.W.; Kozak, R.; Lopaschuk, G.D., et al. The cardiac phenotype induced by PPARalpha overexpression mimics that caused by diabetes mellitus. *J Clin Invest* **2002**, *109*, 121-130, doi:10.1172/JCI14080.

112. Thorens, B.; Mueckler, M. Glucose transporters in the 21st Century. *Am J Physiol Endocrinol Metab* **2010**, *298*, E141-145, doi:10.1152/ajpendo.00712.2009.

113. Kienesberger, P.C.; Lee, D.; Pulinilkunnil, T.; Brenner, D.S.; Cai, L.; Magnes, C.; Koefeler, H.C.; Streith, I.E.; Rechberger, G.N.; Haemmerle, G., et al. Adipose triglyceride lipase deficiency causes tissue-specific changes in insulin signaling. *J Biol Chem* **2009**, *284*, 30218-30229, doi:10.1074/jbc.M109.047787.

114. Pulinilkunnil, T.; Kienesberger, P.C.; Nagendran, J.; Waller, T.J.; Young, M.E.; Kershaw, E.E.; Korbutt, G.; Haemmerle, G.; Zechner, R.; Dyck, J.R. Myocardial adipose triglyceride lipase overexpression protects diabetic mice from the development of lipotoxic cardiomyopathy. *Diabetes* **2013**, *62*, 1464-1477, doi:10.2337/db12-0927.

115. Samovski, D.; Su, X.; Xu, Y.; Abumrad, N.A.; Stahl, P.D. Insulin and AMPK regulate FA translocase/CD36 plasma membrane recruitment in cardiomyocytes via Rab GAP AS160 and Rab8a Rab GTPase. *J Lipid Res* **2012**, *53*, 709-717, doi:10.1194/jlr.M023424.

116. McCommis, K.S.; Douglas, D.L.; Krenz, M.; Baines, C.P. Cardiac-specific hexokinase 2 overexpression attenuates hypertrophy by increasing pentose phosphate pathway flux. *J Am Heart Assoc* **2013**, *2*, e000355, doi:10.1161/JAHA.113.000355.

117. Wu, R.; Smeele, K.M.; Wyatt, E.; Ichikawa, Y.; Eerbeek, O.; Sun, L.; Chawla, K.; Hollmann, M.W.; Nagpal, V.; Heikkinen, S., et al. Reduction in hexokinase II levels results in decreased cardiac function and altered remodeling after ischemia/reperfusion injury. *Circ Res* **2011**, *108*, 60-69, doi:10.1161/CIRCRESAHA.110.223115.

118. Wu, R.; Wyatt, E.; Chawla, K.; Tran, M.; Ghanefar, M.; Laakso, M.; Epting, C.L.; Ardehali, H. Hexokinase II knockdown results in exaggerated cardiac hypertrophy via increased ROS production. *EMBO Mol Med* **2012**, *4*, 633-646, doi:10.1002/emmm.201200240.

119. Bertrand, L.; Horman, S.; Beauloye, C.; Vanoverschelde, J.L. Insulin signalling in the heart. *Cardiovasc Res* **2008**, *79*, 238-248, doi:10.1093/cvr/cvn093.

120. Hue, L.; Beauloye, C.; Marsin, A.S.; Bertrand, L.; Horman, S.; Rider, M.H. Insulin and ischemia stimulate glycolysis by acting on the same targets through different and opposing signaling pathways. *J Mol Cell Cardiol* **2002**, *34*, 1091-1097, doi:10.1006/jmcc.2002.2063.

121. Evans, R.K.; Schwartz, D.D.; Gladden, L.B. Effect of myocardial volume overload and heart failure on lactate transport into isolated cardiac myocytes. *J Appl Physiol (1985)* **2003**, *94*, 1169-1176, doi:10.1152/japplphysiol.00778.2002.

122. Halestrap, A.P.; Price, N.T. The proton-linked monocarboxylate transporter (MCT) family: structure, function and regulation. *Biochem J* **1999**, *343 Pt 2*, 281-299.

123. Valenti, D.; de Bari, L.; Atlante, A.; Passarella, S. L-Lactate transport into rat heart mitochondria and reconstruction of the L-lactate/pyruvate shuttle. *Biochem J* **2002**, *364*, 101-104, doi:10.1042/bj3640101.

124. Frojdo, S.; Vidal, H.; Pirola, L. Alterations of insulin signaling in type 2 diabetes: a review of the current evidence from humans. *Biochim Biophys Acta* **2009**, *1792*, 83-92, doi:10.1016/j.bbadis.2008.10.019.

125. Chadt, A.; Immisch, A.; de Wendt, C.; Springer, C.; Zhou, Z.; Stermann, T.; Holman, G.D.; Loffing-Cueni, D.; Loffing, J.; Joost, H.G., et al. "Deletion of both Rab-GTPase-activating proteins TBC1D1 and TBC1D4 in mice eliminates insulin- and AICAR-stimulated glucose transport [corrected]. *Diabetes* **2015**, *64*, 746-759, doi:10.2337/db14-0368.

126. Montessuit, C.; Lerch, R. Regulation and dysregulation of glucose transport in cardiomyocytes. *Biochim Biophys Acta* **2013**, *1833*, 848-856, doi:10.1016/j.bbamcr.2012.08.009.

127. Shulman, R.G.; Bloch, G.; Rothman, D.L. In vivo regulation of muscle glycogen synthase and the control of glycogen synthesis. *Proc Natl Acad Sci U S A* **1995**, *92*, 8535-8542, doi:10.1073/pnas.92.19.8535.

128. Markou, T.; Cullingford, T.E.; Giraldo, A.; Weiss, S.C.; Alsafi, A.; Fuller, S.J.; Clerk, A.; Sugden, P.H. Glycogen synthase kinases 3alpha and 3beta in cardiac myocytes: regulation and consequences of their inhibition. *Cell Signal* **2008**, *20*, 206-218, doi:10.1016/j.cellsig.2007.10.004.

129. Donthi, R.V.; Ye, G.; Wu, C.; McClain, D.A.; Lange, A.J.; Epstein, P.N. Cardiac expression of kinase-deficient 6-phosphofructo-2-kinase/fructose-2,6-bisphosphatase inhibits glycolysis, promotes hypertrophy, impairs myocyte function, and reduces insulin sensitivity. *J Biol Chem* **2004**, *279*, 48085-48090, doi:10.1074/jbc.M405510200.

130. Pulinilkunnil, T.; An, D.; Yip, P.; Chan, N.; Qi, D.; Ghosh, S.; Abrahani, A.; Rodrigues, B. Palmitoyl lysophosphatidylcholine mediated mobilization of LPL to the coronary luminal surface requires PKC activation. *J Mol Cell Cardiol* **2004**, *37*, 931-938, doi:10.1016/j.yjmcc.2004.07.003.

131. Augustus, A.; Yagyu, H.; Haemmerle, G.; Bensadoun, A.; Vikramadithyan, R.K.; Park, S.Y.; Kim, J.K.; Zechner, R.; Goldberg, I.J. Cardiac-specific knock-out of lipoprotein lipase alters plasma lipoprotein triglyceride metabolism and cardiac gene expression. *J Biol Chem* **2004**, *279*, 25050-25057, doi:10.1074/jbc.M401028200.

132. Varga, Z.V.; Giricz, Z.; Liaudet, L.; Hasko, G.; Ferdinandy, P.; Pacher, P. Interplay of oxidative, nitrosative/nitrative stress, inflammation, cell death and autophagy in diabetic cardiomyopathy. *Biochim Biophys Acta* **2015**, *1852*, 232-242, doi:10.1016/j.bbadis.2014.06.030.

133. Finck, B.N.; Han, X.; Courtois, M.; Aimond, F.; Nerbonne, J.M.; Kovacs, A.; Gross, R.W.; Kelly, D.P. A critical role for PPARalpha-mediated lipotoxicity in the pathogenesis of diabetic cardiomyopathy: modulation by dietary fat content. *Proc Natl Acad Sci U S A* **2003**, *100*, 1226-1231, doi:10.1073/pnas.0336724100.

134. Lee, F.N.; Zhang, L.; Zheng, D.; Choi, W.S.; Youn, J.H. Insulin suppresses PDK-4 expression in skeletal muscle independently of plasma FFA. *Am J Physiol Endocrinol Metab* **2004**, *287*, E69-74, doi:10.1152/ajpendo.00461.2003.

135. Larsen, T.S.; Aasum, E. Metabolic (in)flexibility of the diabetic heart. *Cardiovasc Drugs Ther* **2008**, *22*, 91-95, doi:10.1007/s10557-008-6083-1.

136. Muoio, D.M. Metabolic inflexibility: when mitochondrial indecision leads to metabolic gridlock. *Cell* **2014**, *159*, 1253-1262, doi:10.1016/j.cell.2014.11.034.

137. Carroll, R.; Carley, A.N.; Dyck, J.R.; Severson, D.L. Metabolic effects of insulin on cardiomyocytes from control and diabetic db/db mouse hearts. *Am J Physiol Endocrinol Metab* **2005**, *288*, E900-906, doi:10.1152/ajpendo.00491.2004.

138. Young, M.E.; Guthrie, P.H.; Razeghi, P.; Leighton, B.; Abbasi, S.; Patil, S.; Youker, K.A.; Taegtmeyer, H. Impaired long-chain fatty acid oxidation and contractile dysfunction in the obese Zucker rat heart. *Diabetes* **2002**, *51*, 2587-2595, doi:10.2337/diabetes.51.8.2587.

139. Abel, E.D.; Kaulbach, H.C.; Tian, R.; Hopkins, J.C.; Duffy, J.; Doetschman, T.; Minnemann, T.; Boers, M.E.; Hadro, E.; Oberste-Berghaus, C., et al. Cardiac hypertrophy with preserved contractile function after selective deletion of GLUT4 from the heart. *J Clin Invest* **1999**, *104*, 1703-1714, doi:10.1172/JCI7605.

140. Stenbit, A.E.; Katz, E.B.; Chatham, J.C.; Geenen, D.L.; Factor, S.M.; Weiss, R.G.; Tsao, T.S.; Malhotra, A.; Chacko, V.P.; Ocampo, C., et al. Preservation of glucose metabolism in hypertrophic GLUT4-null hearts. *Am J Physiol Heart Circ Physiol* **2000**, *279*, H313-318, doi:10.1152/ajpheart.2000.279.1.H313.

141. Cai, L.; Kang, Y.J. Oxidative stress and diabetic cardiomyopathy: a brief review. *Cardiovasc Toxicol* **2001**, *1*, 181-193, doi:10.1385/ct:1:3:181.

142. Du, X.; Matsumura, T.; Edelstein, D.; Rossetti, L.; Zsengeller, Z.; Szabo, C.; Brownlee, M. Inhibition of GAPDH activity by poly(ADP-ribose) polymerase activates three major pathways of hyperglycemic damage in endothelial cells. *J Clin Invest* **2003**, *112*, 1049-1057, doi:10.1172/JCI18127.

143. Wakasaki, H.; Koya, D.; Schoen, F.J.; Jirousek, M.R.; Ways, D.K.; Hoit, B.D.; Walsh, R.A.; King, G.L. Targeted overexpression of protein kinase C beta2 isoform in myocardium causes cardiomyopathy. *Proc Natl Acad Sci U S A* **1997**, *94*, 9320-9325, doi:10.1073/pnas.94.17.9320.

144. Kienesberger, P.C.; Pulinilkunnil, T.; Nagendran, J.; Dyck, J.R. Myocardial triacylglycerol metabolism. *J Mol Cell Cardiol* **2013**, *55*, 101-110, doi:10.1016/j.yjmcc.2012.06.018.

145. Lee, W.S.; Kim, J. Peroxisome Proliferator-Activated Receptors and the Heart: Lessons from the Past and Future Directions. *PPAR Res* **2015**, *2015*, 271983, doi:10.1155/2015/271983.

146. Duncan, J.G.; Bharadwaj, K.G.; Fong, J.L.; Mitra, R.; Sambandam, N.; Courtois, M.R.; Lavine, K.J.; Goldberg, I.J.; Kelly, D.P. Rescue of cardiomyopathy in peroxisome proliferator-activated receptor-alpha transgenic mice by deletion of lipoprotein lipase identifies sources of cardiac lipids and peroxisome proliferator-activated receptor-alpha activators. *Circulation* **2010**, *121*, 426-435, doi:10.1161/CIRCULATIONAHA.109.888735.

147. Brindley, D.N.; Kok, B.P.; Kienesberger, P.C.; Lehner, R.; Dyck, J.R. Shedding light on the enigma of myocardial lipotoxicity: the involvement of known and putative regulators of fatty acid storage and mobilization. *Am J Physiol Endocrinol Metab* **2010**, *298*, E897-908, doi:10.1152/ajpendo.00509.2009.

148. Li, P.; Nijhawan, D.; Budihardjo, I.; Srinivasula, S.M.; Ahmad, M.; Alnemri, E.S.; Wang, X. Cytochrome c and dATP-dependent formation of Apaf-1/caspase-9 complex initiates an apoptotic protease cascade. *Cell* **1997**, *91*, 479-489, doi:10.1016/s0092-8674(00)80434-1.

149. de Vries, J.E.; Vork, M.M.; Roemen, T.H.; de Jong, Y.F.; Cleutjens, J.P.; van der Vusse, G.J.; van Bilsen, M. Saturated but not mono-unsaturated fatty acids induce apoptotic cell death in neonatal rat ventricular myocytes. *J Lipid Res* **1997**, *38*, 1384-1394.

150. van de Weijer, T.; Schrauwen-Hinderling, V.B.; Schrauwen, P. Lipotoxicity in type 2 diabetic cardiomyopathy. *Cardiovasc Res* **2011**, *92*, 10-18, doi:10.1093/cvr/cvr212.

151. Ersoy, B.A.; Maner-Smith, K.M.; Li, Y.; Alpertunga, I.; Cohen, D.E. Thioesterase-mediated control of cellular calcium homeostasis enables hepatic ER stress. *J Clin Invest* **2018**, *128*, 141-156, doi:10.1172/JCI93123.

152. Park, M.; Sabetski, A.; Kwan Chan, Y.; Turdi, S.; Sweeney, G. Palmitate induces ER stress and autophagy in H9c2 cells: implications for apoptosis and adiponectin resistance. *J Cell Physiol* **2015**, *230*, 630-639, doi:10.1002/jcp.24781.

153. Sargsyan, E.; Sol, E.R.; Bergsten, P. UPR in palmitate-treated pancreatic beta-cells is not affected by altering oxidation of the fatty acid. *Nutr Metab (Lond)* **2011**, *8*, 70, doi:10.1186/1743-7075-8-70.

154. Imamura, F.; Micha, R.; Wu, J.H.; de Oliveira Otto, M.C.; Otite, F.O.; Abioye, A.I.; Mozaffarian, D. Effects of Saturated Fat, Polyunsaturated Fat, Monounsaturated Fat, and Carbohydrate on Glucose-Insulin Homeostasis: A Systematic Review and Meta-analysis of Randomised Controlled Feeding Trials. *PLoS Med* **2016**, *13*, e1002087, doi:10.1371/journal.pmed.1002087.

155. Qian, F.; Korat, A.A.; Malik, V.; Hu, F.B. Metabolic Effects of Monounsaturated Fatty Acid-Enriched Diets Compared With Carbohydrate or Polyunsaturated Fatty Acid-Enriched Diets in Patients With Type 2 Diabetes: A Systematic Review and Meta-analysis of Randomized Controlled Trials. *Diabetes Care* **2016**, *39*, 1448-1457, doi:10.2337/dc16-0513.

156. Schwingshackl, L.; Hoffmann, G. Monounsaturated fatty acids, olive oil and health status: a systematic review and meta-analysis of cohort studies. *Lipids Health Dis* **2014**, *13*, 154, doi:10.1186/1476-511X-13-154.

157. Listenberger, L.L.; Han, X.; Lewis, S.E.; Cases, S.; Farese, R.V., Jr.; Ory, D.S.; Schaffer, J.E. Triglyceride accumulation protects against fatty acid-induced lipotoxicity. *Proc Natl Acad Sci U S A* **2003**, *100*, 3077-3082, doi:10.1073/pnas.0630588100.

158. Lalia, A.Z.; Lanza, I.R. Insulin-Sensitizing Effects of Omega-3 Fatty Acids: Lost in Translation? *Nutrients* **2016**, *8*, doi:10.3390/nu8060329.

159. Storlien, L.H.; Kraegen, E.W.; Chisholm, D.J.; Ford, G.L.; Bruce, D.G.; Pascoe, W.S. Fish oil prevents insulin resistance induced by high-fat feeding in rats. *Science* **1987**, *237*, 885-888, doi:10.1126/science.3303333.

160. Investigators, O.T.; Bosch, J.; Gerstein, H.C.; Dagenais, G.R.; Diaz, R.; Dyal, L.; Jung, H.; Maggiono, A.P.; Probstfield, J.; Ramachandran, A., et al. n-3 fatty acids and cardiovascular outcomes in patients with dysglycemia. *N Engl J Med* **2012**, *367*, 309-318, doi:10.1056/NEJMoa1203859.

161. Gorski, P.A.; Ceholski, D.K.; Hajjar, R.J. Altered myocardial calcium cycling and energetics in heart failure--a rational approach for disease treatment. *Cell Metab* **2015**, *21*, 183-194, doi:10.1016/j.cmet.2015.01.005.

162. Marks, A.R. Calcium cycling proteins and heart failure: mechanisms and therapeutics. *J Clin Invest* **2013**, *123*, 46-52, doi:10.1172/JCI62834.

163. Zima, A.V.; Bovo, E.; Mazurek, S.R.; Rochira, J.A.; Li, W.; Terentyev, D. Ca handling during excitation-contraction coupling in heart failure. *Pflugers Arch* **2014**, *466*, 1129-1137, doi:10.1007/s00424-014-1469-3.

164. Bers, D.M.; Bassani, J.W.; Bassani, R.A. Na-Ca exchange and Ca fluxes during contraction and relaxation in mammalian ventricular muscle. *Ann N Y Acad Sci* **1996**, *779*, 430-442, doi:10.1111/j.1749-6632.1996.tb44818.x.

165. Kimura, Y.; Kurzydlowski, K.; Tada, M.; MacLennan, D.H. Phospholamban regulates the Ca2+-ATPase through intramembrane interactions. *J Biol Chem* **1996**, *271*, 21726-21731, doi:10.1074/jbc.271.36.21726.

166. MacLennan, D.H.; Kranias, E.G. Phospholamban: a crucial regulator of cardiac contractility. *Nat Rev Mol Cell Biol* **2003**, *4*, 566-577, doi:10.1038/nrm1151.

167. Balke, C.W.; Shorofsky, S.R. Alterations in calcium handling in cardiac hypertrophy and heart failure. *Cardiovasc Res* **1998**, *37*, 290-299, doi:10.1016/s0008-6363(97)00272-1.

168. Bers, D.M. Calcium cycling and signaling in cardiac myocytes. *Annu Rev Physiol* **2008**, *70*, 23-49, doi:10.1146/annurev.physiol.70.113006.100455.

169. Freeman, K.; Lerman, I.; Kranias, E.G.; Bohlmeyer, T.; Bristow, M.R.; Lefkowitz, R.J.; Iaccarino, G.; Koch, W.J.; Leinwand, L.A. Alterations in cardiac adrenergic signaling and calcium cycling differentially affect the progression of cardiomyopathy. *J Clin Invest* **2001**, *107*, 967-974, doi:10.1172/JCI12083.

170. Roderick, H.L.; Higazi, D.R.; Smyrnias, I.; Fearnley, C.; Harzheim, D.; Bootman, M.D. Calcium in the heart: when it's good, it's very very good, but when it's bad, it's horrid. *Biochem Soc Trans* **2007**, *35*, 957-961, doi:10.1042/BST0350957.

171. Belke, D.D.; Swanson, E.A.; Dillmann, W.H. Decreased sarcoplasmic reticulum activity and contractility in diabetic db/db mouse heart. *Diabetes* **2004**, *53*, 3201-3208, doi:10.2337/diabetes.53.12.3201.

172. Lacombe, V.A.; Viatchenko-Karpinski, S.; Terentyev, D.; Sridhar, A.; Emani, S.; Bonagura, J.D.; Feldman, D.S.; Gyorke, S.; Carnes, C.A. Mechanisms of impaired calcium handling underlying subclinical diastolic dysfunction in diabetes. *Am J Physiol Regul Integr Comp Physiol* **2007**, *293*, R1787-1797, doi:10.1152/ajpregu.00059.2007.

173. Trost, S.U.; Belke, D.D.; Bluhm, W.F.; Meyer, M.; Swanson, E.; Dillmann, W.H. Overexpression of the sarcoplasmic reticulum Ca(2+)-ATPase improves myocardial contractility in diabetic cardiomyopathy. *Diabetes* **2002**, *51*, 1166-1171, doi:10.2337/diabetes.51.4.1166.

174. Van den Bergh, A.; Vanderper, A.; Vangheluwe, P.; Desjardins, F.; Nevelsteen, I.; Verreth, W.; Wuytack, F.; Holvoet, P.; Flameng, W.; Balligand, J.L., et al. Dyslipidaemia in type II diabetic mice does not aggravate contractile impairment but increases ventricular stiffness. *Cardiovasc Res* **2008**, *77*, 371-379, doi:10.1093/cvr/cvm001.

175. Sorrentino, A.; Borghetti, G.; Zhou, Y.; Cannata, A.; Meo, M.; Signore, S.; Anversa, P.; Leri, A.; Goichberg, P.; Qanud, K., et al. Hyperglycemia induces defective Ca2+ homeostasis in cardiomyocytes. *Am J Physiol Heart Circ Physiol* **2017**, *312*, H150-H161, doi:10.1152/ajpheart.00737.2016.

176. Abe, T.; Ohga, Y.; Tabayashi, N.; Kobayashi, S.; Sakata, S.; Misawa, H.; Tsuji, T.; Kohzuki, H.; Suga, H.; Taniguchi, S., et al. Left ventricular diastolic dysfunction in type 2 diabetes mellitus model rats. *Am J Physiol Heart Circ Physiol* **2002**, *282*, H138-148, doi:10.1152/ajpheart.2002.282.1.H138.

177. Di Filippo, C.; Cuzzocrea, S.; Rossi, F.; Marfella, R.; D'Amico, M. Oxidative stress as the leading cause of acute myocardial infarction in diabetics. *Cardiovasc Drug Rev* **2006**, *24*, 77-87, doi:10.1111/j.1527-3466.2006.00077.x.

178. Giordano, F.J. Oxygen, oxidative stress, hypoxia, and heart failure. *J Clin Invest* **2005**, *115*, 500-508, doi:10.1172/JCI24408.

179. Yu, T.; Robotham, J.L.; Yoon, Y. Increased production of reactive oxygen species in hyperglycemic conditions requires dynamic change of mitochondrial morphology. *Proc Natl Acad Sci U S A* **2006**, *103*, 2653-2658, doi:10.1073/pnas.0511154103.

180. Liu, J.; Shen, W.; Zhao, B.; Wang, Y.; Wertz, K.; Weber, P.; Zhang, P. Targeting mitochondrial biogenesis for preventing and treating insulin resistance in diabetes and obesity: Hope from natural mitochondrial nutrients. *Adv Drug Deliv Rev* **2009**, *61*, 1343-1352, doi:10.1016/j.addr.2009.06.007.

181. Jain, S.S.; Paglialunga, S.; Vigna, C.; Ludzki, A.; Herbst, E.A.; Lally, J.S.; Schrauwen, P.; Hoeks, J.; Tupling, A.R.; Bonen, A., et al. High-fat diet-induced mitochondrial biogenesis is regulated by mitochondrial-derived reactive oxygen species activation of CaMKII. *Diabetes* **2014**, *63*, 1907-1913, doi:10.2337/db13-0816.

182. Yang, L.; Zhao, D.; Ren, J.; Yang, J. Endoplasmic reticulum stress and protein quality control in diabetic cardiomyopathy. *Biochim Biophys Acta* **2015**, *1852*, 209-218, doi:10.1016/j.bbadis.2014.05.006.

183. Sano, R.; Reed, J.C. ER stress-induced cell death mechanisms. *Biochim Biophys Acta* **2013**, *1833*, 3460-3470, doi:10.1016/j.bbamcr.2013.06.028.

184. Benbrook, D.M.; Long, A. Integration of autophagy, proteasomal degradation, unfolded protein response and apoptosis. *Exp Oncol* **2012**, *34*, 286-297.

185. Groenendyk, J.; Sreenivasaiah, P.K.; Kim, D.H.; Agellon, L.B.; Michalak, M. Biology of endoplasmic reticulum stress in the heart. *Circ Res* **2010**, *107*, 1185-1197, doi:10.1161/CIRCRESAHA.110.227033.

186. Borradaile, N.M.; Han, X.; Harp, J.D.; Gale, S.E.; Ory, D.S.; Schaffer, J.E. Disruption of endoplasmic reticulum structure and integrity in lipotoxic cell death. *J Lipid Res* **2006**, *47*, 2726-2737, doi:10.1194/jlr.M600299-JLR200.

187. Liu, M.; Dudley, S.C., Jr. Targeting the unfolded protein response in heart diseases. *Expert Opin Ther Targets* **2014**, *18*, 719-723, doi:10.1517/14728222.2014.918605.

188. Despa, S.; Margulies, K.B.; Chen, L.; Knowlton, A.A.; Havel, P.J.; Taegtmeyer, H.; Bers, D.M.; Despa, F. Hyperamylinemia contributes to cardiac dysfunction in obesity and diabetes: a study in humans and rats. *Circ Res* **2012**, *110*, 598-608, doi:10.1161/CIRCRESAHA.111.258285.

189. Bishopric, N.H.; Andreka, P.; Slepak, T.; Webster, K.A. Molecular mechanisms of apoptosis in the cardiac myocyte. *Curr Opin Pharmacol* **2001**, *1*, 141-150, doi:10.1016/s1471-4892(01)00032-7.

190. Hengartner, M.O. The biochemistry of apoptosis. *Nature* **2000**, *407*, 770-776, doi:10.1038/35037710.

191. Adams, J.M.; Cory, S. The Bcl-2 protein family: arbiters of cell survival. *Science* **1998**, *281*, 1322-1326, doi:10.1126/science.281.5381.1322.

192. Goldberg, I.J.; Trent, C.M.; Schulze, P.C. Lipid metabolism and toxicity in the heart. *Cell Metab* **2012**, *15*, 805-812, doi:10.1016/j.cmet.2012.04.006.

193. Mittendorfer, B. Origins of metabolic complications in obesity: adipose tissue and free fatty acid trafficking. *Curr Opin Clin Nutr Metab Care* **2011**, *14*, 535-541, doi:10.1097/MCO.0b013e32834ad8b6.

194. Holland, W.L.; Summers, S.A. Sphingolipids, insulin resistance, and metabolic disease: new insights from in vivo manipulation of sphingolipid metabolism. *Endocr Rev* **2008**, *29*, 381-402, doi:10.1210/er.2007-0025.

195. Park, T.S.; Hu, Y.; Noh, H.L.; Drosatos, K.; Okajima, K.; Buchanan, J.; Tuinei, J.; Homma, S.; Jiang, X.C.; Abel, E.D., et al. Ceramide is a cardiotoxin in lipotoxic cardiomyopathy. *J Lipid Res* **2008**, *49*, 2101-2112, doi:10.1194/jlr.M800147-JLR200.

196. Ussher, J.R.; Folmes, C.D.; Keung, W.; Fillmore, N.; Jaswal, J.S.; Cadete, V.J.; Beker, D.L.; Lam, V.H.; Zhang, L.; Lopaschuk, G.D. Inhibition of serine palmitoyl transferase I reduces cardiac ceramide levels and increases glycolysis rates following diet-induced insulin resistance. *PLoS One* **2012**, *7*, e37703, doi:10.1371/journal.pone.0037703.

197. Aburasayn, H.; Al Batran, R.; Ussher, J.R. Targeting ceramide metabolism in obesity. *Am J Physiol Endocrinol Metab* **2016**, *311*, E423-435, doi:10.1152/ajpendo.00133.2016.

198. Weiss, B.; Stoffel, W. Human and murine serine-palmitoyl-CoA transferase--cloning, expression and characterization of the key enzyme in sphingolipid synthesis. *Eur J Biochem* **1997**, *249*, 239-247, doi:10.1111/j.1432-1033.1997.00239.x.

199. Kolesnick, R.N.; Kronke, M. Regulation of ceramide production and apoptosis. *Annu Rev Physiol* **1998**, *60*, 643-665, doi:10.1146/annurev.physiol.60.1.643.

200. Stratford, S.; Hoehn, K.L.; Liu, F.; Summers, S.A. Regulation of insulin action by ceramide: dual mechanisms linking ceramide accumulation to the inhibition of Akt/protein kinase B. *J Biol Chem* **2004**, *279*, 36608-36615, doi:10.1074/jbc.M406499200.

201. Aoki, H.; Kang, P.M.; Hampe, J.; Yoshimura, K.; Noma, T.; Matsuzaki, M.; Izumo, S. Direct activation of mitochondrial apoptosis machinery by c-Jun N-terminal kinase in adult cardiac myocytes. *J Biol Chem* **2002**, *277*, 10244-10250, doi:10.1074/jbc.M112355200.

202. Mapanga, R.F.; Essop, M.F. Damaging effects of hyperglycemia on cardiovascular function: spotlight on glucose metabolic pathways. *Am J Physiol Heart Circ Physiol* **2016**, *310*, H153-173, doi:10.1152/ajpheart.00206.2015.

203. Luo, D.; Dong, X.W.; Yan, B.; Liu, M.; Xue, T.H.; Liu, H.; You, J.H.; Li, F.; Wang, Z.L.; Chen, Z.N. MG132 selectively upregulates MICB through the DNA damage response pathway in A549 cells. *Mol Med Rep* **2019**, *19*, 213-220, doi:10.3892/mmr.2018.9676.

204. Ciechanover, A. The ubiquitin proteolytic system: from a vague idea, through basic mechanisms, and onto human diseases and drug targeting. *Neurology* **2006**, *66*, S7-19, doi:10.1212/01.wnl.0000192261.02023.b8.

205. Glickman, M.H.; Ciechanover, A. The ubiquitin-proteasome proteolytic pathway: destruction for the sake of construction. *Physiol Rev* **2002**, *82*, 373-428, doi:10.1152/physrev.00027.2001.

206. Baumeister, W.; Walz, J.; Zuhl, F.; Seemuller, E. The proteasome: paradigm of a self-compartmentalizing protease. *Cell* **1998**, *92*, 367-380, doi:10.1016/s0092-8674(00)80929-0.

207. Haas, A.L.; Rose, I.A. The mechanism of ubiquitin activating enzyme. A kinetic and equilibrium analysis. *J Biol Chem* **1982**, *257*, 10329-10337.

208. Jackson, P.K.; Eldridge, A.G.; Freed, E.; Furstenthal, L.; Hsu, J.Y.; Kaiser, B.K.; Reimann, J.D. The lore of the RINGs: substrate recognition and catalysis by ubiquitin ligases. *Trends Cell Biol* **2000**, *10*, 429-439, doi:10.1016/s0962-8924(00)01834-1.

209. Herrmann, J.; Wohlert, C.; Saguner, A.M.; Flores, A.; Nesbitt, L.L.; Chade, A.; Lerman, L.O.; Lerman, A. Primary proteasome inhibition results in cardiac dysfunction. *Eur J Heart Fail* **2013**, *15*, 614-623, doi:10.1093/eurjhf/hft034.

210. Hu, J.; Klein, J.D.; Du, J.; Wang, X.H. Cardiac muscle protein catabolism in diabetes mellitus: activation of the ubiquitin-proteasome system by insulin deficiency. *Endocrinology* **2008**, *149*, 5384-5390, doi:10.1210/en.2008-0132.

211. Zheng, Q.; Su, H.; Tian, Z.; Wang, X. Proteasome malfunction activates macroautophagy in the heart. *Am J Cardiovasc Dis* **2011**, *1*, 214-226.

212. Zhu, K.; Dunner, K., Jr.; McConkey, D.J. Proteasome inhibitors activate autophagy as a cytoprotective response in human prostate cancer cells. *Oncogene* **2010**, *29*, 451-462, doi:10.1038/onc.2009.343.

213. Quan, W.; Hur, K.Y.; Lim, Y.; Oh, S.H.; Lee, J.C.; Kim, K.H.; Kim, G.H.; Kim, S.W.; Kim, H.L.; Lee, M.K., et al. Autophagy deficiency in beta cells leads to compromised unfolded protein response and progression from obesity to diabetes in mice. *Diabetologia* **2012**, *55*, 392-403, doi:10.1007/s00125-011-2350-y.

214. Tanida, I. Autophagosome formation and molecular mechanism of autophagy. *Antioxid Redox Signal* **2011**, *14*, 2201-2214, doi:10.1089/ars.2010.3482.

215. Feng, Y.; He, D.; Yao, Z.; Klionsky, D.J. The machinery of macroautophagy. *Cell Res* **2014**, *24*, 24-41, doi:10.1038/cr.2013.168.

216. Wen, X.; Klionsky, D.J. An overview of macroautophagy in yeast. *J Mol Biol* **2016**, *428*, 1681-1699, doi:10.1016/j.jmb.2016.02.021.

217. Lamb, C.A.; Yoshimori, T.; Tooze, S.A. The autophagosome: origins unknown, biogenesis complex. *Nat Rev Mol Cell Biol* **2013**, *14*, 759-774, doi:10.1038/nrm3696.

218. Satoo, K.; Noda, N.N.; Kumeta, H.; Fujioka, Y.; Mizushima, N.; Ohsumi, Y.; Inagaki, F. The structure of Atg4B-LC3 complex reveals the mechanism of LC3 processing and delipidation during autophagy. *EMBO J* **2009**, *28*, 1341-1350, doi:10.1038/emboj.2009.80.

219. Yamada, E.; Singh, R. Mapping autophagy on to your metabolic radar. *Diabetes* **2012**, *61*, 272-280, doi:10.2337/db11-1199.

220. Mindell, J.A. Lysosomal acidification mechanisms. *Annu Rev Physiol* **2012**, *74*, 69-86, doi:10.1146/annurev-physiol-012110-142317.

221. Shen, H.M.; Mizushima, N. At the end of the autophagic road: an emerging understanding of lysosomal functions in autophagy. *Trends Biochem Sci* **2014**, *39*, 61-71, doi:10.1016/j.tibs.2013.12.001.

222. Barth, S.; Glick, D.; Macleod, K.F. Autophagy: assays and artifacts. *J Pathol* **2010**, *221*, 117-124, doi:10.1002/path.2694.

223. Yang, J.; Carra, S.; Zhu, W.G.; Kampinga, H.H. The regulation of the autophagic network and its implications for human disease. *Int J Biol Sci* **2013**, *9*, 1121-1133, doi:10.7150/ijbs.6666.

224. Xie, Z.; Lau, K.; Eby, B.; Lozano, P.; He, C.; Pennington, B.; Li, H.; Rathi, S.; Dong, Y.; Tian, R., et al. Improvement of cardiac functions by chronic metformin treatment is associated with enhanced cardiac autophagy in diabetic OVE26 mice. *Diabetes* **2011**, *60*, 1770-1778, doi:10.2337/db10-0351.

225. Mellor, K.M.; Bell, J.R.; Young, M.J.; Ritchie, R.H.; Delbridge, L.M. Myocardial autophagy activation and suppressed survival signaling is associated with insulin resistance in fructose-fed mice. *J Mol Cell Cardiol* **2011**, *50*, 1035-1043, doi:10.1016/j.yjmcc.2011.03.002.

226. Trivedi, P.C.; Bartlett, J.J.; Perez, L.J.; Brunt, K.R.; Legare, J.F.; Hassan, A.; Kienesberger, P.C.; Pulinilkunnil, T. Glucolipotoxicity diminishes cardiomyocyte TFEB and inhibits lysosomal autophagy during obesity and diabetes. *Biochim Biophys Acta* **2016**, *1861*, 1893-1910, doi:10.1016/j.bbalip.2016.09.004.

227. Schulze, R.J.; Sathyanarayan, A.; Mashek, D.G. Breaking fat: The regulation and mechanisms of lipophagy. *Biochim Biophys Acta Mol Cell Biol Lipids* **2017**, *1862*, 1178-1187, doi:10.1016/j.bbalip.2017.06.008.

228. Ouimet, M.; Franklin, V.; Mak, E.; Liao, X.; Tabas, I.; Marcel, Y.L. Autophagy regulates cholesterol efflux from macrophage foam cells via lysosomal acid lipase. *Cell Metab* **2011**, *13*, 655-667, doi:10.1016/j.cmet.2011.03.023.

229. Hammerling, B.C.; Gustafsson, A.B. Mitochondrial quality control in the myocardium: cooperation between protein degradation and mitophagy. *J Mol Cell Cardiol* **2014**, *75*, 122-130, doi:10.1016/j.yjmcc.2014.07.013.

230. Shires, S.E.; Gustafsson, A.B. Mitophagy and heart failure. *J Mol Med (Berl)* **2015**, *93*, 253-262, doi:10.1007/s00109-015-1254-6.

231. Khalil, B.; El Fissi, N.; Aouane, A.; Cabirol-Pol, M.J.; Rival, T.; Lievens, J.C. PINK1-induced mitophagy promotes neuroprotection in Huntington's disease. *Cell Death Dis* **2015**, *6*, e1617, doi:10.1038/cddis.2014.581.

232. Papadopoulos, C.; Kravic, B.; Meyer, H. Repair or Lysophagy: Dealing with Damaged Lysosomes. *J Mol Biol* **2020**, *432*, 231-239, doi:10.1016/j.jmb.2019.08.010.

233. Radulovic, M.; Schink, K.O.; Wenzel, E.M.; Nahse, V.; Bongiovanni, A.; Lafont, F.; Stenmark, H. ESCRT-mediated lysosome repair precedes lysophagy and promotes cell survival. *EMBO J* **2018**, *37*, doi:10.15252/embj.201899753.

234. Kaushik, S.; Cuervo, A.M. Chaperone-mediated autophagy: a unique way to enter the lysosome world. *Trends Cell Biol* **2012**, *22*, 407-417, doi:10.1016/j.tcb.2012.05.006.

235. Massey, A.C.; Follenzi, A.; Kiffin, R.; Zhang, C.; Cuervo, A.M. Early cellular changes after blockage of chaperone-mediated autophagy. *Autophagy* **2008**, *4*, 442-456, doi:10.4161/auto.5654.

236. Agarraberes, F.A.; Dice, J.F. A molecular chaperone complex at the lysosomal membrane is required for protein translocation. *J Cell Sci* **2001**, *114*, 2491-2499.

237. Kaushik, S.; Cuervo, A.M. The coming of age of chaperone-mediated autophagy. *Nat Rev Mol Cell Biol* **2018**, *19*, 365-381, doi:10.1038/s41580-018-0001-6.

238. Saftig, P.; Schroder, B.; Blanz, J. Lysosomal membrane proteins: life between acid and neutral conditions. *Biochem Soc Trans* **2010**, *38*, 1420-1423, doi:10.1042/BST0381420.

239. Cuervo, A.M.; Dice, J.F. Unique properties of lamp2a compared to other lamp2 isoforms. *J Cell Sci* **2000**, *113 Pt 24*, 4441-4450.

240. Nishino, I.; Fu, J.; Tanji, K.; Yamada, T.; Shimojo, S.; Koori, T.; Mora, M.; Riggs, J.E.; Oh, S.J.; Koga, Y., et al. Primary LAMP-2 deficiency causes X-linked vacuolar cardiomyopathy and myopathy (Danon disease). *Nature* **2000**, *406*, 906-910, doi:10.1038/35022604.

241. Rodriguez-Navarro, J.A.; Kaushik, S.; Koga, H.; Dall'Armi, C.; Shui, G.; Wenk, M.R.; Di Paolo, G.; Cuervo, A.M. Inhibitory effect of dietary lipids on chaperone-mediated autophagy. *Proc Natl Acad Sci U S A* **2012**, *109*, E705-714, doi:10.1073/pnas.1113036109.

242. Schneider, J.L.; Villarroya, J.; Diaz-Carretero, A.; Patel, B.; Urbanska, A.M.; Thi, M.M.; Villarroya, F.; Santambrogio, L.; Cuervo, A.M. Loss of hepatic chaperone-mediated autophagy accelerates proteostasis failure in aging. *Aging Cell* **2015**, *14*, 249-264, doi:10.1111/acel.12310.

243. Cuervo, A.M. Autophagy: in sickness and in health. *Trends Cell Biol* **2004**, *14*, 70-77, doi:10.1016/j.tcb.2003.12.002.

244. Orenstein, S.J.; Cuervo, A.M. Chaperone-mediated autophagy: molecular mechanisms and physiological relevance. *Semin Cell Dev Biol* **2010**, *21*, 719-726, doi:10.1016/j.semcdb.2010.02.005.

245. Sugimoto, S.; Shiomi, K.; Yamamoto, A.; Nishino, I.; Nonaka, I.; Ohi, T. LAMP-2 positive vacuolar myopathy with dilated cardiomyopathy. *Intern Med* **2007**, *46*, 757-760, doi:10.2169/internalmedicine.46.6265.

246. Schilling, J.D.; Machkovech, H.M.; He, L.; Diwan, A.; Schaffer, J.E. TLR4 activation under lipotoxic conditions leads to synergistic macrophage cell death through a TRIF-dependent pathway. *J Immunol* **2013**, *190*, 1285-1296, doi:10.4049/jimmunol.1202208.

247. Ma, X.; Liu, H.; Foyil, S.R.; Godar, R.J.; Weinheimer, C.J.; Hill, J.A.; Diwan, A. Impaired autophagosome clearance contributes to cardiomyocyte death in ischemia/reperfusion injury. *Circulation* **2012**, *125*, 3170-3181, doi:10.1161/CIRCULATIONAHA.111.041814.

248. de Duve, C. The lysosome turns fifty. *Nat Cell Biol* **2005**, *7*, 847-849, doi:10.1038/ncb0905-847.

249. Hu, Y.B.; Dammer, E.B.; Ren, R.J.; Wang, G. The endosomal-lysosomal system: from acidification and cargo sorting to neurodegeneration. *Transl Neurodegener* **2015**, *4*, 18, doi:10.1186/s40035-015-0041-1.

250. Jegga, A.G.; Schneider, L.; Ouyang, X.; Zhang, J. Systems biology of the autophagy-lysosomal pathway. *Autophagy* **2011**, *7*, 477-489, doi:10.4161/auto.7.5.14811.

251. Herb, M.; Gluschko, A.; Schramm, M. LC3-associated phagocytosis - The highway to hell for phagocytosed microbes. *Semin Cell Dev Biol* **2020**, *101*, 68-76, doi:10.1016/j.semcdb.2019.04.016.

252. Schwake, M.; Schroder, B.; Saftig, P. Lysosomal membrane proteins and their central role in physiology. *Traffic* **2013**, *14*, 739-748, doi:10.1111/tra.12056.

253. Saftig, P.; Klumperman, J. Lysosome biogenesis and lysosomal membrane proteins: trafficking meets function. *Nat Rev Mol Cell Biol* **2009**, *10*, 623-635, doi:10.1038/nrm2745.

254. Xiong, J.; Zhu, M.X. Regulation of lysosomal ion homeostasis by channels and transporters. *Sci China Life Sci* **2016**, *59*, 777-791, doi:10.1007/s11427-016-5090-x.

255. Zhang, X.; Cheng, X.; Yu, L.; Yang, J.; Calvo, R.; Patnaik, S.; Hu, X.; Gao, Q.; Yang, M.; Lawas, M., et al. MCOLN1 is a ROS sensor in lysosomes that regulates autophagy. *Nat Commun* **2016**, *7*, 12109, doi:10.1038/ncomms12109.

256. Venkatachalam, K.; Long, A.A.; Elsaesser, R.; Nikolaeva, D.; Broadie, K.; Montell, C. Motor deficit in a Drosophila model of mucolipidosis type IV due to defective clearance of apoptotic cells. *Cell* **2008**, *135*, 838-851, doi:10.1016/j.cell.2008.09.041.

257. Feltes, M.; Gale, S.E.; Moores, S.; Ory, D.S.; Schaffer, J.E. Monitoring the itinerary of lysosomal cholesterol in Niemann-Pick Type C1-deficient cells after cyclodextrin treatment. *J Lipid Res* **2020**, *61*, 403-412, doi:10.1194/jlr.RA119000571.

258. Turk, V.; Stoka, V.; Vasiljeva, O.; Renko, M.; Sun, T.; Turk, B.; Turk, D. Cysteine cathepsins: from structure, function and regulation to new frontiers. *Biochim Biophys Acta* **2012**, *1824*, 68-88, doi:10.1016/j.bbapap.2011.10.002.

259. Kitamoto, S.; Sukhova, G.K.; Sun, J.; Yang, M.; Libby, P.; Love, V.; Duramad, P.; Sun, C.; Zhang, Y.; Yang, X., et al. Cathepsin L deficiency reduces diet-induced atherosclerosis in low-density lipoprotein receptor-knockout mice. *Circulation* **2007**, *115*, 2065-2075, doi:10.1161/CIRCULATIONAHA.107.688523.

260. Felbor, U.; Kessler, B.; Mothes, W.; Goebel, H.H.; Ploegh, H.L.; Bronson, R.T.; Olsen, B.R. Neuronal loss and brain atrophy in mice lacking cathepsins B and L. *Proc Natl Acad Sci U S A* **2002**, *99*, 7883-7888, doi:10.1073/pnas.112632299.

261. Yanagawa, M.; Tsukuba, T.; Nishioku, T.; Okamoto, Y.; Okamoto, K.; Takii, R.; Terada, Y.; Nakayama, K.I.; Kadowaki, T.; Yamamoto, K. Cathepsin E deficiency induces a novel form of lysosomal storage disorder showing the accumulation of lysosomal membrane sialoglycoproteins and the elevation of lysosomal pH in macrophages. *J Biol Chem* **2007**, *282*, 1851-1862, doi:10.1074/jbc.M604143200.

262. Kaminskyy, V.; Zhivotovsky, B. Proteases in autophagy. *Biochim Biophys Acta* **2012**, *1824*, 44-50, doi:10.1016/j.bbapap.2011.05.013.

263. Dubland, J.A.; Francis, G.A. Lysosomal acid lipase: at the crossroads of normal and atherogenic cholesterol metabolism. *Front Cell Dev Biol* **2015**, *3*, 3, doi:10.3389/fcell.2015.00003.

264. Huang, S.C.; Everts, B.; Ivanova, Y.; O'Sullivan, D.; Nascimento, M.; Smith, A.M.; Beatty, W.; Love-Gregory, L.; Lam, W.Y.; O'Neill, C.M., et al. Cell-intrinsic lysosomal lipolysis is essential for alternative activation of macrophages. *Nat Immunol* **2014**, *15*, 846-855, doi:10.1038/ni.2956.

265. Laplante, M.; Sabatini, D.M. mTOR signaling in growth control and disease. *Cell* **2012**, *149*, 274-293, doi:10.1016/j.cell.2012.03.017.

266. Bar-Peled, L.; Sabatini, D.M. Regulation of mTORC1 by amino acids. *Trends Cell Biol* **2014**, *24*, 400-406, doi:10.1016/j.tcb.2014.03.003.

267. Efeyan, A.; Zoncu, R.; Chang, S.; Gumper, I.; Snitkin, H.; Wolfson, R.L.; Kirak, O.; Sabatini, D.D.; Sabatini, D.M. Regulation of mTORC1 by the Rag GTPases is necessary for neonatal autophagy and survival. *Nature* **2013**, *493*, 679-683, doi:10.1038/nature11745.

268. Sancak, Y.; Bar-Peled, L.; Zoncu, R.; Markhard, A.L.; Nada, S.; Sabatini, D.M. Ragulator-Rag complex targets mTORC1 to the lysosomal surface and is necessary for its activation by amino acids. *Cell* **2010**, *141*, 290-303, doi:10.1016/j.cell.2010.02.024.

269. Chantranupong, L.; Wolfson, R.L.; Orozco, J.M.; Saxton, R.A.; Scaria, S.M.; Bar-Peled, L.; Spooner, E.; Isasa, M.; Gygi, S.P.; Sabatini, D.M. The Sestrins interact with GATOR2 to negatively regulate the amino-acid-sensing pathway upstream of mTORC1. *Cell Rep* **2014**, *9*, 1-8, doi:10.1016/j.celrep.2014.09.014.

270. Peng, M.; Yin, N.; Li, M.O. Sestrins function as guanine nucleotide dissociation inhibitors for Rag GTPases to control mTORC1 signaling. *Cell* **2014**, *159*, 122-133, doi:10.1016/j.cell.2014.08.038.

271. Bar-Peled, L.; Schweitzer, L.D.; Zoncu, R.; Sabatini, D.M. Ragulator is a GEF for the rag GTPases that signal amino acid levels to mTORC1. *Cell* **2012**, *150*, 1196-1208, doi:10.1016/j.cell.2012.07.032.

272. Settembre, C.; Fraldi, A.; Medina, D.L.; Ballabio, A. Signals from the lysosome: a control centre for cellular clearance and energy metabolism. *Nat Rev Mol Cell Biol* **2013**, *14*, 283-296, doi:10.1038/nrm3565.

273. Kim, E.; Goraksha-Hicks, P.; Li, L.; Neufeld, T.P.; Guan, K.L. Regulation of TORC1 by Rag GTPases in nutrient response. *Nat Cell Biol* **2008**, *10*, 935-945, doi:10.1038/ncb1753.

274. Oshiro, N.; Rapley, J.; Avruch, J. Amino acids activate mammalian target of rapamycin (mTOR) complex 1 without changing Rag GTPase guanyl nucleotide charging. *J Biol Chem* **2014**, *289*, 2658-2674, doi:10.1074/jbc.M113.528505.

275. Sancak, Y.; Peterson, T.R.; Shaul, Y.D.; Lindquist, R.A.; Thoreen, C.C.; Bar-Peled, L.; Sabatini, D.M. The Rag GTPases bind raptor and mediate amino acid signaling to mTORC1. *Science* **2008**, *320*, 1496-1501, doi:10.1126/science.1157535.

276. Inoki, K.; Li, Y.; Xu, T.; Guan, K.L. Rheb GTPase is a direct target of TSC2 GAP activity and regulates mTOR signaling. *Genes Dev* **2003**, *17*, 1829-1834, doi:10.1101/gad.1110003.

277. Tee, A.R.; Manning, B.D.; Roux, P.P.; Cantley, L.C.; Blenis, J. Tuberous sclerosis complex gene products, Tuberin and Hamartin, control mTOR signaling by acting as a GTPase-activating protein complex toward Rheb. *Curr Biol* **2003**, *13*, 1259-1268, doi:10.1016/s0960-9822(03)00506-2.

278. Cang, C.; Zhou, Y.; Navarro, B.; Seo, Y.J.; Aranda, K.; Shi, L.; Battaglia-Hsu, S.; Nissim, I.; Clapham, D.E.; Ren, D. mTOR regulates lysosomal ATP-sensitive two-pore Na(+) channels to adapt to metabolic state. *Cell* **2013**, *152*, 778-790, doi:10.1016/j.cell.2013.01.023.

279. Marshansky, V.; Futai, M. The V-type H+-ATPase in vesicular trafficking: targeting, regulation and function. *Curr Opin Cell Biol* **2008**, *20*, 415-426, doi:10.1016/j.ceb.2008.03.015.

280. Ganley, I.G.; Lam du, H.; Wang, J.; Ding, X.; Chen, S.; Jiang, X. ULK1.ATG13.FIP200 complex mediates mTOR signaling and is essential for autophagy. *J Biol Chem* **2009**, *284*, 12297-12305, doi:10.1074/jbc.M900573200.

281. Hosokawa, N.; Hara, T.; Kaizuka, T.; Kishi, C.; Takamura, A.; Miura, Y.; Iemura, S.; Natsume, T.; Takehana, K.; Yamada, N., et al. Nutrient-dependent mTORC1 association with the ULK1-Atg13-FIP200 complex required for autophagy. *Mol Biol Cell* **2009**, *20*, 1981-1991, doi:10.1091/mbc.E08-12-1248.

282. Jiang, T.; Harder, B.; Rojo de la Vega, M.; Wong, P.K.; Chapman, E.; Zhang, D.D. p62 links autophagy and Nrf2 signaling. *Free Radic Biol Med* **2015**, *88*, 199-204, doi:10.1016/j.freeradbiomed.2015.06.014.

283. Bellot, G.; Garcia-Medina, R.; Gounon, P.; Chiche, J.; Roux, D.; Pouyssegur, J.; Mazure, N.M. Hypoxia-induced autophagy is mediated through hypoxia-inducible factor induction of BNIP3 and BNIP3L via their BH3 domains. *Mol Cell Biol* **2009**, *29*, 2570-2581, doi:10.1128/MCB.00166-09.

284. Obacz, J.; Pastorekova, S.; Vojtesek, B.; Hrstka, R. Cross-talk between HIF and p53 as mediators of molecular responses to physiological and genotoxic stresses. *Mol Cancer* **2013**, *12*, 93, doi:10.1186/1476-4598-12-93.

285. Chauhan, S.; Goodwin, J.G.; Chauhan, S.; Manyam, G.; Wang, J.; Kamat, A.M.; Boyd, D.D. ZKSCAN3 is a master transcriptional repressor of autophagy. *Mol Cell* **2013**, *50*, 16-28, doi:10.1016/j.molcel.2013.01.024.

286. Martina, J.A.; Chen, Y.; Gucek, M.; Puertollano, R. MTORC1 functions as a transcriptional regulator of autophagy by preventing nuclear transport of TFEB. *Autophagy* **2012**, *8*, 903-914, doi:10.4161/auto.19653.

287. Martina, J.A.; Diab, H.I.; Li, H.; Puertollano, R. Novel roles for the MiTF/TFE family of transcription factors in organelle biogenesis, nutrient sensing, and energy homeostasis. *Cell Mol Life Sci* **2014**, *71*, 2483-2497, doi:10.1007/s00018-014-1565-8.

288. Sardiello, M.; Palmieri, M.; di Ronza, A.; Medina, D.L.; Valenza, M.; Gennarino, V.A.; Di Malta, C.; Donaudy, F.; Embrione, V.; Polishchuk, R.S., et al. A gene network regulating lysosomal biogenesis and function. *Science* **2009**, *325*, 473-477, doi:10.1126/science.1174447.

289. Sakamaki, J.I.; Wilkinson, S.; Hahn, M.; Tasdemir, N.; O'Prey, J.; Clark, W.; Hedley, A.; Nixon, C.; Long, J.S.; New, M., et al. Bromodomain Protein BRD4 Is a Transcriptional Repressor of Autophagy and Lysosomal Function. *Mol Cell* **2017**, *66*, 517-532 e519, doi:10.1016/j.molcel.2017.04.027.

290. Steingrimsson, E.; Copeland, N.G.; Jenkins, N.A. Melanocytes and the microphthalmia transcription factor network. *Annu Rev Genet* **2004**, *38*, 365-411, doi:10.1146/annurev.genet.38.072902.092717.

291. Carr, C.S.; Sharp, P.A. A helix-loop-helix protein related to the immunoglobulin E box-binding proteins. *Mol Cell Biol* **1990**, *10*, 4384-4388, doi:10.1128/mcb.10.8.4384.

292. Fisher, D.E.; Carr, C.S.; Parent, L.A.; Sharp, P.A. TFEB has DNA-binding and oligomerization properties of a unique helix-loop-helix/leucine-zipper family. *Genes Dev* **1991**, *5*, 2342-2352, doi:10.1101/gad.5.12a.2342.

293. Hemesath, T.J.; Steingrimsson, E.; McGill, G.; Hansen, M.J.; Vaught, J.; Hodgkinson, C.A.; Arnheiter, H.; Copeland, N.G.; Jenkins, N.A.; Fisher, D.E. microphthalmia, a critical factor in melanocyte development, defines a discrete transcription factor family. *Genes Dev* **1994**, *8*, 2770-2780, doi:10.1101/gad.8.22.2770.

294. Pogenberg, V.; Ogmundsdottir, M.H.; Bergsteinsdottir, K.; Schepsky, A.; Phung, B.; Deineko, V.; Milewski, M.; Steingrimsson, E.; Wilmanns, M. Restricted leucine zipper dimerization and specificity of DNA recognition of the melanocyte master regulator MITF. *Genes Dev* **2012**, *26*, 2647-2658, doi:10.1101/gad.198192.112.

295. Zhao, G.Q.; Zhao, Q.; Zhou, X.; Mattei, M.G.; de Crombrugghe, B. TFEC, a basic helix-loop-helix protein, forms heterodimers with TFE3 and inhibits TFE3-dependent transcription activation. *Mol Cell Biol* **1993**, *13*, 4505-4512, doi:10.1128/mcb.13.8.4505.

296. Hallsson, J.H.; Haflidadottir, B.S.; Stivers, C.; Odenwald, W.; Arnheiter, H.; Pignoni, F.; Steingrimsson, E. The basic helix-loop-helix leucine zipper transcription factor Mitf is conserved in Drosophila and functions in eye development. *Genetics* **2004**, *167*, 233-241, doi:10.1534/genetics.167.1.233.

297. Rehli, M.; Den Elzen, N.; Cassady, A.I.; Ostrowski, M.C.; Hume, D.A. Cloning and characterization of the murine genes for bHLH-ZIP transcription factors TFEC and TFEB reveal a common gene organization for all MiT subfamily members. *Genomics* **1999**, *56*, 111-120, doi:10.1006/geno.1998.5588.

298. Settembre, C.; Ballabio, A. TFEB regulates autophagy: an integrated coordination of cellular degradation and recycling processes. *Autophagy* **2011**, *7*, 1379-1381, doi:10.4161/auto.7.11.17166.

299. Settembre, C.; De Cegli, R.; Mansueto, G.; Saha, P.K.; Vetrini, F.; Visvikis, O.; Huynh, T.; Carissimo, A.; Palmer, D.; Klisch, T.J., et al. TFEB controls cellular lipid metabolism through a starvation-induced autoregulatory loop. *Nat Cell Biol* **2013**, *15*, 647-658, doi:10.1038/ncb2718.

300. Xu, L.; Massague, J. Nucleocytoplasmic shuttling of signal transducers. *Nat Rev Mol Cell Biol* **2004**, *5*, 209-219, doi:10.1038/nrm1331.

301. Roczniak-Ferguson, A.; Petit, C.S.; Froehlich, F.; Qian, S.; Ky, J.; Angarola, B.; Walther, T.C.; Ferguson, S.M. The transcription factor TFEB links mTORC1 signaling to transcriptional control of lysosome homeostasis. *Sci Signal* **2012**, *5*, ra42, doi:10.1126/scisignal.2002790.

302. Settembre, C.; Zoncu, R.; Medina, D.L.; Vetrini, F.; Erdin, S.; Erdin, S.; Huynh, T.; Ferron, M.; Karsenty, G.; Vellard, M.C., et al. A lysosome-to-nucleus signalling mechanism senses and regulates the lysosome via mTOR and TFEB. *EMBO J* **2012**, *31*, 1095-1108, doi:10.1038/emboj.2012.32.

303. Vega-Rubin-de-Celis, S.; Pena-Llopis, S.; Konda, M.; Brugarolas, J. Multistep regulation of TFEB by MTORC1. *Autophagy* **2017**, *13*, 464-472, doi:10.1080/15548627.2016.1271514.

304. Settembre, C.; Di Malta, C.; Polito, V.A.; Garcia Arencibia, M.; Vetrini, F.; Erdin, S.; Erdin, S.U.; Huynh, T.; Medina, D.; Colella, P., et al. TFEB links autophagy to lysosomal biogenesis. *Science* **2011**, *332*, 1429-1433, doi:10.1126/science.1204592.

305. Pena-Llopis, S.; Vega-Rubin-de-Celis, S.; Schwartz, J.C.; Wolff, N.C.; Tran, T.A.; Zou, L.; Xie, X.J.; Corey, D.R.; Brugarolas, J. Regulation of TFEB and V-ATPases by mTORC1. *EMBO J* **2011**, *30*, 3242-3258, doi:10.1038/emboj.2011.257.

306. Ferron, M.; Settembre, C.; Shimazu, J.; Lacombe, J.; Kato, S.; Rawlings, D.J.; Ballabio, A.; Karsenty, G. A RANKL-PKCbeta-TFEB signaling cascade is necessary for lysosomal biogenesis in osteoclasts. *Genes Dev* **2013**, *27*, 955-969, doi:10.1101/gad.213827.113.

307. Yonekawa, T.; Gamez, G.; Kim, J.; Tan, A.C.; Thorburn, J.; Gump, J.; Thorburn, A.; Morgan, M.J. RIP1 negatively regulates basal autophagic flux through TFEB to control sensitivity to apoptosis. *EMBO Rep* **2015**, *16*, 700-708, doi:10.15252/embr.201439496.

308. Li, Y.; Xu, M.; Ding, X.; Yan, C.; Song, Z.; Chen, L.; Huang, X.; Wang, X.; Jian, Y.; Tang, G., et al. Protein kinase C controls lysosome biogenesis independently of mTORC1. *Nat Cell Biol* **2016**, *18*, 1065-1077, doi:10.1038/ncb3407.

309. Palmieri, M.; Pal, R.; Nelvagal, H.R.; Lotfi, P.; Stinnett, G.R.; Seymour, M.L.; Chaudhury, A.; Bajaj, L.; Bondar, V.V.; Bremner, L., et al. mTORC1-independent TFEB activation via Akt inhibition promotes cellular clearance in neurodegenerative storage diseases. *Nat Commun* **2017**, *8*, 14338, doi:10.1038/ncomms14338.

310. Medina, D.L.; Di Paola, S.; Peluso, I.; Armani, A.; De Stefani, D.; Venditti, R.; Montefusco, S.; Scotto-Rosato, A.; Prezioso, C.; Forrester, A., et al. Lysosomal calcium signalling regulates autophagy through calcineurin and TFEB. *Nat Cell Biol* **2015**, *17*, 288-299, doi:10.1038/ncb3114.

311. Bao, J.; Zheng, L.; Zhang, Q.; Li, X.; Zhang, X.; Li, Z.; Bai, X.; Zhang, Z.; Huo, W.; Zhao, X., et al. Deacetylation of TFEB promotes fibrillar Abeta degradation by upregulating lysosomal biogenesis in microglia. *Protein Cell* **2016**, *7*, 417-433, doi:10.1007/s13238-016-0269-2.

312. Visvikis, O.; Ihuegbu, N.; Labed, S.A.; Luhachack, L.G.; Alves, A.F.; Wollenberg, A.C.; Stuart, L.M.; Stormo, G.D.; Irazoqui, J.E. Innate host defense requires TFEB-mediated transcription of cytoprotective and antimicrobial genes. *Immunity* **2014**, *40*, 896-909, doi:10.1016/j.immuni.2014.05.002.

313. Gray, M.A.; Choy, C.H.; Dayam, R.M.; Ospina-Escobar, E.; Somerville, A.; Xiao, X.; Ferguson, S.M.; Botelho, R.J. Phagocytosis Enhances Lysosomal and Bactericidal Properties by Activating the Transcription Factor TFEB. *Curr Biol* **2016**, *26*, 1955-1964, doi:10.1016/j.cub.2016.05.070.

314. Pastore, N.; Brady, O.A.; Diab, H.I.; Martina, J.A.; Sun, L.; Huynh, T.; Lim, J.A.; Zare, H.; Raben, N.; Ballabio, A., et al. TFEB and TFE3 cooperate in the regulation of the innate immune response in activated macrophages. *Autophagy* **2016**, *12*, 1240-1258, doi:10.1080/15548627.2016.1179405.

315. Nezich, C.L.; Wang, C.; Fogel, A.I.; Youle, R.J. MiT/TFE transcription factors are activated during mitophagy downstream of Parkin and Atg5. *J Cell Biol* **2015**, *210*, 435-450, doi:10.1083/jcb.201501002.

316. Mansueto, G.; Armani, A.; Viscomi, C.; D'Orsi, L.; De Cegli, R.; Polishchuk, E.V.; Lamperti, C.; Di Meo, I.; Romanello, V.; Marchet, S., et al. Transcription Factor EB Controls Metabolic Flexibility during Exercise. *Cell Metab* **2017**, *25*, 182-196, doi:10.1016/j.cmet.2016.11.003.

317. Sha, Y.; Rao, L.; Settembre, C.; Ballabio, A.; Eissa, N.T. STUB1 regulates TFEB-induced autophagy-lysosome pathway. *EMBO J* **2017**, *36*, 2544-2552, doi:10.15252/embj.201796699.

318. Chen, L.; Wang, K.; Long, A.; Jia, L.; Zhang, Y.; Deng, H.; Li, Y.; Han, J.; Wang, Y. Fasting-induced hormonal regulation of lysosomal function. *Cell Res* **2017**, *27*, 748-763, doi:10.1038/cr.2017.45.

319. Ghosh, A.; Jana, M.; Modi, K.; Gonzalez, F.J.; Sims, K.B.; Berry-Kravis, E.; Pahan, K. Activation of peroxisome proliferator-activated receptor alpha induces lysosomal biogenesis in brain cells: implications for lysosomal storage disorders. *J Biol Chem* **2015**, *290*, 10309-10324, doi:10.1074/jbc.M114.610659.

320. Seok, S.; Fu, T.; Choi, S.E.; Li, Y.; Zhu, R.; Kumar, S.; Sun, X.; Yoon, G.; Kang, Y.; Zhong, W., et al. Transcriptional regulation of autophagy by an FXR-CREB axis. *Nature* **2014**, *516*, 108-111, doi:10.1038/nature13949.

321. Decressac, M.; Mattsson, B.; Weikop, P.; Lundblad, M.; Jakobsson, J.; Bjorklund, A. TFEB-mediated autophagy rescues midbrain dopamine neurons from alpha-synuclein toxicity. *Proc Natl Acad Sci U S A* **2013**, *110*, E1817-1826, doi:10.1073/pnas.1305623110.

322. Shin, H.J.; Kim, H.; Oh, S.; Lee, J.G.; Kee, M.; Ko, H.J.; Kweon, M.N.; Won, K.J.; Baek, S.H. AMPK-SKP2-CARM1 signalling cascade in transcriptional regulation of autophagy. *Nature* **2016**, *534*, 553-557, doi:10.1038/nature18014.

323. Du Bois, P.; Pablo Tortola, C.; Lodka, D.; Kny, M.; Schmidt, F.; Song, K.; Schmidt, S.; Bassel-Duby, R.; Olson, E.N.; Fielitz, J. Angiotensin II Induces Skeletal Muscle Atrophy by Activating TFEB-Mediated MuRF1 Expression. *Circ Res* **2015**, *117*, 424-436, doi:10.1161/CIRCRESAHA.114.305393.

324. Pastore, N.; Vainshtein, A.; Klisch, T.J.; Armani, A.; Huynh, T.; Herz, N.J.; Polishchuk, E.V.; Sandri, M.; Ballabio, A. TFE3 regulates whole-body energy metabolism in cooperation with TFEB. *EMBO Mol Med* **2017**, *9*, 605-621, doi:10.15252/emmm.201607204.

325. Steingrimsson, E.; Tessarollo, L.; Reid, S.W.; Jenkins, N.A.; Copeland, N.G. The bHLH-Zip transcription factor Tfeb is essential for placental vascularization. *Development* **1998**, *125*, 4607-4616.

326. Li, L.; Friedrichsen, H.J.; Andrews, S.; Picaud, S.; Volpon, L.; Ngeow, K.; Berridge, G.; Fischer, R.; Borden, K.L.B.; Filippakopoulos, P., et al. A TFEB nuclear export signal integrates amino acid supply and glucose availability. *Nat Commun* **2018**, *9*, 2685, doi:10.1038/s41467-018-04849-7.

327. Kuiper, R.P.; Schepens, M.; Thijssen, J.; van Asseldonk, M.; van den Berg, E.; Bridge, J.; Schuuring, E.; Schoenmakers, E.F.; van Kessel, A.G. Upregulation of the transcription factor TFEB in t(6;11)(p21;q13)-positive renal cell carcinomas due to promoter substitution. *Hum Mol Genet* **2003**, *12*, 1661-1669, doi:10.1093/hmg/ddg178.

328. Slade, L.; Biswas, D.; Ihionu, F.; El Hiani, Y.; Kienesberger, P.C.; Pulinilkunnil, T. A lysosome independent role for TFEB in activating DNA repair and inhibiting apoptosis in breast cancer cells. *Biochem J* **2020**, *477*, 137-160, doi:10.1042/BCJ20190596.

329. Perera, R.M.; Stoykova, S.; Nicolay, B.N.; Ross, K.N.; Fitamant, J.; Boukhali, M.; Lengrand, J.; Deshpande, V.; Selig, M.K.; Ferrone, C.R., et al. Transcriptional control of autophagy-lysosome function drives pancreatic cancer metabolism. *Nature* **2015**, *524*, 361-365, doi:10.1038/nature14587.

330. Evans, T.D.; Zhang, X.; Jeong, S.J.; He, A.; Song, E.; Bhattacharya, S.; Holloway, K.B.; Lodhi, I.J.; Razani, B. TFEB drives PGC-1alpha expression in adipocytes to protect against diet-induced metabolic dysfunction. *Sci Signal* **2019**, *12*, doi:10.1126/scisignal.aau2281.

331. Sergin, I.; Evans, T.D.; Razani, B. Degradation and beyond: the macrophage lysosome as a nexus for nutrient sensing and processing in atherosclerosis. *Curr Opin Lipidol* **2015**, *26*, 394-404, doi:10.1097/MOL.0000000000000213.

332. Sergin, I.; Evans, T.D.; Zhang, X.; Bhattacharya, S.; Stokes, C.J.; Song, E.; Ali, S.; Dehestani, B.; Holloway, K.B.; Micevych, P.S., et al. Exploiting macrophage autophagy-lysosomal biogenesis as a therapy for atherosclerosis. *Nat Commun* **2017**, *8*, 15750, doi:10.1038/ncomms15750.

333. Emanuel, R.; Sergin, I.; Bhattacharya, S.; Turner, J.; Epelman, S.; Settembre, C.; Diwan, A.; Ballabio, A.; Razani, B. Induction of lysosomal biogenesis in atherosclerotic macrophages can rescue lipid-induced lysosomal dysfunction and downstream sequelae. *Arterioscler Thromb Vasc Biol* **2014**, *34*, 1942-1952, doi:10.1161/ATVBAHA.114.303342.

334. Javaheri, A.; Bajpai, G.; Picataggi, A.; Mani, S.; Foroughi, L.; Evie, H.; Kovacs, A.; Weinheimer, C.J.; Hyrc, K.; Xiao, Q., et al. TFEB activation in macrophages attenuates postmyocardial infarction ventricular dysfunction independently of ATG5-mediated autophagy. *JCI Insight* **2019**, *4*, doi:10.1172/jci.insight.127312.

335. Rega, L.R.; Polishchuk, E.; Montefusco, S.; Napolitano, G.; Tozzi, G.; Zhang, J.; Bellomo, F.; Taranta, A.; Pastore, A.; Polishchuk, R., et al. Activation of the transcription factor EB rescues lysosomal abnormalities in cystinotic kidney cells. *Kidney Int* **2016**, *89*, 862-873, doi:10.1016/j.kint.2015.12.045.

336. Song, W.; Wang, F.; Savini, M.; Ake, A.; di Ronza, A.; Sardiello, M.; Segatori, L. TFEB regulates lysosomal proteostasis. *Hum Mol Genet* **2013**, *22*, 1994-2009, doi:10.1093/hmg/ddt052.

337. Tsunemi, T.; Ashe, T.D.; Morrison, B.E.; Soriano, K.R.; Au, J.; Roque, R.A.; Lazarowski, E.R.; Damian, V.A.; Masliah, E.; La Spada, A.R. PGC-1alpha rescues Huntington's disease proteotoxicity by preventing oxidative stress and promoting TFEB function. *Sci Transl Med* **2012**, *4*, 142ra197, doi:10.1126/scitranslmed.3003799.

338. Lieberman, A.P.; Puertollano, R.; Raben, N.; Slaugenhaupt, S.; Walkley, S.U.; Ballabio, A. Autophagy in lysosomal storage disorders. *Autophagy* **2012**, *8*, 719-730, doi:10.4161/auto.19469.

339. Trivedi, P.C.; Bartlett, J.J.; Mercer, A.; Slade, L.; Surette, M.; Ballabio, A.; Flibotte, S.; Hussein, B.; Rodrigues, B.; Kienesberger, P.C., et al. Loss of function of transcription factor EB remodels lipid metabolism and cell death pathways in the cardiomyocyte. *Biochim Biophys Acta Mol Basis Dis* **2020**, *1866*, 165832, doi:10.1016/j.bbadis.2020.165832.

340. Bachar-Wikstrom, E.; Wikstrom, J.D.; Ariav, Y.; Tirosh, B.; Kaiser, N.; Cerasi, E.; Leibowitz, G. Stimulation of autophagy improves endoplasmic reticulum stress-induced diabetes. *Diabetes* **2013**, *62*, 1227-1237, doi:10.2337/db12-1474.

341. Gonzalez-Rodriguez, A.; Mayoral, R.; Agra, N.; Valdecantos, M.P.; Pardo, V.; Miquilena-Colina, M.E.; Vargas-Castrillon, J.; Lo Iacono, O.; Corazzari, M.; Fimia, G.M., et al. Impaired autophagic flux is associated with increased endoplasmic reticulum stress during the development of NAFLD. *Cell Death Dis* **2014**, *5*, e1179, doi:10.1038/cddis.2014.162.

342. Otoda, T.; Takamura, T.; Misu, H.; Ota, T.; Murata, S.; Hayashi, H.; Takayama, H.; Kikuchi, A.; Kanamori, T.; Shima, K.R., et al. Proteasome dysfunction mediates obesity-induced endoplasmic reticulum stress and insulin resistance in the liver. *Diabetes* **2013**, *62*, 811-824, doi:10.2337/db11-1652.

343. Harada, M.; Hanada, S.; Toivola, D.M.; Ghori, N.; Omary, M.B. Autophagy activation by rapamycin eliminates mouse Mallory-Denk bodies and blocks their proteasome inhibitor-mediated formation. *Hepatology* **2008**, *47*, 2026-2035, doi:10.1002/hep.22294.

344. Bartlett, J.J.; Trivedi, P.C.; Yeung, P.; Kienesberger, P.C.; Pulinilkunnil, T. Doxorubicin impairs cardiomyocyte viability by suppressing transcription factor EB expression and disrupting autophagy. *Biochem J* **2016**, *473*, 3769-3789, doi:10.1042/BCJ20160385.

345. Guan, J.; Mishra, S.; Qiu, Y.; Shi, J.; Trudeau, K.; Las, G.; Liesa, M.; Shirihai, O.S.; Connors, L.H.; Seldin, D.C., et al. Lysosomal dysfunction and impaired autophagy underlie the pathogenesis of amyloidogenic light chain-mediated cardiotoxicity. *EMBO Mol Med* **2014**, *6*, 1493-1507, doi:10.15252/emmm.201404190.

346. Matyash, V.; Liebisch, G.; Kurzchalia, T.V.; Shevchenko, A.; Schwudke, D. Lipid extraction by methyl-tert-butyl ether for high-throughput lipidomics. *J Lipid Res* **2008**, *49*, 1137-1146, doi:10.1194/jlr.D700041-JLR200.

347. Breitkopf, S.B.; Ricoult, S.J.H.; Yuan, M.; Xu, Y.; Peake, D.A.; Manning, B.D.; Asara, J.M. A relative quantitative positive/negative ion switching method for untargeted lipidomics via high resolution LC-MS/MS from any biological source. *Metabolomics* **2017**, *13*, doi:10.1007/s11306-016-1157-8.

348. Eskelinen, E.L.; Illert, A.L.; Tanaka, Y.; Schwarzmann, G.; Blanz, J.; Von Figura, K.; Saftig, P. Role of LAMP-2 in lysosome biogenesis and autophagy. *Mol Biol Cell* **2002**, *13*, 3355-3368, doi:10.1091/mbc.e02-02-0114.

349. Aguiar, C.; MacLeod, J.; Yip, A.; Melville, S.; Legare, J.F.; Pulinilkunnil, T.; Kienesberger, P.; Brunt, K.; Hassan, A. Impact of Obesity on Postoperative Outcomes following cardiac Surgery (The OPOS study): rationale and design of an investigator-initiated prospective study. *BMJ Open* **2019**, *9*, e023418, doi:10.1136/bmjopen-2018-023418.

350. Dhanasekaran, D.N.; Reddy, E.P. JNK-signaling: A multiplexing hub in programmed cell death. *Genes Cancer* **2017**, *8*, 682-694, doi:10.18632/genesandcancer.155.

351. Del Re, D.P.; Amgalan, D.; Linkermann, A.; Liu, Q.; Kitsis, R.N. Fundamental Mechanisms of Regulated Cell Death and Implications for Heart Disease. *Physiol Rev* **2019**, *99*, 1765-1817, doi:10.1152/physrev.00022.2018.

352. Peter, A.K.; Bjerke, M.A.; Leinwand, L.A. Biology of the cardiac myocyte in heart disease. *Mol Biol Cell* **2016**, *27*, 2149-2160, doi:10.1091/mbc.E16-01-0038.

353. White, S.M.; Constantin, P.E.; Claycomb, W.C. Cardiac physiology at the cellular level: use of cultured HL-1 cardiomyocytes for studies of cardiac muscle cell structure and function. *Am J Physiol Heart Circ Physiol* **2004**, *286*, H823-829, doi:10.1152/ajpheart.00986.2003.

354. Niso-Santano, M.; Malik, S.A.; Pietrocola, F.; Bravo-San Pedro, J.M.; Marino, G.; Cianfanelli, V.; Ben-Younes, A.; Troncoso, R.; Markaki, M.; Sica, V., et al. Unsaturated fatty acids induce non-canonical autophagy. *EMBO J* **2015**, *34*, 1025-1041, doi:10.15252/embj.201489363.

355. Jaishy, B.; Zhang, Q.; Chung, H.S.; Riehle, C.; Soto, J.; Jenkins, S.; Abel, P.; Cowart, L.A.; Van Eyk, J.E.; Abel, E.D. Lipid-induced NOX2 activation inhibits autophagic flux by impairing lysosomal enzyme activity. *J Lipid Res* **2015**, *56*, 546-561, doi:10.1194/jlr.M055152.

356. Baena, M.; Sanguesa, G.; Hutter, N.; Sanchez, R.M.; Roglans, N.; Laguna, J.C.; Alegret, M. Fructose supplementation impairs rat liver autophagy through mTORC activation without inducing endoplasmic reticulum stress. *Biochim Biophys Acta* **2015**, *1851*, 107-116, doi:10.1016/j.bbalip.2014.11.003.

357. Sauvat, A.; Chen, G.; Muller, K.; Tong, M.; Aprahamian, F.; Durand, S.; Cerrato, G.; Bezu, L.; Leduc, M.; Franz, J., et al. Trans-Fats Inhibit Autophagy Induced by Saturated Fatty Acids. *EBioMedicine* **2018**, *30*, 261-272, doi:10.1016/j.ebiom.2018.03.028.

358. Pulinilkunnil, T.; Kienesberger, P.C.; Nagendran, J.; Sharma, N.; Young, M.E.; Dyck, J.R. Cardiac-specific adipose triglyceride lipase overexpression protects from cardiac steatosis and dilated cardiomyopathy following diet-induced obesity. *Int J Obes (Lond)* **2014**, *38*, 205-215, doi:10.1038/ijo.2013.103.

359. Sharma, S.; Adrogue, J.V.; Golfman, L.; Uray, I.; Lemm, J.; Youker, K.; Noon, G.P.; Frazier, O.H.; Taegtmeyer, H. Intramyocardial lipid accumulation in the failing human heart resembles the lipotoxic rat heart. *FASEB J* **2004**, *18*, 1692-1700, doi:10.1096/fj.04-2263com.

360. Stegemann, C.; Pechlaner, R.; Willeit, P.; Langley, S.R.; Mangino, M.; Mayr, U.; Menni, C.; Moayyeri, A.; Santer, P.; Rungger, G., et al. Lipidomics profiling and risk of cardiovascular disease in the prospective population-based Bruneck study. *Circulation* **2014**, *129*, 1821-1831, doi:10.1161/CIRCULATIONAHA.113.002500.

361. Mihalik, S.J.; Goodpaster, B.H.; Kelley, D.E.; Chace, D.H.; Vockley, J.; Toledo, F.G.; DeLany, J.P. Increased levels of plasma acylcarnitines in obesity and type 2 diabetes and identification of a marker of glucolipotoxicity. *Obesity (Silver Spring)* **2010**, *18*, 1695-1700, doi:10.1038/oby.2009.510.

362. Weiser, A.; Giesbertz, P.; Daniel, H.; Spanier, B. Acylcarnitine Profiles in Plasma and Tissues of Hyperglycemic NZO Mice Correlate with Metabolite Changes of Human Diabetes. *J Diabetes Res* **2018**, *2018*, 1864865, doi:10.1155/2018/1864865.

363. Basu, R.; Oudit, G.Y.; Wang, X.; Zhang, L.; Ussher, J.R.; Lopaschuk, G.D.; Kassiri, Z. Type 1 diabetic cardiomyopathy in the Akita (Ins2WT/C96Y) mouse model is characterized by lipotoxicity and diastolic dysfunction with preserved systolic function. *Am J Physiol Heart Circ Physiol* **2009**, *297*, H2096-2108, doi:10.1152/ajpheart.00452.2009.

364. Dong, S.; Zhang, R.; Liang, Y.; Shi, J.; Li, J.; Shang, F.; Mao, X.; Sun, J. Changes of myocardial lipidomics profiling in a rat model of diabetic cardiomyopathy using UPLC/Q-TOF/MS analysis. *Diabetol Metab Syndr* **2017**, *9*, 56, doi:10.1186/s13098-017-0249-6.

365. Dong, S.; Zhang, S.; Chen, Z.; Zhang, R.; Tian, L.; Cheng, L.; Shang, F.; Sun, J. Berberine Could Ameliorate Cardiac Dysfunction via Interfering Myocardial Lipidomic Profiles in the Rat Model of Diabetic Cardiomyopathy. *Front Physiol* **2018**, *9*, 1042, doi:10.3389/fphys.2018.01042.

366. Koga, H.; Kaushik, S.; Cuervo, A.M. Altered lipid content inhibits autophagic vesicular fusion. *FASEB J* **2010**, *24*, 3052-3065, doi:10.1096/fj.09-144519.

367. Xu, X.; Hua, Y.; Nair, S.; Zhang, Y.; Ren, J. Akt2 knockout preserves cardiac function in high-fat diet-induced obesity by rescuing cardiac autophagosome maturation. *J Mol Cell Biol* **2013**, *5*, 61-63, doi:10.1093/jmcb/mjs055.

368. Ma, X.; Mani, K.; Liu, H.; Kovacs, A.; Murphy, J.T.; Foroughi, L.; French, B.A.; Weinheimer, C.J.; Kraja, A.; Benjamin, I.J., et al. Transcription Factor EB Activation Rescues Advanced alphaB-Crystallin Mutation-Induced Cardiomyopathy by Normalizing Desmin Localization. *J Am Heart Assoc* **2019**, *8*, e010866, doi:10.1161/JAHA.118.010866.

369. Ma, X.; Godar, R.J.; Liu, H.; Diwan, A. Enhancing lysosome biogenesis attenuates BNIP3-induced cardiomyocyte death. *Autophagy* **2012**, *8*, 297-309, doi:10.4161/auto.18658.

370. Ma, X.; Liu, H.; Murphy, J.T.; Foyil, S.R.; Godar, R.J.; Abuirqeba, H.; Weinheimer, C.J.; Barger, P.M.; Diwan, A. Regulation of the transcription factor EB-PGC1alpha axis by beclin-1 controls mitochondrial quality and cardiomyocyte death under stress. *Mol Cell Biol* **2015**, *35*, 956-976, doi:10.1128/MCB.01091-14.

371. Martini-Stoica, H.; Xu, Y.; Ballabio, A.; Zheng, H. The Autophagy-Lysosomal Pathway in Neurodegeneration: A TFEB Perspective. *Trends Neurosci* **2016**, *39*, 221-234, doi:10.1016/j.tins.2016.02.002.

372. Slade, L.; Pulinilkunnil, T. The MiTF/TFE Family of Transcription Factors: Master Regulators of Organelle Signaling, Metabolism, and Stress Adaptation. *Mol Cancer Res* **2017**, *15*, 1637-1643, doi:10.1158/1541-7786.MCR-17-0320.

373. Calcagni, A.; Kors, L.; Verschuren, E.; De Cegli, R.; Zampelli, N.; Nusco, E.; Confalonieri, S.; Bertalot, G.; Pece, S.; Settembre, C., et al. Modelling TFE renal cell carcinoma in mice reveals a critical role of WNT signaling. *Elife* **2016**, *5*, doi:10.7554/eLife.17047.

374. Zhang, H.; Yan, S.; Khambu, B.; Ma, F.; Li, Y.; Chen, X.; Martina, J.A.; Puertollano, R.; Li, Y.; Chalasani, N., et al. Dynamic MTORC1-TFEB feedback signaling regulates hepatic autophagy, steatosis and liver injury in long-term nutrient oversupply. *Autophagy* **2018**, *14*, 1779-1795, doi:10.1080/15548627.2018.1490850.

375. Bartlett, J.J.; Trivedi, P.C.; Pulinilkunnil, T. Autophagic dysregulation in doxorubicin cardiomyopathy. *J Mol Cell Cardiol* **2017**, *104*, 1-8, doi:10.1016/j.yjmcc.2017.01.007.

376. Wang, F.; Pulinilkunnil, T.; Flibotte, S.; Nislow, C.; Vlodavsky, I.; Hussein, B.; Rodrigues, B. Heparanase protects the heart against chemical or ischemia/reperfusion injury. *J Mol Cell Cardiol* **2019**, *131*, 29-40, doi:10.1016/j.yjmcc.2019.04.008.

377. Palmieri, M.; Impey, S.; Kang, H.; di Ronza, A.; Pelz, C.; Sardiello, M.; Ballabio, A. Characterization of the CLEAR network reveals an integrated control of cellular clearance pathways. *Hum Mol Genet* **2011**, *20*, 3852-3866, doi:10.1093/hmg/ddr306.

378. Wang, S.; Ni, H.M.; Chao, X.; Wang, H.; Bridges, B.; Kumer, S.; Schmitt, T.; Mareninova, O.; Gukovskaya, A.; De Lisle, R.C., et al. Impaired TFEB-mediated lysosomal biogenesis promotes the development of pancreatitis in mice and is associated with human pancreatitis. *Autophagy* **2019**, *15*, 1954-1969, doi:10.1080/15548627.2019.1596486.

379. Huang, J.; Wang, X.; Zhu, Y.; Li, Z.; Zhu, Y.T.; Wu, J.C.; Qin, Z.H.; Xiang, M.; Lin, F. Exercise activates lysosomal function in the brain through AMPK-SIRT1-TFEB pathway. *CNS Neurosci Ther* **2019**, *25*, 796-807, doi:10.1111/cns.13114.

380. Pagano, M.; Naviglio, S.; Spina, A.; Chiosi, E.; Castoria, G.; Romano, M.; Sorrentino, A.; Illiano, F.; Illiano, G. Differentiation of H9c2 cardiomyoblasts: The role of adenylate cyclase system. *J Cell Physiol* **2004**, *198*, 408-416, doi:10.1002/jcp.10420.

381. Pan, B.; Zhang, H.; Cui, T.; Wang, X. TFEB activation protects against cardiac proteotoxicity via increasing autophagic flux. *J Mol Cell Cardiol* **2017**, *113*, 51-62, doi:10.1016/j.yjmcc.2017.10.003.

382. Singh, R.; Kaushik, S.; Wang, Y.; Xiang, Y.; Novak, I.; Komatsu, M.; Tanaka, K.; Cuervo, A.M.; Czaja, M.J. Autophagy regulates lipid metabolism. *Nature* **2009**, *458*, 1131-1135, doi:10.1038/nature07976.

383. Vega, R.B.; Huss, J.M.; Kelly, D.P. The coactivator PGC-1 cooperates with peroxisome proliferator-activated receptor alpha in transcriptional control of nuclear genes encoding mitochondrial fatty acid oxidation enzymes. *Mol Cell Biol* **2000**, *20*, 1868-1876, doi:10.1128/mcb.20.5.1868-1876.2000.

384. Matoba, K.; Lu, Y.; Zhang, R.; Chen, E.R.; Sangwung, P.; Wang, B.; Prosdocimo, D.A.; Jain, M.K. Adipose KLF15 Controls Lipid Handling to Adapt to Nutrient Availability. *Cell Rep* **2017**, *21*, 3129-3140, doi:10.1016/j.celrep.2017.11.032.

385. Prosdocimo, D.A.; John, J.E.; Zhang, L.; Efraim, E.S.; Zhang, R.; Liao, X.; Jain, M.K. KLF15 and PPARalpha Cooperate to Regulate Cardiomyocyte Lipid Gene Expression and Oxidation. *PPAR Res* **2015**, *2015*, 201625, doi:10.1155/2015/201625.

386. Takeuchi, Y.; Yahagi, N.; Aita, Y.; Murayama, Y.; Sawada, Y.; Piao, X.; Toya, N.; Oya, Y.; Shikama, A.; Takarada, A., et al. KLF15 Enables Rapid Switching between Lipogenesis and Gluconeogenesis during Fasting. *Cell Rep* **2016**, *16*, 2373-2386, doi:10.1016/j.celrep.2016.07.069.

387. Hsieh, P.N.; Zhou, G.; Yuan, Y.; Zhang, R.; Prosdocimo, D.A.; Sangwung, P.; Borton, A.H.; Boriushkin, E.; Hamik, A.; Fujioka, H., et al. A conserved KLF-autophagy pathway modulates nematode lifespan and mammalian age-associated vascular dysfunction. *Nat Commun* **2017**, *8*, 914, doi:10.1038/s41467-017-00899-5.

388. Wang, Q.; Donthi, R.V.; Wang, J.; Lange, A.J.; Watson, L.J.; Jones, S.P.; Epstein, P.N. Cardiac phosphatase-deficient 6-phosphofructo-2-kinase/fructose-2,6-bisphosphatase increases glycolysis, hypertrophy, and myocyte resistance to hypoxia. *Am J Physiol Heart Circ Physiol* **2008**, *294*, H2889-2897, doi:10.1152/ajpheart.91501.2007.

389. Dyck, J.R.; Cheng, J.F.; Stanley, W.C.; Barr, R.; Chandler, M.P.; Brown, S.; Wallace, D.; Arrhenius, T.; Harmon, C.; Yang, G., et al. Malonyl coenzyme a decarboxylase inhibition protects the ischemic heart by inhibiting fatty acid oxidation and stimulating glucose oxidation. *Circ Res* **2004**, *94*, e78-84, doi:10.1161/01.RES.0000129255.19569.8f.

390. Bouzakri, K.; Austin, R.; Rune, A.; Lassman, M.E.; Garcia-Roves, P.M.; Berger, J.P.; Krook, A.; Chibalin, A.V.; Zhang, B.B.; Zierath, J.R. Malonyl CoenzymeA decarboxylase regulates lipid and glucose metabolism in human skeletal muscle. *Diabetes* **2008**, *57*, 1508-1516, doi:10.2337/db07-0583.

391. Wang, W.; Zhang, L.; Battiprolu, P.K.; Fukushima, A.; Nguyen, K.; Milner, K.; Gupta, A.; Altamimi, T.; Byrne, N.; Mori, J., et al. Malonyl CoA Decarboxylase Inhibition Improves Cardiac Function Post-Myocardial Infarction. *JACC Basic Transl Sci* **2019**, *4*, 385-400, doi:10.1016/j.jacbts.2019.02.003.

392. Yang, L.; Li, P.; Fu, S.; Calay, E.S.; Hotamisligil, G.S. Defective hepatic autophagy in obesity promotes ER stress and causes insulin resistance. *Cell Metab* **2010**, *11*, 467-478, doi:10.1016/j.cmet.2010.04.005.

393. Li, Y.; Chao, X.; Yang, L.; Lu, Q.; Li, T.; Ding, W.X.; Ni, H.M. Impaired Fasting-Induced Adaptive Lipid Droplet Biogenesis in Liver-Specific Atg5-Deficient Mouse Liver Is Mediated by Persistent Nuclear Factor-Like 2 Activation. *Am J Pathol* **2018**, *188*, 1833-1846, doi:10.1016/j.ajpath.2018.04.015.

394. Abe, K.; Yano, T.; Tanno, M.; Miki, T.; Kuno, A.; Sato, T.; Kouzu, H.; Nakata, K.; Ohwada, W.; Kimura, Y., et al. mTORC1 inhibition attenuates necroptosis through RIP1 inhibition-mediated TFEB activation. *Biochim Biophys Acta Mol Basis Dis* **2019**, *1865*, 165552, doi:10.1016/j.bbadis.2019.165552.

395. Neill, T.; Sharpe, C.; Owens, R.T.; Iozzo, R.V. Decorin-evoked paternally expressed gene 3 (PEG3) is an upstream regulator of the transcription factor EB (TFEB) in endothelial cell autophagy. *J Biol Chem* **2017**, *292*, 16211-16220, doi:10.1074/jbc.M116.769950.

396. Anderson, M.E.; Brown, J.H.; Bers, D.M. CaMKII in myocardial hypertrophy and heart failure. *J Mol Cell Cardiol* **2011**, *51*, 468-473, doi:10.1016/j.yjmcc.2011.01.012.

397. Maier, L.S. CaMKIIdelta overexpression in hypertrophy and heart failure: cellular consequences for excitation-contraction coupling. *Braz J Med Biol Res* **2005**, *38*, 1293-1302, doi:10.1590/s0100-879x2005000900002.

398. Teucher, N.; Prestle, J.; Seidler, T.; Currie, S.; Elliott, E.B.; Reynolds, D.F.; Schott, P.; Wagner, S.; Kogler, H.; Inesi, G., et al. Excessive sarcoplasmic/endoplasmic reticulum Ca2+-ATPase expression causes increased sarcoplasmic reticulum Ca2+ uptake but decreases myocyte shortening. *Circulation* **2004**, *110*, 3553-3559, doi:10.1161/01.CIR.0000145161.48545.B3.

399. Kilpatrick, B.S.; Eden, E.R.; Schapira, A.H.; Futter, C.E.; Patel, S. Direct mobilisation of lysosomal Ca2+ triggers complex Ca2+ signals. *J Cell Sci* **2013**, *126*, 60-66, doi:10.1242/jcs.118836.

400. Morgan, A.J.; Davis, L.C.; Wagner, S.K.; Lewis, A.M.; Parrington, J.; Churchill, G.C.; Galione, A. Bidirectional Ca(2)(+) signaling occurs between the endoplasmic reticulum and acidic organelles. *J Cell Biol* **2013**, *200*, 789-805, doi:10.1083/jcb.201204078.

401. Sbano, L.; Bonora, M.; Marchi, S.; Baldassari, F.; Medina, D.L.; Ballabio, A.; Giorgi, C.; Pinton, P. TFEB-mediated increase in peripheral lysosomes regulates store-operated calcium entry. *Sci Rep* **2017**, *7*, 40797, doi:10.1038/srep40797.

402. Li, J.; Ma, W.; Yue, G.; Tang, Y.; Kim, I.M.; Weintraub, N.L.; Wang, X.; Su, H. Cardiac proteasome functional insufficiency plays a pathogenic role in diabetic cardiomyopathy. *J Mol Cell Cardiol* **2017**, *102*, 53-60, doi:10.1016/j.yjmcc.2016.11.013.

403. Kanamori, H.; Takemura, G.; Goto, K.; Tsujimoto, A.; Mikami, A.; Ogino, A.; Watanabe, T.; Morishita, K.; Okada, H.; Kawasaki, M., et al. Autophagic adaptations in diabetic cardiomyopathy differ between type 1 and type 2 diabetes. *Autophagy* **2015**, *11*, 1146-1160, doi:10.1080/15548627.2015.1051295.

404. Li, Z.L.; Woollard, J.R.; Ebrahimi, B.; Crane, J.A.; Jordan, K.L.; Lerman, A.; Wang, S.M.; Lerman, L.O. Transition from obesity to metabolic syndrome is associated with altered myocardial autophagy and apoptosis. *Arterioscler Thromb Vasc Biol* **2012**, *32*, 1132-1141, doi:10.1161/ATVBAHA.111.244061.

405. Puertollano, R.; Ferguson, S.M.; Brugarolas, J.; Ballabio, A. The complex relationship between TFEB transcription factor phosphorylation and subcellular localization. *EMBO J* **2018**, *37*, doi:10.15252/embj.201798804.

406. McLendon, P.M.; Robbins, J. Proteotoxicity and cardiac dysfunction. *Circ Res* **2015**, *116*, 1863-1882, doi:10.1161/CIRCRESAHA.116.305372.

407. Janikiewicz, J.; Hanzelka, K.; Dziewulska, A.; Kozinski, K.; Dobrzyn, P.; Bernas, T.; Dobrzyn, A. Inhibition of SCD1 impairs palmitate-derived autophagy at the step of autophagosome-lysosome fusion in pancreatic beta-cells. *J Lipid Res* **2015**, *56*, 1901-1911, doi:10.1194/jlr.M059980.

408. Las, G.; Serada, S.B.; Wikstrom, J.D.; Twig, G.; Shirihai, O.S. Fatty acids suppress autophagic turnover in beta-cells. *J Biol Chem* **2011**, *286*, 42534-42544, doi:10.1074/jbc.M111.242412.

409. Boland, B.; Yu, W.H.; Corti, O.; Mollereau, B.; Henriques, A.; Bezard, E.; Pastores, G.M.; Rubinsztein, D.C.; Nixon, R.A.; Duchen, M.R., et al. Promoting the clearance of neurotoxic proteins in neurodegenerative disorders of ageing. *Nat Rev Drug Discov* **2018**, *17*, 660-688, doi:10.1038/nrd.2018.109.

410. Pi, H.; Li, M.; Tian, L.; Yang, Z.; Yu, Z.; Zhou, Z. Enhancing lysosomal biogenesis and autophagic flux by activating the transcription factor EB protects against cadmium-induced neurotoxicity. *Sci Rep* **2017**, *7*, 43466, doi:10.1038/srep43466.

411. Morgan, M.J.; Liu, Z.G. Programmed cell death with a necrotic-like phenotype. *Biomol Concepts* **2013**, *4*, 259-275, doi:10.1515/bmc-2012-0056.

412. Brady, O.A.; Jeong, E.; Martina, J.A.; Pirooznia, M.; Tunc, I.; Puertollano, R. The transcription factors TFE3 and TFEB amplify p53 dependent transcriptional programs in response to DNA damage. *Elife* **2018**, *7*, doi:10.7554/eLife.40856.

413. Nijman, S.M.; Hijmans, E.M.; El Messaoudi, S.; van Dongen, M.M.; Sardet, C.; Bernards, R. A functional genetic screen identifies TFE3 as a gene that confers resistance to the anti-proliferative effects of the retinoblastoma protein and transforming growth factor-beta. *J Biol Chem* **2006**, *281*, 21582-21587, doi:10.1074/jbc.M602312200.

414. Song, E.; Da Eira, D.; Jani, S.; Sepa-Kishi, D.; Vu, V.; Hunter, H.; Lai, M.; Wheeler, M.B.; Ceddia, R.B.; Sweeney, G. Cardiac Autophagy Deficiency Attenuates ANP Production and Disrupts Myocardial-Adipose Crosstalk Leading to Increased Fat Accumulation and Metabolic Dysfunction. *Diabetes* **2020**, 10.2337/db19-0762, doi:10.2337/db19-0762.

415. Porter, K.; Nallathambi, J.; Lin, Y.; Liton, P.B. Lysosomal basification and decreased autophagic flux in oxidatively stressed trabecular meshwork cells: implications for glaucoma pathogenesis. *Autophagy* **2013**, *9*, 581-594, doi:10.4161/auto.23568.

416. Unuma, K.; Aki, T.; Funakoshi, T.; Yoshida, K.; Uemura, K. Cobalt protoporphyrin accelerates TFEB activation and lysosome reformation during LPS-induced septic insults in the rat heart. *PLoS One* **2013**, *8*, e56526, doi:10.1371/journal.pone.0056526.

417. Prosdocimo, D.A.; Anand, P.; Liao, X.; Zhu, H.; Shelkay, S.; Artero-Calderon, P.; Zhang, L.; Kirsh, J.; Moore, D.; Rosca, M.G., et al. Kruppel-like factor 15 is a critical regulator of cardiac lipid metabolism. *J Biol Chem* **2014**, *289*, 5914-5924, doi:10.1074/jbc.M113.531384.

418. Hussain, R.; Zubair, H.; Pursell, S.; Shahab, M. Neurodegenerative Diseases: Regenerative Mechanisms and Novel Therapeutic Approaches. *Brain Sci* **2018**, *8*, doi:10.3390/brainsci8090177.

Appendix A. Copyright Permissions

Dear Ms Purvi Trivedi

We hereby grant you permission to reprint the material below at no charge **in your thesis** subject to the following conditions:

1. If any part of the material to be used (for example, figures) has appeared in our publication with credit or acknowledgement to another source, permission must also be sought from that source. If such permission is not obtained then that material may not be included in your publication/copies.

2. Suitable acknowledgment to the source must be made, either as a footnote or in a reference list at the end of your publication, as follows:
"This article was published in Publication title, Vol number, Author(s), Title of article, Page Nos, Copyright Elsevier (or appropriate Society name) (Year)."

3. Your thesis may be submitted to your institution in either print or electronic form.

4. Reproduction of this material is confined to the purpose for which permission is hereby given

5. This permission is granted for non-exclusive world **English** rights only. For other languages please reapply separately for each one required. Permission excludes use in an electronic form other than submission. Should you have a specific electronic project in mind please reapply for permission.

6. As long as the article is embedded in your thesis, you can post/ share your thesis in the University repository

7. Should your thesis be published commercially, please reapply for permission.

8. Posting of the full article/ chapter online is not permitted. You may post an abstract with a link to the Elsevier website www.elsevier.com, or to the article on ScienceDirect if it is available on that platform.

Thanks & Regards,
Roopa Lingayath
Sr Copyrights Coordinator – Copyrights Team
ELSEVIER | Health Content Operations
E-mail: r.lingayath@elsevier.com | url: www.elsevier.com